



Universitat de Lleida

## Development of new therapeutic strategies for Spinal Muscular Atrophy

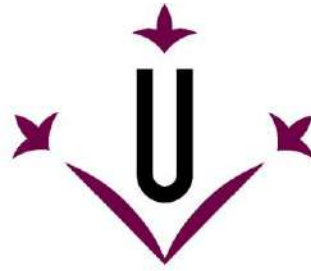
Sandra De la Fuente Ruiz

<http://hdl.handle.net/10803/669753>

**ADVERTIMENT.** L'accés als continguts d'aquesta tesi doctoral i la seva utilització ha de respectar els drets de la persona autora. Pot ser utilitzada per a consulta o estudi personal, així com en activitats o materials d'investigació i docència en els termes establerts a l'art. 32 del Text Refós de la Llei de Propietat Intel·lectual (RDL 1/1996). Per altres utilitzacions es requereix l'autorització prèvia i expressa de la persona autora. En qualsevol cas, en la utilització dels seus continguts caldrà indicar de forma clara el nom i cognoms de la persona autora i el títol de la tesi doctoral. No s'autoritza la seva reproducció o altres formes d'explotació efectuades amb finalitats de lucre ni la seva comunicació pública des d'un lloc aliè al servei TDX. Tampoc s'autoritza la presentació del seu contingut en una finestra o marc aliè a TDX (framing). Aquesta reserva de drets afecta tant als continguts de la tesi com als seus resums i índexs.

**ADVERTENCIA.** El acceso a los contenidos de esta tesis doctoral y su utilización debe respetar los derechos de la persona autora. Puede ser utilizada para consulta o estudio personal, así como en actividades o materiales de investigación y docencia en los términos establecidos en el art. 32 del Texto Refundido de la Ley de Propiedad Intelectual (RDL 1/1996). Para otros usos se requiere la autorización previa y expresa de la persona autora. En cualquier caso, en la utilización de sus contenidos se deberá indicar de forma clara el nombre y apellidos de la persona autora y el título de la tesis doctoral. No se autoriza su reproducción u otras formas de explotación efectuadas con fines lucrativos ni su comunicación pública desde un sitio ajeno al servicio TDR. Tampoco se autoriza la presentación de su contenido en una ventana o marco ajeno a TDR (framing). Esta reserva de derechos afecta tanto al contenido de la tesis como a sus resúmenes e índices.

**WARNING.** Access to the contents of this doctoral thesis and its use must respect the rights of the author. It can be used for reference or private study, as well as research and learning activities or materials in the terms established by the 32nd article of the Spanish Consolidated Copyright Act (RDL 1/1996). Express and previous authorization of the author is required for any other uses. In any case, when using its content, full name of the author and title of the thesis must be clearly indicated. Reproduction or other forms of for profit use or public communication from outside TDX service is not allowed. Presentation of its content in a window or frame external to TDX (framing) is not authorized either. These rights affect both the content of the thesis and its abstracts and indexes.



Universitat de Lleida

# Development of new therapeutic strategies for Spinal Muscular Atrophy

Sandra De la Fuente Ruiz

2020





**Universitat de Lleida**

## **TESI DOCTORAL**

Development of new therapeutic strategies for  
Spinal Muscular Atrophy

Sandra De la Fuente Ruiz

Memòria presentada per optar al grau de Doctor per la Universitat de Lleida

Programa de Doctorat en Salut

Directora i Tutora

Rosa M<sup>a</sup> Soler Tatché

2020



This thesis has been funded by:

- Ajuts per a personal predoctoral de la Universitat de Lleida en formació i ajuts Jade Plus per a l'any 2015-2018
- Ajuts de Promoció de la Recerca en Salut 2018 del IRBLleida i Diputació de Lleida
- Ministerio de Economía y competitividad (Gobierno de España)-Instituto de Salud Carlos III, Fondo de Investigaciones Sanitarias, Unión Europea, Fondo Europeo de Desarrollo Regional (FEDER), "Una manera de hacer Europa". Convocatoria 2014 (PI14/0060).
- Ministerio de Economía y competitividad (Gobierno de España)-Instituto de Salud Carlos III, Fondo de Investigaciones Sanitarias, Unión Europea, Fondo Europeo de Desarrollo Regional (FEDER), "Una manera de hacer Europa". Convocatoria 2017 (PI17/00231).



**RESUM·RESUMEN·ABSTRACT**

---





## RESUM

L'Atròfia Muscular Espinal (AME) és una malaltia neurodegenerativa greu i la primera causa genètica de mort infantil. S'origina per la pèrdua o mutació del gen *Survival Motor Neuron 1* (SMN1) que causa una deficiència de la proteïna de Survival Motor Neuron (SMN). La reducció d'aquesta proteïna condueix principalment a la degeneració de les motoneurons (MNs) de la medulla espinal i, en conseqüència, produeix atròfia i feblesa del múscul esquelètic. Actualment, només es coneix parcialment quins mecanismes cel·lulars i moleculars exactes són els responsables de la pèrdua de funció de les MNs. La reducció de SMN causa degeneració de les neurites i mort cel·lular sense característiques apoptòtiques clàssiques. L'autofàgia és un procés important i altament regulat, essencial per a l'eliminació d'òrgans danyats i substàncies o proteïnes tòxiques a través de la degradació amb els lisosomes. L'autofàgia és especialment important en cèl·lules post-mitòtiques, com les MNs, on l'acumulació d'autofagosomes provoca la interrupció del transport axonal, la interferència del trànsit intracel·lular i la degeneració de les neurites.

El que és ben sabut en l'AME és que el nivell intracel·lular de proteïna SMN defineix l'inici i la gravetat de la malaltia i això està parcialment determinat pel nombre de còpies del gen SMN2, la duplicació centromèrica de SMN i el principal modificador de l'AME. Per aquesta raó, comprendre els processos que regulen la degradació de SMN amb la finalitat d'identificar compostos que augmentin els nivells de proteïnes és el principal objectiu en el desenvolupament terapèutic per a l'AME. Les calpaïnes són una família de proteases dependents de calci que s'han relacionat amb trastorns musculars i malalties neurodegeneratives. Específicament, s'ha descrit en el múscul que SMN pot ser proteolitzada per calpaïna. L'activitat de la calpaïna també està involucrada en la regulació de l'autofàgia mitjançant la modulació de múltiples de les proteïnes involucrades en el procés.

L'objectiu en el present treball ha estat analitzar la desregulació de l'autofàgia i determinar la participació de la calpaïna en la regulació de la proteïna SMN en les MNs per a aprofundir en l'origen de la neurodegeneració i desenvolupar un nou enfocament terapèutic per a l'AME. Per aquesta finalitat, hem analitzat marcadors autofàgics en diferents models *in vitro* d'AME, tant de ratolí com d'humà. Els resultats van mostrar que,

tant els autofagosomes com els nivells de LC3 es troben augmentats en les mostres d'AME en comparació amb els controls, la qual cosa suggereix una desregulació del procés d'autofàgia al llarg de la progressió de la malaltia. A més, la reducció dels nivells endògens de calpaína utilitzant un shRNA van mostrar un augment dels nivells de Smn i LC3, alhora que prevenia la degeneració neurítica que es produeix en les MNs de ratolí afectats per AME. Es van obtenir resultats similars en experiments *in vitro* utilitzant un inhibidor farmacològic de calpaína, la calpeptina. Tanmateix, l'activació de la calpaína produïda per condicions despolarizants induïa la proteólisis de l' $\alpha$ -fodrina i de SMN, la qual cosa confirma que calpain regula directament els nivells de proteïna SMN en les MNs. A més, el tractament amb calpeptina *in vivo* va millorar significativament l'esperança de vida i la funció motora de dos models de ratolins amb AME, la qual cosa demostra la utilitat potencial dels inhibidors de la calpaína en la teràpia per a la malaltia. Finalment, l'anàlisi de la via de la calpaína en ratolins i models cel·lulars humans d'AME va indicar un augment de l'activitat de la calpaína en les MNs amb nivells reduïts de SMN. Per tant, els nostres resultats demostren que l'activitat de la calpaína es troba sobreactivada en les MNs d'AME i que la seva inhibició pot tenir un efecte beneficiós sobre el fenotip de la malaltia a través de l'augment de SMN i la regulació del procés d'autofàgia en les MNs de la medul·la espinal.

## RESUMEN

La atrofia muscular espinal (AME) es una enfermedad neurodegenerativa grave y la primera causa genética de muerte infantil. Se origina por la pérdida o mutación del gen *Survival Motor Neuron 1* (SMN1) que causa una deficiencia de la proteína de Survival Motor Neuron (SMN). La reducción de esta proteína conduce predominantemente a la degeneración de las motoneuronas (MNs) de la médula espinal y, en consecuencia, produce atrofia y debilidad del músculo esquelético. Actualmente, solo se conoce parcialmente que mecanismos celulares y moleculares exactos son los responsables de la pérdida de función de las MNs. La reducción de SMN causa degeneración de neuritas y muerte celular sin características apoptóticas clásicas. La autofagia es un proceso importante y altamente regulado, esencial para la eliminación de orgánulos dañados y sustancias o proteínas tóxicas a través de la degradación con los lisosomas. La autofagia es especialmente importante en células post-mitóticas, como las MNs, donde la acumulación de autofagosomas provoca la interrupción del transporte axonal, la interferencia del tráfico intracelular y la degeneración de las neuritas.

Lo que es bien sabido en la AME es que el nivel intracelular de proteína SMN define el inicio y la gravedad de la enfermedad y esto está parcialmente determinado por el número de copias del gen SMN2, la duplicación centromérica de SMN y el principal modificador de la AME. Por esa razón, comprender los procesos que regulan la degradación de SMN con la finalidad de identificar compuestos que aumentan los niveles de proteínas es el principal objetivo en el desarrollo terapéutico de AME. Las calpaínas son una familia de proteasas dependientes de calcio que se han relacionado con trastornos musculares y enfermedades neurodegenerativas. Específicamente, se ha descrito en el músculo que SMN puede ser proteolizada por calpaína. La actividad de la calpaína también está involucrada en la regulación de la autofagia mediante la modulación de múltiples de las proteínas involucradas en el proceso.

El objetivo en el presente trabajo ha sido analizar la desregulación de la autofagia y determinar la participación de la calpaína en la regulación de la proteína SMN en las MNs para profundizar en el origen de la neurodegeneración y desarrollar un nuevo enfoque terapéutico para la AME. Con este fin, hemos analizado marcadores autofágicos en diferentes modelos in vitro de AME, tanto de ratón como de humano. Los resultados

mostraron que los autofagosomas y los niveles de LC3 se encuentran aumentados en las muestras de AME en comparación con los controles, lo que sugiere una desregulación del proceso de autofagia a lo largo de la progresión de la enfermedad. Además, la reducción de los niveles endógenos de calpaína utilizando un shRNA mostraron un aumento de los niveles de Smn y LC3, a la vez que previene la degeneración neurítica que se produce en las MNs de ratón afectados por AME. Se obtuvieron resultados similares en experimentos *in vitro* utilizando un inhibidor farmacológico de calpaína, la calpeptina. Asimismo, la activación de calpaína producida por condiciones despolarizantes inducía la proteólisis de  $\alpha$ -fodrina y de SMN, lo que confirma que calpain regula directamente los niveles de proteína SMN en las MNs. Además, el tratamiento con calpeptina *in vivo* mejoró significativamente la esperanza de vida y la función motora de dos modelos de ratones con AME, lo que demuestra la utilidad potencial de los inhibidores de la calpaína en la terapia para la enfermedad. Finalmente, el análisis de la vía de la calpaína en ratones y modelos celulares humanos de AME indicó un aumento de la actividad de la calpaína en las MNs con niveles reducidos de SMN. Por lo tanto, nuestros resultados demuestran que la actividad de la calpaína se encuentra sobreactivada en las MNs de AME y su inhibición puede tener un efecto beneficioso sobre el fenotipo de la enfermedad a través del aumento de SMN y la regulación del proceso de autofagia en las MNs de la médula espinal.

**ABSTRACT**

Spinal Muscular Atrophy (SMA) is a severe neurodegenerative disease and the first genetic cause of infant death. It is originated by the deletion or mutation of *Survival Motor Neuron 1* (SMN1) gene causing a Survival Motor Neuron (SMN) protein deficiency. The reduction of this protein predominantly leads to the degeneration of spinal cord motoneurons (MNs) and consequently produces skeletal muscle atrophy and weakness. The exact cellular and molecular mechanisms responsible for MN loss of function are only partially known. SMN reduction causes neurite degeneration and cell death without classical apoptotic features. Autophagy is an important and highly regulated process, essential for the removal of damaged organelles and toxic substances or proteins through lysosome degradation. This mechanism is specifically important in post-mitotic cells like MNs where autophagosome accumulation causes axonal transport disruption, interference of intracellular space trafficking, and neurite degeneration.

What is well known in SMA is that intracellular SMN protein levels are critical to define the disease onset and severity, and this is partially determined by the number of copies of SMN2, the centromeric duplication of the SMN gene and the main modifier of SMA. For that reason, understanding the processes of SMN stability and degradation to identify compounds that increase protein levels is a major goal in SMA therapeutics development. Calpains are a family of calcium-dependent proteases that have been related to muscle disorders and neurodegenerative diseases. Specifically, it has been described in muscle that SMN can be a proteolytic target of calpain. Calpain activity is also involved in autophagy regulation by modulation of multiple proteins involved in the process.

The objectives in the present work have been to analyze the autophagy deregulation and determine the involvement of calpain in SMN protein regulation on MNs, in order to deepen in the origin of neurodegeneration and to develop a new therapeutic approach for SMA disease. To this end, we have analyzed autophagic markers in different mouse and human SMA *in vitro* models. The results showed that autophagosomes and LC3 levels were increased in SMA samples compared to controls, suggesting a deregulation of the autophagy process throughout the disease progression. Moreover, calpain knockdown using an shRNA approach showed an increase of both, Smn and LC3 levels and prevented neurite degeneration occurred in SMA affected mouse MNs. Similar results were obtained

in *in vitro* experiments using a pharmacological calpain inhibitor, calpeptin. Likewise, calpain activation produced by depolarized conditions induced  $\alpha$ -fodrin and SMN proteolysis, confirming that calpain directly regulates the SMN protein level in MNs. Additionally, calpeptin *in vivo* treatment significantly improved the lifespan and motor function of two severe SMA mouse models, demonstrating the potential utility of calpain inhibitors in SMA therapeutics. Finally, the analysis of calpain pathway members in mice and human cellular SMA models indicated an increase of calpain activity in SMN-reduced MNs. Thus, our results show that calpain activity is increased in SMA MNs and its inhibition may have a beneficial effect on the SMA phenotype through the increase of SMN and the regulation of the autophagy process in spinal cord MNs.

## **ACKNOWLEDGMENTS**

---





Para mí, presentar esta tesis doctoral es mucho más que un simple trámite. La realización de esta tesis constituye un motivo de genuina satisfacción, en parte generado por el orgullo personal del esfuerzo realizado para ofrecer nuevos conocimientos en la Atrofia Muscular Espinal, y en parte porque representa el final de una etapa formativa que empezó hace diez años con mi entrada en la Universidad. Un periodo que ha pasado por buenos y malos momentos, por periodos de frustración y de entusiasmo, pero que ha sido una grandiosa experiencia, no solo a nivel profesional, sino también a nivel personal, y de la que he disfrutado de cada momento, de cada experimento y de cada proyecto.

Esta aventura por supuesto no se supera sola, sino que siempre cuenta con el esfuerzo de un grupo humano que nos aliena y nos anima a la realización de nuestras investigaciones. Es por ello que quiero dar las gracias a todas esas personas que han sido tan importantes para mí en estos años, y que estoy segura que lo continuaran siendo en el futuro.

Para empezar, quiero agradecer de manera especial a mi tutora y directora de tesis. Rosa, muchas gracias por la oportunidad y por confiar en mi para hacer la tesis. Gracias por todo lo que me has enseñado y ayudado en estos años, por las tardes discutiendo resultados, por los consejos que me han guiado en este camino, y en general por cuidarme desde el primer momento. Para mi has sido una mentora y una segunda madre. Sé que, aunque me vaya, siempre podré contar con tus palabras de ánimo. Espero algún día poder ser una investigadora tan capaz como tú.

A Ana, por enseñarme todo lo relacionado con los cultivos primarios de motoneuronas, la producción de lentivirus y western blot.

A Alba, que durante este tiempo nos hemos ido conociendo casi como hermanas, gracias por los momentos de cotilleo, por esas míticas aventuras en los congresos, por las risas en los seminarios y fuera de ellos, y por esa maravillosa chaqueta quita-fríos.

Quiero agradecer también a todo el laboratorio de Bioquímica, a Kim, Elisa, Jordi, Fabien, Roser, Elena, Marta y Arabela. Ha sido un placer compartir laboratorio con vosotros. Gracias por hacer tan fácil la vida en el laboratorio, por el buen rollo que siempre generáis, por compartir vuestro entusiasmo y pasión por la ciencia, por los consejos y la ayuda que siempre brindáis despreocupadamente, por las charlas en las horas de café, y por darnos siempre una visión diferente de todo.

Quiero agradecer también al resto de becarios e investigadores de los departamentos de medicina experimental y ciencias médicas básicas por los buenos momentos compartidos y la buena predisposición a ayudar. Gracias a todos por esos fines de semana de vermuteo que se alargan todo el día, por hacer más amenas esas tardes eternas en el laboratorio, por esos ratos de café que eran como agua en el desierto, por las cenas, salidas, charlas, y en general por todo el tiempo que hemos pasado juntos y que ha hecho de estos años un recuerdo inolvidable. Gracias Moni, Albi, Javi, Elena, Iván, Nuria, Marta, Arabela, Sara, Silvia, Irene, Turi, Carles, Ares, etc.

A Rosa y a Myriam, por ser responsables de mi estancia en la Universidad de Hasselt, que ha sido una experiencia inolvidable tanto a nivel de formación como a nivel personal. I would like to thank professor Hendrix for receiving me to his laboratory and for the enjoyable barbeque. To Stefannie for the nice welcome during my stay and for all that you taught me. Thanks to all the people from the group for being so friendly with me, you treated me as one of the group and for the nice farewell dinner when I was leaving. Thanks, Selien for letting me work with you and for all the talks about science and life. Thanks to all the people I met in Hasselt that made my internship as a memorable part of my life. I will never forget you. Thank you, Pascal, for being such a good friend, thanks for all the moments shared together, for all the scientific advice and all the jokes.

A mis padres, que se alegraron como nadie cuando empecé a cobrar de la beca de doctorado. Gracias por enseñarme a hacer las cosas con pasión y dedicación, a no rendirme nunca y dar siempre lo mejor de mí. Sin vuestro esfuerzo no hubiera podido llegar hasta donde estoy ahora. Gracias papa, mama y Esther, por confiar y creer en mí, por vuestro apoyo incondicional para seguir siempre adelante, los estilismos para los congresos y los ánimos mientras escribo la tesis. A mis yayos, que desde que me vine a Lleida habéis sido los proveedores oficiales de tupperes, que siempre os habéis preocupado de mi bienestar y, aun sin entender lo que hago, aun me preguntáis cómo van los estudios. A toda mi familia, que os he dedicado menos tiempo del que os merecáis debido al trabajo, gracias por entenderme y dedicarme esos fines de semana de comilonas y desconexión. Gracias porque os debo todo lo que soy.

Y gracias a Marc, porque no sé qué hubiera hecho sin ti. Gracias por ser siempre mi mayor apoyo, por tus ánimos en mis momentos de flaqueza, por alegrarte conmigo en los buenos

momentos, por tu cariño incondicional y por la paciencia (de campeonato) que has demostrado conmigo (sobre todo este último año). Por ayudarme a sobrevivir al estrés y no dejar que me rinda nunca, por acompañarme en las agotadoras noches preparando posters, tesis y resultados, por aguantar escuchándome hablar de calpains y autofagia a todas horas, gracias de todo corazón.

Gracias a toda la gente que me ha ayudado a llegar hasta aquí.



## INDEX

---



## INDEX

<b>ABBREVIATIONS</b>	<b>1</b>
<b>INTRODUCTION</b>	<b>7</b>
<b>1. The Human Nervous System</b>	<b>9</b>
1.1. Motoneurons (MNs)	10
1.1.1. Upper MNs	10
1.1.2. Lower MNs	11
1.2. Generation of MNs	14
1.3. Columnar organization of spinal cord MNs	16
<b>2. Spinal muscular atrophy</b>	<b>19</b>
2.1. SMA clinical classification	20
2.1.1. SMA type 0 or prenatal	21
2.1.2. SMA type 1 or infantile	21
2.1.3. SMA type 2 or intermediate	22
2.1.4. SMA type 3 or juvenile	22
2.1.5. SMA type 4 or adult	22
2.2. Molecular and genetic basis of the disease	23
2.2.1. SMN gene (SMN1 and SMN2)	24
2.2.2. Genotype-phenotype correlation	25
2.3. SMN protein	27
2.3.1. SMN functions	28
2.4. SMA pathology	34
2.4.1. Motoneuron alteration	34
2.4.2. One protein, two hypothesis	35
2.4.3. Other cell types affected: SMA as a multisystemic disease	37
2.5. SMA therapies	42
2.5.1. Current treatment	43
2.5.2. New therapies	47
2.6. SMN models	60
2.6.1. <i>Schizosaccharomyces pombe</i>	60
2.6.2. <i>Caenorhabditis elegans</i>	61
2.6.3. <i>Drosophila melanogaster</i>	61
2.6.4. <i>Danio rerio</i>	62



2.6.5. Mus musculus	62
<b>3. Autophagy</b>	<b>68</b>
3.1. Autophagy machinery	70
3.1.1. Initiation	71
3.1.2. Phagophore nucleation	73
3.1.3. Phagophore elongation	75
3.1.4. Lysosomal fusion and degradation	78
3.2. Autophagy and neurodegeneration	79
<b>4. Calpain</b>	<b>81</b>
4.1. Calpain family	81
4.2. Calpain activity and specificity	85
4.3. Calpain regulation	86
4.3.1. Calcium	86
4.3.2. Small regulatory subunit	86
4.3.3. Calpastatin	87
4.4. Calpain and neurodegeneration	89
<b>HYPOTHESIS AND OBJECTIVES</b>	<b>91</b>
<b>MATERIALS AND METHODS</b>	<b>95</b>
<b>1. Mouse lines and colony maintenance</b>	<b>97</b>
1.1. CD1 mouse model	97
1.2. SMA transgenic mouse models	98
1.2.1. Smn -/-; SMN2 +/+ or MutSMA	98
1.2.2. Smn -/-; SMN2 +/+; SMN $\Delta$ 7 +/+ or SMN $\Delta$ 7	99
1.2.3. Genotype	100
<b>2. Primary Cell culture</b>	<b>103</b>
2.1. Precoating plates	103
2.2. Cell culture media and solutions	104
2.3. Mouse motoneuron primary culture	105
<b>3. Cell lines culture</b>	<b>110</b>
3.1. Human Embryonic Kidney Cell Line (HEK 293T)	110
3.1.1. Maintenance	110
3.1.2. Freezing and thawing	111
3.2. Human fibroblast cell lines	111

3.2.1. Maintenance	113
3.2.2. Freezing and thawing	114
3.3. Human-induced Pluripotent Stem Cells (iPSC)	114
3.3.1. Cell culture media and solutions	115
3.3.2. MNs differentiation protocol	116
<b>4. shRNA interference by lentiviral transduction</b>	<b>117</b>
4.1. shRNA construct	118
4.2. Lentivirus production	119
4.3. Virus titration	122
4.4. Lentiviral transduction of primary cell cultures	123
<b>5. List of cell cultures drugs</b>	<b>124</b>
<b>6. Evaluation of neuronal viability in culture</b>	<b>125</b>
6.1. MNs survival	125
6.2. Neuronal degeneration	126
6.3. Apoptosis nucleus quantification	126
<b>7. Immunofluorescence technique</b>	<b>127</b>
7.1. Cell culture immunofluorescence	128
7.2. Tissue immunofluorescence	129
7.2.1. Tissue preparation and cryopreservation	129
7.2.2. Immunofluorescence protocol	129
7.3. List of antibodies	130
7.4. Quantification and analysis	131
7.4.1. Cell fluorescence measurements	131
7.4.2. Spots number quantification	132
<b>8. Protein analysis technique</b>	<b>133</b>
8.1. Protein extraction	133
8.1.1. Cell culture	133
8.1.2. Tissue	134
8.2. Protein concentration quantification	134
8.3. Electrophoresis in SDS-polyacrylamide gel	135
8.4. Protein transference to a PVDF membrane	136
8.5. Protein immunodetection	136
8.5.1. List of antibodies	137
<b>9. Reverse Transcriptase Quantitative PCR</b>	<b>138</b>

9.1. RNA purification	138
9.2. Reverse transcriptase PCR	139
9.3. Quantitative PCR	142
<b>10. Mouse in vivo treatment</b>	<b>143</b>
10.1. Physical parameters	143
10.2. Motor and behaviour test	144
10.2.1. Righting Reflex	145
10.2.2. Tube test	146
<b>11. Statistics</b>	<b>147</b>
<b>RESULTS</b>	<b>149</b>
<b>CHAPTER 1: Autophagy modulators regulate SMN protein stability in Motoneurons.</b>	<b>151</b>
1. Smn reduction causes an increase of neurite degeneration in cultured MNs	155
2. Increase of autophagy markers expression in SMA mice MNs	157
3. Differential autophagy alteration in cultured human fibroblast	161
4. Autophagy dysregulation in human SMA differentiated MNs	164
5. Effect of Calpain knockdown on autophagy markers and Smn in cultured spinal cord MNs	170
6. Calpain Knockdown prevents Smn reduction caused by membrane depolarization	176
7. Calpain shRNA increases Smn and prevents neurite degeneration in SMA mutant MNs	178
<b>CHAPTER 2: Calpeptin treatment regulates SMN and has protective effects in mouse models of Spinal Muscular Atrophy.</b>	<b>183</b>
1. Calpeptin treatment increases Smn protein level in cultured spinal cord MNs	187
2. High potassium treatment induces direct cleavage of Smn in culture MNs	189
3. Calpeptin treatment increases autophagy markers in mouse MNs	192
4. Calpeptin treatment increases Smn protein level in SMA mutant MNs	194
5. Calpeptin treatment in human SMN reduced cells	197
6. Effect of calpeptin and mTOR independent autophagy inducers treatment on CD1 MNs	199
7. Calpeptin administration extends survival in MutSMA and SMNDelta7 mice	201
8. Calpeptin treatment improves Motor function in SMA mice	204
<b>CHAPTER 3: Calpain pathway is altered in Spinal Muscular Atrophy models.</b>	<b>209</b>
1. Calpain activity is increased in mouse SMA MNs	213

2. Calpain activity is altered in SMA human SMA cells	216
3. Smn and calpain are modulated with calpeptin treatment in spinal cord of SMNDelta7 mouse model	219
4. Smn, calpain and calpastatin immunofluorescence in calpeptin-treated SMNDelta7 MNs	221
5. Calpastatin peptide as a treatment to inhibit calpain	226
<b>DISCUSSION</b> _____	<b>231</b>
<b>CONCLUSIONS</b> _____	<b>251</b>
<b>REFERENCES</b> _____	<b>255</b>
<b>PUBLICATIONS</b> _____	<b>293</b>



## **ABBREVIATIONS**

---



30K: 30 mM of KCl	CBS: Calcium-Binding Sites
3-MA: 3-methyladenine	CBSW: Calpain-type $\beta$ Sandwich Domain
50Resv: 50 nM of Resveratrol	ChAT: Choline Acetyltransferase
AAV: Adeno-Associated Virus	CMV: Cytomegalovirus
AD: Alzheimer disease	CNS: Central Nervous System
ALS: Amyotrophic Lateral Sclerosis	CT-1: Cardiotrophin-1
ANS: Autonomic Nervous System	CTCF: Corrected Total Cell Fluorescence
ASO: Antisense Oligonucleotide	CysPc: Cysteine Protease domain
Atg: Autophagy-related genes	DcpS: Decapping Scavenger enzyme
A $\beta$ : beta-amyloid plaques	DIV: Days <i>In Vitro</i>
BBB: Blood-Brain Barrier	DMSO: Dimethyl sulfoxide
BDNF: Brain-Derived Neurotrophic	DRG: Dorsal Root Ganglia
bFGF: basic Fibroblast Growth Factor	E12.5: Embryonic day 12.5
BMPs: Bone Morphogenetic Protein family	EMA: European Medicines Agency
BSA: Bovine Serum Albumin	ENS: Enteric Nervous System
<i>C. elegans</i> : Caenorhabditis elegans	ER: Endoplasmic Reticulum
C1–C7: Cervical spinal cord segments	ESS: Exonic Splicing Silencer
C2L: Calcium-binding motif	EV: Empty Vector
Ca <sup>2+</sup> : Calcium	FDA: Food and Drug Administration
Calpain-1 or $\mu$ -calpain: heterodimer formed by CAPN1 and CAPNS1	FF: Fast-twitch Fatigable
Calpain-2 or m-calpains: heterodimer formed by CAPN2 and CAPNS1	FFR: Fast-twitch Fatigable-Resistant
CAPN1: Calpain gene (from 1 to 16)	Fwd: Forward primer
CAPNS1: Smaller calpain regulatory subunit (1 and 2)	GADPH: Glyceraldehyde-3-Phosphate Dehydrogenase
CAST: Calpastatin gene	GDNF: Glial cell-Derived Neurotrophic Factor
CBs: Cajal Bodies	GFP: Green Fluorescent Protein



HD: Huntington diseases	mRNA: messenger RNA
HDACs: Histone deacetylases	mTOR: Mammalian Target of Rapamycin
HEK 293T: Human Embryonic Kidney Cell Line	mTORC1: mTOR complex 1
HGF: Hepatocyte growth factor	mTORC2: mTOR complex 2
HLS: Hind-limb score	MutSMA: <i>Smn<sup>-/-</sup></i> ; <i>SMN2<sup>+/+</sup></i> mouse model
HMC: Hypaxial Motor Column	NAIP: Neuronal Apoptosis Inhibitory Protein
hnRNPs: Heterogeneous nuclear ribonucleoproteins	NBM: Neurobasal medium
HRP: Horseradish Peroxidase	NMJ: Neuromuscular junction
HS: Horse serum	NTFs medium: NBM complete supplemented with NTFs
I3P: Inositol (1,4,5)P3	NTFs: Neurotrophic factors
IGF-1: Insulin-like Growth Factor 1	P/O: Poly-DL-ornitin
iPSC: induced Pluripotent Stem Cells	P5: Postnatal day 5 (from 0 to 15)
IQ: Calmodulin-interacting domain	p62: Sequestosome 1
KCl: Potassium chloride	PC1: Protease Core domain (1 and 2)
L1–L5: Lumbar spinal cord segments	PCD: Programmed Cell Death
LAMP-2A: Lysosomal-associated membrane protein 2A	PD: Parkinson disease
LC3: Microtubule-associated protein light chain 3	PE: Phosphatidylethanolamine
LIR: LC3-interacting region	PEF(L): Penta EF-hand domain in the large subunit
LMC: Lateral Motor Column	PEF(S): Penta EF-hand domain in the small subunit CAPNS1
miRNA: microRNA	PEI: Polyethyleneimine
MIT: Microtubule-Interacting and Transport domain	PFA: Paraformaldehyde
MMC: Median Motor Column	PGC: Preganglionic Column
MNs: Motoneurons	PI: Phosphatidylinositol
	PI3K: Phosphoinositide 3-kinases

PI3KC3: Class III PI3K	shCalp: shRNA specific for Calpain-1
PI3P: Phosphatidylinositol triphosphate	Shh: Sonic hedgehog morphogen
PLS3: Plastin 3	shRNA: Short hairpin RNA
PMC: Phrenic Motor Column	siRNA: small interfering RNA
PNS: Peripheral Nervous System	SK channel: calcium-activated K channel
PRL: Prolactin	SMA: Spinal Muscular Atrophy
PVDF: polyvinylidene difluoride	SMN: Human Survival Motor Neuron gene
RA: Retinoic Acid	SMN: Human Survival Motor Neuron protein
RBPs: mRNA-Binding Proteins	<i>Smn-1</i> : SMN gene in <i>C. elegans</i>
Rev: Reverse primer	<i>SMN1</i> : Telomeric gene for SMN
RISC: RNA-Induced Silencing Complex	<i>SMN2</i> : Centromeric gene for SMN
RNAi: RNA interference	SMN $\Delta$ 7: <i>Smn</i> <sup>-/-</sup> ; SMN2 <sup>+/+</sup> SMN $\Delta$ 7 <sup>+/+</sup> mouse model
RNP: Ribonucleoprotein complex	SMN $\Delta$ 7: SMN gene without exon 7
RR: Righting Reflex	snoRNAs: Small nucleolar RNAs
rRNA: Ribosomal RNA	snRNP: Small nuclear ribonucleoprotein
RT-qPCR: Reverse Transcriptase quantitative PCR	SNS: Somatic Nervous System
<i>S. cerevisiae</i> : <i>Saccharomyces cerevisiae</i>	SOH: SOL-Homology domain
<i>S. pombe</i> : <i>Schizosaccharomyces pombe</i>	T1-T12: Thoracic spinal cord segments
SAC: spinal accessory Column	TBST: Tris Buffered Saline with Tween 20
SC: Subcutaneous injection	TFM: Tissue Freezing Medium
SD: Standard Deviation	TT: Tube Test
SDS: Sodiumdodecylsulfate	TU: Transducing Units
SDS-PAGE: SDS polyacrylamide gel electrophoresis	Ub: Ubiquitin
SEM: Standard Error Mean	UBD: Ubiquitin-Binding Domain
SFR: Slow-twitch Fatigable-Resistant	UPS: Ubiquitin-Proteasome System

VPA: Valproic Acid

WNT: Wingless-type MMTV integration protein

WT: Wild Type

*ySMN*: SMN gene in *S. pombe*

Zn: Zinc-finger motif

## **INTRODUCTION**

---



## 1. The Human Nervous System

The human nervous system is the most intricate and organized structure of the body. Among other decisive functions, it is responsible for integrating, monitoring and conducting the stimuli captured from sensory receptors to the spinal cord and brain, and sending them back to other parts of the body by using a specific cell type, the neurons. As with the rest of the upper vertebrates, the human nervous system is subdivided into two main parts: the central nervous system (CNS) (formed by the brain and the spinal cord) and the peripheral nervous system (PNS) (composed of sensory neurons, ganglia and nerves that carry impulses to and from the CNS). At the same time, the PNS has two branches, subdivided according to the direction of nerve spread. Sensory or afferent neurons transmit nerve impulses from sensory organs to the CNS, while motor or efferent neurons transmit CNS impulses to the effector muscles through the somatic nervous system (SNS) or autonomic nervous system (ANS) glands (Nieuwenhuys et al., 2008).

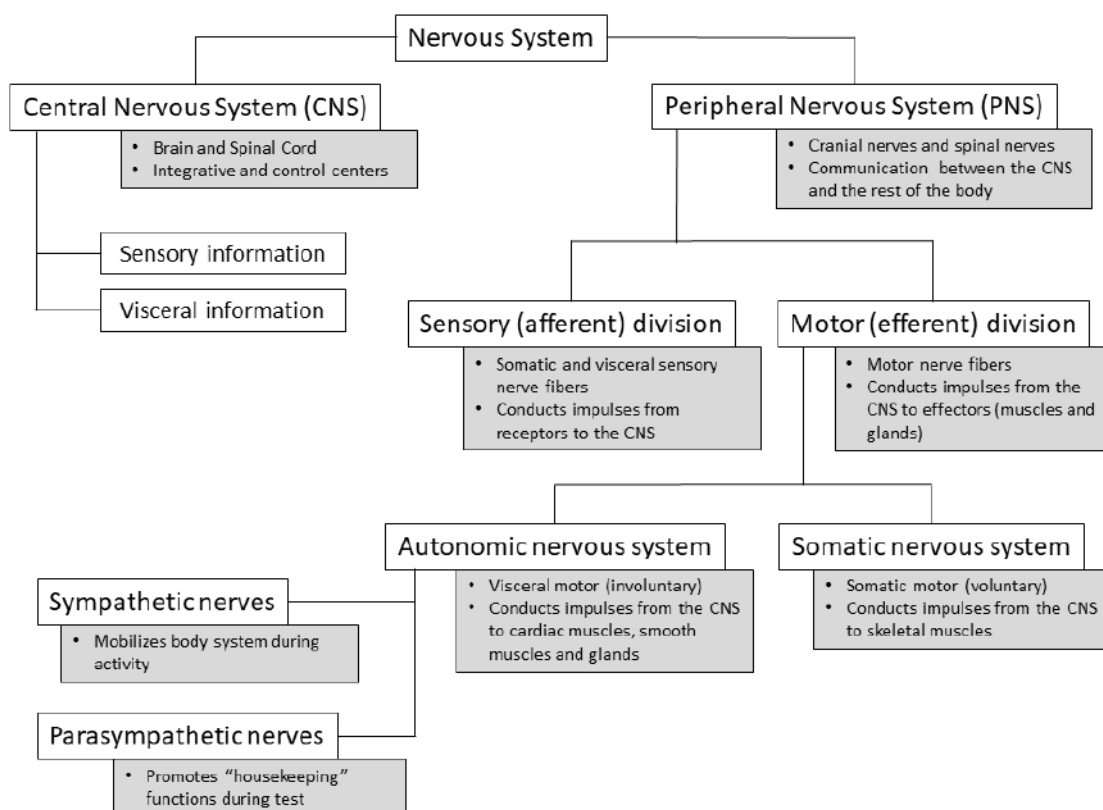


**Figure 1. Diagram showing the organization of the vertebrate nervous system.** The nervous system is a highly complex system that in vertebrates consist of two parts, the central nervous system (CNS) and the peripheral nervous system (PNS). The CNS englobed the brain and spinal cord while the PNS

consists mainly of nerves, that connect the CNS to every other part of the body. Nerves that transmit signals from the body to the CNS are called sensory or afferent while those nerves that transmit information from the brain are called motor or efferent. The PNS is divided into the somatic (mediate voluntary movement) and the autonomic (involuntary movement), further subdivided into the sympathetic (activated in cases of emergencies) and the parasympathetic nervous systems (activated in a relaxed state) (Based on Nieuwenhuys et al., 2008).

### 1.1. Motoneurons (MNs)

Motoneurons (MNs) are neuronal cells located within the CNS responsible for generating and transmitting the nerve impulses that produce muscle contraction. The networks that control the locomotion processes are known as motor circuits and pathological disturbances of these circuits are involved in many neurodegenerative diseases. MNs are exceptional cell types divided into two main populations depending on the location: upper and lower MNs. Despite sharing nomenclature, these two categories must be considered as distinct entities due to their differences.

	Upper MNs	Lower MNs
Location	Brain cortex	Brainstem and Spinal cord
Cell type	Betz cells	Multipolar
Neurotransmitter	Glutamate	Acetylcholine
Target	Within the CNS	Outside the CNS
Symptoms upon lesion	Spasticity	Paralysis

**Table 1. Characteristics of upper and lower MNs.** These neurons differ not only by their location but also by their cellular characteristics and their functions (Stifani, 2014).

#### 1.1.1. Upper MNs

Upper MNs soma are located in the pre-motor and primary motor regions of the cerebral cortex. These MNs are a type of giant pyramidal cells known as pyramidal cells of Betz or Betz cells located in the fifth layer of the grey matter. Those cells are the neurons responsible for planning and directing body movements by sending their axons downward and connecting with the lower MNs in the spinal cord. Since upper MNs are exclusively

confined to the CNS, the connections are essentially glutamatergic (Purves et al., 2001). Clinical symptoms of upper MN alterations include uncontrolled movement, reduced sensitivity to superficial reflex stimulation and spasticity (Ivanhoe and Reistetter, 2004; Stifani, 2014).

### 1.1.2. Lower MNs

In the present thesis, we have focused on the study of spinal cord MNs since those cells are affected in the Spinal Muscular Atrophy (SMA) disease. Lower MNs are located in the nuclei of the cranial nerves in the brainstem and the ventral horn of the spinal cord. These neurons project their axonal extensions outside the CNS to, directly (performing synapses with skeletal muscle) or indirectly (through the ganglia of the sympathetic system) innervate their effector targets to control muscle contraction. Lower MNs are cholinergic and receive inputs from upper MNs (complex circuits) or sensory neurons and interneurons (local circuits, such as reflex control) (de Lahunta and Glass, 2009). Since muscle control has no alternative route to convey the information, when lower MNs are lost or degenerated the clinical symptom developed is the paralysis (Purves et al., 2001).

According to the type of target they innervate, lower MNs are subclassified into three groups:

- **Branchial MNs.** These are basically MNs in the brainstem that together with sensory neurons form the cranial nuclei, the trigeminal (V), facial (VII), glossopharyngeal (IX), vagus (X) and accessory (XI), innervate the muscles of the face and neck (Chandrasekhar, 2004).
- **Visceral MNs.** These neurons belong to the ANS and are responsible for the control of smooth muscle and glands. Visceral MNs constitute an anatomical and functional exception of lower MNs since those neurons do not directly connect to the final effector. Instead, visceral MNs in the CNS connect with ganglionic neurons of the PNS, which in turn target the final effector. The ANS can be divided into two systems: the sympathetic and the parasympathetic (Purves et al., 2001).



- **Somatic MNs.** Cell soma of these neurons are located in the ventral horn of the spinal cord and control skeletal muscles. The remarkable characteristic of somatic MNs is their long axonal extension which constitutes an exceptional and unique anatomical feature. Each MN together with the muscle fibres it innervates form the structure known as **motor unit**. The innervation pattern of the skeletal muscle requires a high degree of coherent organization, achieved by MNs homogeneity. Each MN innervates muscle fibres from a single type. Depending on the muscle fibre type they innervate, somatic MNs can be divided into 3 groups: alpha, beta, and gamma (Kanning et al., 2010; Stifani, 2014).

**Alpha MNs ( $\alpha$ -MNs):** are the most abundant type and exclusively innervate extrafusal muscle fibres, the key to muscle contraction. Alpha MNs are characterized by a large soma and a well-characterized neuromuscular ending, known as neuromuscular junction (NMJ). They receive monosynaptic innervation directly from sensory neurons and play an important role in the spinal reflex circuitry. Alpha MNs are classified according to the contractile properties of the extrafusal fibre they innervate, their size, conductivity and neuronal excitability (Burke et al., 1973).

- **Slow-twitch fatigable-resistant (SFR).** SFR MNs are recruited first during muscle contraction. They establish their NMJ with slow contraction muscle fibres that respond to a lower stimulation threshold. They even have the capacity of maintaining a remaining activity even after the stimulation ceased (Lee and Heckman, 1998). As a consequence, SFR MNs are responsible for the maintenance of body posture, which does not require excessive contraction force but prolonged. SFR MNs tend to have a smaller soma and reduced axons with a conduction velocity of 85 m/s (Burke et al., 1973).
- **Fast-twitch fatigable (FF).** FF MNs innervate fibres of rapid contraction and have the largest soma with a remarkable dendritic arborisation and lots of presynaptic terminals (Cullheim et al., 1987). They are important for movements that require short impulses but with a strong contraction. Usually, FF MNs firing after the initial recruitment of SFR MNs giving extra strength to the activated muscle. The conduction velocity is 100 m/s (Burke et al., 1973).

- **Fast-twitch fatigable-resistant (FFR).** Little is known about FFR MNs physiology but it is considered that they have intermediate characteristics between FF and SFR MNs.

**Beta MNs ( $\beta$ -MNs):** Beta MNs are poorly characterized, anatomically  $\beta$ -MNs are smaller and less abundant than other somatic MNs subtypes. They innervate both intrafusal and extrafusal muscle fibres (Bessou et al., 1965) and control both muscle contraction and receptiveness of the sensory feedback from muscle spindles. Further molecular and electrical properties remain to be identified. Beta MNs are further subdivided into 2 types: static, innervating extrafusal fibres and increasing the firing rate, and dynamic, that innervate intrafusal fibres and increase the stretch-sensitivity.

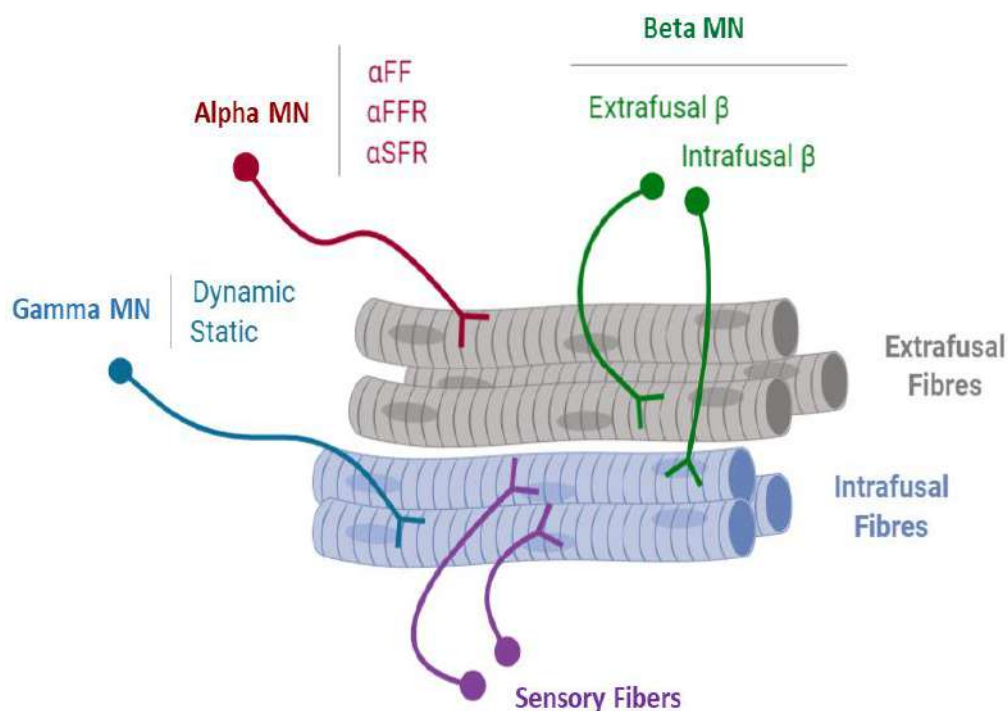


**Figure 2. Classification of the Somatic MNs according to the type of muscle they innervate.** Schematic illustration of muscle fibres innervated by the different types of MNs. Alpha MN (red) innervates extrafusal muscle fibres (grey), gamma MN (blue) connects to intrafusal fibres (light blue) within the muscle spindle whereas beta MNs (green) can innervate both types. Sensory neurons (purple) carry information from the intrafusal fibres to the CNS. Usually, a single MN innervate multiple fibres all of the same type; however, for the schematic simplicity, only one fibre is represented (Based on Stifani, 2014).

**Gamma MNs ( $\gamma$ -MNs):** Gamma MNs innervate exclusively the sensitivity of muscle spindles and regulate complex functions in motor control. Gamma MNs are characterized by slow axonal conduction, due to the smaller axon diameter and lower degree of arborisation. They receive innervation of proprioceptive sensory neurons only indirectly, therefore  $\gamma$ -MNs do not participate directly in spinal reflexes (Eccles et al., 1960). They also do not have any motor function but contribute to the modulation of muscle contraction through direct stimulation of intrafusal muscle fibres by increasing the tension of the fibres and therefore mimicking the stretch of the muscle. There are 2 types of  $\gamma$ -MNs: dynamic, enhancing dynamic sensitivity and static, that enhance stretch sensitivity.

## 1.2. Generation of MNs

During the early stage of embryogenesis, the ectoderm undergoes a process called neurulation in which it folds inward and leads to the formation of three ectodermal masses: the cells of the neural crest, which will form most of the PNS and several non-neural cell types; the external ectoderm, which will generate the epidermis; and the neural tube, which will originate the CNS (Purves et al., 2003).

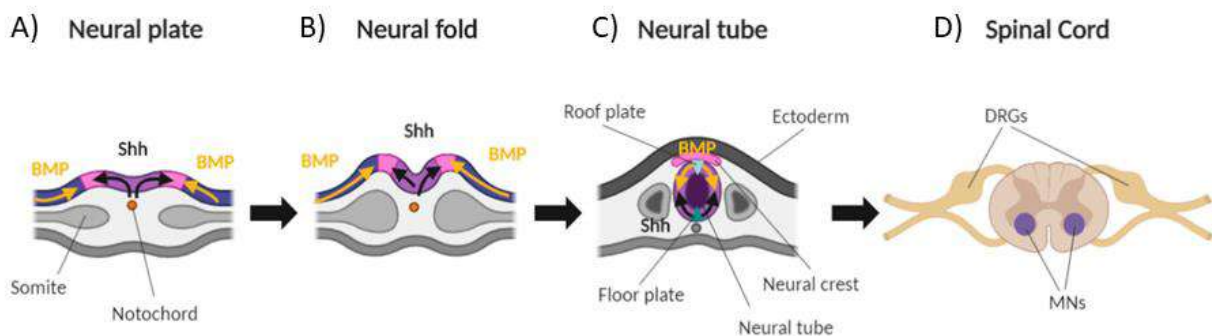


**Figure 3. Spinal cord developmental.** **A)** Initially, the neural plate is formed from the cells of the neuroectoderm, **B)** which folds to form the neural tube. **C)** The dorso-ventral polarization of the neural tube, mainly determined by the signalling of Shh and BMP is produced by the roof Plate and the floor Plate. **D)** Finally, MNs localize in the ventral area of the spinal cord (Based on Purves et al., 2003).

Initially, in the neural tube, the rostro-caudal and dorso-ventral axes are specified through gradients of signalling molecules along each axis, which provide a roadmap to guide the differentiation of the neuronal types in each region (Jessell, 2000).

Along the rostro-caudal axis, the neural tube is specified in the main components of the CNS, including the brain, midbrain, hindbrain and spinal cord. The main signalling of the caudalization process is produced by the effect of the paraxial mesoderm surrounding the neural tube. This expresses the aldehyde dehydrogenase 1 A2 (ALDH1A2 or RALDH2) (Niederreither et al., 1997), which converts retinaldehyde into retinoic acid (RA) (Pierani et al., 1999). The RA is crucial for the initial differentiation of neurons from the hindbrain and spinal cord from those in the forebrain and midbrain (Maden, 2007).

On the other hand, the dorso-ventral axis develops as a result of members of the wingless-type MMTV integration site family (WNT) (Sokol, 1999) and the bone morphogenetic protein family (BMPs) (Mehler et al., 1997) and their regulators Noggin (NOG), Chordin (CHRD), and Follistatin (FST) (Streit et al., 1998; Zimmerman et al., 1996) that are secreted by the roof-plate in a decreasing dorsal to ventral gradient. These signals are complemented by the increasing dorso-ventral gradient of sonic hedgehog morphogen (Shh) secreted by the notochord (formation from the mesoderm) as well as the floor-plate (Yamada et al., 1991). Molecularly, Shh binds to the patched homolog 1 receptor (PTCH1) (Stone et al., 1996) and initiates a transcriptional cascade that will end with the induction or suppression of different transcription factors in a gradient-dependent manner (Briscoe et al., 2000).

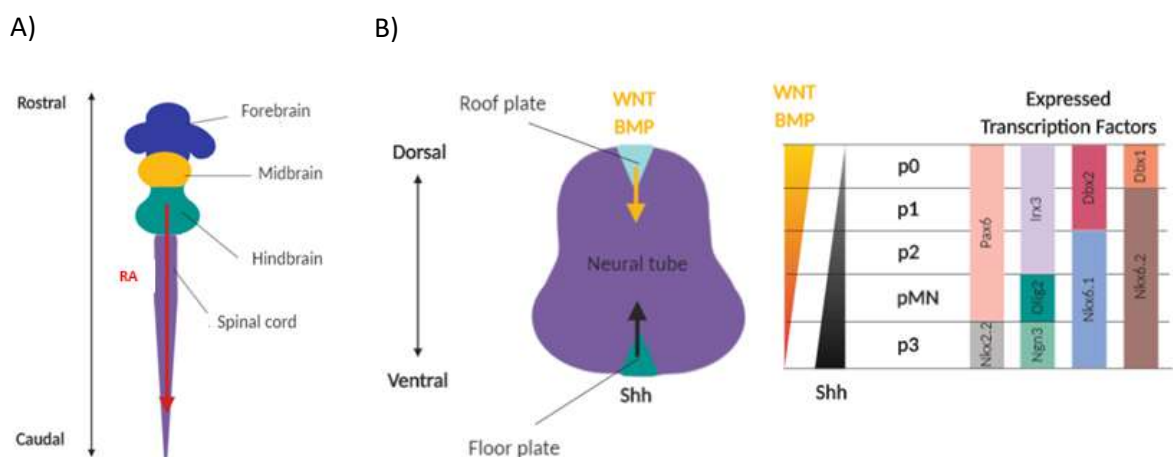


**Figure 4. Spinal cord differentiation axis and MNs specification. A)** RA signalling primarily determines the rostro-caudal axis and the differentiation of the hindbrain and spinal cord during development. **B)** Dorso-ventral polarization of the neural tube by BMPs, WNT (roof-plate) and Shh (floor-plate). This signalling creates a gradient that determines the differentiation and localization of the different subtypes of neurons in the neural tube. Mature MNs derived from the pMN domain (Based on Purves et al., 2003).

Eventually, these gradients lead to the appearance of 5 ventral progenitor domains (p0, p1, p2, pMN and p3), each defined by the expression of a unique combination of transcription factors that will end into the generation of a specific neuronal subtype, including MNs (reviewed in Lu et al., 2015).

Spinal cord MNs derive exclusively from the progenitor domain of pMN which by the effect of Shh downstream signalling activates the homeodomain proteins Nkx6.1, Olig2 and Nkx2.2 while repressing the expression of Pax6, Irx3, Dbx1 and Dbx2 (Briscoe et al., 2000; Jessell, 2000). In the MNs progenitors the expression of Nkx6.1 acts by repressing the other progenitor domains, while the presence of Olig2 promotes the expression of Ngn2, which is important for the exit of the cell cycle, as well as for the induction of typical transcription factors of mature MN such as Hb9 (Mnx1), Isl1, Isl2 and Lhx3 (Jessell, 2000). Ultimately, to become mature MNs, progenitors must leave the cell cycle and enter the process of differentiation in a series of strictly regulated events during neurogenesis.

### 1.3. Columnar organization of spinal cord MNs

The MNs subtypes are distributed along the spinal cord in an organized system to perform their functions on a daily basis. These distinctive anatomical structures, resembling columns, extend along the rostro-caudal axis, called **motor column** and appeared during the development of the MNs due to the Hox transcription factor family (Dasen and Jessell, 2009). Each column possesses a specific gene expression profile as well as a uniform axonal projection pattern.

Traditionally, four main columns have been described, the median motor column (MMC), the lateral motor column (LMC), the hypaxial motor column (HMC), and the preganglionic column (PGC), but in the last years, two less well-characterized motor columns have included, the spinal accessory column (SAC) and the phrenic motor column (PMC) (reviewed in Stifani, 2014).

- **The medial motor column (MMC).** MMC MNs are found along the entire rostro-caudal axis of the spinal cord in the medial region of the ventral spinal cord. MMC MNs project their axons towards the axial musculature (intercostal and body wall muscles) mainly involved in the maintenance of the body posture. These MNs are characterized by the co-expression of MNX1, ISL1/2, and LHX3.

- **The lateral motor column (LMC).** LMC MNs are located in the most lateral portion of the ventral spinal cord at the brachial (C5 to T1) and lumbar (L1–L5) level. These MNs innervate ventral and dorsal muscles of the extremities and therefore are characterized by the expression of ISL2, FOXP1, and ALDH1A2.
- **The hypaxial motor column (HMC).** HMC MNs target the body wall musculature composed of the intercostal and abdominal muscles essentially involved in breathing. HMC MNs are only present at thoracic segments, specifically, in the ventro-lateral area of the spinal cord. Molecularly, HMC MNs are determined by the expression of MNX1, ISL1, ETV1 and low levels of ISL2.
- **The preganglionic column (PGC).** PGC MNs do not innervate skeletal muscles but instead project their axons towards the sympathetic ganglia neurons. These MNs are involved in the stimulation of smooth muscles as well as in the control of glandular secretions. PGC MNs are located at the thoracic and upper lumbar spinal segments (T1–L2) but can also be found in the sacral segments (S2–S4). PGC MNs can be defined by the SMAD1 expression.
- **The spinal accessory column (SAC).** SAC MNs are a very peculiar population with transitional characteristics between the hindbrain and cervical MNs. SAC segment expands through the cervical segment (C1–C5) and the MNs are positioned in the intermedia-lateral region. SAC MNs innervate mastoid muscles and four muscles of the neck (Sternomastoid, Cleidotrapezius, Cleidomastoid, and Acromiotrapezius). SAC MNs are distinguished from other MNs by the expression of ALCAM, ISL1, RUNX1 and PHOX2B.
- **The phrenic motor column (PMC).** Little is known about PMC MNs. They are found in the cervical segments C3–C5 and innervate specifically a particular muscle: the diaphragm. This muscle is essential for breathing, both conscious and unconscious, and therefore is under constant rhythmic activity. Because of its unique function, PMC MNs are required to produce a continuous rhythmic firing just after birth and throughout life. In terms of molecular characteristics, PMC MNs are under the control of HOX5 patterning and express POU3F1, ISL1/2, and MNX1.

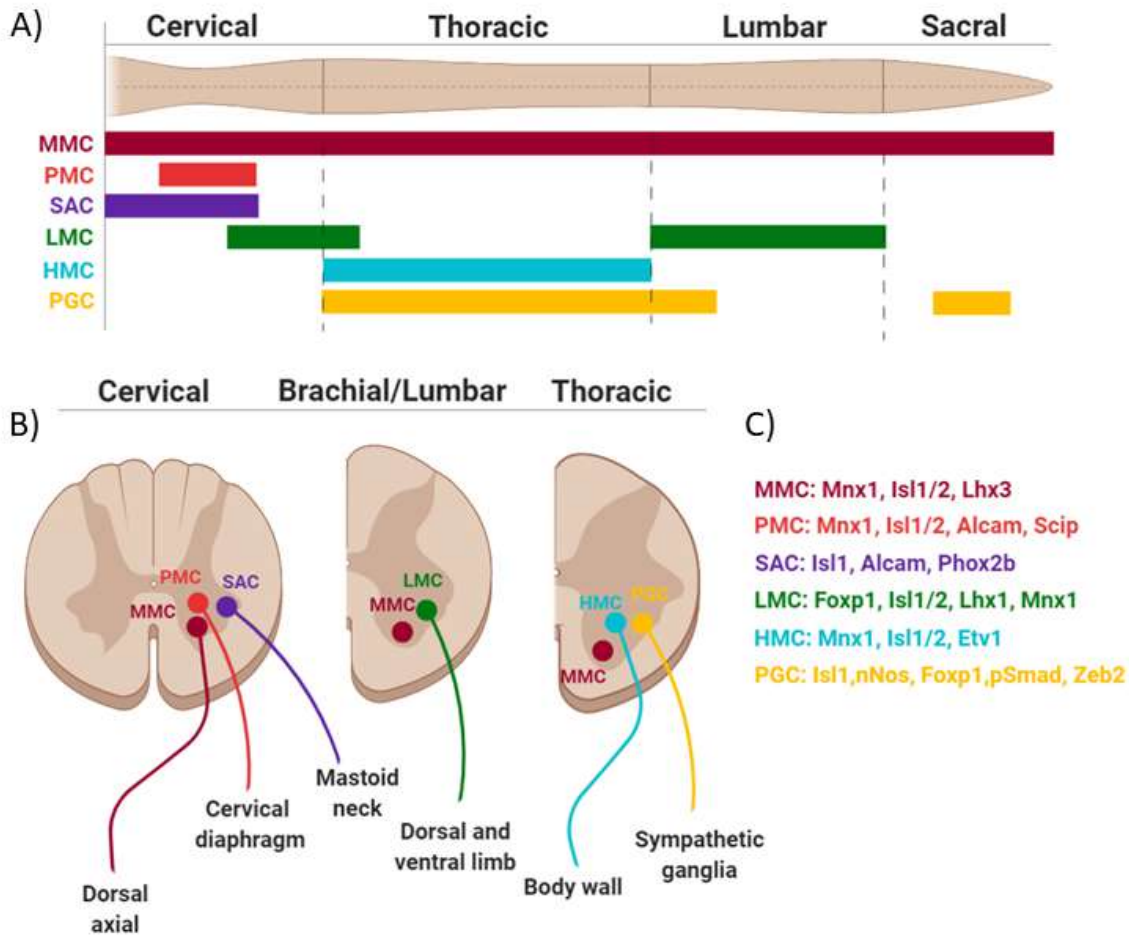


**Figure 5. Segmental organization of motor columns on the spinal cord and innervation target. A)** Scheme summarizing the segmental distribution of spinal motor columns: MMC present all along the rostro-caudal axis, PMC confined between C3 and C5, SAC restricted to C1 – C5, LMC located at limb levels: brachial (C5-T1) and lumbar segments (L1 – L5), HMC exclusive of the thoracic segment and PGC that extends through the thoracic segments until the second lumbar segments (L2) and the sacral segments 2 and 4 (S2 – S4). **B)** Schematic summarizing of a transversal section of the spinal cord at cervical, brachial/lumbar and thoracic levels with the axonal projections of the MNs of each motor column and their innervation target. **C)** Specific molecular markers of MNs from each of the motor column (Based on Stifani, 2014).

Within the motor column, the SAC segments are the only representative of the branchial MNs category whereas the PGC are formed by visceral MNs. The rest of the columns, MMC, HMC, PMC, and LMC are constituted by somatic MNs. The set of MNs that project their axons to the same skeletal muscle is called **pool**. MN pools respect a topographic organization share morphological and molecular properties and allow muscle coordination to perform complex movements. A typical MNs pool usually has one-third of  $\gamma$ -MNs and a variable ratio of all  $\alpha$ -MNs subtypes, SFR, FF and FFR. Thus, each pool has a characteristic

ratio of MNs types depending on the motor unit that they innervate to adapt to its function (reviewed by Kania, 2014).

The study and characterization of the different subpopulations of MNs are crucial, especially in the study of neurodegenerative diseases, because each subpopulation has different degrees of vulnerability. This is the case of the Spinal Muscular Atrophy (SMA) disease where motor units with rapid contractile properties, the  $\alpha$ -MNs FF, are more vulnerable and degenerate faster than others that are more resistant to degeneration processes (such as motor units that participate in eye movement or sphincter contraction) (reviewed in Kanning et al., 2010)).

## 2. Spinal muscular atrophy

Spinal muscular atrophy (SMA) is a term that includes a group of autosomal recessive disorders primarily characterized by the progressive degeneration of the  $\alpha$ -MNs (hereinafter referred to as MNs) located in the anterior horn of the spinal cord. The neurodegenerative process occurring in these cells causes the main symptoms of SMA, proximal muscle wasting and paralysis, but also other common complications described, such as pulmonary problems, spine deformities, swallowing difficulties and gastrointestinal dysfunction. Regardless of the symptoms, cognition in these infants is not affected (Kolb and Kissel, 2015).

The disease was first described by Guido Werdnig and Johann Hoffman in early 1890, as a disorder of progressive muscular weakness of onset in infancy that resulted in premature death, though the age of death was variable (Kolb and Kissel, 2015). One hundred years later the disease was associated with a specific genetic locus, thanks to the work of Dr Judith Melki, a neuropediatric and researcher at the Institute of Health and Medical Research (INSERM) of France (Melki et al., 1990). Specifically, SMA has been related to two genes located in the long arm of the chromosome 5 (5q13.1): the *Survival Motor Neuron (SMN)* (Lefebvre et al., 1995) gene that acts as a disease-determining gene, and the *Neuronal Apoptosis Inhibitory Protein (NAIP)* gene that probably acts as a phenotype modifier (Roy et al., 1995).



Owing to an intrachromosomal duplication event, humans possess two copies of the *SMN* gene: the *SMN1* gene and the *SMN2* gene (Lefebvre et al., 1995). The most common cause of SMA, around 95% of cases, is the homozygous deletion or mutation of *SMN1* gene in patients, while the *SMN2* gene is retained at a variable number of copies. Without *SMN1* gene, *SMN2* provides sufficient residual full-length protein for cellular viability, but it is not enough to maintain MNs survival (Lefebvre et al., 1997; Wirth, 2000). Consequently, SMA is a disease produced by low levels of protein and not by total ablation.

SMA has an incidence of about 1/6000–10,000 live births, out of which about 60% develop the most severe form of the disease, what makes SMA the most common fatal neuromuscular disease in infants and constitute one of the most frequent autosomal recessive disorders, right after cystic fibrosis (Pearn, 1978). Nowadays the carrier frequency, one in 54 for the world population and one in 35 in the European population, meaning that in Spain there are approximately 1,000,000 carriers of the disease and about 1,500 families that have or have had affected relatives (Verhaart et al., 2017).

### **2.1. SMA clinical classification**

SMA is highly variable and there is a wide spectrum of clinical severity, because of that the disease is classified into four types (Type 1-4) based on the age of onset and the maximum motor function achieved. Some authors incorporate an extra SMA subtype, the Type 0 or embryonic. The disease diagnosis and classification are usually first made by clinical parameters, muscle atrophy, tremor, weakness, loss of reflexes, abnormal tongue movements (fasciculation) and denervation on EMG; and then confirmed by genetic test (Kolb and Kissel, 2015; Russman, 2007).

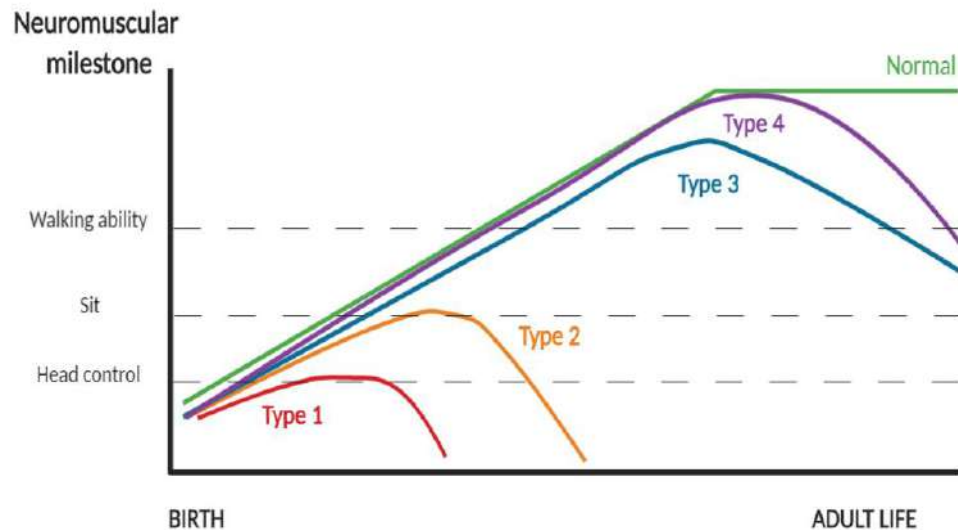


**Figure 6. Neuromuscular milestones and trajectories from birth to adult life in SMA types.** SMA type 1 (red) has an acute phase with rapid decline, where patients only achieve poor head control. Type 2 (orange) patients, without intervention, are able to sit but never achieve independent walking. SMA type 3 (blue) and 4 (purple) have a late-onset with a more stable deterioration that allows them to maintain the walking ability for years. Type 0 trajectories are not represented. Normal neuromuscular development is shown as a green line (Serra-Juhe and Tizzano, 2019).

### 2.1.1. SMA type 0 or prenatal

SMA type 0 describes a disease with a prenatal onset. Neonates who have type 0, suffer a severe weakness and hypotonia and a history of decreased fetal movements. Tongue fasciculations and respiratory distress make a requirement of respiratory assistance within hours of life. Patients also suffer from autonomic dysfunction, and in some cases, congenital heart defects (septal defects). Life-expectancy is reduced and most are unable to survive beyond 6 months of age (Dubowitz, 1999; Macleod et al., 1999).

### 2.1.2. SMA type 1 or infantile

SMA type 1, also known as Werdnig-Hoffmann disease, is the most common and severe form of SMA. SMA Type 1 becomes evident rapidly after birth within the first 6 months of life. By definition, patients never achieve the ability to sit unassisted due to general hypotonia, poor head control and reduced or absent tendon reflexes (usually manifested as “frog-leg” posture). Affected infants can also show swallowing weakness and fasciculations. The hypotonia will progressively affect the intercostal muscles, sparing of

the diaphragm and producing breathing problems, which generally result fatally before the to 2 years of life. The prognosis varies depending on the severity, treatments are typically nutritional and respiratory support which help to prolong life expectancy (Finkel et al., 2014; Thomas and Dubowitz, 1994).

### **2.1.3. SMA type 2 or intermediate**

SMA type 2 symptoms appear typically between 6 to 18 months of age and describe children able to sit unassisted, but that never achieve independent walking. Intermediate SMA is characterized by proximal weakness that is more severe in legs earlier than in arms, and lack of reflexes. Many comorbidities have been described due to muscular weakness, such as complications of bone and articulation development and progressive scoliosis. The combination of intercostal muscle weakness, thorax deformities and scoliosis results in significant respiratory insufficiency disease that may require supportive care. Life expectancy is reduced, but survival and progression depend on different factors especially supportive care that can help patients survive to adolescence and in some cases into adulthood (Mercuri et al., 2016).

### **2.1.4. SMA type 3 or juvenile**

SMA type 3 is also referred as Kugelberg-Welander disease. This form of SMA has been subdivided depending on disease onset: type 3a includes patients with earlier onset, between 18 months and 3 years old while type 3b embraces those with a later onset, between ages 3 and 21 years old. Individuals with SMA type 3 are able to walk unassisted but show difficulties at running, climbing steps, or rising from a chair. Eventually, at some point in their lifetime, progressive proximal weakness of the legs makes patients end up needing a wheelchair. As happens in SMA type 2, comorbidities such as scoliosis and respiratory muscle weakness are common. With appropriate treatment, life expectancy is not altered in this group (Mercuri et al., 2016; Zerres et al., 1997).

### **2.1.5. SMA type 4 or adult**

The adult-onset form is the mildest form of SMA and also the rarest because it only represents less than 5% of SMA cases. It mainly occurs in men. The disease begins after the age of 21, usually after the third decade of life. It is manifested as a gradual proximal

weakness of the extremities but other complications (swallowing and respiratory dysfunction) are rare. Life expectancy is unaffected but it is frequent that the person requires to use a wheelchair to move (Piepers et al., 2008).

SMA Type	Age of onset	Diagnostic features	Age at death	Proportion of total SMA (%)
Type 0	Prenatal	Reduced movement in utero. Respirator required at birth	< 6 months	-
Type 1	< 6 months	Poor muscle tone and lack of movement. Never able to sit.	< 2 years	60
Type 2	< 18 months	Cannot sit or walk unaided	2 - 10 years	27
Type 3	>18 months	May lose the ability to walk in their adulthood	Normal life expectancy	12
Type 4	Adult-hood (> 21 years)	Mild proximal muscle weakness	Normal life expectancy	1

**Table 2. Classification and clinical features of human SMA types.** SMA is classified into 5 types (Type 0-4) based in the age of onset, maximum motor function achieved and clinical severity.

## 2.2. Molecular and genetic basis of the disease

As mentioned, SMA is an autosomal recessive neuromuscular disorder. In order to identify the cause of the disease, in 1990 genetic analyses were carried out in patients with SMA type 1, 2 and 3. These studies allowed to locate the region q11.2-13.3 of chromosome 5 that contained the gene responsible for the disease (Melki et al., 1990).

This locus is a complex area that contains an inverted chromosomal duplication of more than 500 kb with multiple repeated sequences, a characteristic that makes it predisposed to deletions (Melki et al., 1994). It is in this area where the *survival motor neuron (SMN)* gene is found (Lefebvre et al., 1995). In humans, and due to the genomic duplication of the area, there are two copies of the *SMN* gene: the telomeric form (*SMN1*) and the centromeric form (*SMN2*). Subsequent studies made it possible to determine specifically that the genetic lesion causing SMA in 95% of patients is the homozygous deletion of the *SMN1* gene. (Lefebvre et al., 1997).



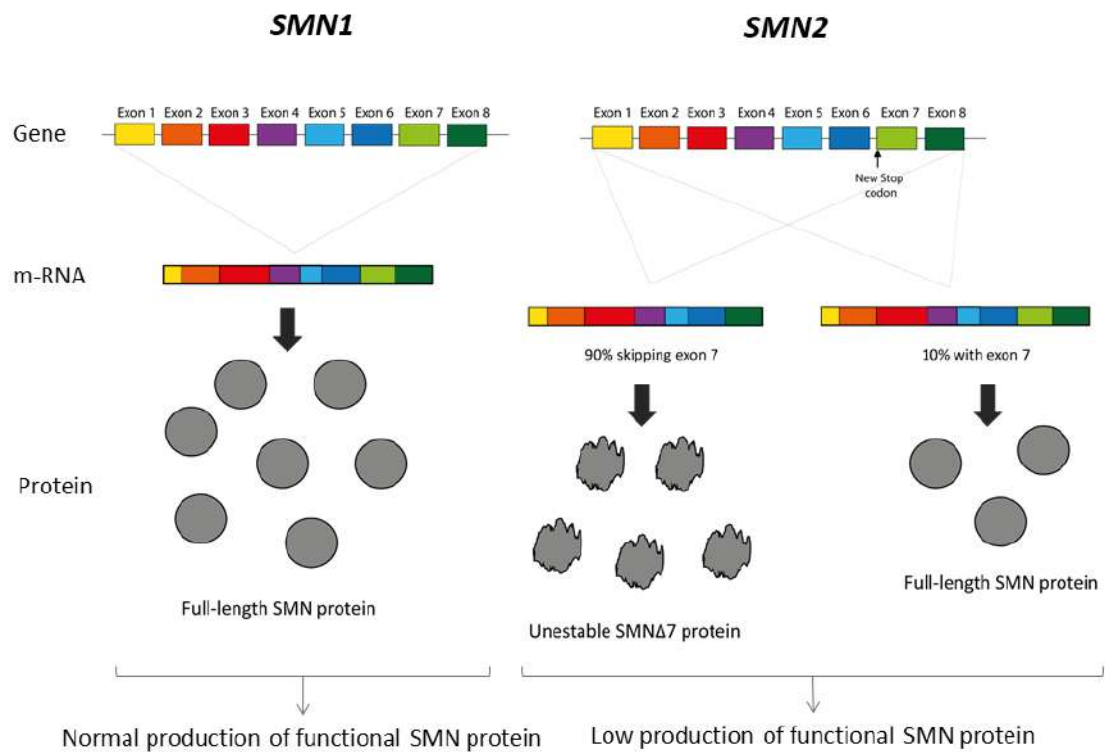


**Figure 8. Transcription of the *SMN1* and *SMN2* genes.** In the *SMN1* gene, all the transcripts encode for the complete SMN protein (full-length SMN) producing the majority of the protein in the cells (normal levels). In contrast, in the *SMN2* gene, 90% of the transcripts encodes for a truncated protein (without exon 7) that degrades rapidly. Only 10% of mRNAs contain exon 7 which results in low levels of SMN protein that are insufficient to prevent the degeneration of MNs in SMA disease (Based on Kolb et al., 2015).

Under normal conditions, SMN protein is produced at normal levels, by the *SMN1* gene but a small amount is produced by *SMN2*. However, in SMA patients, when both alleles of the *SMN1* gene are lost, SMN protein production derives from the *SMN2* gene, which cannot compensate *SMN1* loss and results in reduced levels of SMN in the cells.

### 2.2.2. Genotype-phenotype correlation

But how the defect in a single gene can produce such a wide range of clinical severity? The riddle's solution lies in the genetic duplication of *SMN1*, the *SMN2* gene.

*SMN2* occurred by an evolutionary event about 5 million years ago, just before the separation of human and chimpanzee lineages. While chimpanzees have two identical *SMN* copies, in humans the duplication created *SMN2*, generating the gene and the SMA disease-

specific of humans. Even more, during gene duplication, *SMN1* gene remained in a single copy *per* chromosome, but the number of *SMN2* copies in the genome could vary between 0 and 8.

In 1995 when the group of Lefebvre and collaborators began studying the genomic DNA of SMA patients using agarose electrophoresis, they observed that *SMN2* gene band appeared more intense in type 3 SMA than in type 1 SMA patients. Subsequent genotype/phenotype studies confirmed that, among the SMA types, exists a correlation between the number of *SMN2* gene copies and the severity of the disease (Lefebvre et al., 1995; Mailman et al., 2002). As the number of *SMN2* copies increases, more quantity of stable full-length SMN protein is produced and less severe the disease is. Patients with the severe form of SMA, type 1, usually have one or two copies of *SMN2*, while type 2 and type 3 SMA patients mostly have 3 and 4 *SMN2* copies respectively.

SMA Type	SMN2 copies	Levels of SMN produced (%)
Type 0	1	5
Type 1	1-2	10
Type 2	2-3	15
Type 3	3-4	20
Type 4	>4	25

**Table 3. Number of copies and amount of produced SMN in SMA types.** *The number of copies of the SMN2 gene determines the amount of produced SMN protein and therefore correlates with the severity of the SMA (Based on Mailman et al., 2002).*

However, even though *SMN2* copy number is the main determinant of the disease, it cannot solely explain the variation of clinical severity observed in SMA phenotype. This is the case of discordant patients, where SMA patients with the same number of *SMN2* copies have different symptoms suggesting the existence of other phenotypic modifying factors (Calucho et al., 2018).

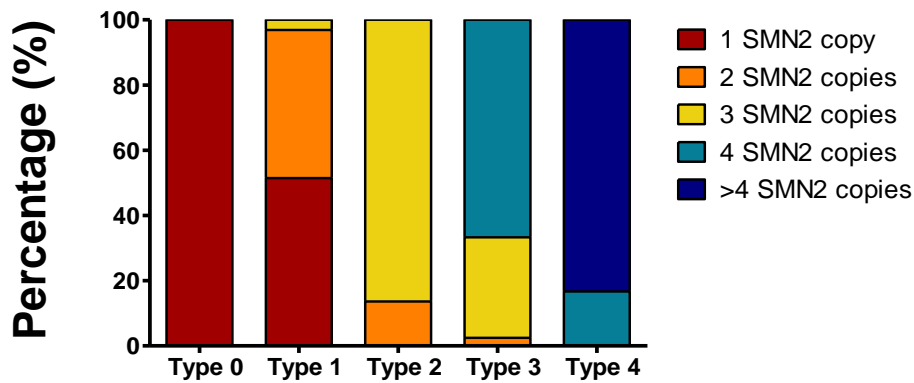


**Figure 9. Percentage of patients' number of copies for each SMA type.** In 1995 it was discovered the genotype/phenotype correlation between the number of copies of the SMN2 gene and the severity of the SMA (Based on Mailman et al., 2002).

### 2.3. SMN protein

SMN is a ubiquitous protein constitutively expressed in all cell types. The isoform of SMN resulting from the full-length transcript is a 294 amino acid protein with a molecular weight about 38 kDa in Western blot analysis (Coover et al., 1997; Lefebvre et al., 1997). SMN has been implicated in a range of cellular processes (Singh et al., 2017). In the nucleus, SMN localizes inside the Cajal bodies (CBs) in dot-like structures called 'gems' (Liu and Dreyfuss, 1996; Young et al., 2000). In this location, SMN performs an important role in assembling small nuclear ribonucleoprotein (snRNP) particles (Fischer et al., 1997), and also gathering of small nucleolar RNAs (snoRNAs) and pre-mRNA splicing sites (Pellizzoni et al., 1998). On the other hand, SMN has a granular pattern distribution in the cytoplasm, neuronal growth cones and neuronal extensions (Fallini et al., 2010) and participates in actin cytoskeleton dynamics, mRNA transport, bioenergetics pathways, ubiquitin (Ub) homeostasis and synaptic vesicle release (Singh et al., 2017). Therefore, SMN is a multifunctional protein that can bind to several proteins and participate in different physiological processes, but it is still unclear what is the critical function disrupted by low levels of SMN.

Structurally, the SMN protein contains several functional motifs. From N-terminus to C-terminus:

- The basic/lysine-rich domain, mainly encoded by exon 2, is responsible for the interaction between SMN and RNA in the Gems structures (Lorson et al., 1998).



- Tudor domain is a highly conserved motif that mediates de interaction of SMN with other proteins through the binding of the arginine glycine motifs and facilitating the assembly of spliceosomes. It also promotes the nuclear localization of SMN (Selenko et al., 2001).
- The proline-rich domain is encoded by exons 4, 5 and 6 and responsible for the binding of profilins, the key proteins in regulating actin dynamics (Gieseemann et al., 1999).
- YG box or tyrosine/glycine-rich region participates in SMN self-oligomerisation by the formation of stable glycine-zipper structure, indicating that YG box plays a role in SMN stability (Lorson et al., 1998). It has been demonstrated that this domain is important for post-transcriptionally modifications that determine SMN location and, consequently, its function. The two main modifications that have been described are acetylation which promotes the cytoplasmic localisation and increases its half-life (Lafarga et al., 2018), and phosphorylation that promotes SMN localisation to CBs (Husedzinovic et al., 2014).

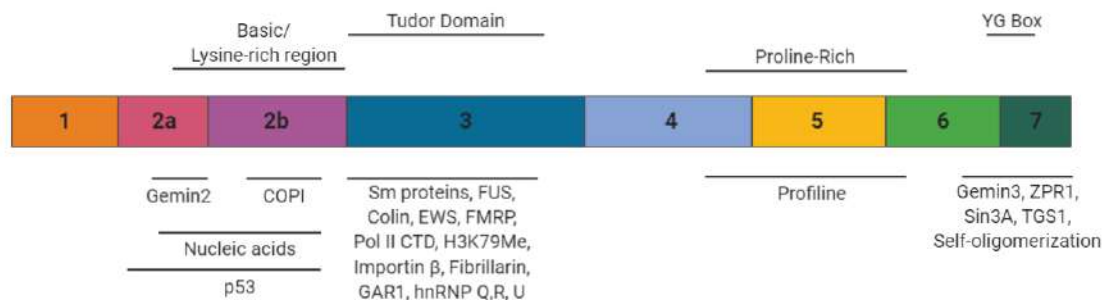


**Figure 10. Structure of SMN protein.** Schematic representation of the SMN protein codified by the exons 1-7. SMN domains are indicated above and proteins that interact with SMN are shown below (Based on Singh et al., 2017).

### 2.3.1. SMN functions

Over the years, it has been demonstrated that SMN is able to interact with a large number of proteins, which means that SMN may be involved in several cellular processes (Singh et al., 2017). Currently, to consider that SMN is interacting with a protein forming a functional

complex, four criteria methods have been developed. Those criteria are: a reciprocal immunoprecipitation of the endogenous forms; possibility to isolate the complex containing SMN and the interacting protein from cells or tissues samples; co-localization of both proteins by immunofluorescence analysis; and the complex containing SMN and the protein in question should show a functional deficit under SMN reduction condition. The first and only identified complex that achieved the four criteria has been the one that involves SMN in the snRNP assembly (Burghes and Beattie, 2009)

### **Modulation of the ribonucleoprotein assembly**

The role of SMN in snRNP assembly is considered the canonical function of SMN and even though it is the most studied and well characterized, there are several unresolved issues that need further investigation. The snRNP are RNA-protein complexes essential for the formation of the spliceosome, which is required to remove introns from unmodified pre-mRNA. snRNPs are composed of a U snRNA (U1, U2, U4, U5, U11 or U12) bound to a set of seven Sm proteins (Matera and Wang, 2014). Sm proteins can spontaneously associate with snRNA *in vitro*, although this process completely lacks specificity (Raker et al., 1999). *In vivo*, to generate active snRNP particles, a heptameric ring of Sm proteins is precisely assembled to the U snRNP through the mediation of the SMN complex (Pellizzoni et al., 2002). In the cytoplasm, SMN monomers self-associate to form SMN oligomers that subsequently will form a macro complex together with the proteins, Gemin2, also called survival of motor neuron protein-interacting protein 1 (SIP1), Gemin 3–8 and UNR interacting protein (UNRIP), and ATP because the assembly reaction is ATP dependent (Fischer et al., 1997; Pellizzoni, 2007; Raker et al., 1999). The interaction between SMN complex with the snRNPs is produced in the cytoplasm and translocated to the nuclear bodies termed “Gems”. Interestingly, MNs from Type 1 SMA patients showed a reduced number of Gems (Lorson et al., 1998).

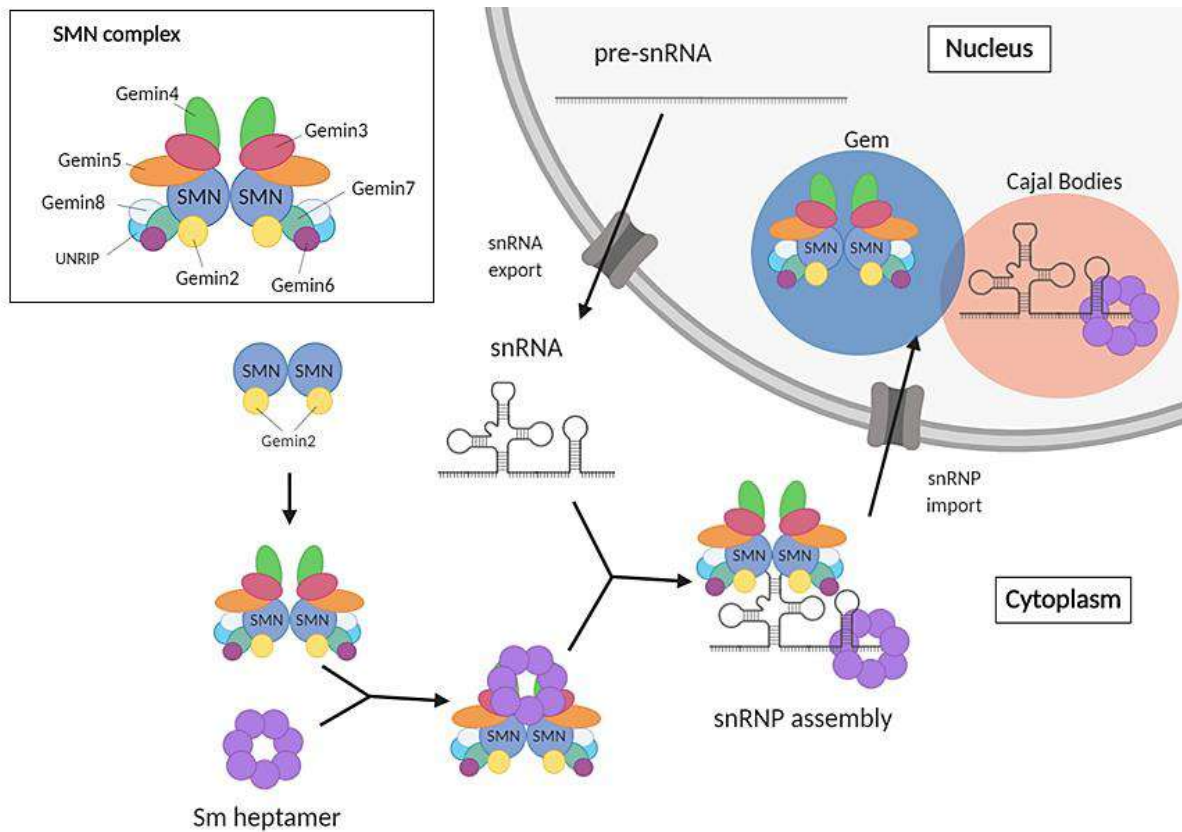


**Figure 11. SMN function in the snRNPs assembly.** In the cytoplasm, SMN oligomers form a macro complex with Gemin proteins (2-8) and UNRIP. The formed SMN complex binds with an Sm heptamer. In the meantime, snRNAs are transcribed in the nucleus and exported to the cytoplasm. Following export, the snRNAs bind to the SMN complex with the Sm proteins to the 3'-end and the complete complex is imported back to the nucleus (Based on Pellizzoni et al., 2001).

In addition, SMN has tightly been associated in the assembly and metabolism of other ribonucleotide complexes, like snoRNPs proteins that act as guides for the posttranscriptional processing and modification of ribosomal RNA (rRNA) (methylation and pseudouridylation) (Pellizzoni et al., 2001).

### **Stabilization and transport of mRNA through the axon**

The pieces of evidence that connect SMN in mRNA trafficking are multiples, including the observation of SMN in the dendrites, axons and growth cones of cultured MNs by using electron microscopy (Pagliardini et al., 2000). Using live-cell imaging, it has also been observed, SMN positive puncta actively transported bi-directionally along the axons (Zhang et al., 2003).

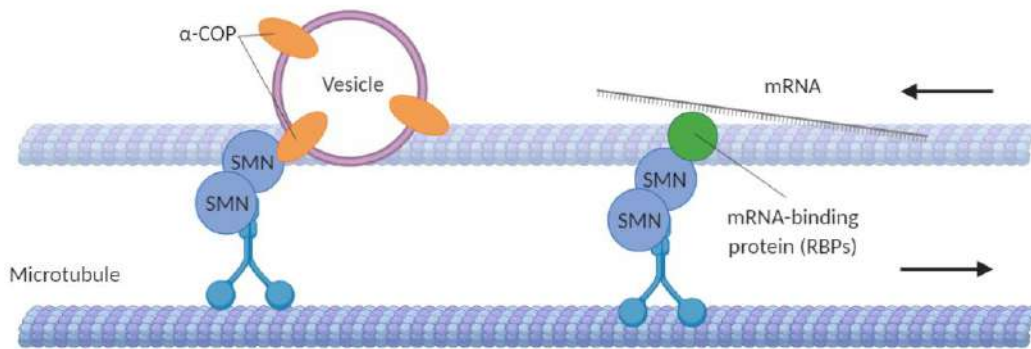


**Figure 12. SMN function in the transport of mRNA at the axon terminal.** SMN participates in axonal transport in two different ways. On one hand, SMN binds to the  $\alpha$ -COP protein of the Golgi-derived vesicles involved in the transport through the neurites. On the other hand, SMN acts as a chaperone promoting the association of mRNA-binding proteins (RBPs) with mRNA transcripts, while linking the complex to the cytoskeleton (Based on Chaytow et al., 2018).

In this context, SMN could be involved in axonal transport by two different ways. In the first pathway, SMN binds to the  $\alpha$ -COP subunit of the COPI vesicle, a Golgi-derived vesicular transport system involved in intracellular trafficking in neurites and necessary for the maturation of these neuronal cell processes (Peter et al., 2011; Todd et al., 2013). It would suggest that the role of SMN in trafficking can be involved in neuronal outgrowth and formation. On the second pathway, SMN was found to be associated, via its Tudor domain, with several mRNA-binding proteins (RBPs) (such as KSRP (Tadesse et al., 2008), FMRP (Piazzon et al., 2008), HuD (Hubers et al., 2011), FUS (Groen et al., 2013) and IMP1 (Fallini et al., 2014)). Thus, SMN would be acting as a molecular chaperone that promotes the molecular interaction of RBPs to mRNA transcripts, but also the binding of RBPs to the cytoskeleton in order to stabilize and facilitate trafficking. The transportation of mRNA transcripts along the axon is important because it provides rapid protein turnover in distal regions of the neuron (Fallini et al., 2012; Glock et al., 2017).

### Translation of mRNA transcripts

Recent evidences have also pointed out that SMN could be involved in the local translation of mRNA (Fallini et al., 2016). It was previously reported that SMN deficiency severely disrupted local protein synthesis within the axon without any change in soma protein translation (Fallini et al., 2016). This suggests a link between the role of SMN in mRNA

trafficking and translation and, nowadays we know that SMN alters the local translatoome through several mechanisms. Among them, the best characterized are the direct association of SMN with polyribosomes to regulate the availability of ribosomal units for local translation and consequently suppressing translation (Sanchez et al., 2013), and the up-regulation of microRNAs that are associated with increased cell proliferation through the mTOR pathway (Weeraratne et al., 2012). Even so, these mechanisms are not very well known and future experiments will be necessary to finally corroborate this SMN function.

### **Modulation of cytoskeleton dynamics**

Three interesting points have been observed related to SMN protein and cytoskeleton activity. The first arises from the fact that one of the mRNAs transported in the axon by SMN is  $\beta$ -actin mRNA, a protein essential for cytoskeletal dynamics and growth cone formation (Rossoll et al., 2003). In addition, it has been observed that in the extension of neurites SMN colocalizes with Profilin 2a (Sharma et al., 2005). Profilin 2a is a protein expressed in the nervous system that participates in the regulation of actin turnover by promoting actin polymerisation. SMN modulates profilin activity by the direct interaction of Profilin 2a with the proline-rich domain of the SMN protein (Nölle et al., 2011).

Finally, the study of discordant SMA patients, two brothers carrying the same alleles of *SMN1* and *SMN2* and showing different phenotypes, exposed one of the first known genetic modifiers of SMA: the protein plastin 3 (PLS3). PLS3 is a highly conserved protein involved in axonogenesis by bounding actin filament and stabilizing growth cones. More recent studies have demonstrated that PLS3 protein levels directly depend on SMN and that reduction of PLS3 during SMA aggravates the disease phenotypes (Hao et al., 2012; Oprea et al., 2008).

Despite all this, it remains to be determined the exact mechanisms that link SMN to the regulation of the dynamics of the cytoskeleton, and whether the effect is really direct, or just the result of SMN's involvement in the mRNA trafficking of components of the cytoskeleton.

### Cellular homeostasis

Besides the previously described SMN functions, the reduction of SMN protein levels have also been related to alterations in multiple cellular processes, but the mechanism underlying these changes is still poorly understood.

In several murine models of SMA, it has been identified endosomal defects in the NMJ, causing a synapse disruption, but also in non-neural tissue (Dimitriadi et al., 2016). Similarly, it has been observed that in SMN depletion models, there is an increase in the number of autophagosomes. It is debatable whether this deregulation of autophagy is protective or harmful to the cell, but together with the results that autophagy modulators can alter SMN protein levels, it indicates a relationship between SMN and autophagy (Garcera et al., 2013; Periyakarupiah et al., 2016). Recently, SMN deficiency has also been linked to changes in oxidative stress, mitochondrial dysfunction and transport and impairment of bioenergetic pathways, but the results are still preliminary and conflicting and need deeper analysis (Chaytow et al., 2018).

It is important to note that, to date, none of these roles has been identified as uniquely responsible for SMA pathophysiology.

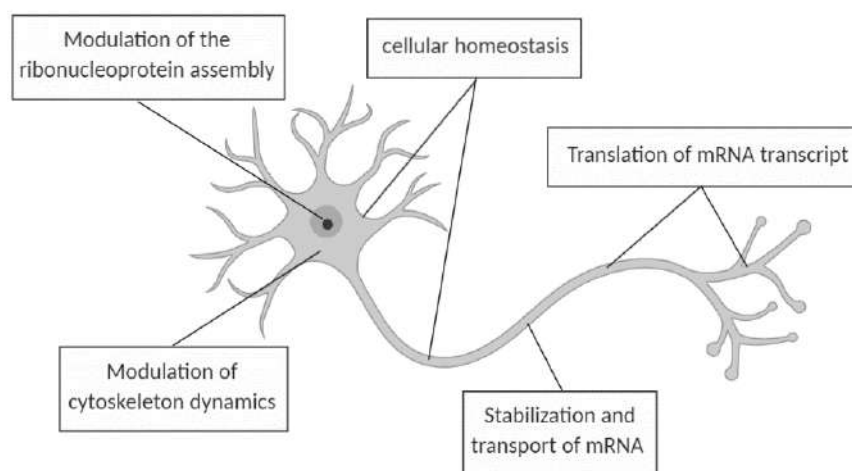


**Figure 13. Summary of the described cellular functions of SMN in neuronal cells.** The information that SMN is present in different areas of the MNs reinforces the idea that it has more specific functions beyond its classical function in the nucleus regulating the small nuclear ribonucleoprotein (snRNP) biogenesis (Based on Singh et al., 2017).

## 2.4. SMA pathology

### 2.4.1. Motoneuron alteration

The main pathological characteristic observed in SMA patients is the specific loss of MNs in the ventral horn of the spinal cord which results in muscular atrophy. Other less common MNs features in SMA are: the altered positioning (heterotopia) of MNs in the ventral white matter (Simic et al., 2008), swelling and chromatolysis with accumulation of phosphorylated neurofilaments, vesicles and ribosomes in the soma of these cells. In infrequent cases, these pathological features are also observed in DRG neurons and brain structures such as the thalamus (Monani and De Vivo, 2014). However, these cellular pathological features of SMA are usually described from the analysis of autopsy tissue samples from patients with severe forms of the disease. This means that, in addition to the limited availability of material, these data only reflect the final stage of the disease (Crawford and Pardo, 1996). Thus, it must be considered that the loss of MNs is probably the consequence of neurodegenerative alterations previously occurring in these cells.

To overcome these limitations and to be able to study the alterations of the early pathology of SMA, several SMA animal models have been generated. In contrast to the mentioned observations, in SMA mouse models it has been detected a similar number of MNs in the spinal cord at birth in SMA mutants compared with their control littermates (Hsieh-Li et al., 2000; Le et al., 2005; Monani et al., 2000). Only the 20–35% reduction of those cells at post-symptomatic stages have been described, despite the severe neuromuscular degeneration of these SMA mutants (Monani et al., 2000; Tarabal et al., 2014). Moreover, recent data suggest that synaptic defects followed by axonal degeneration can be the first pathological sign of the disease (Kariya et al., 2008; Tarabal et al., 2014). These alterations indicate that the loss of MNs soma occurs subsequent to abnormalities in MNs function at the distal end.

These defects of the NMJ take place early in the disease progress at both the pre- and post-synaptic terminal and are characterized by impaired neurotransmitters release, synaptic accumulation of neurofilament proteins, significant nerve terminal loss and reduced maturation of acetylcholine receptor clusters. Specific findings in the axons show defects that include truncated and branched axons (Cifuentes-Diaz et al., 2002; Dachs et al., 2011; Kariya et al., 2008; Kong et al., 2009; MCGovern et al., 2008; Murray et al., 2008; Tarabal et

al., 2014). Although it is currently unclear how low levels of SMN cause the selective vulnerability of MNs, these defects are indicative that SMA pathology may be the consequence of failed synaptic maintenance and axonal alterations (Fallini et al., 2012).

#### 2.4.2. One protein, two hypothesis

Although the genetic basis of SMA is well known and is a disease that has been studied for a long time, there are still many questions without a clear answer. How can *SMN* gene defects lead to a MNs disease? Two hypotheses have been postulated trying to explain the specific sensitivity of MNs in SMA. The first hypothesis suggests that the reduction of SMN levels produces a direct disruption on the biogenesis of the snRNPs affecting the splicing of a select group of pre-mRNA which are important for MNs, and the second hypothesis, postulates that SMA would specifically affect MNs due to an explicit role of SMN in these cells, related to axonal transport and maintenance. A third option is also possible if we consider that both hypotheses are connected. The reduction in the assembly of snRNPs could produce a decrease in the splicing of specific and crucial genes for axonal transport and maintenance in MNs (**Figure 14**). Currently, there are evidences that support both hypotheses, but there is still no clear indication of which one is the correct.

##### Hypothesis 1, snRNPs biogenesis alteration

According to this hypothesis, the residual low levels of functional SMN protein produced during the disease might be sufficient for the maintenance of snRNPs assembly and pre-mRNA splicing in most cell types, but not in MNs. This specific vulnerability of MNs to abnormal splicing would be a consequence of higher cellular energy requirements (Simic, 2008).

The pieces of evidence supporting this hypothesis showed that snRNP assembly activity was reduced in SMA patient cells (Gabanella et al., 2007; Wan et al., 2005). Therefore, if this hypothesis is correct, we should expect modifications of snRNP assembly in other cell types with a high RNA turnover, such as hepatocytes or other types of neurons, like, the pyramidal cells of the hippocampus, proprioceptive sensory neurons or the Purkinje cells, which it appears they are not that affected in the disease. Moreover, other described results could contradict this hypothesis. For example, there are some SMA-causing mutations in the *SMN1* gene, that displayed no defect in snRNP biogenesis (Shpargel and



Matera, 2005). Similarly, when the severe SMA and the SMN $\Delta$ 7 mouse model were compared, no differences in snRNP assembly activity were observed, despite the significant differences in lifespan between the two models (~9 days) (Gabanella et al., 2007). Consequently, examining different SMA animal models suggest that deficits in snRNP maturation and abnormal splicing are unlikely to be sufficient to initiate SMA pathogenesis (Bäumer et al., 2009; Rajendra et al., 2007). As a result, it cannot be excluded that the SMN protein may have an additional function in the cell which is independent of snRNP biogenesis but probably which is more specific for MNs.

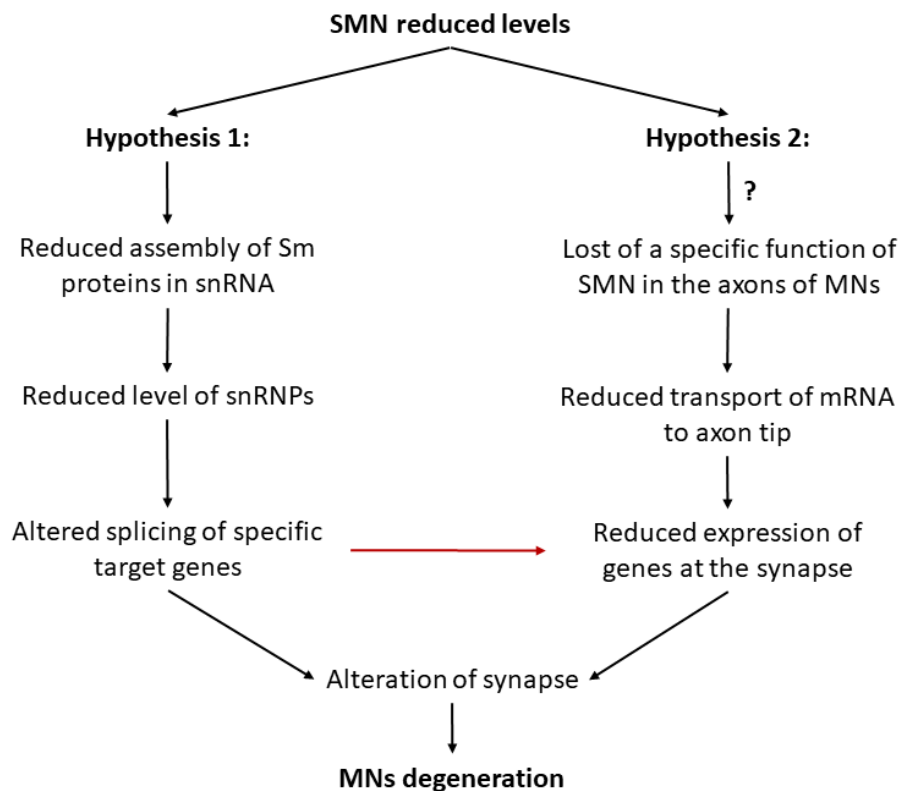


**Figure 14. Hypotheses proposed to explain how reduced SMN levels cause MNs affection.** Two mechanisms have been proposed to explain how low levels of SMN protein mainly affect MNs. A third option (red arrow) unites the two hypotheses by where the reduction of snRNP assembly causes a decrease in the splicing of a target gene that is critical for the transport of mRNA to the MN synapse (Based on Burghes and Beattie, 2009).

### **Hypothesis 2, specific SMN function in MNs**

SMN protein has been detected in MN axons and growth cones in complexes that do not contain Sm proteins or are associated with the snRNPs assembly. It has also been demonstrated that SMN is actively transported (anterograde and retrograde) through the axon in cultured MNs. Moreover, in cells affected by SMA, the SMN axonal complex is interrupted (Briese et al., 2005; Rossoll and Bassell, 2009). This hypothesis has been strengthened by the findings observed in animal models. For example, the elimination of SMN in zebrafish leads to specific axonal defects (truncated and branched axons) in MNs (McWhorter et al., 2003). Likewise, a similar phenotype, short axons with small growth cones, and a reduction of  $\beta$ -actin mRNA transport was observed in cultured MNs of SMA mice (Rossoll et al., 2003).

However, it is still unclear whether these axonal defects result from the loss of a specific function of SMN in the MNs axons or they are another consequence of snRNPs biogenesis alteration. In addition, this specific SMN axonal function would not fully explain the specificity of MNs since SMN is found in the axons of all neurons, and there are neurons with prolongations as long as MNs. In conclusion, there are evidences that SMN has a role in the MNs axon, however, there are no conclusive evidences and additional studies are required.

#### **2.4.3. Other cell types affected: SMA as a multisystemic disease**

Whether there is a specific function of SMN in MNs axon or the alteration of snRNPs biogenesis, why are MNs the main target of SMN deficiency? Truthfully, only MNs are affected in SMA? Over the years many studies have described non-motor abnormalities in severe forms of SMA that might also contribute to the overall pathology.

In humans, SMN protein is expressed at early stages of embryonic development and is present at high levels in most tissues, including spinal cord, skeletal muscle, heart, kidneys, spleen, liver and lungs (A. Nash et al., 2017; Hamilton and Gillingwater, 2013). This ubiquitous expression implies that in patients with severe SMA phenotypes, protein deficiency may have other consequences that are not immediately evidenced due to their short life expectancy, but which may contribute to the disease pathology.

This has led to suggest that there is a gradient of susceptibility to SMN reduction where MNs are at one end of the spectrum (**Figure 15**). Nowadays this hypothesis is known as the “**threshold hypothesis**” (Hamilton and Gillingwater, 2013; Sleigh et al., 2011b). According to this hypothesis, regardless of the SMN function, when SMN protein is reduced, MNs are the first affected cells since they are the most sensitive cell type to SMN level changes. This would drive the MNs to a process of progressive degeneration. As the levels of SMN are further reduced, the range of affected cells becomes greater, to a point of universal cell degeneration, where there is not enough SMN protein for any cell type to survive.

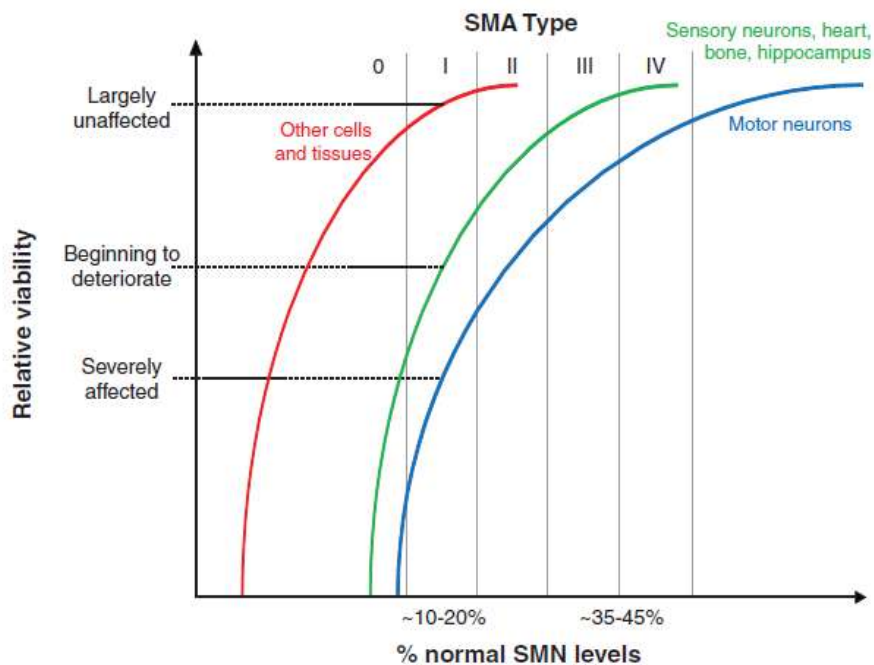


**Figure 15. Representative scheme of the threshold hypothesis in the SMA.** This theory may explain why MNs are the most severely affected cells by the depletion of SMN. Although SMN is a ubiquitous protein, there is a differential susceptibility of different types of cells and tissues to the protein reduction. MNs are at one end of the resistance spectrum and therefore have a higher vulnerability. As protein levels decrease further, additional tissues such as bone, heart and sensory neurons are affected (Sleight et al., 2011).

An important consequence of this new hypothesis is that it considers SMA as a multisystemic disorder, where not only MNs but other cell types are affected and susceptible to degeneration. Another important consequence is that when developing new treatments, it must be taken into account that they must be administered systematically

to have a greater chance of success. In addition, a better understanding of this differential susceptibility is likely to offer more information about the role of SMN in MNs.

### **Skeletal muscle alteration**

The most clearly affected systems after MNs is the skeletal muscle. It has been described that patients with SMA suffer muscular atrophy, characterized by the presence of atrophic and less organized myotubes interspersed with hypertrophic fibres. These alterations do not occur uniformly. The trunk, thigh and arm muscles are the most severely affected and can be detected in SMA fetuses, which indicates a delay in growth and muscle maturation (Durmus et al., 2017; Martínez-Hernández et al., 2009). Analysis of degenerative changes in muscle cells using an SMA mouse model has corroborated defective skeletal muscle development accompanied by a prominent muscle satellite cell apoptosis (Dachs et al., 2011).

During SMA, muscle involvement is due to indirect effects caused by denervation, as well as to direct effects caused by the reduction of SMN levels in the muscle cells itself. It is known that the survival of muscle fibres is closely related and depends on the cell contact with the innervating MNs. Therefore, the degeneration of MNs and NMJ can contribute significantly to muscular atrophy (Greensmith and Vrbová, 1997). However, studies in murine models have shown that atrophy (and increased levels of cell death) can also occur independently of nerve degeneration (Murray et al., 2008) by specifically reducing SMN protein only in muscle cells but not in MNs. *In vitro* studies have shown that the reduction of SMN in muscle cells produces decreased proliferation, defects in the fusion of myoblasts and malformed myotubes (Boyer et al., 2013; Bricceno et al., 2014; Hayhurst et al., 2012; Shafey et al., 2005).

Despite evidences supporting the direct role for SMN in skeletal muscle, restoring SMN in SMN-reduced muscle cells is insufficient to correct the disease pathology (Gavrilina et al., 2008). Although abnormalities in skeletal muscle are also likely to contribute to the pathogenesis of SMA, the degree to which they participate remains unclear and further research is required.

### **Cardiovascular system alteration**

In patients with severe SMA cardiac abnormalities and arrhythmias have been reported as one of the most common peripheral phenotypes (Rudnik-Schöneborn et al., 2008). At the final stages of the disease, severe SMA mouse models have shown to display bradycardia and to develop dilated cardiomyopathy with a reduction of heart muscle contractility (Bevan et al., 2010; Heier et al., 2010). Usually, it has also been reported vascular defects like distal digital necrosis (Somers et al., 2012). It is still under study if these structural defects in the heart and vascular system are due to aberrant autonomic signalling or a direct effect of SMN in heart and vascular development. It is also unknown if these defects can exist independently of MNs pathology and muscle paralysis.

However, it is well-known that high *SMN2* copy numbers are sufficient to compensate and prevent these defects in non-severe SMA types (Types 3 and 4) but insufficient in the most severe patients (Bianco et al., 2015).

### **Peripheral nervous system alteration**

Studies of end-staged mouse models of SMA and post-mortem patient spinal cords samples showed clear signs of astrogliosis (Kumagai and Hashizume, 1982; Tarabal et al., 2014). Astrocytes support neuronal development and synapse formation and their alteration can inhibit axon regeneration. Although the mechanisms are still unknown, in SMA mouse models the restoration of SMN levels in astrocytes increased lifespan, improved the function of the motor unit and normalized NMJ defects, even though it does not prevent MNs degeneration (Rindt et al., 2015).

Other neuronal cell types modified in SMA are Schwann cells and DRG neurons. These cells developed abnormalities in the mutant SMA mouse. Specifically, it was observed that Schwann cells did not wrap axons compactly producing an expansion of the nodes of Ranvier, which translates into an incorrect neuronal transmission (Hao et al., 2015). On the other hand, DRG neurons showed chromatolysis and degeneration, associated with strong dysfunction of proprioceptive synaptic inputs (Fletcher et al., 2017; Mentis et al., 2011; Tisdale and Pellizzoni, 2015).

### **Enteric Nervous System alteration**

SMN reduction causes defects in the enteric nervous system (ENS) (Gombash et al., 2015). These, in turn, contribute to dysfunction of the gastrointestinal tract producing severe diarrhea, reduced number and altered morphology of the villi in the small intestine and early submucosal edema. These effects are the direct consequence of SMN reduction in the ENS and confirm, that even in a less degree other neurons are affected during SMA (Schreml et al., 2013; Shababi et al., 2014).

### **Reproductive tissue alteration**

Severe types of SMA disease do not reach the age for reproduction and consequently, it is not possible to report the effects of SMN deficiency on fertility. However, the use of intermediate mouse models of SMA, allowed to determine that affected mice had significantly smaller testis, degenerated seminiferous tubules, impairment in spermatogenesis and differential expression and splicing of over 3,700 genes within the testes. Females do not show any reproductive abnormalities. These findings suggest that SMN deficiency leads to an aberrant reproductive phenotype in males, even though these observations have not been assessed in humans (Ottesen et al., 2016).

### **Mineral and metabolic alterations**

The skeletal system is also affected in patients with SMA. Recent studies have observed that the reduction of SMN levels in humans causes osteoporotic phenotype with a decrease in bone mineral density and higher levels of bone resorption (Khatri et al., 2008). These defects traduce as a higher risk of suffering fractures in the forearm, hands, femur, legs, and vertebrae. The severity of these symptoms is closely related to the stage of the disease, the degree of ambulation and treatment. It is not known whether these symptoms are a consequence of a specific role of SMN in skeletal development and bone remodelling or due to the weakened state and lack of weight load in these patients (Vai et al., 2015; Vestergaard et al., 2001).

Likewise, SMA patients, other metabolic alterations have been reported, such as abnormalities in the pancreas and the liver. These alterations result in hyperglycemia, iron

overload, and reduced body size subsequent to abnormal and reduced secretion of liver-like insulin-like growth factor 1 (IGF-1) (Bowerman et al., 2012b; Vitte et al., 2004).

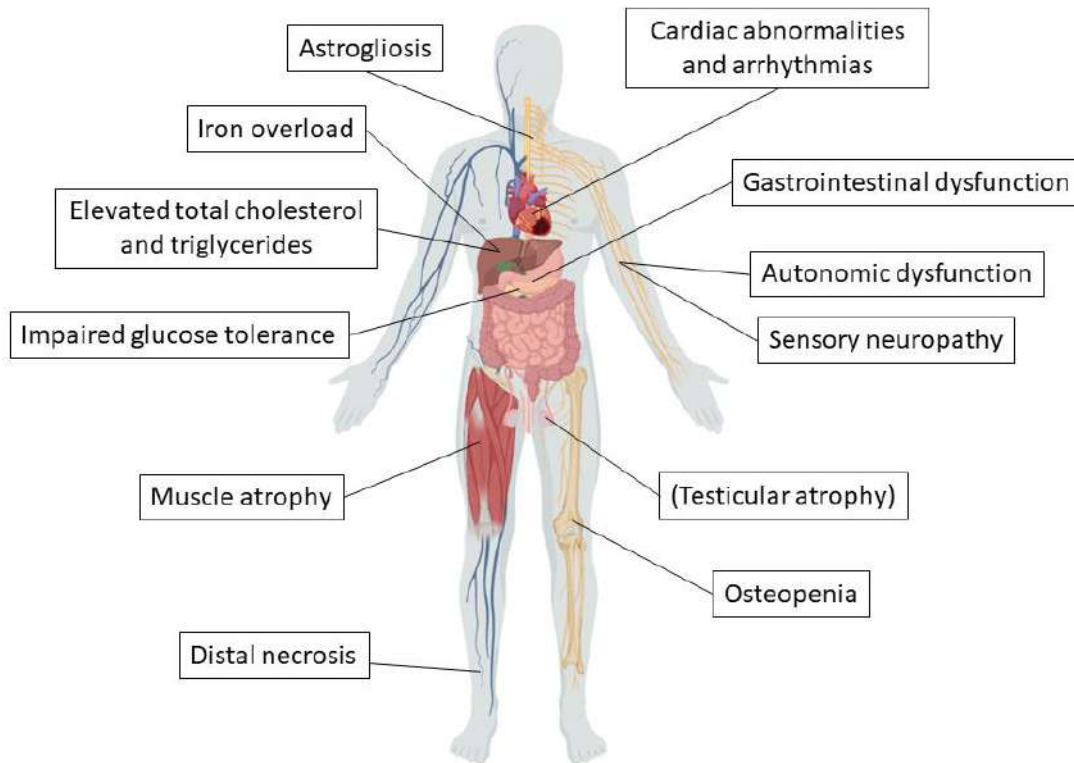


**Figure 16. Overview of the systemic alterations known to be affected in SMA.** Besides the muscular atrophy, numerous tissues and organs are also known to be affected during the disease. Testicular atrophy is in parenthesis since reproductive alteration has only been possible reported in some SMA mouse models (Based on A. Nash et al., 2017).

## 2.5. SMA therapies

SMA has no cure but there are several treatments that help control the symptoms of the disease (Finkel et al., 2018; Mercuri et al., 2018). Moreover, in recent years several experimental therapies have been approved by the Food and Drug Administration (FDA) and the European Medicines Agency (EMA) and are currently being administered in patients and other therapies, are now in the pipeline and could reach the patients in the coming years.

### 2.5.1. Current treatment

#### **Paralysis**

SMA is characterized by progressive muscle weakness and atrophy. In the most severe cases, these atrophy ends up producing muscular paralysis. To maintain muscle strength and prevent stiff joints, controlled physiotherapy and exercise are recommended. However, as the disease progresses, orthopaedic supports for arms and legs, orthopaedic walking devices, walking racks, voice synthesizers and wheelchairs may be required (Finkel et al., 2018; Mercuri et al., 2018).

#### **Pulmonary complications**

During SMA the intercostal muscles are also weakened and it makes patients depend exclusively on the diaphragm (which only becomes involved in later stages) to breathe, leading to progressive respiratory deterioration. This causes hypoventilation during sleep, impaired cough with an inadequate clearance of lower airway secretions and recurrent pneumonia. The decrease in respiratory function usually ends in the death of patients due to respiratory failure. The existing management to treat respiratory problems include, breathing exercises, oral suction of the mucus to clear the throat, vaccination against flu and, in the most severe cases, assisted ventilation to support breathing (Finkel et al., 2018; Mercuri et al., 2018).

#### **Orthopaedic Complications**

One of the most common complications in SMA patients is the development of scoliosis, joint contractures and hip dislocations. Without treatment, progressive scoliosis can affect lung function and cardiac function, in severe cases. Initially, the treatment for spinal problems is the use of a back clamp, to force the spine to develop properly and support the back. In more severe cases, surgery is required to straighten the spine with metal hooks and rods (Finkel et al., 2018; Mercuri et al., 2018).

#### **Nutritional problems**

Gastrointestinal dysmotility in SMA causes delayed gastric emptying, constipation, aspiration and gastroesophageal reflux. If the muscles of the jaw and throat are also



affected can cause difficulties in swallowing and feeding, which consequently leads to weight loss and affects growth in children. Growth failure and nutritional problems can be treated with a strictly regulated diet or with feeding tubes in the most serious cases (Finkel et al., 2018; Mercuri et al., 2018).

### **Metabolic acidosis**

Aberrant glucose metabolism can lead to severe metabolic acidosis with dicarboxylic aciduria and low serum carnitine concentrations, which can be prevented by avoiding prolonged fasting in SMA patients (Finkel et al., 2018; Mercuri et al., 2018).

### **Non-specific medications**

In the SMA it is common to use medications that have not been specifically designed for this disease. They are used to treat specific symptoms or prevent complications of SMA. The most common is the use of muscle relaxants (such as baclofen, tizanidine, or benzodiazepines) to prevent stiffness and muscle strain (spasticity) and medications such as Botox (onabotulinumtoxinA), amitriptyline, Robinul (glycopyrrolate), or AtroPen (atropine) used to prevent excessive saliva production and jaw spasms (Finkel et al., 2018; Mercuri et al., 2018).

### **Nusinersen**

Nusinersen (SPINRAZA-Biogen; Cambridge, MA, USA) was the first approved treatment for SMA (FDA, December 2016). The good results obtained in the ENDEAR clinical trial were decisive (n = 121, in a randomized, double-blind, controlled study with phase III simulation in patients with SMA type 1). In this trial with only 6 administrations of Nusinersen (approximately 1 year of treatment), 30% of patients improved motor function and achieved some motor milestone (holding their heads, sitting or standing) while in the control group any patient obtained these achievements (Finkel et al., 2017). Extended trials with Nusinersen have shown that the treatment is able to avoid mortality, respiratory requirements, and maintain a normal or almost normal development in SMA patients when the treatment is presymptomatic (Neil and Bisaccia, 2019).

Nusinersen is an antisense oligonucleotide (ASO) modified with 29-O- (2-methoxyethyl). ASOs are short synthetic nucleotide chains designed to bind to specific mRNAs by base pairing hybridization. Specifically, nusinersen is addressed to ESS in intron 7 of the *SMN2* pre-mRNA. The drug displaces the hnRNP (heterogeneous nuclear ribonucleoproteins) from ESS by facilitating the correct splicing of *SMN2* transcripts, including exon 7 and resulting in the production of full-length SMN. This produces an increase in the levels of functional SMN protein in the cells and delays the progression of the symptoms of the disease (**Figure 17**) (Chiriboga, 2017).

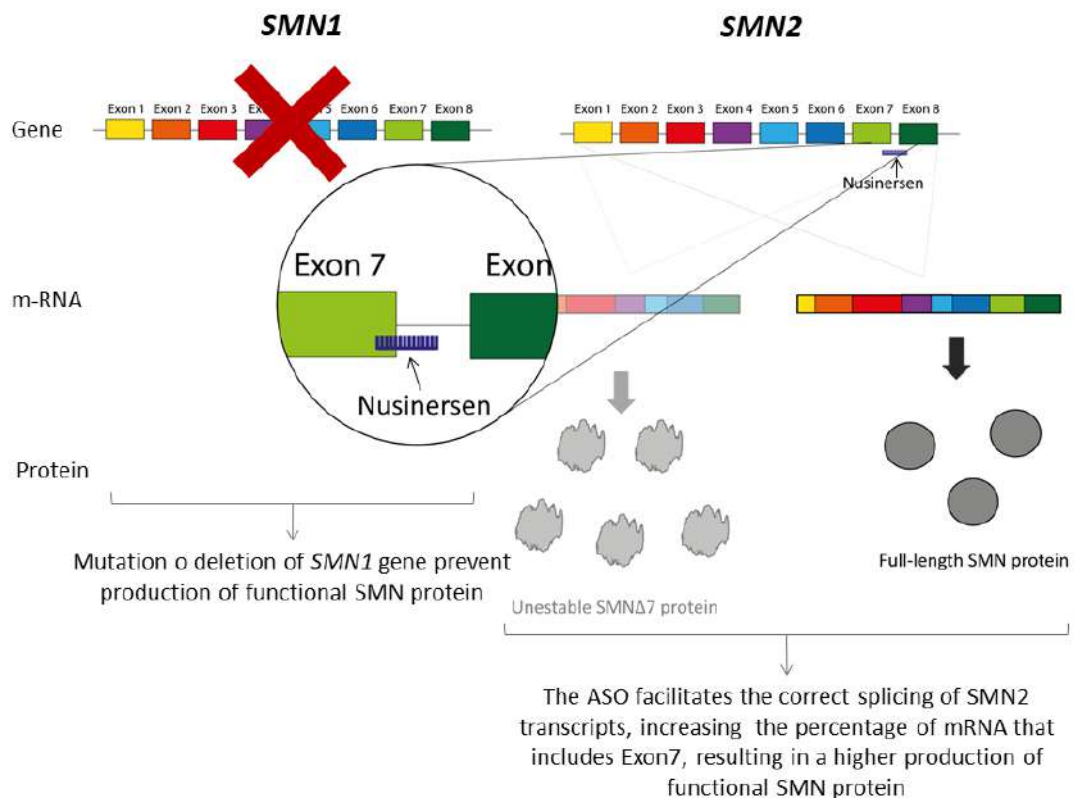


**Figure 17. Mechanism of action of Nusinersen.** Nusinersen is an antisense oligonucleotide (ASO) specifically designed to bind to the ESS (exonic splicing silencer) of intron 7 in the *SMN2* pre-mRNA. The treatment facilitated the correct splicing of the mRNA, increasing the levels of full-length SMN protein in the cells (Based on Chiriboga, 2017).

ASOs molecules are not able to cross the blood-brain barrier, so they must be administered directly into the CNS, by intrathecal injection (lumbar puncture). The dosage regimen is in an injectable solution of 12 mg / 5 ml *per* administration with controlled speed for 1-3

minutes. The administration pattern begins with 3 initial doses separated fourteen days (days 1, 15, 30) and 35 days after the fourth (day 60). Maintenance doses are administered every four months for life (Chiriboga, 2017). The price of each vial of Nusinersen 12mg vial of 5ml (in injectable solution) costs \$ 70,000 with an annual cost of \$ 750,000 in the first year of treatment and \$ 375,000 for the following years.

Like any, treatment nusinersen has adverse effects both by the treatment itself and by the intrathecal administration. The most common adverse effects described are: fever, headache, back pain, vomiting, proteinuria, thrombocytopenia, secondary thrombosis, lower respiratory tract infection with airway obstruction (atelectasis), urinary tract infection, hyponatremia (low sodium concentration in the blood), weight loss and meningitis infections associated with lumbar puncture (Aslan et al., 2019; Chiriboga, 2017).

### **Zolgensma**

Onasemnogene abeparvovec, formerly known as AVXS-101, was first developed by AveXis with the brand name of Zolgensma (Novartis). It is the first gene therapy and the second approved drug (currently only in the U.S.) for the treatment of SMA. The FDA approved (May, 2019) the use of Zolgensma under certain conditions. In the last clinical trial, of the two that have been carried out, the results are very promising. In the last trial, funded by NeuroNEXT project (n = 16 SMA affected babies type 1 and n = 27 healthy babies) it was reported an improvement in motor function and increase of survival at 24 months of monitoring of 100% versus 38% (compared to results obtained in a previous study (NN101) with untreated patients of similar age and characteristics) (Al-Zaidy et al., 2019a).

Zolgensma uses gene therapy to restore functional SMN protein levels in cells. It works by using a genetically modified adeno-associated virus (AAV) with a hybrid cytomegalovirus (CMV) enhancer/chicken- $\beta$ -actin promoter vector to integrate a functional copy of the *SMN1* gene into the nuclei of MNs patients (Rao et al., 2018).

The unique treatment is administered intravenously once in a lifetime. Its administration is only indicated to SMA type 1 patients under two years of age with bi-allelic mutations in the *SMN1* gene. The actual recommended dosage of Zolgensma is  $1.1 \times 10^{14}$  vector genomes *per* kg of body weight. Its main drawback and the reason why this drug is under

controversy is its high price, established at \$ 2.1 million. It is currently the world's most expensive drug (Malone et al., 2019).

As side effects, Zolgensma may interact with corticosteroids and certain vaccines, such as MMR (measles, mumps, rubella vaccine) and varicella, induce vomits and can raise liver enzymes (aminotransferases) producing acute serious liver injury. It should be noted that there is not yet a complete list of side effects, which could lead to other complications not yet described (Rao et al., 2018).

### 2.5.2. New therapies

Despite the spectacular effects described for the two SMA treatments approved, it should not be forgotten that long-term effectiveness and safety are not known for any of the therapies. Likewise, they also have limitations, apart from their side effects, their high price may not make them accessible to everyone. This is the reason to continue investigating this disease, not only to understand the genetic and molecular complexity of SMA but also to develop new potential therapeutic approaches.

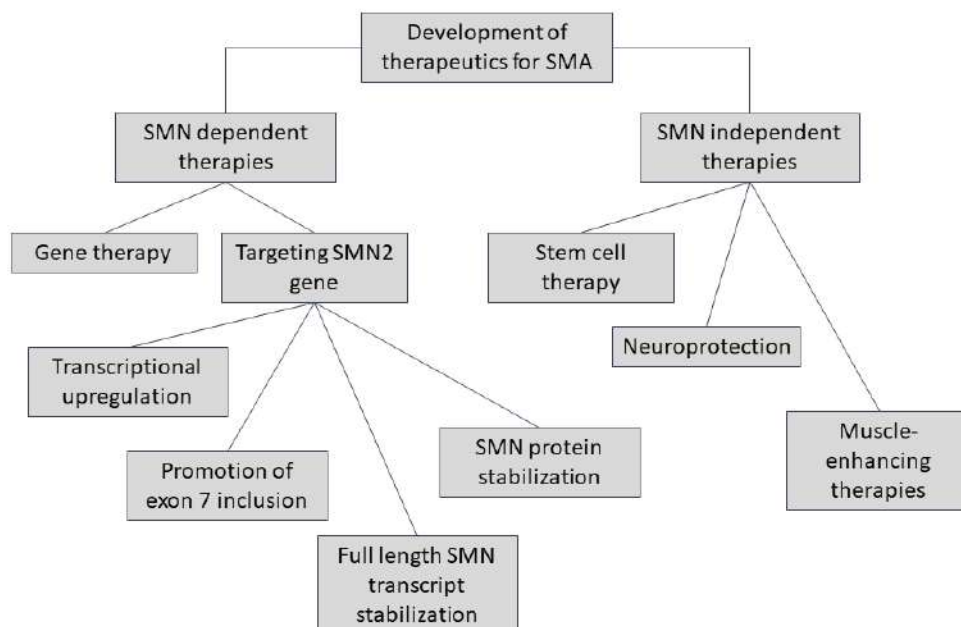


**Figure 18. Strategies in the development of new therapies for SMA.** The general treatment strategies for SMA are focused on strategies that try to compensate fully or in part for the absence of SMN1 (using gene therapy to restore it or targeting the SMN2 gene locus) or using strategies that do not depend on the SMN protein level (Based on Tariq et al., 2013).

Currently, SMA therapies are characterized by their mechanisms of action, if their objective is to increase the levels of SMN, directly or indirectly, they are called SMN-dependent therapies, while if the main target is not to modify SMN protein levels, they are called SMN-independent therapies (**Figure 18**) (Parente and Corti, 2018; Shorrocks et al., 2018; Tariq et al., 2013; Waldrop and Kolb, 2019).

### **SMN dependent therapies**

As described, there is an inverse correlation between SMN protein levels and the severity of SMA disease. It involves that increasing the levels of SMN could prevent the degeneration of MNs and therefore the development of SMA. There are two main mechanisms to achieve it, by replacing the affected gene or by targeting the *SMN2* gene.

### ***Gene therapy***

Gene therapy is currently one of the most encouraging therapeutic advances in SMA. This category includes the FDA-approved treatment, Onasemnogene abeparvovec/AVXS-101/Zolgensma (see above, section "*current therapies*"), but also others under development such as Genzyme and Genethon gene therapy that are currently in clinical trials.

This technique is based on the haploinsufficiency of the disease, where the introduction of a single functional copy of *SMN1* is sufficient to correct the disease. The *SMN1* gene is cloned into cDNA and packaged into a viral vector, generally an AAV type 8 and 9. These viral vectors are ideal for *SMN1* administration in SMA since they are a serotype of AAV that can cross the blood-brain barrier (BBB) and transduce neuronal cells (Schuster et al., 2014).

Trials in animals and patients using gene therapy demonstrate an extension of lifespan, usually accompanied by a general improvement in neurophysiology function and an essential rescue of the phenotype (Foust et al., 2010; Passini et al., 2010; Valori et al., 2010). The main limitations of this therapeutic approach are: clinical safety, both for the use of adenovirus, and for barriers between species, the possibility of an immune response to AAV, which may limit its effectiveness, the cost of virus production and the need for early pre-symptomatic intervention, which limits its possibilities of use as a treatment

(MacKenzie, 2010). Based on current data from clinical trials, no long-term safety or toxicity problems have been observed, even at high doses of AVV. Long-term monitoring is also important to understand the persistence of the therapeutic effect. The provisional long-term follow-up has shown sustained improvements and without security problems (Al-Zaidy et al., 2019b). However, the question of how much virus is excessive remains and highlights the importance of considering a more specific route of administration (intrathecal administration) and lower volumes to try to reduce the risk.

### ***Targeting SMN2 gene***

Therapies targeting the *SMN2* gene in SMA patients can be achieved through different pathways and are also significant for the development of SMA drug treatment.

#### *Transcriptional upregulation*

This therapeutic approach was the first developed and is based on the inhibition of histone deacetylases (HDACs). HDACs repress transcription of genes, including *SMN2*, by chromatin condensation. Its inhibition in SMA patients will potentially increase the rate of transcription of the *SMN2* gene producing more full-length SMN transcripts and protein resulting in a beneficial effect. Several HDAC inhibitors have been studied in cell culture, mouse models and clinical trials as a potential therapy for SMA. However, up to now, the consensus is that even well tolerated (Andreassi et al., 2004; Chang et al., 2001; Tsai et al., 2008), any of the HDAC inhibitors treatments produce a significant clinical improvement in SMA patients (Mercuri et al., 2007; Swoboda et al., 2009).

One of the most interesting HDAC treatments in clinical trials is Valproic acid (VPA) which is currently in phase III to evaluate changes in muscle strength and functionality. Results have shown that VPA treatment has no sufficient beneficial effect on motor function and improvement in survival, but it did provide some significant and interesting outcomes. When VPA was administrated in SMA patients, only one-third of the treated patients did show a slight improvement in motor function and had an increase of *SMN2* transcript levels (Darbar et al., 2011; Krosschell et al., 2018). Investigation of the responsiveness to VPA revealed that beneficial effects were only evident in young SMA type 2 patients and that the non-responder patients have CD36 overexpression that prevents SMN expression (Garbes et al., 2013). As a side effect of this drug, VPA induces a deficit in free plasma

carnitine that can lead to toxicity in the liver, which can be solved by supplementation with levocarnitine during the treatment. These findings make it interesting to speculate the potential usefulness of VPA as an early treatment in SMA patients who are ineligible for other SMN-targeted therapies and have low levels of CD36.

More recent studies show motivating results with the use of the hormone prolactin (PRL). This drug is approved for the treatment of lactation deficient mothers (Powe et al., 2010) and is capable to cross the BBB. In studies with animal models, PRL treatment showed that it is able to specifically inducing the transcription of the *SMN2* gene by activation of the JAK2/STAT5 pathway. *SMN2* gene contains a STAT5 transcription binding motifs (Farooq et al., 2011). This might prove to be beneficial in all types of SMA patients since they only have *SMN2* copies as a source of SMN protein. Besides, since PRL has already been approved in humans, it can outperform other compounds that have not yet been tested for clinical safety and join proximately the list of medications that may have therapeutic potential for SMA.

#### *Promotion of exon 7 inclusion*

Another SMA treatment strategy explored is the production of a full-length transcript from the *SMN2* gene by promoting exon 7 inclusion. The most promising compounds that suppress exon 7 skipping are the ASOs, complementary molecules to *SMN2* exon 7 pre-mRNA sequence that inhibit the binding of negative splicing (Singh et al., 2009). The FDA-approved Nusinersen/Spinraza is the best representative of this group of molecules (see section "*current therapies*") (Chiriboga, 2017; Parente and Corti, 2018).

The major obstacle using ASOs for SMA therapeutics, is their clinical safety, immune response affectation, the quantity of administered ASO, the need for repeated lumbar puncture and the cost of production. To overcome some of these effects, small molecule-based pharmacological approaches that increase the production of full-length *SMN2* mRNA have been developed in parallel. The mechanism of action of these modulatory small molecules is based on the direct interaction with two different sites in the pre-mRNA of *SMN2*, which stabilizes an unidentified ribonucleoprotein complex (RNP), ensuring the correct splicing of the *SMN2* gene (Sivaramakrishnan et al., 2017). These orally bioavailable small molecule-based approaches are more tolerable than ASOs and because of the

systemic administration, the effect is not only restricted to the CNS but also affects other organs. The major concern related to the small molecule-based approach is the risk of off-target effects given that, unlike ASOs and gene therapy, this approach is not completely specific and can affect the expression of other genes. Initial studies in mouse models of SMA with small molecule-based therapies have shown improvement in motor function, protection of the neuromuscular system from degeneration and increased survival (Naryshkin et al., 2014). Currently, the most promising therapies in clinical trials are the LM1070 and the RG7916 (Parente and Corti, 2018).

Branaplam or LMI070 (Novartis, Basilea, Svizzera) compound began to be tested in clinical trials in April 2015, in an open-label, multi-part, phase I/II study with SMA type 1 patients with two copies of *SMN2*. The main objectives were to evaluate the efficacy, safety, tolerability, pharmacokinetics and pharmacodynamics of the oral administration (once a week over a 13-week trial period). Initial results suggested some improvements in motor function and indicated adverse events that were mostly mild and reversible. However, parallel toxicology studies conducted in animals showed unexpected toxicities to the peripheral nerves and spinal cord, testes and blood vessels in the kidney. This forced temporarily to stop the trial that was discontinued in mid-2016. Nowadays, the trial has been resumed with close monitoring of the patients (Charnas et al., 2017).

Risdiplam/RG7916 (RO7034067, Roche, Basel, Svizzera) is the second small molecule *SMN2*-splicing modifier in clinical trials. After the conclusion of a phase I study in August 2016 in healthy volunteers that helped to establish the optimal treatment dose and corroborate the increase in full-length *SMN2* mRNA levels, RG7916 is now being tested in 3 parallel phase II clinical trials in Europe in SMA patients. The Firefish trial is an open-label (without placebo) trial that assesses the effectiveness of orally daily dose of RG7916 in patients with SMA type 1 aged between 1 and 7 months with two copies of *SMN2*. Sunfish is the second RG7916 phase II clinical trial. During the first part of the trial, it was assessed the safety of the optimal dose and, in the second part, it was investigated the effectiveness of RG7916 in type 2 and type 3 SMA patients aged 2–25 years. In contrast to Firefish, the Sunfish trial is a randomized, double-blind and placebo-controlled clinical trial. Initial results from these studies showed moderate benefits of the therapy on the SMA patients. Finally, the Jewelfish trial is a 2-years trial that assesses the daily doses of RG7916



treatment in adults and children with SMA type 2 and 3, who were previously treated with other *SMN2*-targeting small molecule therapies (Mercuri et al., 2017).

Although the initial results of the trials with small molecule-based therapies indicate limited functional improvement, their oral administration makes them more flexible, easier and safer to administer than ASOs or viral gene therapy. Therefore, it is expected that these drugs, if formally approved, may play a significant role in the clinic of the SMA in the coming years.

#### *Full-length SMN transcript stabilization*

In the recent years, a new approach has been developed with the objective of stabilizing the full-length mRNA produced by the *SMN2* gene and potentially increase the production of functional SMN protein. This new group of molecules bind to the Decapping Scavenger (DcpS) enzyme, part of the RNA degradation machinery, opening the enzyme to a catalytically inactivated conformation (Singh et al., 2008; Tariq et al., 2013). The inhibition ultimately blocks the breakdown of *SMN2* mRNA and consequently increasing SMN protein (Singh et al., 2008). In a different approach, the activation of the p38 pathway results in the binding of HuR protein to the specific AU rich element region in its 3' UTR (which normally marks the mRNA for degradation) of SMN mRNA and stabilizes the transcript. Importantly, in any of these transcript stabilization approaches alterations in the transcription process were observed (Farooq et al., 2009).

The quinazoline RG3039 (developed by Repligen, in partnership with Pfizer) is nowadays the only disease-modifying therapy of this category that has entered the clinical trials. Preclinical studies using SMA mouse models revealed that RG3039 successfully pass through the BBB to reach affected neurons and increase the motor function and survival in a dose-dependent manner (Van Meerbeke et al., 2013). Using these studies to estimate the optimal dose of RG3039 in humans, in 2014, the first clinical trial started with healthy volunteers. The initial objective was to evaluate the compound's safety, tolerability, pharmacodynamics, and mode of action of an oral administration in a single or multiple ascending doses. The results demonstrate that RG3039 was well-tolerated and successfully blocked more than 90% of DcpS for at least 48 hours, however, the treatment did not change SMN protein level in blood. As a consequence, Pfizer concluded that at the tested

dose RG3039 would be ineffective in SMA patients and suspended all further work with this drug (Whitehouse, 2012).

#### *SMN protein stabilization*

The mechanisms regulating SMN protein levels into the cells are not fully understood. Therefore, this alternative potential therapeutic approach has been less explored than others at the clinical level. The regulation of SMN has been related to the proteasome (Burnett et al., 2009), but it is not ruled out that other pathways may participate in its intracellular turnover. As one of the proteins degraded by the ubiquitin-proteasome pathway, SMN is targeted with polyUb molecules by the action of the enzymes E1 (Ub activating enzyme), E2 (Ub conjugating enzyme) and E3 (Ub ligase). This posttranslational modification marks the protein for destruction by the proteasome complex.

Bortezomib is the first therapeutic proteasome inhibitor approved to be used in humans. In Europe, this anti-cancer drug is prescribed for the treatment of recurrent multiple myeloma and mantle cell lymphoma (Hambley et al., 2016; Sonneveld and Broijl, 2016). *In vitro* and *in vivo* studies have shown an inhibition of SMN proteolysis accompanied by an increase in the protein levels. However, the main concern for bortezomib as a possible SMA therapy is that this drug is not able to cross the BBB (Kwon et al., 2011).

Strategy	Treatment	ClinicalTrials Identifier	Sponsors	Phase	Initiation date	Estimated completion date	Delivery method	Dosing	Target population	Objectives
Promotion of exon 7 inclusion	Branaplan	NCT02268552	Novartis Pharmaceuticals (Europe)	I-II	April 2015	July 2020	O	Once weekly	Type 1 (with 2 copies of SMN2)	-Evaluate safety, tolerability, PK, PD and efficacy -Estimate the MTD -Identify safe long term dose and optimal durable efficacy dosing regimen
SMN gene replacement therapy	AVXS-101 (Zolgensma)	NCT03837184	AveXis, Inc (Asia)	III	February 2019	April 2021	IV	One time (single dose)	Type 1 (with biallelic mutation of SMN1 and 2 copies of SMN2)	-Evaluate the efficacy
		NCT03381729	AveXis, Inc. (United States)	I	December 2017	June 2021	IT	One time (3 potential doses)	3 copies of SMN2 biallelic deletion of SMN1	- Assess the safety and tolerability by the incidence and SAE - Determine Optimal Dose
		NCT03505099	AveXis, Inc. (United States)	III	April 2018	October 2020	IV	One time (single dose)	Pre-symptomatic with biallelic mutation of SMN1 and 2 or 3 copies of SMN2	-Evaluate the safety and efficacy
		NCT03306277	AveXis, Inc.	III	October 2017	November 2019	IV	One time (single dose)	Type 1	-Evaluate survival, achievement of developmental milestone and ability to remain independent of ventilatory support
		NCT03461289	AveXis, Inc. (Europe)	III	August 2018	November 2020	IV	One time (single dose)	Type 1	-Evaluate efficacy in motor function
SMN2 splicing modifier	Nusinersen (spinraza)	NCT04042025	AveXis, Inc. (Australia, Europe, Canada, Europe, Asia and United States)	IV	October 2019	December 2034	IV and IT	One time (single dose)	Type 1, 2 and 3 already receiving AVXS-101	-Continuous monitoring of safety as well as monitoring of continued efficacy (developmental milestones) and durability of response
		NCT04050852	NYU Langone Health (New York)	I	July 2019	July 2020	IT	All previous tested doses	Patients who are approved and maintained on nusinersen treatment	-Determine changes in pulmonary function and respiratory muscle strength thought the first year of treatment
		NCT02594124	Biogen (United States and Australia)	III	November 2015	August 2023	IT	-	Patients who previously participated in investigational studies of Nusinersen	-Evaluate long-term efficacy, safety, tolerability and incidence of AE

SMN2 splicing modifier	Nusinersen (spinraza)	NCT02386553	Biogen (United States)	II	May 2015	January 2022	IT	-	Genetically diagnosed and presymptomatic under 6 weeks at first dose	-Examine the efficacy of multiple doses in the ability to remain independent of ventilatory support	
		<a href="#">NCT04089566</a>	Biogen	II-III	September 2019	February 2020	IT	3 loading doses (every 14 days) and then every 4 months	Homozygous biallelic deletion of SMN1	-Clinical efficacy of treatment, safety, tolerability PK	
	Risdiplam RO7034067	<a href="#">NCT03032172</a>	Hoffmann-La Roche (United states and Europe)	II	March 2017	December 2021	O	Once daily	Patients previously treated with Risdiplam, nusinersen, olesoxime or Zolgensma	-Investigate the safety, tolerability, PK, and PD	
		<a href="#">NCT03779334</a>	Hoffmann-La Roche (United States)	II	August 2019	June 2021	O	Once daily	Genetically diagnosed and presymptomatic under 6 weeks at first dose	-Investigate the efficacy, safety, PK and PD	
		NCT02913482	Hoffmann-La Roche (United States)	II-III	December 2016	November 2023	O	Once daily	Type 1	-Assess safety, tolerability, PK, PD, and efficacy in motor function -Determine AE and SAEs	
		NCT02908685	Hoffmann-La Roche (Canada Europe, United States, China, Japan and Turkey)	II-III	October 2016	September 2019	O	-	Type 2 and 3	-Evaluate safety, tolerability, PK, PD and efficacy in the Total Motor Function	
		<a href="#">NCT03920865</a>	Hoffmann-La Roche	I	May 2019	October 2019	O	Single dose	Healthy participant with Normal Hepatic Function	-Effect of Hepatic Impairment, PK, safety and tolerability	
		<a href="#">NCT03988907</a>	Hoffmann-La Roche (United States)	I	June 2019	October 2019	O	Once daily (Multiple doses tested)	Healthy participants	-Evaluate safety, tolerability, and PK -Effect of Risdiplam on the PK of Midazolam	
	Histone deacetylase inhibitor	Valproate + Levocarnitine	<a href="#">NCT01671384</a>	All India Institute of Medical Sciences, New Delhi (India)	III	August 2013	December 2016	O	Once daily	Patients aged 2 to 15 year-old with already registered in myopathy	-Evaluate efficacy in muscle power

**Table 4. SMN dependent therapies clinical trials (to October, 2019): 18 Studies found for SMA drug-interventional with an SMN dependent approach in ClinicalTrials.gov. Status are: Active, recruiting (green); Unknown (red). Abbreviations: Oral (O), intravenous (IV), intrathecal (IT), pharmacokinetics (PK), Adverse Events (AE), Serious Adverse Events (SAEs), Maximum Tolerated Dose (MTD).**

### **SMN independent therapies**

Parallel to the first-generation SMN-dependent therapies progression, several SMN-independent therapies have been developed and currently are under clinical research. These second-generation therapies are focused on the replacement or protection of the SMA affected cells and the enhancement of muscle strength.

#### ***Stem cell therapy***

Stem cell therapy has generated a lot of attention and expectations as a treatment for many diseases, including SMA. Its mechanism of action is based on the replacement of lost MNs or by supporting the population of existing neurons.

Although investigations have been carried out with primary murine neural stem cells and embryonic stem cell-derived neural stem cells in animal models of SMA with certain positive results (improvement of neuromuscular phenotype and survival), it remains unclear whether this effect is for the replacement of the MNs or a neuroprotection effect (Corti et al., 2010, 2009; Simone et al., 2014). Furthermore, there are several limitations to the use of this therapy. Although it is possible to differentiate induced pluripotent stem cells (iPSC) to MNs, the lentiviral vectors necessary to produce iPSC are not suitable for humans due to their mutagenic and carcinogenic potential. On the other hand, there are limitations of large-scale production and transplantation and development of these cells in the patient's CNS (Gorecka et al., 2019; Steinbeck and Studer, 2015).

#### ***Neuroprotection therapies***

Neuroprotective molecules pursue to protect the secondary function and survival of MNs during the development of SMA. Although these therapies can have positive effects on their own, it is expected that they can become very successful when used in combination with other SMN-dependent therapies. There is no specific mechanism of action within this category but includes any therapy that has a neuroprotective function. The best known are Olesoxime and Mestrinon.

Olesoxime (TRO19622; Roche, Basel, Svizzera; initially developed by Trophos, Marseille, France) is a cholesterol-like compound with a neuroprotective function that does not regulate upward SMN levels. Its mechanism of action is not fully understood, but it is

believed that it interacts directly with mitochondrial membranes and/or components of the mitochondrial permeability pore and decreases its fluidity. It prevents excessive membrane permeability under stress conditions and preserves mitochondrial function (Bordet et al., 2010). The route of administration is oral. The drug entered clinical trials as a possible treatment of SMA after the demonstration of its neuroprotective properties *in vitro* and *in vivo* on SMA murine models. In the first 12-month clinical trial (multicenter, randomized, adaptive, double-blind, placebo-controlled study with SMA type 2 and 3 patients, aged 3–25 years) clinical evidences did not establish a risk-benefit profile for this treatment approach, but a delay of neuromotor impairment was seen when comparing patients treated with the control group (Bertini et al., 2017; Dessaud et al., 2014). However, a following trial, after 18 months of treatment, the administration of olesoxime had to be stopped, because deterioration of motor function was observed.

Mestinon (pyridostigmine bromide) is a cholinesterase inhibitor drug commonly used for treating myasthenia gravis (Maggi and Mantegazza, 2011) and now it is under investigation as a possible neuroprotective treatment for SMA. Mestinon reversibly inhibits the acetylcholinesterase enzyme-inducing an increase of the acetylcholine levels as well as the duration of the signalling. Therefore, Mestinon facilitates the nerve signal transmission at the NMJ, which it has been already demonstrated to be affected in SMA. The drug is currently in phase II of a clinical trial with SMA type 2, 3 and 4 patients (ages 12 and above, who are able to walk). The double-blind test over placebo ended in January 2018 but so far no results have been published (Stam et al., 2018).

### ***Muscle-Enhancing Drugs***

Muscular symptoms represent an important part of SMA phenotype and therapeutic approaches focused on muscle protection can be strategically important to slow the disease progression. The muscle-enhancing group englobes therapies aimed to improve neuromuscular function and muscular weakness and fatigue by enhancing the ability of muscles to contract and increasing muscle mass. Some of these therapeutical agents have shown effect correcting the SMA phenotype and have been now introduced in clinical trials. The two more promising are CK-107 and SRK-015 (Parente and Corti, 2018).

CK-2127107, known as CK-107 (2-aminoalkyl-5-N-heteroarylpyrimidine; Cytokinetics, South San Francisco, California, USA) is a troponin complex activator. It slows the rate of calcium ( $\text{Ca}^{2+}$ ) release from fast skeletal muscle troponin, sensitizing the sarcomere to  $\text{Ca}^{2+}$ . Consequently, the contractile response to nerve signalling is increased, improving muscle function. Currently in a phase II clinical trial (double-blind, randomized, placebo-control groups) in patients with SMA type 2, 3 and 4, ambulant and non-ambulant, with 12 years or more. The trial was completed in May 2018 but there are no public results yet (Shorrock et al., 2018).

SRK-015 (Scholar Rock) is a selective monoclonal antibody that inhibits myostatin, a protein responsible for muscle growth inhibition. Specifically, SRK-015 binds to myostatin and delays protease cleavage preventing latent myostatin activation and leads to an increase of muscle cell growth and differentiation. Preclinical studies using animal models have shown that SRK-015 treatment increased muscle mass and strength and helps to maintain healthy muscle function (Long et al., 2019). After entering clinical trials for SMA in 2018, SRK-015 has been shown to be well-tolerated across all tested doses and now, in phase II clinical trial, it is being tested in combination with SMN-targeted therapies in SMA type 2 and 3 patients (Shorrock et al., 2018).

Increasing evidence also suggests that therapeutic approaches targeting NMJs preservation may be beneficial for SMA pathology. Moreover, some of the already described treatments such as ASOs or SMN upregulation therapies significantly improve neuromuscular transmission (reviewed in Boido and Vercelli, 2016). To date, one of the most promising approaches that specifically target NMJs is Agrin. Agrin is a synaptogenic molecule important for NMJ formation and stabilization of AChR clusters at synaptic sites (Witzemann, 2006) which is abnormally expressed in SMA models (Arnold et al., 2004; Zhang et al., 2013). Direct administration of an active splice variant form of agrin, NT-1654, has shown beneficial effects on muscle fibres and NMJs stabilization, delaying muscular atrophy, improving motor performance and extending survival in SMA (Boido et al., 2018). Showing that therapies focused on NMJ preservation may result in an interesting approach to take into consideration for future clinical trials.

Strategy	Treatment	ClinicalTrials Identifier	Sponsors	Phase	Initiation date	Estimated completion date	Delivery method	Dosing	Target population	Objectives
Neuroprotection	Adipose derived mesenchymal stem cell	<a href="#">NCT02855112</a>	Tehran University of Medical Sciences (Iran)	I-II	June 2015	December 2016	IT	Every 3 weeks (3 doses tested)	Patients age under 12 month	-Evaluate changes in action potential of muscles and overall survival
	Pyridostigmine Bromide (Mestinon)	<a href="#">NCT02227823</a>	Centre Hospitalier Régional de la Citadelle (Belgium)	II	July 2014	July 2017	IV	3 times a day	Type 3 (with impaired NMJ)	-Evaluate safety and efficacy on the motor function
Neuroprotection (anti-inflammatory)	Celecoxib	<a href="#">NCT02876094</a>	Hugh McMillan, Children's Hospital of Eastern Ontario (Canada)	II	January 2019	July 2020	O	Once daily	Type 2 and 3	-Determine safety and AEs
Muscle-Enhancing drug	SRK-015	<a href="#">NCT03921528</a>	Scholar Rock, Inc. (United States)	II	April 2019	January 2021	IV	Once every 4 weeks	Type 2 and 3	-Evaluate the efficacy and safety
Muscle-Enhancing drug (potassium channel -blocking)	Amifampridine Phosphate	<a href="#">NCT03781479</a>	Catalyst Pharmaceuticals, Inc (Italy)	II	January 2019	December 2019	O	Doses 3 to 4 times a day	Type 3	-Evaluate safety, tolerability and efficacy in muscular function
		<a href="#">NCT03819660</a>	Catalyst Pharmaceuticals, Inc (Italy)	II	March 2019	December 2020	O	3 to 4 times a day	Type 3	-Determine long term safety, AE and SAEs

**Table 5. SMN independent therapies clinical trials (to October, 2019): 6 Studies found for SMA drug-interventional with an SMN independent approach in ClinicalTrials.gov. Status are: Active, recruiting (green); Active, not recruiting; Unknown (red). Abbreviations: Oral (O), intravenous (IV), intrathecal (IT), pharmacokinetics (PK), pharmacodynamics (PD), Adverse Events (AE), Serious Adverse Events (SAEs), Maximum Tolerated Dose (MTD).**



## 2.6. SMN models

Animal models are essential to understand the pathophysiology of the diseases. Likewise, animal models are necessary to identify and evaluate newly developed therapies (Edens et al., 2015; Monani and De Vivo, 2014; Schmid and DiDonato, 2007). SMA is an exclusively human disease, and given its complex genetic and molecular basis, its recreation in other species has postured serious challenges. Although the sequence and function of the SMN protein are conserved in all species during evolution, the gene duplication that created *SMN2* is unique to humans (reviewed in Wirth et al., 2017). Moreover, the complete deletion of the unique copy of the *Smn* gene in nonhumans animals is embryonic lethal (Schrank et al., 1997). Therefore, SMA animal models require a minimum level of SMN protein to be viable, either by the residual activity of their endogenous single *Smn* gene or by the presence of a human-*SMN2*-like gene.

### 2.6.1. *Schizosaccharomyces pombe*

The yeast model due to its simplicity has widely been used in the genetic study of basic eukaryotic cell biology. The two commonly used species are *Saccharomyces cerevisiae* (*S. cerevisiae*) and *Schizosaccharomyces pombe* (*S. pombe*), but only *S. pombe* has an ortholog of the human *SMN* gene known as *Yab8*, or *ySMN*, whereas *S. cerevisiae* has no demonstrable *SMN* ortholog (Owen et al., 2000).

In general, the *ySMN* gene translates a protein significantly similar to the human SMN at the amino and carboxy-terminal level but with a very poor internal homology. For instance, the *ySMN* lacks the RNA binding domain (Talbot et al., 1997). On the other hand, the *ySMN* protein is capable of binding to human SMN to form a complex. The location of the protein is both the nucleus and the cytoplasm, but the small size of *S. pombe* nucleus makes it impossible to characterize the subnuclear localization of *ySMN* (Paushkin et al., 2000).

The *ySMN* maintains the essentiality role for viability in *S. pombe* although this phenotype cannot be rescued by exogenously supplied human SMN. Overexpression of *ySMN* is not lethal but results in a deleterious phenotype of a retarded growth (Paushkin et al., 2000). These observations suggest an essential function of SMN conserved in eukaryotes and *S. pombe* model has occasionally been used to study protein interactions of SMN.

### 2.6.2. *Caenorhabditis elegans*

The *Caenorhabditis elegans* (*C. elegans*) genome contains a single *SMN* gene, which encodes a protein 36% identical to the human ortholog (Bertrand et al., 1999). The complete inactivation of the endogenous *C. elegans* *SMN* gene, the *Smn-1* gene, does not produce a total defect to the development of embryos, due to the relatively large maternal contribution of SMN protein to the fertilized oocyte. This effect occurs in this nematode, but also other invertebrates, such as the fruit fly *Drosophila melanogaster*, or fish models such as *Danio rerio* (Schmid and DiDonato, 2007). It is important to consider this limitation, especially when studying the effect of Smn protein on embryonic development. The elimination of the *smn-1* coding region through a null mutation, the *smn-1* (ok355) causes severe defects such as developmental arrest, lifespan reduction and progressive loss of motor functions (Briese et al., 2009). However, a point mutation in *smn-1*, the *smn-1* (cb131), that mimics a mutation of human SMA disease, causes minor disturbances, such as weak motor defects and a slightly reduced lifespan (Sleigh et al., 2011).

*C. elegans* as a model of SMA disease has been used extensively for the identification of phenotype modifying genes that may become potential therapeutic targets (Dimitriadi et al., 2010). One of the most promising identified genes is the small conductance calcium-activated K channel (SK channel) gene. SK channels are a type of ionic channel activated by increases of intracellular  $Ca^{2+}$  levels and are essential to regulate hyperpolarization caused by action potentials. When the SK channel was pharmacologically activated with Riluzole, the motor functions of the *C. elegans* mutant, *smn-1* (ok355), were improved. Subsequent studies in rat models with Smn deficiency showed that the same treatment restored axon growth in hippocampal neurons (Dimitriadi et al., 2013). Therefore, the *C. elegans* mutants represent an efficient tool to perform large-scale screens to discover unknown modifiers of SMN function.

### 2.6.3. *Drosophila melanogaster*

The *Drosophila* genome contains an orthologous copy of the *SMN* gene, the *Smn*, with a 41% sequence homology to the human gene. The expression of truncated forms of Smn in *Drosophila* causes dominant-negative developmental arrest in the pupal state and lethality (Miguel-Aliaga et al., 2000). Likewise, in the *Drosophila* models where the human *SMN1*

transgene containing SMA-causing mutations were introduced, it was observed a reduction in excitatory postsynaptic currents, disorganized MNs buttons, loss of glutamate receptors in the NMJs and compromised motor capacities (Chan et al., 2003).

*Drosophila* mutants are used as an SMA model, combining genetic screens and bioinformatics analyses to study genes that interact with *Smn*. Up to now, more than a hundred candidates of *Smn*-interacting genes have been identified including, RNA splicing factors (Sen et al., 2013), members of the BMP signalling pathways (Chang et al., 2008) and genes involved in endocytosis and RNA processing (Dimitriadi et al., 2010).

#### **2.6.4. Danio rerio**

*Smn* protein in zebrafish shares 49% homology with the human protein (Bertrand et al., 1999). As an SMA model, the first approach was to introduce an antisense morpholino (oligomer molecule commonly used to modify gene expression in zebrafish) to knockdown the endogenous protein (with ~ 60% *Smn* protein level reduction). The results showed many aspects of MNs defects previously observed in other models, including truncation and ectopic branching of motor axons (McWhorter et al., 2003). Mutations in the endogenous zebrafish gene that recapitulates SMA human mutations showed a deleterious phenotype characterized by reduced body axis length and overall size, and a selective decrease in the synaptic vesicle protein SV2 (Boon et al., 2009). Recently, a new transgene zebrafish SMA model was generated by expressing the human *SMN2* together with endogenous *smn* mutations to create a model genetically comparable to the human SMA pathology (Hao et al., 2011). Due to the easy genetic and molecular manipulation, the rapid and ex-utero development, zebrafish is an invaluable model to develop the knowledge of SMA disease development and progression, as well as to perform drug testing.

#### **2.6.5. Mus musculus**

From all current models to study the basic pathogenesis of SMA, the most relevant is the transgenic mouse models due to the similarities with the human neuromuscular system, and the facility of genetic manipulation. Mice contain a single *Smn* gene similar to the human *SMN1*. This orthologous contains the same "C" nucleotide at the +6 position on exon 7, and is located in mouse chromosome 13 in the region, equivalent to human chromosome 5q13 (DiDonato et al., 1997).

Homozygous removal of *Smn* in mice leads to an early embryonic lethal phenotype caused by massive cell death in the formation of blastocysts (Schrack et al., 1997). To circumvent this fatal phenotype multiple approaches have been developed to produce SMA models, from tissue-specific *Smn* knockout to human *SMN2* transgene introduction. Among the most notable effects, the specific knockout of *Smn* in neuronal cells produces a progressive loss of MNs and axon degeneration (Frugier et al., 2000), while the muscle tissue-specific knockout leads to muscle necrosis with a dystrophic phenotype ending in paralysis and death (Cifuentes-Diaz et al., 2001).

The introduction of several copies of human *SMN2* transgene allows embryonic survival while retaining the criteria for an SMA model. The severity of the phenotypic signs correlates with the number of the *SMN2* copies and the amount of full-length SMN protein produced, as it happens in human patients (Park et al., 2010; Schrack et al., 1997). For instance, *Smn*<sup>-/-</sup>; *SMN2* mice is one of the most severely affected SMA models that only produces around 15% of full-length *SMN2* transcript and typically do not survive after the first post-natal week (Monani et al., 2000). Conversely, the introduction of eight copies of the *SMN2* transgene expressed normal wild-type or even bigger levels of the SMN protein and is completely asymptomatic and indistinguishable from healthy, non-transgenic animals (Hsieh-Li et al., 2000; Monani et al., 2000). The same happens to heterozygous animals (*Smn*<sup>+/-</sup>) that do not develop the SMA phenotype (Bowerman et al., 2014; Schrack et al., 1997). These data provide direct evidence as it occurs in humans, SMA phenotype develops when the loss of at least 85% of the normal SMN levels is evident (Bowerman et al., 2012).

Recently other interesting mouse models have been generated. For example, the introduction of the partially functional human *SMN1* gene without exon 7 in the *Smn*<sup>-/-</sup>; *SMN2* mice, produces additional *SMN $\Delta$ 7* protein and increase survival for one week and presents severe motor deficits (Le et al., 2005), or the *Smn*<sup>2B/-</sup> mice that carry an endogenous mutation in the *Smn* gene that mimics the human *SMN2* gene and recreate an intermediate form of SMA with a significantly longer asymptomatic phase and an average lifespan of 30 days (Bowerman et al., 2012; Hammond et al., 2010).

Up to now, multiple mouse models of SMA have been developed over the years, recreating different ranges of the disease severity. Each of these models is useful to study different

aspects of the pathology and test therapeutic approaches. Severe mouse models of SMA have no chronic phase and are suitable for modelling severe infantile SMA. Whereas longer-lived mice that recreate intermediate forms of SMA are more suitable for the evaluation of non-SMN therapies or long-term defects in non-neuronal cells that might emerge over time. Thus mouse models remain an important system for increasing our understanding of the SMA disease process and in the evaluation of potential therapeutic approaches.

In reference to the mouse models used in this study, the specific information is detailed in the “Materials and methods” section.

Genotype	Molecular mutation	Phenotype	Survival	References
<i>Smn</i> <sup>-/-</sup> <i>Smn</i> <sup>-/-</sup> ; <i>SMN2</i> (2 <i>Hung</i> ) <sup>+/+</sup>	Knockout of endogenous <i>Smn</i> gene Knockout of endogenous <i>Smn</i> with a transgene of human <i>SMN2</i> , <i>SERF1</i> and part of <i>NAIP</i>	-Embryonic dead prior to uterine implantation -Rescues embryonic lethality of <i>Smn</i> <sup>-/-</sup> -Loss of thick myelinated MNs -Decreased MNs number -MNs axon degeneration -Decreased diameter of muscle fibres -Muscle atrophy -Subcutaneous edema -Low body weight -Paralysis -Respiratory distress	Embryonic lethal Transgene copy number correlates with disease severity, which ranges from death within 1 week to normal survival	(Schrank et al., 1997) (Hsieh-Li et al., 2000)
<i>Smn</i> <sup>-/-</sup> ; <i>SMN2</i> (89 <i>Ahmb</i> ) <sup>+/+</sup>	Knockout of endogenous <i>Smn</i> with a transgene containing the human <i>SMN2</i> locus	-Rescues <i>Smn</i> <sup>-/-</sup> – embryonic lethality -Vacant or partially occupied motor endplates -Abnormal neurofilament accumulations in presynaptic MNs -Decreased muscle fibre diameter -Low body weight -Paralysis -Respiratory distress	Transgene copy number correlates with disease severity, which ranges from death within 6 hours to normal survival	(Monani et al., 2000)
<i>Smn</i> <sup>F/Δ7</sup> ; <i>NSE-Cre</i> <sup>+</sup>	<i>Cre-loxP</i> -mediated heterozygous deletion of <i>Smn</i> exon 7 in neuronal cells	-Muscle denervation -Abnormal neurofilament accumulations in presynaptic MNs -Aberrant cytoskeletal organization -Neurogenic atrophy of skeletal muscle -Paralysis	Mean lifespan: 25 days	(Cifuentes-Diaz et al., 2002; Frugier et al., 2000)
<i>Smn</i> <sup>F/Δ7</sup> ; <i>HSA-Cre</i> <sup>+</sup>	<i>Cre-loxP</i> -mediated deletion of <i>Smn</i> exon 7 in myoblasts and post-mitotic fused myotubes of skeletal muscle in a constitutive heterozygous <i>Smn</i> Δ7	-Progressive myopathy -Extensive mononuclear cell infiltration -Necrosis of muscle fibres -variable muscle fibre diameter -Paralysis	Mean lifespan: 33 days	(Cifuentes-Diaz et al., 2001)

<i>Smn</i> <sup>+/-</sup> ; <i>Gemin2</i> <sup>+/-</sup>	Heterozygous deletion of <i>Smn</i> and <i>Gemin2</i>	-Enhanced MNs degeneration -Reduction of Sm protein levels in MNs nucleus -Defect in snRNP assembly	Still alive at 150 days (5 months)	(Jablonka et al., 2002)
<i>Smn</i> <sup>-/-</sup> ; <i>SMN2</i> (89A <i>hmb</i> ) <sup>+/-</sup> ; <i>SMN1</i> (A2G) <sup>+/-</sup>	Knockout of endogenous <i>Smn</i> with heterozygous human <i>SMN2</i> expression and the human <i>SMN1</i> carrying the A2G missense mutation	- MNs degeneration -Axon degeneration, loss and sprouting -Muscle atrophy -Abnormal EMG patterns -Muscle weakness -Reduced activity	Mean lifespan: 227 days (7-8 months)	(Monani et al., 2003)
<i>Smn</i> <sup>+/-</sup> ; <i>HSA-Cre</i> <sup>+</sup>	<i>Smn</i> <sup>+/-</sup> mice with Cre- <i>loxP</i> -mediated deletion of <i>Smn</i> exon 7 in post-mitotic fused myotubes of skeletal muscle.	-Motor performance similar to controls within the first 6 month of age -Severe myopathic process -No affection of satellite cells -Severe reduction of muscle mass	Mean lifespan: 240 days (8 months)	(Nicole et al., 2003)
<i>Smn</i> <sup>+/-</sup> ; <i>NSE-Cre</i> <sup>+</sup>	<i>Smn</i> <sup>+/-</sup> mice with Cre- <i>loxP</i> -mediated deletion of <i>Smn</i> exon 7 in neuronal tissue	-Progressive axonal degeneration -Progressive loss of MNs in the spinal cord -MNs atrophy	Mean lifespan: 31 days	(Ferri et al., 2004)
<i>Smn</i> <sup>+/-</sup> ; <i>Alfp-Cre</i> <sup>+</sup>	<i>Smn</i> <sup>F7/F7</sup> mice with Cre- <i>loxP</i> -mediated deletion of <i>Smn</i> exon 7 in hepatocytes	-Dramatic liver atrophy -Severe liver dysfunction -Iron overload -Lack of regeneration	Late embryonic lethality at E18	(Vitte et al., 2004)
<i>Smn</i> <sup>-/-</sup> ; <i>SMN2</i> (89A <i>hmb</i> ) <sup>+/-</sup> ; <i>SMNΔ7</i> <sup>+/-</sup>	Transgene containing human <i>SMN2Δ7</i> cDNA in the <i>Smn</i> <sup>-/-</sup> ; <i>SMN2</i> <sup>+/-</sup> background	-Decreased body weight -Impaired righting response -Abnormal gate -Impaired balance and limb coordination -Skeletal muscle fibre atrophy -Abnormal cardiac morphology and function	Mean lifespan: 15 days	(Le et al., 2005)
<i>Smn</i> <sup>-/-</sup> ; <i>SMN2</i> <sup>+/-</sup> ; <i>SMN1</i> (A111G) <sup>+/-</sup>	<i>SMN1</i> transgene containing the human allele A111G (SMA type 1 and 2) in the <i>Smn</i> <sup>-/-</sup> ; <i>SMN2</i> <sup>+/-</sup> background	-Low snRNP assembly activity -Hypertrophy of gastrocnemius fibres -No obvious SMA phenotype	Survival over 1 year	(Workman et al., 2009)
<i>Smn</i> <sup>-/-</sup> ; <i>SMN2</i> <sup>+/-</sup> ; <i>SMN1</i> (VDQNKKE) <sup>+/-</sup>	<i>SMN1</i> transgene containing exons 1-6 with an additional motif in the <i>Smn</i> <sup>-/-</sup> ; <i>SMN2</i> <sup>+/-</sup> background	-Low snRNP assembly activity	Lifespan from 2 to 6 days	(Workman et al., 2009)

<i>Smn</i> <sup>2B/-</sup>	Knock in heterozygous mice with an <i>Smn</i> gene harbouring three nucleotide substitutions within the exonic splicing enhancer of exon 7	-Smaller body size -MNs number reduction -Increase in profilin Ila staining intensity -Reduced levels of plastin 3 protein -Sarcomeric defects	Mean lifespan: 28 days	(Bowerman et al., 2009)
<i>Smn</i> <sup>-/-</sup> ; <i>SMN2</i> ( <i>N11</i> ) <sup>+/+</sup> ; <i>SMN2</i> ( <i>N46</i> ) <sup>+/+</sup>	Mice with knock out of endogenous <i>Smn</i> with three copies of the human <i>SMN2</i> transgene. Generated by crossing the strains N11 (that carries one copy of <i>SMN2</i> on chromosome 18) and N46 (that carries two <i>SMN2</i> copies at a single insertion site on chromosome 3)	-Diminished weight gain -Muscle weakness Reduced ability to perform in the negative geotaxis test -Behavioural defects in the tube and in the rope tests -Reduced Compound Muscle Action Potential amplitude and extended latency and duration -Sensory defects -MNs loss -Degeneration and decrease in the number of myelinated axons -Decrease in muscle fibre diameter -Neurofilament accumulation at the synaptic boutons -NMJ disorganization -Denervated endplates -Respiratory impairments	Mean lifespan: 14 days	(Michaud et al., 2010)
<i>Smn</i> <sup>+/+</sup> ; <i>SMN2</i> ( <i>89Ahmb</i> ) <sup>+/+</sup> ; <i>Olig2-Cre</i> <sup>+</sup>	<i>Smn</i> <sup>+/+</sup> ; <i>SMN2</i> <sup>+/+</sup> mice with <i>Cre-loxP</i> -mediated deletion of <i>Smn</i> exon 7 in spinal cord motor neuron progenitor cells	- Neuromuscular weakness -Peripheral and central synaptic defects -Electrophysiological abnormalities of the NMJ -Muscle atrophy -MNs degeneration	~70% of mutants survived up to 12 months	(Park et al., 2010)
<i>Smn1</i> <sup>tm1Cald/tm1Cald</sup> ; <i>Cre</i> <sup>Esr1</sup> and <i>Smn1</i> <sup>tm2Cald/tm2Cald</sup> ; <i>Cre</i> <sup>Esr1</sup>	Cre inducible hypomorphic <i>Smn</i> alleles that mimic <i>SMN2</i> splicing. Are specifically designed to generate each three independent lines (homozygous, heterozygous and by Cre induction)	-When Cre induction at early embryonic state rescue embryonic lethality -Heterozygous have no SMA phenotype	Homozygous alleles are embryonic lethal (E12.5-E15.5); Heterozygous have normal lifespan	(Hammond et al., 2010)

**Table 6. Mouse models of SMA. Mouse models with different cellular levels of *Smn*, allow the dissection of biological processes and assessment of gene and protein function in a mammalian context and are a useful preclinical tool for testing potential therapies.**



### 3. Autophagy

The term 'autophagy', literally meaning "self-eating", was first coined by Christian de Duve in 1963 referring to a previous observation made by Keith R. Porter and his student Thomas Ashford at the Rockefeller Institute, where they described lysosomes-like structures containing mitochondria and other intracellular structures in rat liver perfused with glucagon (Deter and De Duve, 1967). Nowadays we know that the pathway involves the formation of unique structures that sequester the target cargos, engulf and deliver them into the lysosome for degradation (Dikic and Elazar, 2018; Ravanan et al., 2017).

This self-digesting mechanism is an essential and highly regulated pathway that in physiological conditions plays a "housekeeping" role by removing non-functional long-lived, aggregated and misfolded proteins, clearing damaged organelles, such as mitochondria, endoplasmic reticulum (ER) and peroxisomes, and eliminating intracellular pathogens. Therefore, autophagy has been linked to a variety of biological functions related to development, cellular differentiation, defence against pathogens, oxidative stress and nutritional starvation (Badadani, 2012). Moreover, its deregulation has also been related to non-apoptotic cell death (Edinger and Thompson, 2004).

Autophagy is conserved throughout the eukaryotes and is present in all species from slime mould to mammals, passing through plants, worms, flies and fish, allowing the study of its molecular machinery of regulation and execution in model organisms such as yeasts, principally *Saccharomyces cerevisiae*. Currently, 32 different **autophagy-related genes (Atg)** have been identified by genetic screening in yeast permitting the identification of their respective orthologues in other species (King, 2012; Nakatogawa et al., 2009).

Based on the mechanism by which intracellular materials are delivered for degradation, three forms of autophagy have been identified: microautophagy, chaperone-mediated autophagy and macroautophagy (Hayat, 2017).

- **Microautophagy** is the degradation process where the cellular contents are directly taken up by invaginations of the lysosomal membrane without any vesicular transport.

- **Chaperone-mediated autophagy**, the targeted proteins containing a consensus KFERQ sequence are recognised by the chaperon protein HSC70. The proteins are then translocated across the lysosomal membrane by a membrane receptor called LAMP-2A (lysosomal-associated membrane protein 2A) resulting in their unfolding and degradation. This process is highly specific as the cargo's recognition and degradation is only made for the proteins that have the consensus sequence.

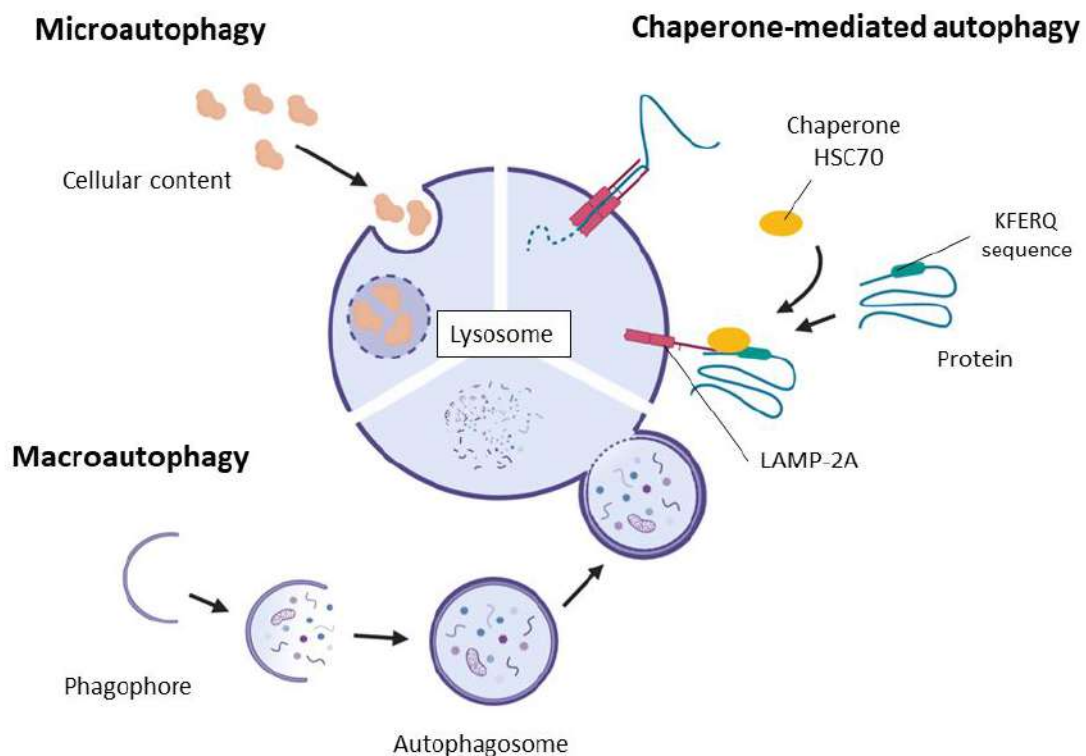


**Figure 19. Autophagy types in mammalian cells.** Microautophagy involves the direct uptake of the cargo through invagination of the lysosomal membrane without vesicular transport. Chaperone-mediated autophagy degrades individual proteins that contain the KFERQ recognition sequence. The targeted protein enters the lysosome directly through the LAMP-2A membrane receptor. Macroautophagy is based on the formation of double-membrane cytosolic vesicles, called autophagosomes, to sequester and transport the cargo to the lysosome. The three types of autophagy lead to degradation of the cargo and release of decomposition products back into the cytosol for reuse by the cell (Based on Hayat, 2017).

- **Macroautophagy**, usually referred to as autophagy, among the three types, is the major prevalent pathway used by cells to remove the damaged cellular organelles and other related debris. This form of autophagy delivers cytoplasmic cargo to the lysosome through the formation of special double-membrane structures called autophagosomes. These intermediary vesicles entrap the cellular contents and targeted proteins and eventually fuses with the lysosome to form an autophagolysosome.

### 3.1. Autophagy machinery

Autophagy is a highly regulated pathway active at basal levels in most cell types. However, autophagy can be activated in response to several stress conditions, such as nutrient deprivation and/or low cellular energy levels, and mediating signalling pathways that converge to the autophagosome formation (He and Klionsky, 2009). Once an autophagy activation signal is induced, the process is orchestrated in five key stages: initiation, phagophore nucleation, phagophore elongation, fusion with the lysosome and degradation by lysosomal proteases of engulfed molecules.

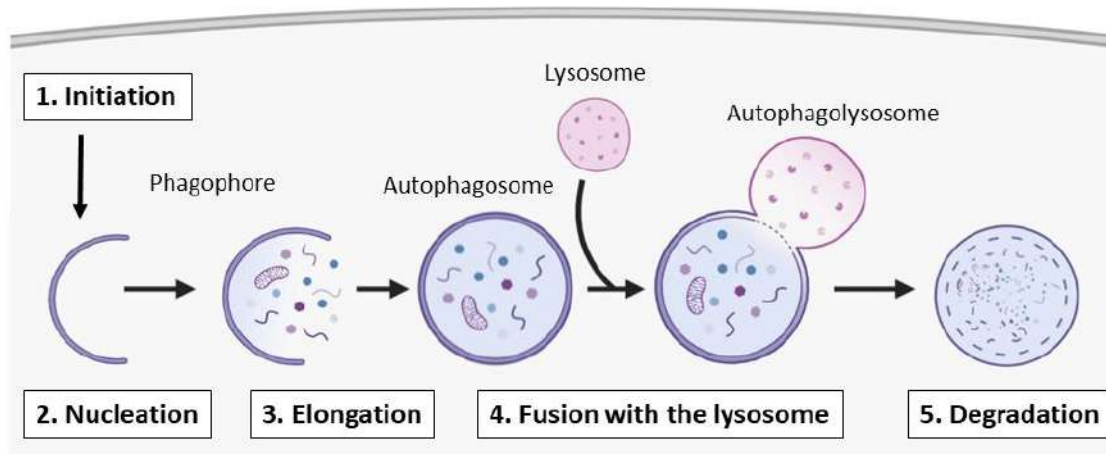


**Figure 20. Steps during the autophagy process.** 1. Initiation of the process by activation of the autophagy signalling pathways. 2. Autophagosome nucleation. 3. Elongation and capture of cytoplasmic components, to form the autophagosome. 4. Fusion of the autophagosome with the lysosome to form the autophagolysosome. 5. Degradation of the cargo by the hydrolases from the lysosome.

### 3.1.1. Initiation

#### Autophagy signalling pathways

Among several components involved in the tight regulation of autophagy, mTORC1 is a key player directing the autophagy pathway in response to environmental and physiological stresses. However, apart from the regulation of autophagy by mTORC1, several mTOR-independent autophagy pathways have been described.

#### *mTOR-dependent autophagy pathway*

The classical regulation of autophagy is ruled by the target of rapamycin (mTOR) kinase, which negatively regulates this process. The serine/threonine-protein kinase mTOR is a signalling control point downstream of growth factor receptor signalling, hypoxia, ATP levels and insulin signalling. This kinase nucleates two structurally and functionally different complexes named mTOR complex 1 (mTORC1) and mTOR complex 2 (mTORC2) (Kim and Guan, 2015; Paquette et al., 2018).

mTORC1 consists of the catalytic subunit Raptor (regulatory-associated protein of mTOR), PRAS40 (proline-rich Akt substrate of 40 kDa), mLST8 (mammalian lethal with SEC13 protein 8) and DEPTOR (DEP-domain containing mTOR-interacting protein). On the other hand, mTORC2 comprises mLST8 (mammalian lethal with SEC13 protein 8,) Rictor (rapamycin sensitive companion of mTOR), mSin1 (mammalian stress-activated mitogen-activated protein kinase-interacting protein 1) and Protor (protein observed with rictor) subunits (Laplanche and Sabatini, 2012; Ravanan et al., 2017). Essentially, autophagy is controlled by mTORC1 and only an indirect effect on autophagy through mTORC1 activation was reported for mTORC2 (Oh et al., 2010; Zinzalla et al., 2011).

In mammalian cells, Atg13 binds to FIP200 through the mediation of Unc-51-like kinase 1 (ULK1) protein to form the stable complex ULK1–Atg13–FIP200 (RB1-inducible coiled-coil protein 1). This complex is responsible to initiate the autophagic pathway downstream of mTORC1. Under growth-promoting conditions, mTOR kinase is activated downstream of Akt kinase and PI3-kinase to inhibit autophagy and promote growth through induction of ribosomal protein expression and increased protein translation. This autophagy inhibition is due to the direct interaction of mTORC1 with the ULK1–Atg13–FIP200 complex

phosphorylating and inactivating the kinase activity of Atg13 and ULK1. Conversely, during starvation conditions, mTORC1 is inhibited by the activity of Tsc1 and Tsc2 (Tuberous sclerosis complex 1 and 2) dissociating from the ULK1–Atg13–FIP200 complex. This leads to dephosphorylation and activation of ULK1 which phosphorylates Atg13, FIP200 and ULK1 itself. In consequence, autophagy is activated promoting the recycling of intracellular constituents as a source of energy (Ganley et al., 2009; Hosokawa et al., 2009; Jung et al., 2009; Sarkar, 2013).

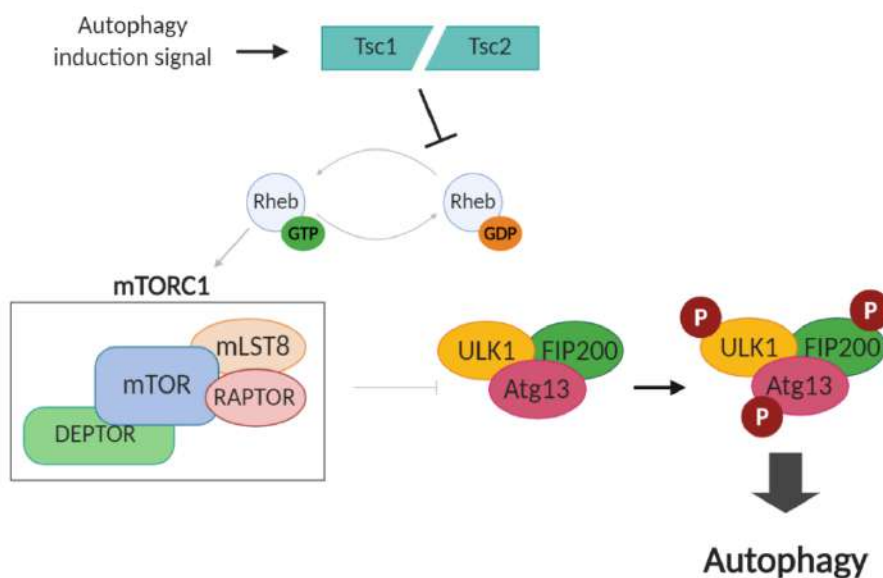


**Figure 21. Initiation of autophagy via the mTOR pathway.** When autophagy inducing signal starts the Tsc1 and Tsc2 proteins are activated and indirectly inhibit mTORC1. The inactivation of mTORC1 allows the activation of the ULK1-Atg13-FIP200 complex.

### ***mTOR-independent autophagy pathway***

Aside from the regulation of autophagy by mTORC1, several mTOR independent autophagy pathways have been described. Those pathways are in most cases chemical perturbations that are able to induce autophagy and facilitate the clearance of autophagy substrates without inhibiting mTOR activity. For example, increases in the levels of Inositol(1,4,5)P<sub>3</sub>, also known as Inositol triphosphate (I<sub>3</sub>P), or the second messenger cAMP, inhibit the autophagosome synthesis (Noda and Ohsumi, 1998; Sarkar et al., 2005). In these cases, autophagy is modulated without affectation of mTOR activity, but the exact mechanism by

which it occurs is virtually unknown. Nevertheless, it is interesting to highlight that both, cAMP and I3P signalling converges into an increase of cytosolic  $\text{Ca}^{2+}$ .

Subsequent studies have found that elevation of cytosolic  $\text{Ca}^{2+}$  may have complex effects in autophagy impairment, at the level of both autophagosome formation and autophagosome-lysosome fusion. Increases of cytosolic  $\text{Ca}^{2+}$  can activate calpains, which are calcium-dependent cysteine proteases (Goll et al., 2003) and some evidences suggest that calpain is a downstream mediator of the autophagy-regulatory effects of free cytosolic  $\text{Ca}^{2+}$  (Williams et al., 2008). Moreover, calpains have been related to the cleavage multiple autophagic proteins (Weber et al., 2019), including Beclin 1 (Russo et al., 2011) and Atg5 (Yousefi et al., 2006).

### **3.1.2. Phagophore nucleation**

During the first step of the autophagosome formation in mammals, cytoplasmic components including organelles, are sequestered by a unique membrane structure called phagophore (Hurley and Young, 2017).

This process is initiated after the activation of the ULK1 kinase activity that phosphorylates Atg13, FIP200 and ULK1 itself. Once phosphorylated, the 3 proteins form a complex with Atg101 and triggers the phagophore nucleation by phosphorylating components of the class III PI3K (PI3KC3) complex I. The PI3KC3 complex I is the main responsible of phagophore nucleation and is formed by: the class III PI3K vacuolar protein sorting 34 (VPS34), Beclin 1, Atg14, the activating molecule in Beclin 1-regulated autophagy protein 1 (AMBRA1) and the general vesicular transport factor (p115) (Dikic and Elazar, 2018; Hurley and Young, 2017).

One of the most important phosphorylations by ULK1 is in AMBRA1 which induces its dissociation and translocates from the dynein motor complex to the ER where binds Beclin 1 (Di Bartolomeo et al., 2010). Active Beclin 1 selectively involved VPS34 in the autophagy process and promotes its catalytic activity. VPS34 is unique amongst PI3-kinases and is the only enzyme to be assigned as class III in mammals. VPS34 only uses phosphatidylinositol (PI) as a substrate to generate phosphatidylinositol triphosphate (PI3P), which is an essential component for the nucleation of the phagophore and recruitment of other Atg proteins (Nascimbeni et al., 2017).

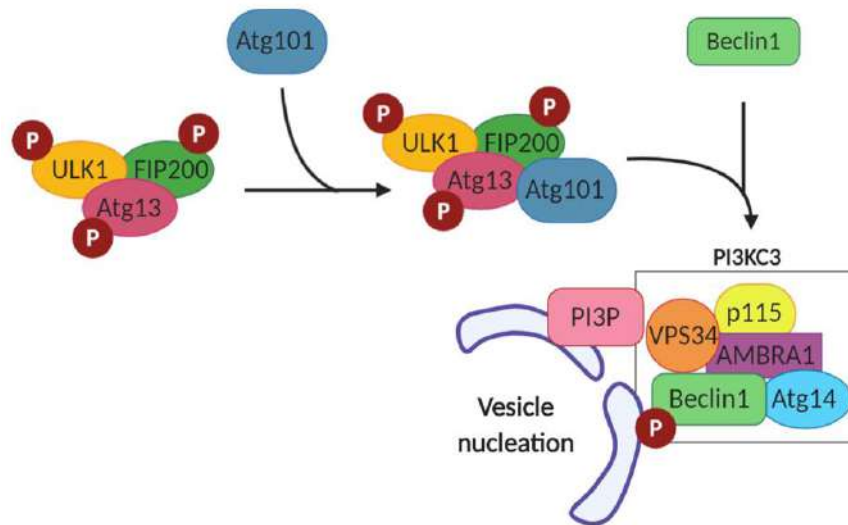


**Figure 22. Autophagosome nucleation signalling pathway.** When the ULK1-Atg13-FIP200 complex is activated binds to Atg101. The formed complex triggers the phagophore nucleation by phosphorylating components of the class III PI3K (PI3KC3) complex (VPS34, Beclin 1, Atg14, AMBRA1, p115).

### Membrane source

The source of the autophagosome membrane is still a controversial area in an active investigation. It is known that the phagophore derives from lipid bilayer, forming a double-membraned structure that is in dynamic equilibrium with other cytosolic membrane structures (Tooze and Yoshimori, 2010). Different autophagosome sources have been suggested in mammalian cells like ER (Hayashi-Nishino et al., 2009), mitochondria (Hailey et al., 2010), Golgi apparatus (Ge et al., 2013), endosomal compartments (Orsi et al., 2012), plasma membrane (Puri et al., 2013) and nuclear envelope (English et al., 2009). Moreover, given the relative lack of transmembrane proteins in the autophagosomal membranes, it is not yet possible to completely exclude *de novo* membrane formation from cytosolic lipids, although it has only been demonstrated in yeast (Noda et al., 2002). Nonetheless, in eukaryotes, autophagosome membranes seem to initiate primarily from the ER, since phagophore membranes were observed cradled and interconnected within a subdomain of the ER (Axe et al., 2008; Hamasaki et al., 2013; Hayashi-Nishino et al., 2009; Ylä-Anttila et al., 2009).

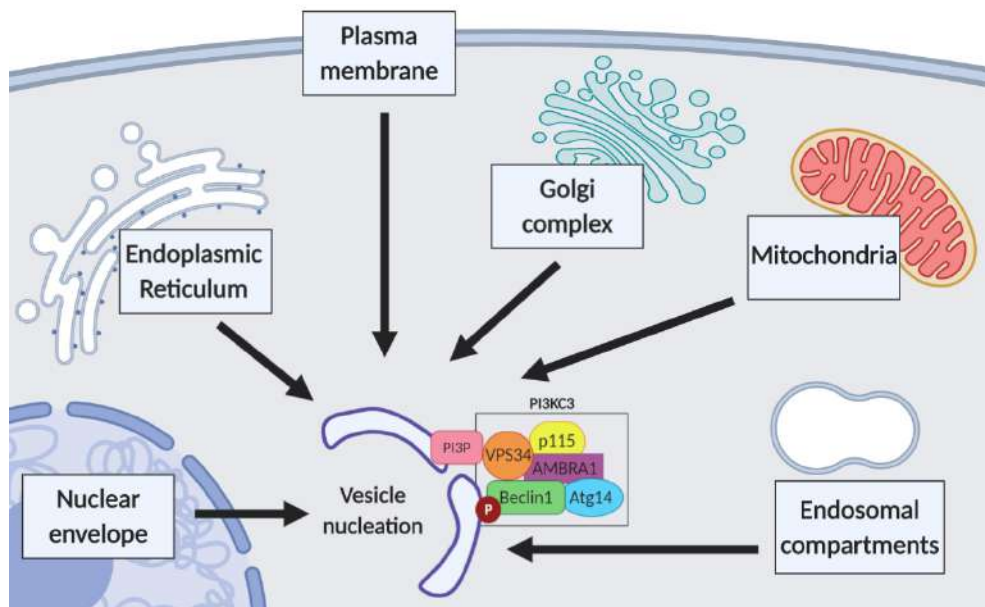


**Figure 23. Potential phagophore membrane sources.** Up to now, it has been suggested that the double-membraned structure can be formed from ER, mitochondria, Golgi apparatus, endosomal compartments, plasma membrane and nuclear envelope.

### 3.1.3. Phagophore elongation

During phagophore elongation, the double-membrane structure expands to engulf the intracellular cargo as a simple sequestration process where no degradation occurs. The entire elongation mechanism is undertaken by two ubiquitin-like systems that are crucial in autophagy, the Atg5-Atg12 conjugation step and the LC3 processing step (Glick et al., 2010; Kirkin et al., 2009).

#### Atg5-Atg12 conjugation

The Atg5-Atg12 complex formation starts with the E1 like enzyme Atg7, which binds to a glycine residue of Atg12 monomer in an ATP-dependent manner. Activated Atg12 is covalently linked to Atg5 by the action of the E2- like Ub carrier protein Atg10. Conjugated Atg5-Atg12 complexes in pairs link with Atg16L dimers to form the multimeric complex Atg5-Atg12-Atg16L. This complex associates with the extending phagophore, adding the proper curvature of the phagophore and is essential for the LC3 lipidation (Otomo et al., 2013). Atg5-Atg12 conjugation is independent of autophagy activation. Moreover, once



the autophagosome is formed Atg5–Atg12–Atg16L dissociates from the membrane to degradation, making conjugated Atg5–Atg12 as a relatively poor marker of autophagy (Glick et al., 2010).

### **LC3 processing**

The E1-like enzyme Atg7 also participates in the second Ub-like system involved in autophagosome formation, activating the processed LC3 (microtubule-associated protein light chain 3). Pro-LC3 is expressed in most cell types as a full-length cytosolic protein. When autophagy is induced pro-LC3 is proteolytically processed at its C-terminal end by the cysteine protease Atg4, generating LC3I and exposing a glycine residue that is essential for its conjugation with phosphatidylethanolamine (PE). Then, Atg7 activates LC3I in an ATP-dependent manner and transfers it to Atg3 (a different E2-like carrier protein) that conjugate PE to the carboxyl group on the glycine residue to generate a membrane-anchored lipidated form of LC3, known as LC3II (Eskelinen, 2005).

LC3II is recruited and integrated into the inner and outer surface of the growing phagophore. LC3II induces the elongation and sealing of the phagophore to form the double membrane structure called autophagosome and participates in the cargo selection for degradation. For efficient LC3 recruitment, Atg3 requires stimulation of Atg5–Atg12 conjugate. Thus, LC3 processing is increased during autophagy and remains associated with the autophagosome membrane until the fusion with the lysosome occurs. After this, the LC3II at the inner surface is degraded along with the cargo, while the LC3II at the outer surface of the membrane dissociates and degrades through the proteasome. This makes the processed LC3 levels a key marker to measure autophagy levels in cells (Glick et al., 2010; Tanida et al., 2008; Tanida and Waguri, 2010).

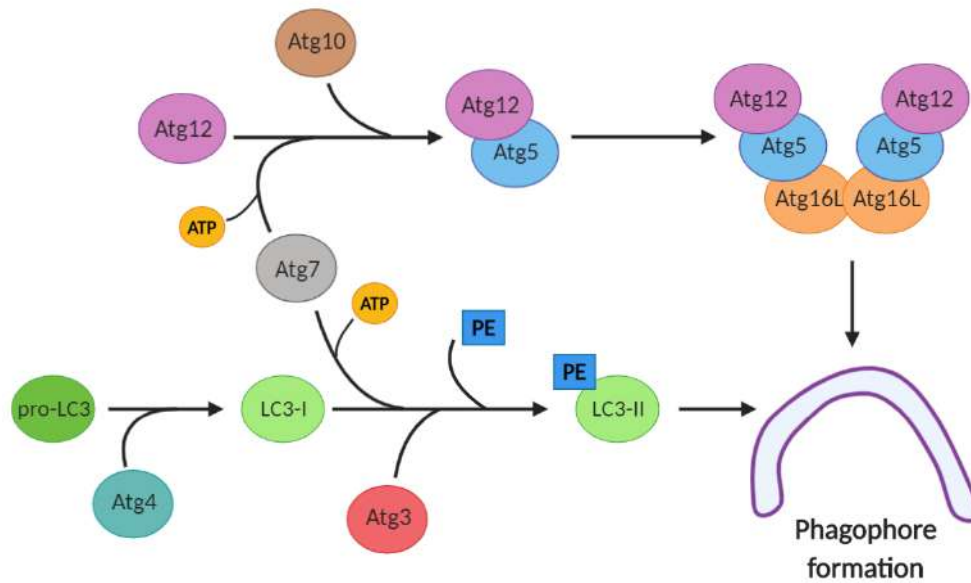


**Figure 24. Phagophore elongation signalling pathway.** The binding of a glycine molecule to Atg12 by the action of the enzyme Atg7 promotes its binding to Atg5 thanks to the carrier protein Atg10. Pairs of conjugated Atg5 – Atg12 complexes link with Atg16L dimers to form the multimeric complex Atg5 – Atg12 – Atg16L. On the other hand, pre-LC3 is processed by Atg4 exposing a glycine residue that is essential for its conjugation to PE by Atg7 and Atg3.

### Selection of cargo

Autophagy was initially characterized as an indiscriminate degradation system that randomly englobes cytoplasmic content induced by nutrient deprivation, but recent studies clearly have shown that autophagy has a selectivity of the substrate (Stolz et al., 2014). In a well-known example, aggregates or aberrant-folded proteins are tagged with polyUb chains which are recognized by the receptor Sequestosome 1 (SQSTM1)/p62 through its ubiquitin-binding domain (UBD) (Bjørkøy et al., 2005; Liu et al., 2016; Pankiv et al., 2007). There are other UBD-containing receptors such optineurin (OPTN) (Wild et al., 2011), TOLL-interacting protein (TOLLIP) (Lu et al., 2014), Tax1 binding protein 1 (TAX1BP1), nuclear dot protein 52 (NDP52)/CALCOCO2 (Newman et al., 2012), and 26S proteasome regulatory subunit (RPN10) (Marshall et al., 2015) with similar functions. All these receptors have in common an LC3-interacting region (LIR) motif in their sequences that binds with LC3. Therefore, these receptors function as a bridge between Ub cargo and autophagosomes, enhancing the incorporation of the cargo into these structures for subsequent lysosomal degradation (Bjørkøy et al., 2005; Pankiv et al., 2007).

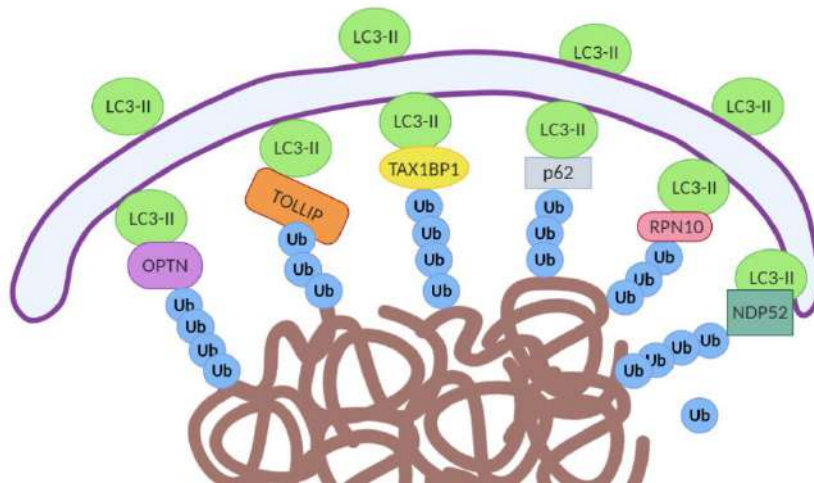


**Figure 25. Cargo selection in the autophagy vesicles in mammals.** Autophagy is a selective degradation system where ubiquitinated aggregated proteins are recognized by cargo receptors. These receptors have in common an LC3-interacting region (LIR) motif in their sequences that allows interaction with the LC3II.

#### 3.1.4. Lysosomal fusion and degradation

Once the expanding ends of the phagophore completely fuse to form the autophagosome, the next step of maturation in the autophagy process is its fusion with the specialized endosomal compartment lysosome to form the autophagolysosome (Klionsky et al., 2014). Some studies have suggested that previous to the fusion with the lysosome, the autophagosome fuse with early and late endosomes. This union is known as amphisomes and provides to the nascent autophagosomes the machinery and pH conditions that are required for lysosome fusion (Eskelinen, 2005; Tooze et al., 1990). The autophagosome formation is relatively understudied but, the small G protein Rab7 and the cytoskeleton have an important role in this part of the process (Gutierrez et al., 2004; Jäger et al., 2004; Webb et al., 2004).

When this self-degradative process starts lysosomal acid proteases and hydrolases degraded indistinctly the inner membrane of the autophagosome and the cytoplasm-contained materials. Regarding the enzymes involved in the degradation process, cathepsin proteases B and D are the best known (Koike et al., 2005) but Lamp-1 and Lamp-2 are also critical for functional autophagy maturation, as the targeted deletion of these proteins inhibits the process (Tanaka et al., 2000). Degraded material forming monomeric units

(mainly amino acids) is exported to the cytosol by the lysosomal amino acid transporter 1 and 2 (LYAAT-1 and LYAAT-2, respectively) to be reused. Other amino acid effluxers and vacuolar permeases have been postulated that can participate in the process, but so far they have not been found in mammals. The contribution of autophagy to reuse other macromolecules such as lipids and carbohydrates is unknown (Sagné et al., 2001).

### **3.2. Autophagy and neurodegeneration**

As mentioned, autophagy is essentially a recycling process of biosynthetic building blocks that help to maintain cell viability. Active autophagy is particularly important for neurons to sustain homeostasis. Neurons are post-mitotic cells that must survive for an entire lifetime and consequently cannot dilute out proteotoxins by cell division. These cells also present the unique, highly complex and polarized morphology of an extended axon. This structure essentially works for communication between neurons by carrying electrical and chemical information over long distances (up to 1 meter in length in adult humans) (Maday, 2016). These particularities make it critical for neurons to have robust quality control mechanisms to ensure protein quality and organelles to support their long-term viability and functionality.

In a healthy nervous system, autophagy has been related, to the elimination of aggregated and misfolded proteins and damaged organelles. Additionally, it is involved in the regulation of neurogenesis and developmental organization processes (Fimia et al., 2007), support of neuronal stem cell pools (Komatsu et al., 2007) and ensuring axonal homeostasis (Wang et al., 2013).

The importance of autophagy in neuronal viability is further emphasised by the ubiquitous deletion of core autophagy genes in various animal models. In the absence of autophagy, these studied models suffer from embryonic lethality to a neurodegenerative phenotype, characterized by the accumulation of ubiquitylated protein aggregates, axonal swelling and neuronal death (Hara et al., 2006; Komatsu et al., 2006). Furthermore, during the aging process, the deterioration capacity of the proteasome activity overloads the autophagy system (Dikic, 2017) inducing an accumulation of intraneuronal aggregates of misfolded proteins (Ravikumar et al., 2002).

All these evidences strongly suggest that autophagy dysregulation may play an important role in neurodegenerative disorders, like Amyotrophic Lateral Sclerosis (ALS), Parkinson disease (PD), Alzheimer disease (AD), and Huntington disease (HD), where the accumulation of misfolded proteins is a common pathological hallmark (reviewed in Menzies et al., 2015). Furthermore, analysis of post-mortem brain samples from PD, ALS and HD patients have shown dysfunctional lysosomes and dysregulation of autophagy (Fujikake et al., 2018; Guo et al., 2018).

In HD, the accumulation of autophagosomes is caused by the sequestration and inactivation of mTOR and p62 by mutant huntingtin protein which leads to an increase of autophagosome formation and impaired in cargo loading (Martinez-Vicente et al., 2010; Sarkar and Rubinsztein, 2008). Mutant huntingtin also inactivates Rhes, an autophagy regulator that accelerates autophagy by inhibiting the interaction of Beclin 1 with Bcl-2 (Mealer et al., 2014). Comparable results were obtained in ALS, where it was described a reduction of functional receptors for selective autophagy (p62, optineurin and TBK1) producing disruption of autophagic degradation of mutant SOD1 and TDP-43 proteins (Gal et al., 2009; Teyssou et al., 2013) and reduction of dysfunctional mitochondria clearance (Richter et al., 2016). In contrast, during PD pathogenesis inclusions of  $\alpha$ -synuclein have shown to specifically affect autophagy activity during the maturation of autophagosomes and their fusion with lysosomes, exacerbating pathogenic mechanisms (Button et al., 2017; Sánchez-Danés et al., 2012; Tanik et al., 2013). Furthermore, mutations of Parkin pathway disrupt lysosomal pH maintenance and autophagosome-lysosome fusion, producing defects in the mitophagy process (Chen et al., 2017).

Several studies of autophagy in AD pathogenesis have reported the degradation of the neurotoxic extracellular beta-amyloid (A $\beta$ ) plaques by autophagy and the presence of autophagosome vesicles in the affected cells (Nixon et al., 2005; Yu et al., 2005). Likewise, it has been observed that in AD patients Beclin 1 is transcriptionally suppressed (Pickford et al., 2008). Genetic studies have also identified additional proteins involved in autophagy during AD, such as the phosphatidylinositol binding clathrin assembly protein (PICALM), an endocytic trafficking regulator involved in autophagosome formation and maturation (Moreau et al., 2014).

Taken together, evidences indicate the important role of autophagy and its dysregulation in the pathogenesis of neurodegenerative diseases. However, exact mechanisms of autophagy alterations and regulations remain to be further investigated to be able to develop new and efficient therapeutic strategies.

## 4. Calpain

### 4.1. Calpain family

Calpains are an evolutionarily conserved family of proteases derived from an ancestral branch of the superfamily of the papains (Marchler-Bauer et al., 2009). The name of calpain comes from **Calcium** ion-dependent **papain**-like cysteine protease (Suzuki, 1991). In 1964, the first member of the family was described in rat brain (Guroff, 1964) and all members are characterized by calcium-dependent activity and a well-conserved cysteine protease domain called CysPc motif (Campbell and Davies, 2012; Goll et al., 2003).

Humans express 15 calpain genes, named from CAPN1 to CAPN3 and from CAPN5 to CAPN16, two calpain small regulatory subunit genes, CAPNS1 and CAPNS2, and one calpastatin gene, CAST. Each of these calpain genes generates one or more transcripts to constitute a whole calpain family of more than 50 molecules (Ono et al., 2016a; Sorimachi et al., 2011).

The two most extensively studied calpains are the ubiquitous mammalian  $\mu$ -calpain and m-calpain (also called calpain I and calpain II) which are activated *in vitro* by micromolar and millimolar  $\text{Ca}^{2+}$  concentration, respectively. Both are heterodimers consisting of a common smaller calpain regulatory subunit (CAPNS1) and a different, larger catalytic calpain subunit (CAPN1 and CAPN2, respectively). CAPN1 and CAPN2 are almost 60% identical in their protein sequences (Goll et al., 2003; Ono and Sorimachi, 2012).

The domain structure of the **catalytic subunits** of  $\mu$ -calpain and m-calpain defines the term "classical" calpains. This "classical" structure is composed by the catalytic domain CysPc, the C2L (Calcium-binding motif) domain and PEF (Penta EF-hand) domain. The group includes nine out of the fifteen calpains, CAPN 1, 2, 3, 8, 9 and 11 to 14. The presence of the

PEF domain is structurally important since it is involved in dimerization, either heterodimerization with the small subunits or homodimerization (Maki et al., 2002). On the other hand, “non-classical” calpains, CAPN 5, 6, 7, 10,15 and 16, are the ones that contain the CysPc but exclude C2L and/or PEF domains (Sorimachi et al., 1993).

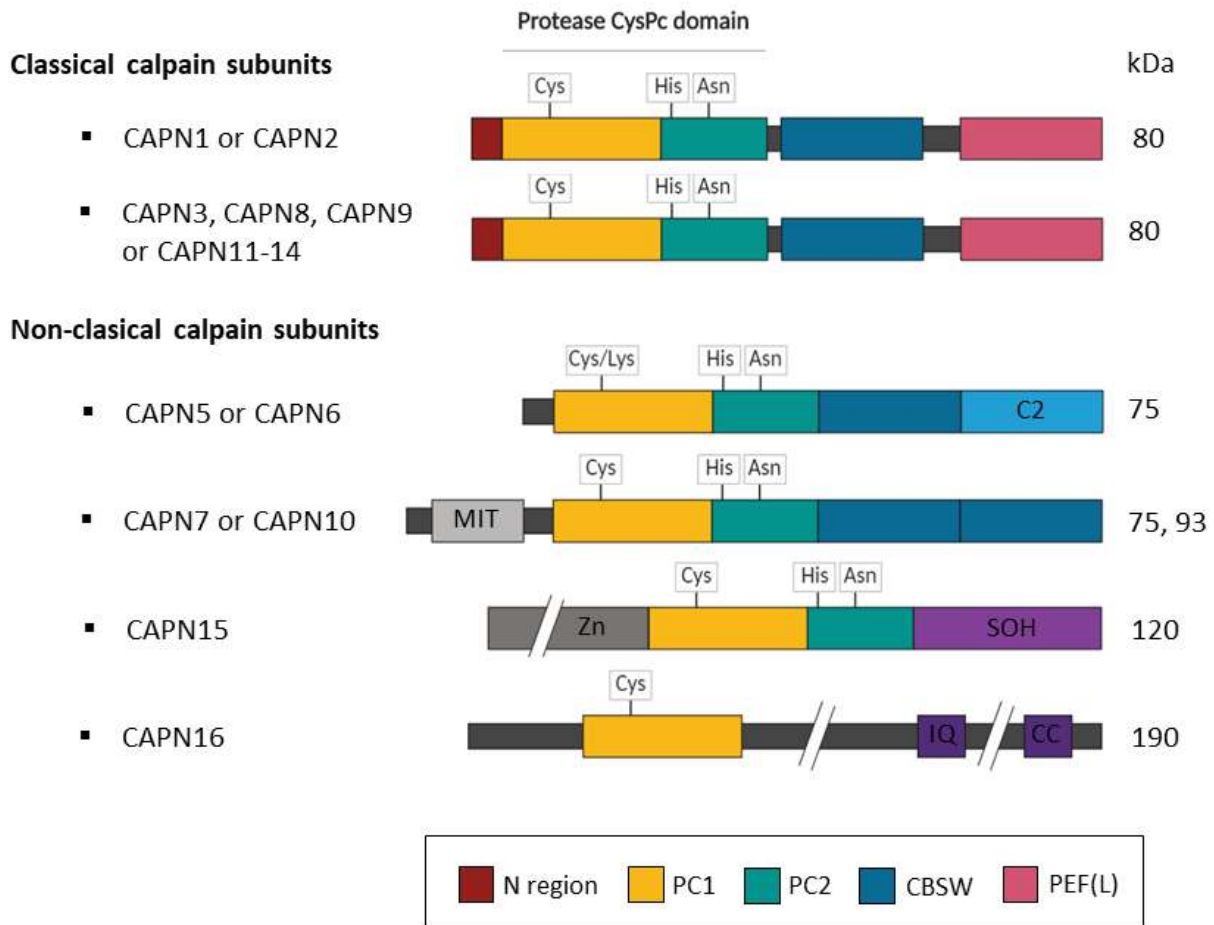


**Figure 26. Structure and classification of catalytic subunits of human calpains.** Calpains are structurally classified into two types: classical, with domain structures that are identical to those of CAPN1 and CAPN2, and non-classical. CysPc, cysteine protease domain, calpain-type; PC, protease core 1 and 2; CBSW, calpain-type  $\beta$  sandwich domain; PEF(L), penta EF-hand domain in the large subunit; C2L, calcium-binding motif; MIT, microtubule-interacting and transport domain; Zn, zinc-finger motif; SOH, SOL-homology domain; IQ, calmodulin-interacting domain (Based on Ono et al., 2016b).

Calpains can also be classified due to their expression profile. Most of the calpains, including the classical calpain catalytic subunits, CAPN1 and CAPN2, are ubiquitously expressed, but six calpain genes are considered to be tissue-specific according to the

expression of their major protein products: CAPN3 in skeletal muscle (Sorimachi et al., 1989), CAPN6 in placenta and embryonic striated muscle (Dear and Boehm, 1999), CAPN8 and CAPN9 in gastrointestinal tract (Sorimachi et al., 1993), CAPN11 in testis (Dear et al., 1999) and CAPN12 in hair follicles (Dear et al., 2000). It is extensively assumed that while ubiquitous calpains play a fundamental role in all cells, tissue-specific calpains might be involved in more specific cellular functions and, when defective, cause disorders specific to the tissues in which they are expressed. However, pathogenic alterations of some ubiquitous calpain can lead to deficiencies in specific tissues (for example CAPN1 reduction affects neuronal cells and CAPN5 reduction to the eyes) (Mahajan et al., 2012; Wang et al., 2016).

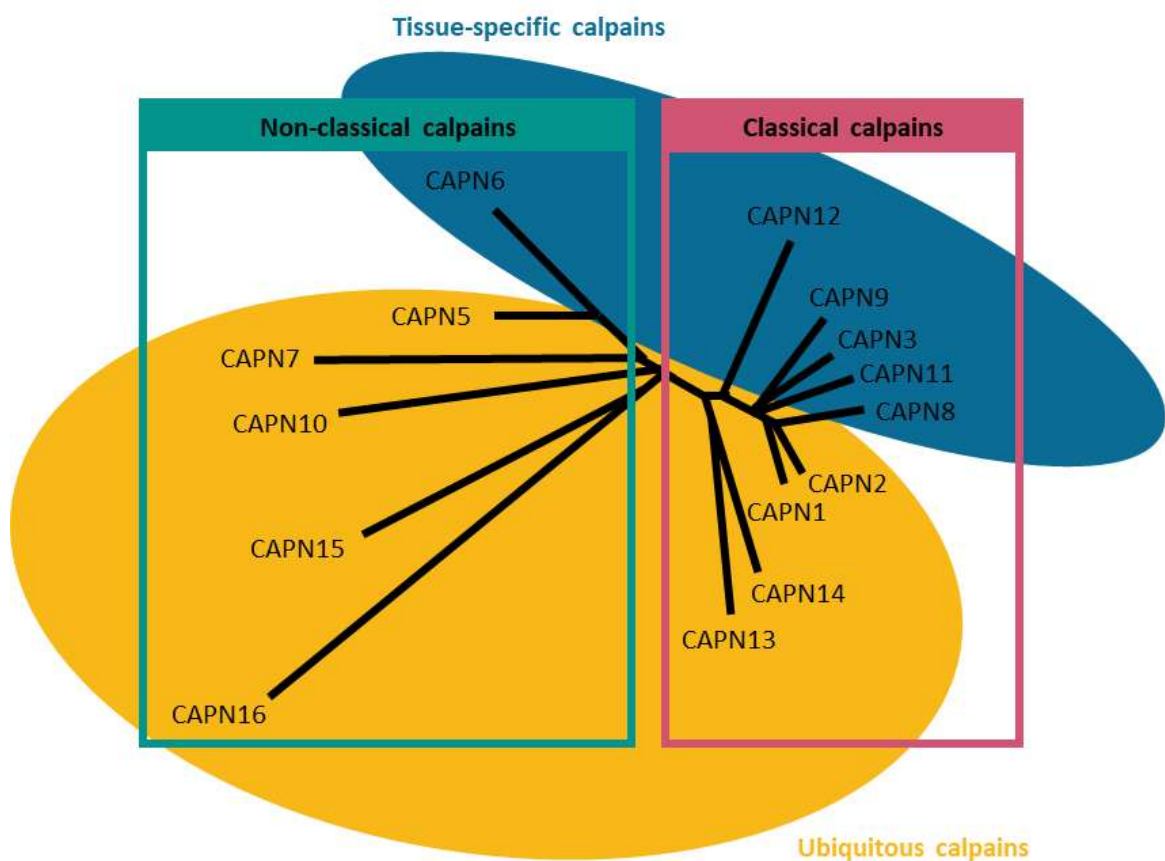


**Figure 27. Phylogenetic tree of human calpains and their classification.** Calpains can be classified based on domain structure, classical (pink rectangle) or non-classical (turquoise rectangle), or based on the expression patterns tissue-specific (blue) and ubiquitous (yellow) (Sorimachi et al., 2013).



Gene	Protein	Chromosome location	Expression	Cellular location
<b>CAPN1</b>	Calpain-1 catalytic subunit	<i>11q13</i>	Ubiquitous	Cytoplasm and cell membrane
<b>CAPN2</b>	Calpain-2 catalytic subunit	<i>1q41-q42</i>	Ubiquitous (except erythrocytes)	Cytoplasm and cell membrane
<b>CAPN3</b>	Calpain-3	<i>15q15.1-q21.1</i>	Skeletal muscle	Cytoplasm
<b>CAPN5</b>	Calpain-5	<i>11q14</i>	Abundant in testis and brain	Cytoplasm, cell Surface, focal adhesions and extracellular exosome
<b>CAPN6</b>	Calpain-6	<i>Xq23</i>	Embryonic muscles and placenta	Perinuclear region and spindle
<b>CAPN7</b>	Calpain-7	<i>3p24</i>	Ubiquitous	Nucleus
<b>CAPN8</b>	Calpain-8	<i>1q41</i>	Gastrointestinal tracts	Cytoplasm and Golgi apparatus
<b>CAPN9</b>	Calpain-9	<i>1q42.11-q42.3</i>	Gastrointestinal tracts	Cytoplasm
<b>CAPN10</b>	Calpain-10	<i>2q37.3</i>	Ubiquitous	Cytoplasm, mitochondria and plasma membrane
<b>CAPN11</b>	Calpain-11	<i>6q12</i>	Testis	Acrosomes
<b>CAPN12</b>	Calpain-12	<i>19q13.2</i>	Hair follicle	Cytoplasm
<b>CAPN13</b>	Calpain-13	<i>2p22-p21</i>	Ubiquitous	Cytoplasm
<b>CAPN14</b>	Calpain-14	<i>2p23.1-p21</i>	Ubiquitous	Cytoplasm
<b>CAPN15</b>	Calpain-15	<i>16p13.3</i>	Ubiquitous	Cytoplasm
<b>CAPN16</b>	Calpain-16	<i>6q24.3</i>	Ubiquitous	-
<b>CAPNS1</b>	Calpain small subunit 1	<i>19q13</i>	Ubiquitous	Cytoplasm and cell membrane
<b>CAPNS2</b>	Calpain small subunit 2	<i>16q13</i>	Ubiquitous	Cytoplasm and cell membrane
<b>CAST</b>	Calpastatin	<i>5q15-21</i>	Ubiquitous	Cytoplasm, cell membrane and endoplasmic reticulum

**Table 7. Human calpain genes and their representative products.** Calpain genes are distributed along the human genome and can be classified due to their expression profile.

#### 4.2. Calpain activity and specificity

As mentioned above, calpains are a family of proteases whose activity depends on  $\text{Ca}^{2+}$  bindings. Although the exact mechanism of calpain activation is still under study, 3D analysis of the crystal structure of calpains helped to understand this mechanism. The protease activity in calpains is formed by two separated core domain structures, PC1 and PC2, both located in the CysPc domain (Murachi, 1989). In the absence of  $\text{Ca}^{2+}$ , PC1 and PC2 are aligned in the same plane and separated from each other (Baki et al., 1996; Brown and Crawford, 1993). When activation, two  $\text{Ca}^{2+}$  ions bind the Calcium-Binding Sites (CBS) of PC1 and PC2 (Sorimachi et al., 2013).  $\text{Ca}^{2+}$  binding itself does not induce any dramatic change in the PC domains, but permit to rearrange and connect them forming a functional active site cleft. The key movement in this rearrangement is the repositioning of the Cys115 (calpain-1 numbering) close to the His272 while the residue Trp298 moves to an exposed position in the cleft. The formed cleft in the core domains after activation is deep and narrow only allowing the substrate to fit the cleft in an extended conformation. This explains the calpain's preference for digesting mainly inter-domain unstructured regions (Campbell and Davies, 2012; Hanna et al., 2008; Moldoveanu et al., 2002).

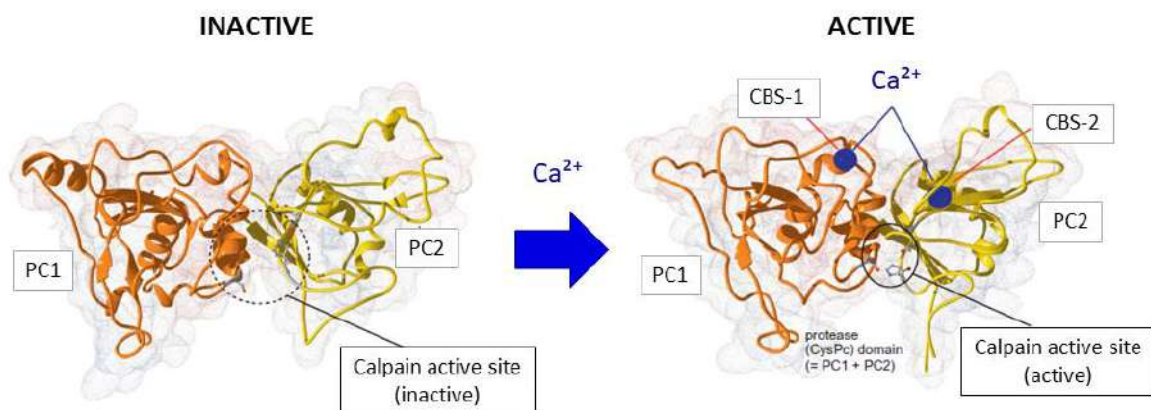


**Figure 28. Three-dimensional structures of the inactive and active form of human calpain CysPc domain.** Catalytic CysPc domain is composed by the protease core 1 and protease core 2 (PC1 and PC2). In the absence of  $\text{Ca}^{2+}$ , PC1 and PC2 are aligned on the same plane and separated from each other. The active site cleft is (circled in black) created by the rearrangement of PC1 and PC2 due to the binding of two  $\text{Ca}^{2+}$  ions (blue balls) in the Calcium Binding Site (CBS 1 and 2) (Sorimachi et al., 2013).

Calpains directly recognize the substrate even it appears to lack a clear cleavage sequence specificity. Some calpain sequence preferences have been reported, like Leu in position P2, Thr or Arg, in P1 and Pro residue in position P3 (duVerle et al., 2010; Tompa et al., 2004), but the concrete regulation governing calpains' substrate specificity is still unknown. Nowadays, it is extensively accepted that calpain process the substrate preferably in the peptide backbone atoms, which may explain the apparently low amino acid sequence selectivity for calpain substrates (Goll et al., 2003).

Calpains proteolyze most of their substrates in a limited number of cleavage sites producing larger fragments, rather than completely degrading to small polypeptides. This action of calpains on their substrates is known as "proteolytic processing" and suggest that calpains have a modulatory nature over the substrate (Goll et al., 2003; Suzuki et al., 2004). However, its biological functions and therapeutic potential remain poorly understood.

#### **4.3. Calpain regulation**

It is known that calpains participate in many physiological and pathological processes and understanding the exact mechanisms of calpains activity regulation will help to develop new therapeutic strategies. There are three main intracellular levels of calpain activity regulation: the binding of  $\text{Ca}^{2+}$ , the small regulatory subunit and calpastatin.

##### **4.3.1. Calcium**

Calpains are some of the very few proteases that are directly activated by  $\text{Ca}^{2+}$ . Apart from the two  $\text{Ca}^{2+}$  ions that bind the CysPc domain and help to form the active site of the protein, up to eight more ions can bind to different positions of the PEF domains. The binding of these extra  $\text{Ca}^{2+}$  to the protein is believed to have a modulatory function protecting against spontaneous activation rather than being the primary regulators of calpain activity, as originally thought. For example, calcium-binding to the PEF domains barely changes the secondary structure but induces displacement of the N-terminal region from the protease core region (Ono and Sorimachi, 2012).

##### **4.3.2. Small regulatory subunit**

CAPNS1 is composed by a glycine-rich domain and a PEF(S) domain. While the hydrophobic glycine-clusters are usually autolyzed during the activation, the EF-hand motifs mediate the

interaction with CAPN1 and CAPN2 to generate the heterodimeric conventional calpains  $\mu$ -calpain and m-calpain, respectively. CAPNS1 also binds to other calpains, such as CAPN9 (Ono and Sorimachi, 2012). Under basal conditions, CAPNS1 is essential for the enzymatic activity and protein stability of  $\mu$ -calpain and m-calpain as disruption of CAPNS1 causes the down-regulation of both proteins (Arthur et al., 2000; Tan et al., 2006). It also exists a paralogue of the gene, CAPNS2, which until today has no known function in physiological conditions (Schád et al., 2002).

### 4.3.3. Calpastatin

The calpain family also includes an endogenous calpain inhibitor, Calpastatin (CAST). At present, it is the only absolutely specific inhibitor for classical calpains that does not inhibit any other proteases. It is able to inhibit with the same susceptibility  $\mu$ -calpain, m-calpain, calpain-8 (CAPN8), calpain-9 (CAPN9–CAPNS1), and the heterodimer calpain-8/9 (CAPN8–CAPN9) but not calpain-3 (CAPN3). However, it is suggested that Calpain-3 can proteolyze calpastatin *in vivo* with an unknown physiological significance (Ono et al., 2016b, 2004; Wendt et al., 2004).

Calpastatin sequence is poorly conserved between species, but its general structure formed by 4 tandemly repeated calpain inhibitory units is maintained (Domain 1-4). Each of these inhibitory units contains three highly conserved regions, A, B, and C. B region is a consensus sequence responsible for calpain inhibition, whereas A and C bind calpain but have no inhibitory activity on its own. Consequently, each inhibitory domain can inhibit one calpain independently with variable efficiency (Emori et al., 1987; Maki et al., 1987a, 1987b), but only in the presence of  $\text{Ca}^{2+}$  (Hanna et al., 2007; Wendt et al., 2004). Calpastatin also has two extra domains, XL and L, both without inhibitory activity, but able to interact with calpain in the absence of  $\text{Ca}^{2+}$ . These two domains are usually exposed to alternative splicing (Goll et al., 2003; Melloni et al., 2006; Takano et al., 1999).

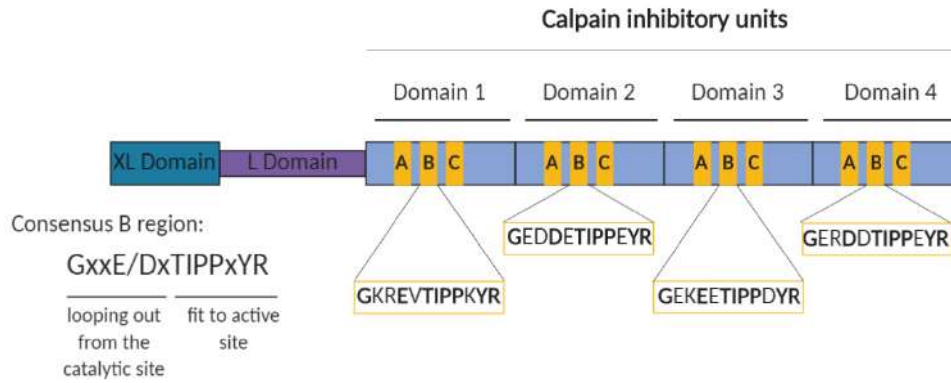


**Figure 29. Structure of the longest isoform of human calpastatin.** Calpastatin is composed of XL and L domains and four repetitive inhibitory units (labelled as domains 1 to 4). Each inhibitory unit contains A-, B- and C-regions important for the inhibitory activity of calpastatin. Consensus aa sequence in B-region directly interacts with the active site of calpain and is maintained in all the inhibitory units (Based on Ono and Sorimachi, 2012).

Calpastatin is what is defined as an intrinsically unstructured molecule, a protein that does not have a stable structure unless it binds to another protein. Each inhibitory sequence interacts with the calpain-type  $\beta$ -sandwich (CBSW) domain while, at the same time, loop out and around the active site. This calpastatin–CBSW interaction appears to be the key for calpastatin specificity while at the same time, it protects calpastatin itself from proteolysis (Hanna et al., 2008; Moldoveanu et al., 2008).

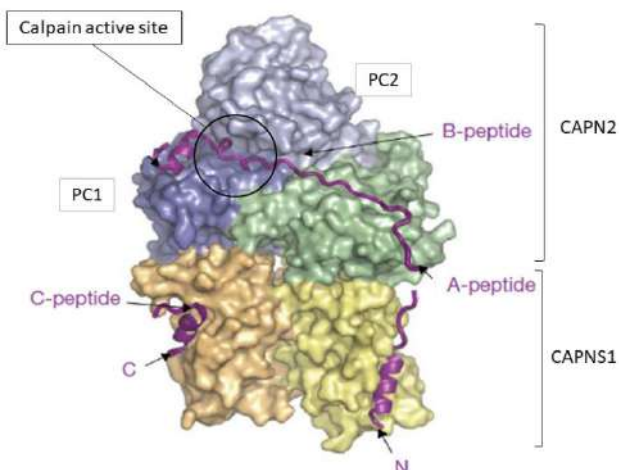


**Figure 30. Mechanism of calpain inhibition by calpastatin.** Three-dimensional structure of calpain-2 heterodimer (formed by CAPN2 and CAPNS1) is bound to domain 4 of calpastatin (purple). Domain 4 is one of the four calpain inhibitory units of calpastatin, which is unstructured in the absence of calpain. When inhibiting calpain, domain 4 changes to a three  $\alpha$ -helices conformation that wraps up calpain. Helices in A- and C- regions bind the PEF domains (PEF(S) and PEF(L), yellow and orange, respectively) while helix in B-region, binds the protease core CysPc formed by the protease core (PC1 and PC2, blue and light blue) (Hanna et al., 2008).

#### 4.4. Calpain and neurodegeneration

Neurodegeneration is defined as a complex and multifactorial process that determines the progressive loss of the function and structure of neurons and that eventually can end in neuronal cell death. The exact mechanism of neurodegeneration is still unknown and its origin may vary in the different neurodegenerative diseases.

Calpains are a cysteine-protease family tightly regulated and with a massive proteolytic activity. During aging, it is known that the over-activation of calpains occurs by a decline in the regulatory mechanisms (calpastatin protein level and  $\text{Ca}^{2+}$  homeostasis) (Benuck et al., 1996; Ferreira, 2012). However, this protease seems to be abnormally activated under pathological neurodegenerative conditions characterized by abnormal elevated intracellular  $\text{Ca}^{2+}$  levels (Bezprozvanny, 2009) such as in AD (Mahaman et al., 2019), PD (Mouatt-Prigent et al., 1996), HD (Gafni and Ellerby, 2002; Paoletti et al., 2008), and ALS (Yamashita et al., 2012). Interestingly, several studies have also reported an association of calpain activity with the fragmentation of the proteins involved in these disorders, leading to the generation of breakdown products that are significantly more toxic compared to the full-length protein. This includes the  $\alpha$ -synuclein protein in PD, TDP-43 in ALS and htt in HD (Dufty et al., 2007; Gafni and Ellerby, 2002; Yamashita et al., 2012).

In PD and HD,  $\alpha$ -synuclein accumulation and mutant htt, respectively, are the promoters of the initial disruption of  $\text{Ca}^{2+}$  homeostasis that leads to calpain activation perpetuating this cellular deleterious effects (Crocker et al., 2003; Kolobkova et al., 2017). However, in ALS  $\text{Ca}^{2+}$  alterations and calpain overactivation are due to an upregulation of the  $\text{Ca}^{2+}$ -permeable AMPA receptors (Yamashita et al., 2012). In AD calpain overactivation results from several factors, including intracellular  $\text{Ca}^{2+}$  dysregulation (Pierrot et al., 2006) and decreased calpastatin levels in the affected cells (Rao et al., 2008). Experiments performed using AD models have also demonstrated that accumulation of  $\text{A}\beta$  oligomers causes these dysregulation (Ferreira, 2012). All these neurodegenerative diseases share in common that the inhibition of calpain, using a specific inhibitor molecule or by overexpression of calpastatin, significantly reduces protein aggregates and ameliorates the pathology (Crocker et al., 2003; Gafni et al., 2004; Medeiros et al., 2012; Wright and Vissel, 2016), suggesting that calpain activation participates in the neurodegeneration process.



## **HYPOTHESIS AND OBJECTIVES**

---





## HYPOTHESIS

SMN levels are fundamental in the progress of MNs degeneration in SMA pathology. Therefore, protein stability regulation and SMN increase constitutes a significant strategy to develop new SMA therapeutic approaches.

Alterations of autophagy and calpain intracellular pathways have been related to neurodegeneration. In the present study, we hypothesize that these mechanisms may regulate SMN levels and degeneration of spinal cord MNs in SMA disease.

## OBJECTIVES

1. Analyse autophagy markers in cultured SMA cellular models.
2. Effect of calpain knockdown on autophagy regulation and Smn in mouse spinal cord control and SMA MNs.
3. Analyse the effect of calpain activity regulation on the Smn protein level in cultured mouse MNs.
4. Evaluate calpeptin in vivo administration on survival and motor function of two severe SMA mouse models.
5. Characterization of the calpain pathway in SMA models.



## **MATERIALS AND METHODS**

---



## 1. Mouse lines and colony maintenance

CD1 mice and two severe SMA transgenic mouse model, FVB.Cg-Tg(SMN2)<sup>89Ahmb</sup>Smn1<sup>tm1Msd</sup>/J (Smn<sup>-/-</sup>; SMN2<sup>+/+</sup> or MutSMA) and FVB.Cg-Grm7<sup>Tg(SMN2)89Ahmb</sup>Smn1<sup>tm1Msd</sup> Tg(SMN2\*delta7) 4299Ahmb/J (Smn<sup>-/-</sup>; SMN2<sup>+/+</sup> SMNΔ7<sup>+/+</sup> or SMNΔ7) were used. Transgenic mice were kindly provided by Dr Josep Esquerda and Dr Jordi Caldero (Universitat de Lleida-IRBLLEIDA). All animal procedures were performed in the *Estabulari de rosegadors* (University of Lleida), where all conditions were maintained in accordance to the European Committee Council Directive and the norms established by the Generalitat de Catalunya (published as a law in the Diari Oficial de la Generalitat de Catalunya [DOGC] 2073, 1995) about Animal Care guidelines. Mice were housed in propylene cages (33 cm × 18 cm × 14 cm) at an ambient temperature of 22 ± 2 °C, relative humidity of 40% ± 10% and on a 12 /12 hours light/dark cycle (light period from 07:30 until 19:30). Mice were provided with ad libitum water and rodent chow (nº 2018, Envigo). All the experiments were previously evaluated and approved by the University of Lleida Advisory Committee on Animal Services.

### 1.1. CD1 mouse model

The CD1 mouse is an outbred stock that was first produced by Charles River Laboratories in 1959. This stock originally derived from the Lynch's Swiss mice, by Roswell Park Memorial Institute, (Buffalo, New York) and the Institute of Cancer Research (Fox Chase, Philadelphia, Pennsylvania). CD1 mouse is the most common non-consanguineous mouse in the world. It is an inexpensive, robust and readily available outbred population with a docile temperament, and excellent maternal characteristics, that has a high efficient breeding and large litter sizes (average number of animals *per* litter: 11.5). It also shows a high incidence of retinal degeneration.

Due to its characteristics, CD1 mouse line is commonly used in toxicology, cancer research, ageing studies, trans-genesis experiments and as a surgical model (Chia et al., 2005; Rice and O'Brien, 1980). In the present study, the CD1 mouse model was used due to the large number of embryos *per* pregnancy and to obtain cells with unaltered Smn protein level.

## 1.2. SMA transgenic mouse models

### 1.2.1. *Smn*<sup>-/-</sup>; *SMN2*<sup>+/+</sup> or MutSMA (The Jackson Laboratory, Sacramento, USA, stock 005024)

The SMA transgenic mice were created in two steps. First, the *Smn* knockout mice were generated in the laboratory of Dr Michael Sendtner at the University of Wurzburg, by disruption of Exon 2 of the endogenous mouse *Smn* gene using a targeting vector encoding a neomycin cassette. On the other hand, the *SMN2* transgene was created in the laboratory of Dr Arthur Burghes at Ohio State University when a genomic fragment encoding the human *SMN2* promoter and gene was integrated into intron 4 of the *Grm7* gene. Transgenic *SMN2* mice were bred to the *Smn* mutant mice to obtain the double mutant mice.

Homozygous mice for the targeted mutant *Smn* allele and carriers of *SMN2* transgene are noticeably smaller than normal littermates and died shortly after birth (survive for only 4-6 days). From postnatal day 2, they exhibit symptoms and neuropathology like decreased suckling and movement, laboured breathing and tremoring limbs, similar to patients afflicted with type 1 SMA. Histological analysis indicates that at P5 affected mice exhibit a 35% loss of MNs from the spinal cord, absence or near absence of intranuclear aggregates of the *Smn* protein ('gems') and muscle fibres (quadriceps and gastrocnemius assayed) atrophy (Monani et al., 2000; Schrank et al., 1997).



**Figure 31. Severe SMA mouse model *Smn*<sup>-/-</sup>; *SMN2*<sup>+/+</sup> or MutSMA photographed at postnatal day 4 (P4) with a normal littermate. This severe SMA mouse model survive only up to 6 days.**

The colony was maintained by continuously crossing heterozygous mice (*Smn*<sup>+/-</sup>; *SMN2*<sup>+/+</sup>). Other two different genotypes were obtained with a probability of 25%; wild-types (*Smn*<sup>+/+</sup>; *SMN2*<sup>+/+</sup>, referred as WT and used as a positive control) and mutant animals (*Smn*<sup>-/-</sup>; *SMN2*<sup>+/+</sup>, referred as MutSMA).

**1.2.2. *Smn*<sup>-/-</sup>; *SMN2*<sup>+/+</sup>; *SMNΔ7* <sup>+/+</sup> or *SMNDelta7* (The Jackson Laboratory, Sacramento, USA, stock 005025)**

Transgenic mice for human SMN2 cDNA lacking exon 7 (*SMNDelta7*) under the control of the human SMN2 promoter were obtained in Dr Arthur Burghes laboratory. Founder *SMNdelta7* transgenic allele mice were bred with heterozygous *Smn*<sup>+/-</sup>; *SMN2*<sup>+/+</sup> mice to obtain the triple mutant mouse who harbours two transgenic alleles and a single targeted mutant.

Mutant mice that are homozygous for the targeted mutant *Smn* allele and homozygous for the two transgenic alleles (*Smn*<sup>-/-</sup>; *SMN2*<sup>+/+</sup>; *SMNΔ7* <sup>+/+</sup>, referred as *MutDelta7*) exhibit symptoms and neuropathology similar to patients afflicted with type 1 SMA. At birth, mutants are noticeably smaller than normal littermates and starting at day 5, they show progressive muscle weakness that gets more pronounced over the following week (abnormal gait, shakiness in the hind limbs and a tendency to fall over). Immunocytochemical analysis indicates that dystrophin expression is normal, however, fibres isolated from the gastrocnemius muscle of a mutant clearly show evidence of atrophy. Mean survival was originally reported to be ~13 days (Le et al., 2005).



**Figure 32. SMA mutant mouse *Smn*<sup>-/-</sup>; *SMN2*<sup>+/+</sup>; *SMNΔ7* <sup>+/+</sup> or *SMNDelta7* together with a normal littermate photographed at postnatal day 10 (P10). The addition of a copy of the human SMN2 cDNA lacking exon 7 extends survival up to 13 days.**

Two other *SMNDelta7* mice genotypes were generated: heterozygous (*Smn*<sup>+/-</sup>; *SMN2*<sup>+/+</sup>; *SMNΔ7* <sup>+/+</sup>) exclusively used for colony maintenance, and wild-types (*Smn*<sup>+/+</sup>; *SMN2*<sup>+/+</sup>; *SMNΔ7* <sup>+/+</sup>, referred as WT and used as a positive control).



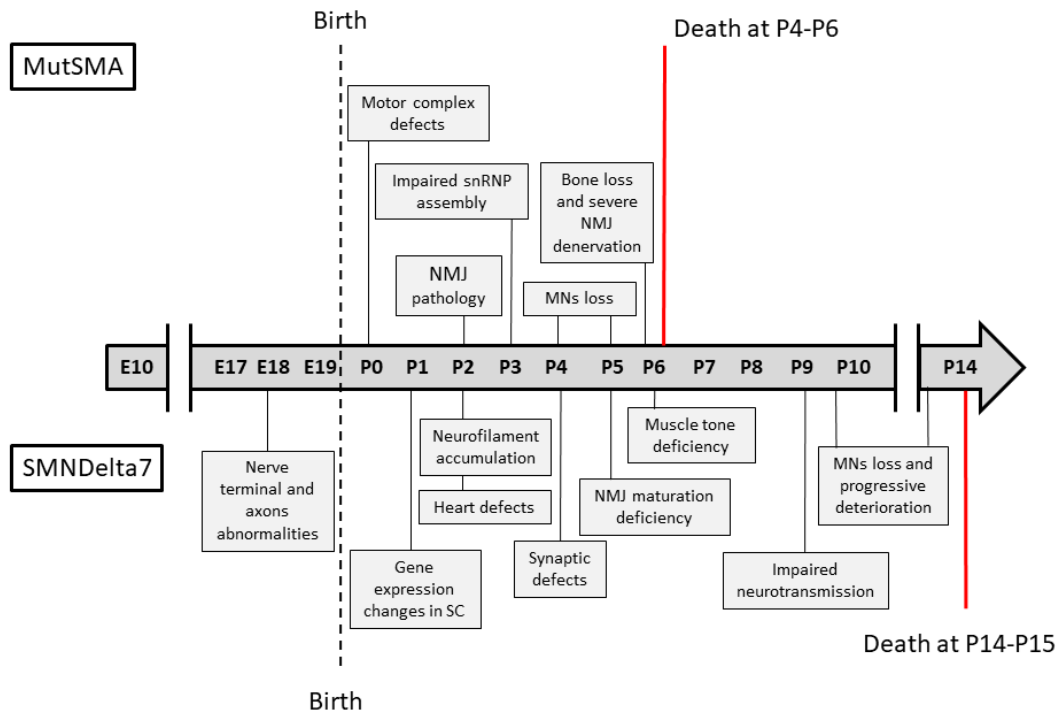


**Figure 33. Timeline of major cellular and symptomatic events in MutSMA (*Smn*<sup>-/-</sup>; *SMN2*<sup>+/+</sup>) and SMNDelta7 (*Smn*<sup>-/-</sup>; *SMN2*<sup>+/+</sup>; *SMNΔ7*<sup>+/+</sup>) mouse models of SMA. MN, motor neuron; NMJ, neuromuscular junction; SC, spinal cord and snRNP, small nuclear ribonucleoprotein (Based on James N Sleight et al., 2011).**

### 1.2.3. Genotype

#### DNA extraction

To obtain genomic DNA the REExtract-N-Amp Tissue PCR Kit (Sigma, St Louis, MO, USA) was used. For colony maintenance and *in vivo* treatment, neonatal offspring were marked (ear puncher or tattoo) and a fragment of the tail/ear was collected. For MNs purification, E12.5 embryos were removed from the uterus and the head was snipped.

The DNA from the portion of tissue (head, tail or ear) was obtained in 6 steps suggested by the provider as follow:

1. Placed the tissue from each animal in a separate 1.5 polypropylene tube.
2. Prepared the extract solution following the proportion:

[ 3 volumes of Extract solution  
1 volume of Tissue prep

Add 50 µl of extract solution to each sample.

3. Incubate 10 minutes at room temperature
4. Heat the samples to 95°C for 3 minutes.
5. Add 50µl of neutralization buffer to each sample and mix accurately or vortex them.
6. Centrifuge samples a maximum speed for 10 minutes and collect the supernatant in a new tube. The extract is ready for PCR to be used immediately or stored at 4°C up to 6 months.

### **Genotyping PCR SMA Mice**

The REDExtract-N-Amp Tissue PCR Kit contains a reaction mixture that contains the buffer, salts, dNTPs, and the Taq polymerase and it is optimized specifically for use with the extraction reagents. It also includes a JumpStart™ Taq antibody for hot start PCR which prevents the premature activation of the DNA Taq polymerase at room temperature and enhances specificity.

Both SMA mouse models were genotyped by using the same pairs of primers. The primers used for the PCR amplification were designed for The Jackson Laboratory (ordered at Sigma at 100 µM):

- Forward (Fwd): common for wild type (WT) mouse *Smn* gene and the interrupted *Smn* gene.

**5' CTCCGGGATATTGGGATTG 3'**

- Reverse 1 (Rev1): specific for the WT *Smn* gene.

**5' GGTAACGCCAGGGTTTTCC 3'**

- Reverse 2 (Rev2) or Cassette: is the reverse primer specific for the *Smn* gene interrupted by the neomycin resistance cassette.

**5' TTTCTTCTGGCTGTGCCTT 3'**

The PCR reaction mixture was prepared following the protocol:

Reagents	
Buffer Red extraction	4,65 $\mu$ l
Sterile miliQ water	x $\mu$ l (up to the final volume)
Fwd primer	1.2 $\mu$ M
Rev1 primer	1.2 $\mu$ M
Rev2 primer / Cassette	1.2 $\mu$ M
DNA Sample	5-20 ng
<b>Total volume: 10 <math>\mu</math>l</b>	

**Table 8. Genotype PCR mix preparation.**

The PCR cycling parameters were:

Step	Temperature	Time	Cycles
Initial Denaturation	94 °C	5 minutes	1
Denaturation	94 °C	30 seconds	35
Annealing	62 °C	1 minute	
Extension	72 °C	1 minutes	
Final Extension	72 °C	7 minutes	1
Final Hold	4 °C	Indefinitely	

**Table 9. Genotype PCR cycling parameters.**

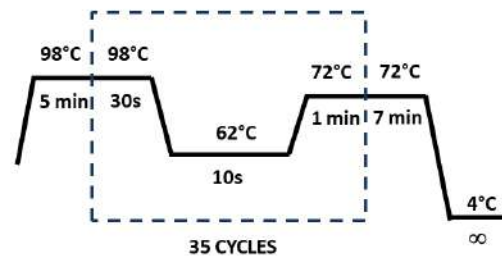


**Figure 34. Schematic representation of genotype PCR cycling parameters.**

## Electrophoresis

The REExtract-N-Amp PCR ReadyMix contains REDTaq® dye, an inert dye that acts as a tracking dye and allows for convenient laddering of PCR reactions directly onto agarose gels for analysis. We use 1% agarose gel for the DNA separation and SYBR Safe (1:10,000; added to the gel) as a dye.

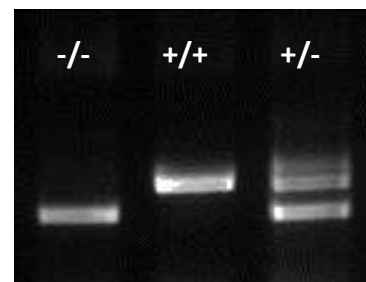


**Figure 35. Genotypes in a 1% agarose gel.** Mutant (-/-) and WT (+/+) shown as a single band, while heterozygous present 2 bands.

After the electrophoresis, the gel was developed using the ultraviolet sample tray support on a Gel Doc™ EZ Imager. As a result, we obtained: an amplification of 800Kb DNA product that corresponding to endogenous Mouse *Smn* gene (WT (+/+)); a single fragment of 500Kb corresponding to the neomycin resistance cassette (mutants (-/-)); and a combination of both fragments in the heterozygous samples (+/-).

## 2. Primary Cell culture

### 2.1. Precoating plates

#### Polyornitin (P/O) coated- plates

To prepare the culture dishes a 35 µg/ml solution of poly-DL-ornitin (P/O) (Sigma, Stock solution of 10mg/ml) was prepared in Boric-Borate buffer (150mM sodium tetraborate, 150mM boracic acid, pH 8.3). Four well tissue culture plates (M4 plates) were covered with 350 µl/ well and incubated for 2-4 hours or overnight at room temperature. After incubation, plates were rinsed 3 times with sterile miliQ water and air-dried at room temperature for 15 minutes. Plates can be stored at 4°C up to 2 weeks or used immediately.

For cell culture immunofluorescence analysis, cells where growth in sterilised 15-mm glass coverslips placed in M4 plates. For that use, a small drop of P/O (50-80 µl) is placed in the centre of the coverslip.

### Laminin coated-plates

After P/O coating, plates were treated with laminin (Sigma, stock solution 1mg/ml) diluted in L-15 medium at a final concentration of 3.8 µg/ml. M4 wells were covered with an adequate volume of the laminin solution (330 - 350 µl/ well or 50-80 µl/ coverslip-well).

Laminin was incubated for a minimum of 2 hours at 37°C into a CO<sub>2</sub> incubator. Laminin-coated plates can be stored in the incubator up to one week. Laminin solution was removed immediately before plating.

## 2.2. Cell culture media and solutions

All the media and solutions used in cell culture experiments were sterilized using 0.22 µm filters.

Media and Solutions	Components
<b>GHEBS solution</b>	137mM NaCl, 2.6 mM KCl, 25mM Glucose (Sigma), 25mM Hepes (Gibco, Life technologies), 20 µg/ml Penicillin - Streptomycin
<b>Leibovitz's L-15 Medium Complete (L-15 complete)</b>	Leibovitz's L-15 Medium (L-15 medium) (Gibco, Life technologies, ref:11415-049) supplemented with horse serum (HS) (2% v/v) (Gibco, Life technologies), N2 (1% v/v) (Gibco; Invitrogen), 20 mM Glucose (Sigma) and 0.1 mg/ml P/S
<b>Neurobasal Medium complete (NBM complete)</b>	Neurobasal Medium (NBM) (Gibco, Life technologies, ref:21108-049) supplemented with B27 (2% v/v) (Gibco; Invitrogen), HS (2% v/v), L-glutamine (125 mM) (Gibco; Invitrogen) and 2-mercaptoetanol (25 µM) (Sigma)
<b>NBM+NTFs (NTFs medium)</b>	NBM complete supplemented with neurotropic factors (NTFs) (GDNF, HGF and CT-1 at 10 ng/ml and BDNF at 1 ng/ml (Bio-nova))
<b>Bovine Serum Albumin (BSA) 4%</b>	BSA 7.5% (Sigma) diluted with L-15 medium

**Table 10. Primary cell culture media and solution.** All media and solution were prepared fresh and sterilized before use.

### 2.3. Mouse motoneuron primary culture

One of the most common sources of MNs cultures is obtained from the dissociation of E12.5 -E13 (12.5 or 13 days of gestation) embryonic spinal cords. MNs constitute only a minor population of neurons developed towards postmitotic stages at early embryonic nervous system development. During the embryonic development, approximately one-half of the MNs initially generated are lost during a wave of programmed cell death (PCD). In mouse, this pattern of naturally-occurring MNs PCD occurs at E11.5 to E15.5 (Yamamoto and Henderson, 1999). At E12.5-E13 development stage, MNs are already formed, but the axonal extension and this naturally occurring cell death have not occurred yet. Additionally, at this point, MNs are larger and less dense than the remaining cells of the spinal cord and can be easily isolated using density gradient centrifugation (Arce et al., 1999; Wiese et al., 2010).

Spinal cord MNs were obtained from mouse embryos from CD1 or SMA transgenic mouse models at embryonic stage 12.5- 13 (E12.5- E13). We isolated MNs using two-step centrifugation through a density gradient that allows us a 97% culture purity that can be maintained for up to 2 weeks. In all experiments, 20-24 hours after purification, the cell medium was replaced with fresh NTFs medium supplemented with aphidicolin. Aphidicolin is a DNA polymerase inhibitor that was added to avoid the growth of mitotic cells that have been able to reach the final culture of MNs.

#### Spinal Cord dissection

Initially, adult-pregnant mice were sacrificed by cervical dislocation and embryos were removed from the uterus and transferred to a plate with GHEBS buffer solution. Embryos' head were snipped (**Figure 36.1**), to facilitate future manipulation, and fixed upside-down by using small needles in a silicon support plate fill with GHEBS. Spinal cords were dissected firstly by cutting the tail and opening the dorsal part of the embryo with a longitudinal cut in the middle of the spinal cord area (1-2 mm of depth) (**Figure 36.2**). When spinal cord got exposed, dorsal horns were removed and discarded (**Figure 36.3**), because MNs are situated in the ventral part of the spinal cord.

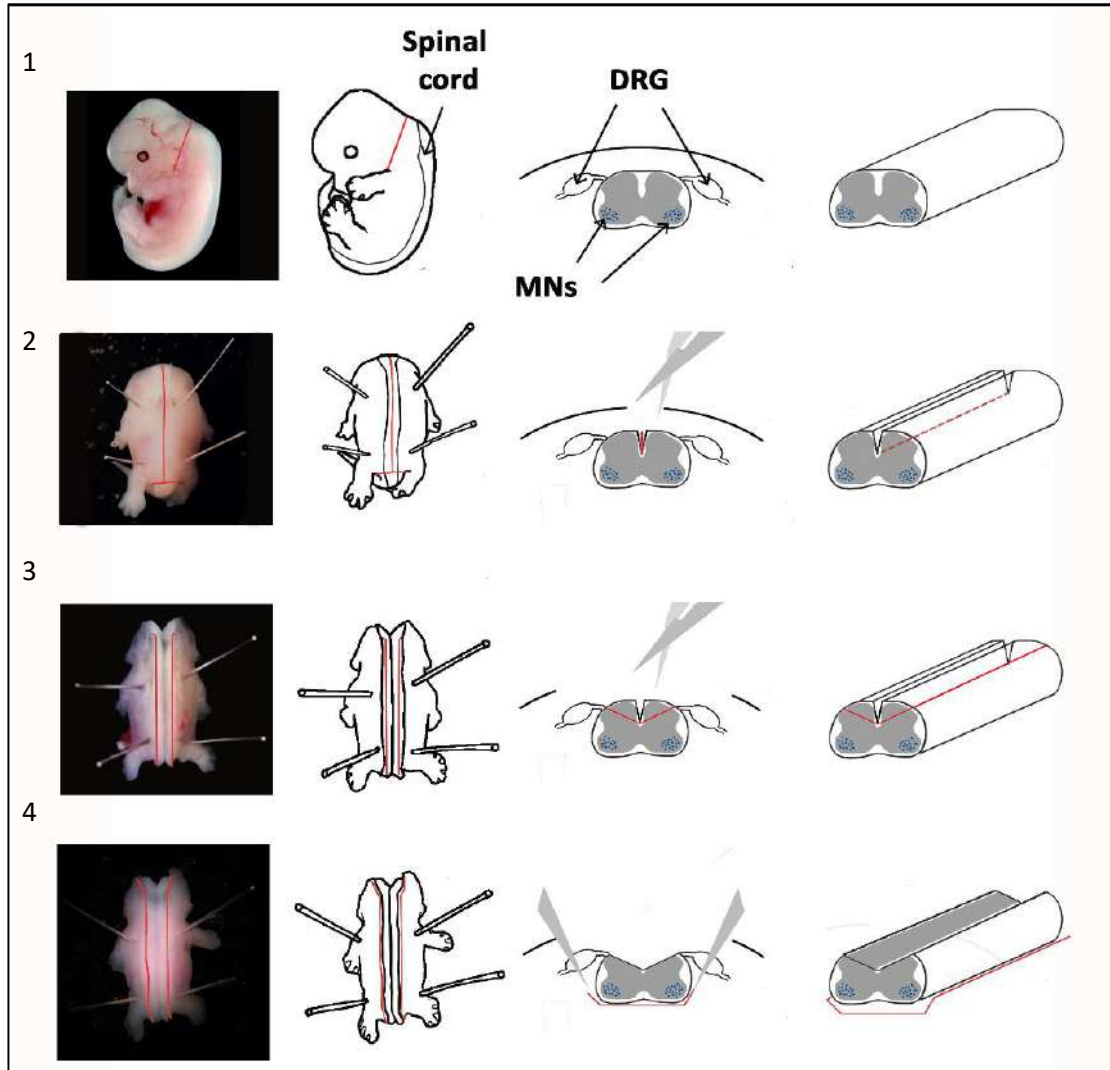


**Figure 36. Dissection of mouse embryo spinal cord.** Embryos head is snipped to allow upside-down position. Once spinal cord is exposed, the dorsal horns are removed and the remaining part of the spinal cord was carefully separated from the rest of the body.

The remaining part of the spinal cord was carefully separated from the rest of the body using a small and thin dissection tweezer (**Figure 36.4**). When the spinal cord was isolated from the rest of the body the meninges were removed (**Figure 37**). This step is important to prevent the presence of other cells type in the purified culture. Each spinal cord was chopped in 2-3 mm fragments (4-5 pieces) and transferred to a conic tube fill with GHEBS. Spinal cords were pooled in groups of 4 *per* tube.

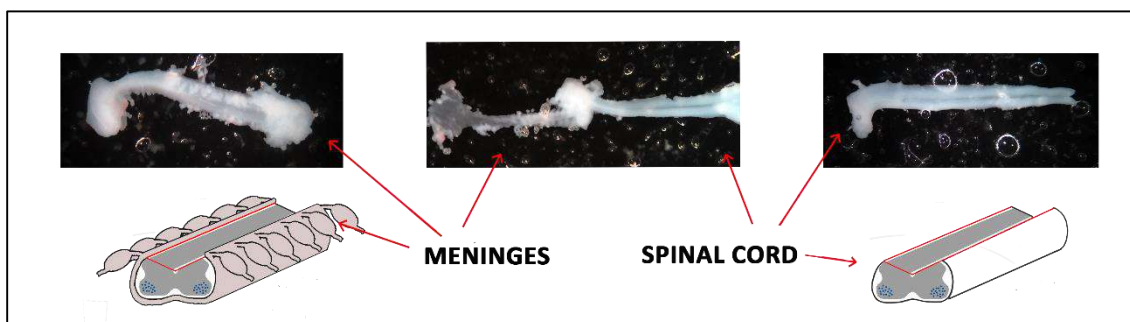


**Figure 37.** *Detail of the separation of the meninges from the spinal cord. After separation of the spinal cord from the rest of the body the meninges are separated to prevent the presence of other cells type in the purified culture. The meninges are separate from the tissue by simply peeling them.*

### **Mouse MNs isolation**

The purification process starts with an enzymatic and mechanical dissociation and ends with MNs separation by using a density gradient. This process has to be done rapidly, but always being soft and precise with the sample. We obtain approximately  $2.5 \times 10^4$  to  $4 \times 10^4$  MNs *per* spinal cord.

1. When the spinal cord dissection was finished the fragments were washed twice with clean GHEBS solution and incubated in GHEBS containing trypsin (Sigma, final concentration 0.025%) for 8-10 minutes at 37°C shaking frequently.
2. The fragments were mechanically dissociated on 4% BSA medium containing DNase (final concentration 0.1-0.14 mg/ml) using a Blue Tip. This step could be repeated up to three times, depending on the size of the fragments.
3. After tissue disgregation, the pieces were incubated for 2 minutes to precipitate, and the supernatant containing the dissociated cells was collected and place in a conic tube.
4. In the tube containing the dissociated cells 4 ml of 4% BSA solution was slowly added, creating a two-phase gradient and centrifuged 5 minutes at 6500g (Relative Centrifugal Force or G-force).



5. The pellet was completely resuspended in 1 ml of L-15 complete medium.

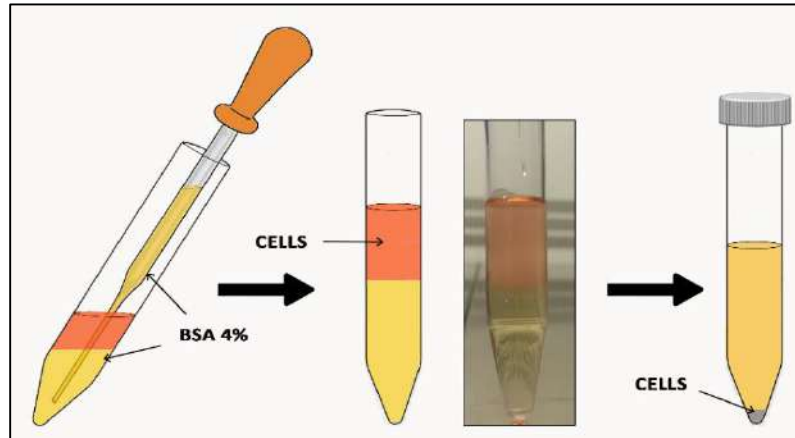


**Figure 38. Graphic representation of the centrifugation step of the cells in a 4% BSA gradient.** In this step, the 4% BSA is carefully added to the bottom of the tube containing the dissociated cell solution.

6. The last step is the density gradient isolation made using a freshly prepared 12.5 % Optiprep™ solution (Axis-Shield, Oslo, Norway, diluted in GHEBS solution) in a flat bottom tube. Optiprep™ is the commercial name for a medium based on iodixanol, a non-ionic chemical, with a density of  $1.320 \pm 0.001$  g/ml at  $20^{\circ}\text{C}$ . The cell solution was slowly added over this Optiprep™ solution, creating two differentiated phases and centrifuged 10 minutes at 520g.

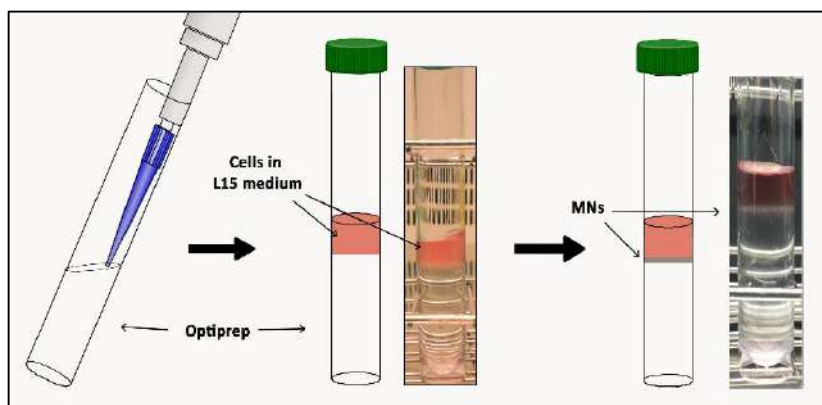


**Figure 39. Graphic representation of the Optiprep™ gradient centrifugation step.** In this step, the dissociated cell solution is carefully added to the top over the Optiprep™ solution.

### Plating and cell culture

After the centrifugation, a pale band between the Optiprep™ and the L-15 complete medium was obtained. This interface corresponds to the MNs and 0.5 ml was carefully collected in each tube and deposit in a sterile new tube.

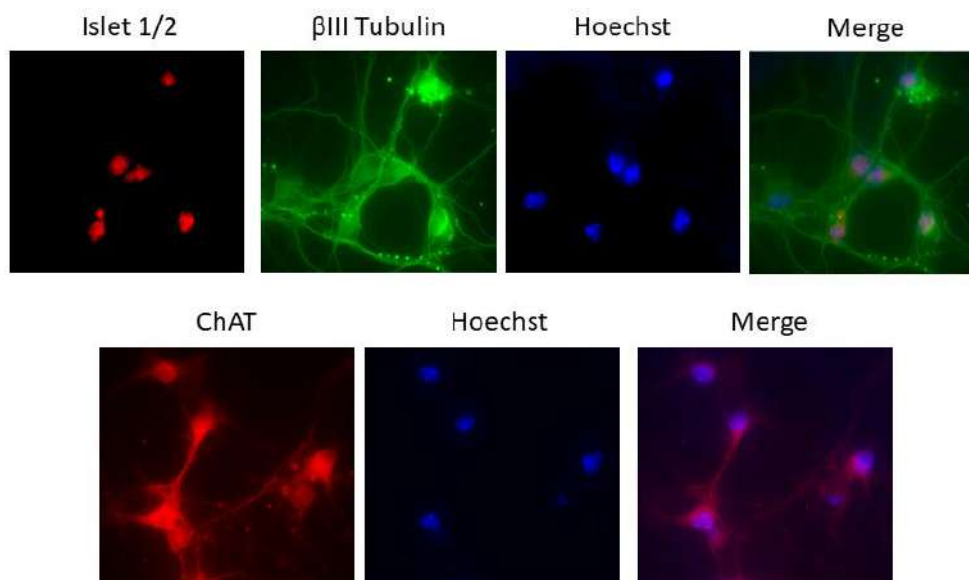


**Figure 40. Immunofluorescence of MNs markers in mouse isolated MNs.** Isolated MNs were fixed after 6 days in culture and immunofluorescence was performed using different specific MNs markers to demonstrate the efficacy of the isolation process. **Top photos:** Islet1/2 (Red), B-III Tubulin (Green). **Bottom photos:** Choline Acetyltransferase (ChAT).

Isolated MNs were counted on a Burker chamber and plated either using 15-mm glass coverslips placed in 4-well tissue culture dishes for immunofluorescence (7,000 cells/cm<sup>2</sup>) or in 4-well tissue culture dishes (Nunc, Thermo Fisher Scientific, Madrid, Spain) for survival experiments (8,000 cells/cm<sup>2</sup>), neurite degeneration evaluation (5,000 cells/cm<sup>2</sup>), and western blot analysis (26,000 cells/cm<sup>2</sup>).

Cells were directly plated in NTFs medium and keep for up to 12-15 days in a CO<sub>2</sub> incubator. To avoid the potential growth of non-neuronal cells in the culture, aphidicolin (2μg/ml; Sigma) was added to the culture medium 24 hours after isolation.

### 3. Cell lines culture

#### 3.1. Human Embryonic Kidney Cell Line (HEK 293T)

The 293T cell line was created in the laboratory of Michele Calos by transfection of the human kidney 293 epithelium cell line with a gene encoding the simian virus 40 (SV40) large T antigen (SV40T-antigen) and a neomycin resistance gene. The constitutive expression of SV40T-antigen, that bind to SV40 origin of replication, enhances the protein expression and production of many viral vectors such as oncoretroviruses and lentiviruses. HEK 293T line also has favourable tissue culture, transfection, DNA replication and gene expression. We use this cell line to produce and test the lentivirus used in our experiments.

##### 3.1.1. Maintenance

The maintenance of HEK 293T cells was performed in 100 mm plates (p100) (Falcon, BD Bioscience) with DMEM supplemented medium:

Media and Solutions	Components
293T medium	Dulbecco's Modified Eagle Medium (DMEM) (Gibco, Life Technologies, ref:41966-29) supplemented with 20 µg/ml Penicillin-Streptomycin and 10% (v/v) of HI-Fetal Bovine Serum (FBS) (Gibco, Invitrogen)

**Table 11. HEK 293T cells media.** Cell media was prepared fresh before use directly in the medium botte and maintained at 4 °C.

When they reached 80-90% of confluence, cells were detached mechanically and centrifuged for 6500g for 5 minutes. We resuspended and plated the 293T cells at 1:4, 1:10 or 1:20 in 10ml of the 293T Medium and incubated at 37°C in a controlled atmosphere (5% CO<sub>2</sub>) incubator. The culture medium was changed every 2 or 3 days. For lentivirus production, we plated the cells in 0.2% gelatine-coated dishes.

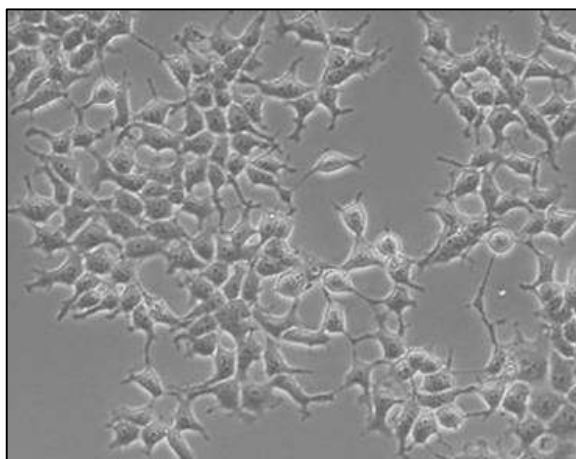


**Figure 41. Representative culture of HEK 293T cells.** Cells were cultured for 1 day in 293T medium.

### 3.1.2. Freezing and thawing

To thaw HEK 293T cells, the vials (preserved in liquid nitrogen) were warmed at 37 ° using the water bath (20-40 seconds). Once thawed, cells were collected in a 15 ml Falcon conical bottom centrifuge tube and DMEM medium was added to reach a final volume of 10ml. Then, cells were centrifuged at 6500g for 5 minutes, resuspended in 293T medium and grown in p100 dishes placed in a CO<sub>2</sub> incubator.

To freeze the HEK 293T cell line, the cells were detached mechanically using 1-2ml of culture medium and collected in a conical bottom tube. DMEM medium was added to a final volume of 10 ml and centrifuged for 5 minutes at 6500g. The cell pellet was resuspended in freezing medium (90% HI-FBS and 10% DMSO (Sigma)) at  $2 \times 10^6$  cells/ml. One ml was distributed in each cryogenic vial (corning, 2ml tube) and kept inside a thermo flask at -80° for 24 hours for a slow freezing process and then kept in liquid nitrogen.

## 3.2. Human fibroblast cell lines

To study the effect of our treatments and to further characterize SMA pathology, we obtain 4 untransformed human cell lines from primary fibroblasts from Coriell Cell Repositories. We purchased 2 cell lines of SMA patients, 1 unaffected carrier, 1 Huntington disease-related patient.

### GM03813 Fibroblast cell line

Untransformed fibroblast cell line obtained from a skin biopsy (arm) of a 3-year-old (at sampling) American Caucasian male clinically affected with SMA.

As described in the Coriell Cell Repository: *“Born after full-term uncomplicated pregnancy; rolled over at 6 months old, began babbling at 9 months old, by 12 months old, there was marked muscle atrophy and weakness; absent deep tendon reflexes and constipation”*

The donor subject has a homozygous deletion of exon 7 and 8 in the *SMN1* gene and 3 copies of the *SMN2* gene. First classified as type 1 SMA was re-classify as type 2 due to onset features and *SMN2* dosage. He has a similarly affected brother (not in the repository).

#### **GM09677 Fibroblast cell line**

Untransformed fibroblast cell line obtained from a biopsy of the eye lens of a 2-year-old (at sampling) Polish/German Caucasian male clinically affected with SMA.

As described in the Coriell Cell Repository: *“Expired at age 23 months; showed hypotonia, decreased muscle bulk, absent deep tendon reflexes, possible fasciculations, normal creatine phosphokinase (CPK) and abnormal Electromyography (EMG)”*.

The donor subject was homozygous for a deletion of exons 7 and 8 of the *SMN1* gene with only 3 copies of the *SMN2* gene and categorize as type 1 SMA (muscle biopsy was consistent with the diagnosis). No previous cases in the family.

#### **GM03814 Fibroblast cell line**

Untransformed fibroblast cell line obtained from a biopsy skin biopsy (arm) of an American Caucasian female clinically unaffected. Mother of two affected children: 1st child is GM03813 and 2nd child is not in the repository. The analysis revealed that donor subject is heterozygous for deletion of exons 7 and 8 in the *SMN1* gene (has 1 copy of the *SMN1* gene) and 5 copies of the *SMN2* gene.

#### **GM02183 Fibroblast cell line**

Untransformed fibroblast cell line obtained from a 21-year-old (at sampling) female with 50% of probability to be affected with Huntington disease (57-year-old affected father). Unknown *SMN1* alterations and *SMN2* gene copies but unaffected with SMA.

### 3.2.1. Maintenance

Cells were grown in 60 mm diameter culture plates (p60) (Falcon, BD Bioscience) using the following medium:

Media and Solutions	Components
<b>Fibroblast Growth medium</b>	Minimum Essential Medium Eagle (MEME) (Sigma, Life science, ref: M2279) supplemented with non-inactivated FBS (Gibco, Invitrogen) (15% v/v), 0.5 M of L-Glutamine (Gibco; Invitrogen), 1% (v/v) of MEME non-essential amino acids (Gibco; Invitrogen) and 20 µg/ml Penicillin - Streptomycin

**Table 12. Fibroblast cell lines media.** Cell media was prepared fresh before use directly in the medium bottle and maintained at 4 °C.

At 80-90% of confluence, cells were washed once with 5ml of Hanks' Balanced Salt Solution (Sigma) and detached using 0.25% of Trypsin-EDTA (Sigma) for 3-4 minutes at 37°. To stop trypsin reaction, DMEM-10% FBS was added (5ml of DEMEM-FBS for 1ml of trypsin solution). After 3 minutes' centrifugation at 6500g, cells were re-suspended in 1ml of Fibroblast Growth medium and plated at 1:3 or 1:4 dilutions.

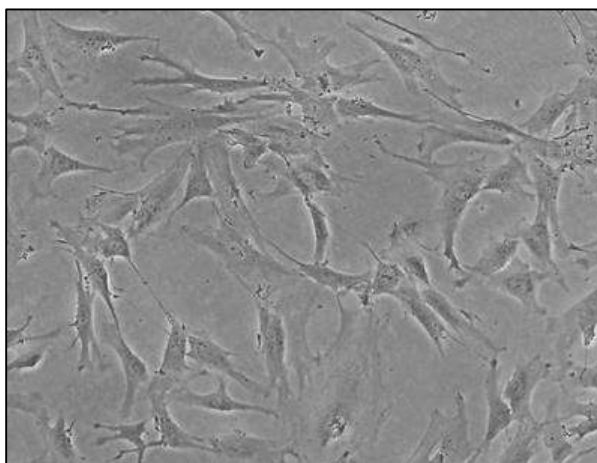


**Figure 42. Representative culture of the human fibroblast cell line (GM03814).** Cells were cultured for 2 days in Fibroblast Growth medium.

### 3.2.2. Freezing and thawing

Cryopreserved vials (liquid nitrogen) were warmed for 20-40 seconds on a water bath at 37 °C. Once thawed, cells were collected in a 15 ml Falcon conical bottom centrifuge tube and 5 ml of Fibroblast Growth medium were added. After 3 minutes of centrifugation (6500g). Cells were re-suspended in Fibroblast Growth medium and cultured in p60 dishes into a CO<sub>2</sub> incubator.

To freeze the fibroblast cell lines, cells were detached and after centrifugation (3 minutes at 6500g) were resuspended in the Fibroblast freezing medium (95% Fibroblast Growth medium and 5% DMSO (Sigma)). Cells were frozen at a ratio of  $5 \times 10^5$  cells/ml. One ml was added in each cryogenic vial (corning, 2ml tube) and kept inside a thermos flask at -80° for 24 hours for a slow freezing process and then kept in liquid nitrogen.

### 3.3. Human-induced Pluripotent Stem Cells (iPSC)

The use of animal models is sometimes limited by inherent differences between species. In order to evaluate previously observed alterations in MNs primary cultures from SMA mice models, we developed in the laboratory the culture of differentiated human MNs from iPSC. To this aim, we purchased from Coriell Institute for Medical Research the GM23411\*B iPSC cell line used as a control (Control) and GM23240\*B iPSC cell line derived from an SMA type 2 patient (SMA). Control and SMA cells were differentiated to MNs as described below.

#### GM23411\*B iPSC cell line

GM23411\*B iPSC cell line derived from the human fibroblast cell GM00041 (Coriell Institute for Medical Research). The untransformed fibroblast cell line was obtained from a skin biopsy (arm) of a 3-month-old (at sampling) Puerto Rican female apparently healthy. The human Fibroblast cell line was reprogrammed with six factors (OCT4, SOX2, KLF4, CMYC, NANOG, LIN28) using retroviral vectors.

#### GM23240\*B iPSC cell line

GM23240\*B iPSC cell line derived from the human fibroblast cell GM03813 (described above). The donor subject has a homozygous deletion of exon 7 and 8 in the *SMN1* gene

and 2 copies of the SMN2 gene and was classified as type 2 SMA. Human fibroblast cell line reprogrammed with four factors (Oct4, Sox2, Nanog, Lin28) using lentivirus vector

### 3.3.1. Cell culture media and solutions

Media and Solutions	Components
<b>hES Media</b>	KnockOut Dulbecco's Modified Eagle Medium (KO DMEM) (Gibco, Life technologies, ref:10829018) supplemented with KO Serum replacement (20% v/v) (Gibco, Life technologies), 2-mercaptoethanol (0.1 mM) (Sigma), L-glutamine (0.1 mM) (Gibco; Invitrogen), basic fibroblast growth factor (bFGF) (6 ng/ml) (Peprotech) and non-essential amino acids (1% v/v) (Gibco; Invitrogen)
<b>MEF-conditioned hES Media</b>	hES Media supplemented with additional 4 ng/ml of bFGF (Peprotech) and the rock inhibitor Y27632 (10 $\mu$ M)
<b>Neural Epithelial Induction Media (NEPIM)</b>	DMEM/F-12 (Gibco, Life technologies, ref:11320033) and Neurobasal Medium (NBM) (Gibco, Life technologies, ref:21108-049) 1:1 supplemented with B27 (Gibco, Life technologies), L-glutamine (Gibco, Life technologies), NEAA (Gibco; Invitrogen), ascorbic acid (0.1 mM) (Sigma), CHIR99021 (3 mM) (Cayman), SB431512 (2 mM) (Cayman) and DMH1 (2 mM) (Cayman)
<b>MNs Progenitors (MNP Media)</b>	NEPIM containing retinoic acid (RA) (0.1 $\mu$ M) (Sigma), purmorphamine (0.5 $\mu$ M) (Cayman) and VPA (0.5 mM) (Sigma)
<b>MNs Induction Media</b>	NEPIM plus RA (0.5 $\mu$ M) (Sigma) and purmorphamine (0.1 $\mu$ M) (Cayman)
<b>MNs Maturation Media</b>	MN Induction medium supplemented with Compound E (0.1 $\mu$ M) (Sigma), CNTF (20 ng/ml) (Bio-nova) and IGF-1 (20 ng/ml) (Peprotech)

**Table 13. Human MNs differentiation cell culture medium.** All media and solution were prepared fresh and sterilized before use.

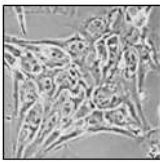
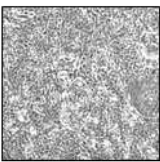
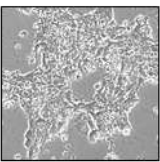
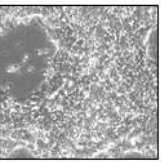
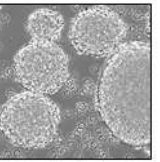
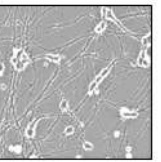


### 3.3.2. MNs differentiation protocol

MNs differentiation was performed following the protocol described previously (Du et al., 2015) with minor modifications established by Dr Manuel Portero's laboratory (Universitat de Lleida-IRBLLLEIDA).

Human iPSCs were cultured on a layer of irradiated mouse embryonic fibroblasts (Gibco) in regular hES media. When large undifferentiated colonies were observed we started the differentiation process by generation of neuroepithelial cells. For that, iPSCs were dissociated with Accutase (Gibco) following manufacturer indications and plated on Geltrex (Gibco)-coated plates in MEF-conditioned hES medium at 20 000 cells/cm<sup>2</sup>. Twenty-four hours later, neuroepithelial induction medium fresh medium was added.

Medium was changed every two days and maintained in this condition for 6 days. To generate motoneuron progenitors (MNP), cells were dissociated with Accutase, plated at a density of 30000-50000 cells/cm<sup>2</sup> on matrigel-coated dishes and MNPs Media and expanded for around 6 days. At this point, MNPs can be split once a week (always replating at 30000-50000 cells/cm<sup>2</sup>) for additional 5 passages, before losing the potential of forming MNs, or cells can be freeze in standard 10% DMSO freezing media.

Days in vitro	0	2	4	6	8	10	12	14	16	18	20	22	24	26	28	30
hiPSCs maintenance	Neuroepithelial Induction				MNs specification						MNs induction			MNs Maturation		
hiPSCs	Neuroepithelial progenitors				MNs progenitors I			MNs progenitors II			Neurospheres			hMNs		
																
Coating: irradiated mouse embryonic fibroblasts	Coating: Geltrex				Coating: Matrigel			Coating: Matrigel			Coating: non cell-culture treated plates			Coating: P/O-Laminin		
Medium: hES Media	Medium: MEF-conditioned hES Media (24h) and NEPIM				Medium: MNPs Media			Medium: MNPs Media supplemented with VPA			Medium: MNs Induction Media			Medium: MNs Maturation Media		

**Figure 43. Differentiation process from hiPSCs to mature MNs.** The total differentiation process takes approximately 30 days before we obtain mature MNs

For the final step of MNs formation, MNPs were detached with Accutase and cultured (at 1.000.000/ml) in suspension in MN Induction medium (non cell-culture treated plates). The medium was changed every two days and six days later, neurospheres were dissociated with Accumax Dissociation Medium (Invitrogen) and plated on laminin-coated plates (as described in “2.1. Precoating plates” from “*Materials and Methods*” section) in MNs maturation medium. For western blot analysis, cells were plated on laminin-coated four-well dishes at 20.000 cells/cm<sup>2</sup> of density and maintained with MN maturation medium during 6 days. For immunofluorescence experiments, 25.000 cells were plated on laminin-coated 1 cm<sup>2</sup> glass coverslips, maintained in the MN maturation medium and fixed in 4% paraformaldehyde (PFA) in PBS.

#### **4. shRNA interference by lentiviral transduction**

The RNA interference (RNAi) is a technique of gene silencing at the post-transcriptional state that reduces mRNA expression in living cells. Several types of small RNA molecules have been described for silencing target genes, the most widely used are the small interfering RNA (siRNA) sequences. These molecules are sized 21 to 25 nucleotides and are produced from a precursor of double-stranded RNA that may vary in size and origin.

Short hairpin RNA (shRNA), is an artificial RNA molecule slightly larger and precursor of siRNA, with a tight hairpin-like turn that has a relatively low rate of degradation and turnover, and allows a durable gene silencing.

shRNAs can be introduced inside the cells using lentivirus and, unlike siRNA, shRNA is produced inside the cell nucleus and transported to the cytoplasm via the microRNA (miRNA) export pathway. There, the shRNA is processed into siRNA by Dicer, an enzyme that degrades the double-stranded RNA precursors. The new-formed siRNA is engaged in a silencing complex called RISC (RNA-Induced Silencing Complex) for an optimal RNAi processing activity.

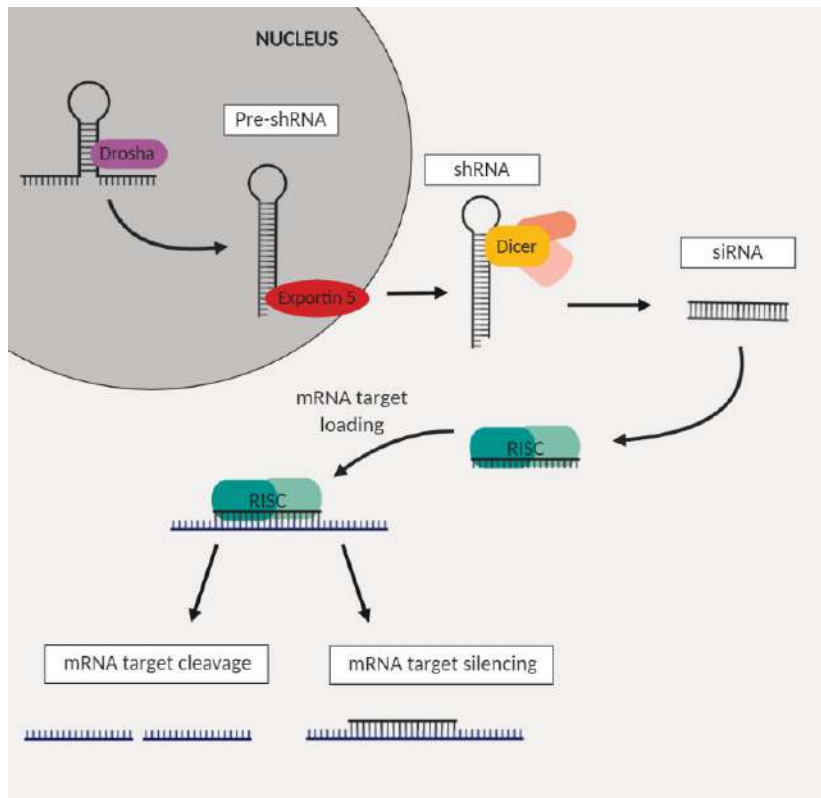


**Figure 44. Mechanism of shRNA induced gene silencing.** Pre-shRNA in the nucleus is processed by Drosha and exported to the cytoplasm by Exportin 5. After association with Dicer, the loop sequence is removed and processed as siRNA. After association with RISC and removal of one of the RNA strands, they target mRNAs with complementary sequence, inducing mRNA degradation or silencing (Based on Hannon and Rossi, 2004).

The incorporation of the siRNA into the RISC complex induces the separation of the siRNA into two strands: the sense (passenger) strand that is degraded and the antisense (guide) strand that directs RISC to mRNA that has a complementary sequence. In case of perfect complementarity, RISC cleaves the mRNA while in case of partial complementarity, RISC represses translation of the mRNA. In both cases leading as results in the silencing of the target gene (Reviewed in Hannon and Rossi, 2004).

#### 4.1. shRNA construct

In the present study, we knockdown the  $\mu$ -calpain protein expression using an shRNA introduced into the cell by lentiviral transduction. The shRNA and lentivirus design was mainly performed by Dra Ana Garcerá and Dra Myriam Gou-Fabregas. The shRNA was design based on an RNAi sequence using the informatics online tool, siDESIGN<sup>®</sup> and sDirect with the following parameters:

- To be a siRNA for the Open Reading Frame of Calpain (between the first 130 to 240 nucleotides)
- To have a percentage of G-C between 30 and 52
- Exclusion of all patterns AAA and TTT
- Elimination of sequences that recognize non-specific sequences
- Omit sequences with more than 9 continued C/G

The resulting shRNA was a double strain DNA with the following structure:

#### Forward

5'-GATCCCCGCGCCAAGCAGGTAACCTTATTCAAGAGATAAGTTACCTGCTTGGCGCTTTTT-3'

#### Reverse

5'-AGCTAAAAAGCGCCAAGCAGGTAACCTTATCTCTTGAATAAGTTACCTGCTTGGCGGGG-3'

Both sequences were ordered at Invitrogen (Custom Primers Order) and cloned into the lentiviral vector pLVTHM (Tronolabs).

## 4.2. Lentivirus production

Lentivirus, a subset of retroviruses, are the most common tool used to introduce a gene or DNA into cells. These viruses are based on HIV-1 and integrate randomly into the host genome enabling long term transgene expression in both dividing and non-dividing cells. Because of this stable integration, lentiviruses have mutagenic potential. To reduce the risk of infection during the processes of production and manipulation 2<sup>nd</sup> and 3<sup>rd</sup> generation of lentiviral systems were designed. These lentiviral system have eliminated five of the nine HIV-1 genes, leaving only the genes essential for transcriptional and post-transcriptional functions, structural utilities and enzymatic components, and splitting them across multiple plasmids (usually 3).

In our laboratory we used a second-generation system that has the following components:

- **Lentiviral transfer plasmid** encoding our insert of interest (we used the pLVTHM (Tronolabs) plasmid). Here the transgene sequence is flanked by long terminal repeat (LTR) sequences, which facilitates the integration of the transfer plasmid

sequences into the host genome. This vector also contains the Green Fluorescent Protein (GFP) under the control of an EF-1  $\alpha$  promoter to monitor the transduction efficiency.



**Figure 45. pLVTHM lentiviral transfer plasmid structure.**

**EF-1 $\alpha$  promoter:** Elongation Factor 1 promoter

**cPPT (central Polypurine Tract):** 118 bp sequence derived from the HIV-1 pol gene that increases the efficiency of transduction of lentiviral vectors

**WPRE (Woodchuck hepatitis virus Posttranscriptional Regulatory Element):** Posttranscriptional regulatory element of hepatitis virus from Woodchuck that is incorporated to increase transgene expression

**H1 promoter:** promoter of the H1 gene a ribonucleic component of the RNase P

**SIN (Self-Inactivating):** modified 3' LTR region of the virus, so that the lentiviral vectors self-inactivate once integrated into the host genome. The process occurs because this deleted region is copied into the 5' LTR once integrated, reducing vector genome mobilization and the influence of the LTR on endogenous cell promoters near the integration site

- **Packaging plasmid.** Is the vector that contains all the proteins necessary for the packaging of the virus. We used the psPAX2 (Tronolabs) plasmid.

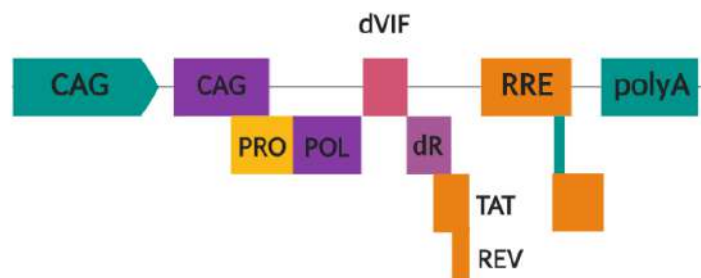


**Figure 46. psPAX2 packaging plasmid structure.**

**GAG:** gene coding for different nucleocapside and matrix proteins

**POL:** gene that codes for a reverse transcriptase, a protease and an integrase

**TAT:** gene coding for a protein necessary for the transactivation

**REV:** gene coding for a protein necessary for transport regulation and RNA processing

**RRE (Rev-Responsive Element):** necessary for the REV sequence action

- **Envelope plasmid.** Is the vector that codifies for the Vesicular Stomatitis Virus (VSV) protein responsible for the infection process. In our case, we used the pM2 (Tronolabs).



**Figure 47. pM2 envelope plasmid structure.**

**VSVG:** heterologous gene of the G protein of the VSV. It is flanked by a CMV promoter and a polyA tail

Lentiviruses were produced using the HEK 293T cells and the polyethyleneimine (PEI) (Sigma) cell transfection method. PEI is obtained by polymerization of ethylenimine, forming a highly branched network with a high cationic potency that condenses DNA into positively charged particles which bind to anionic cell surface residues inducing cell endocytosis. Once inside the cell protonation of the amines results in an influx of counterions and a lowering of the osmotic potential. Osmotic swelling results and bursts the vesicle releasing the polymer-DNA complex into the nucleus and the cytoplasm. PEI is highly used in biology laboratories, especially in tissue culture, but if used in excess could result in cell toxicity (Vancha et al., 2004).

PEI was prepared at an initial concentration of 20% (equivalent of 8 mM PEI (Aldrich) and 4.5 M equivalents of Nitrogen) and later diluted in milliQ water to a stock concentration of 200 mM at pH 5.6. To generate the final transfection reagent, PEI was diluted at a final concentration of 10 $\mu$ M. The reagent can be stored at -20 $^{\circ}$ C in aliquots.

The protocol for the lentivirus production was:

**Day 0:** The day before transfection, HEK 293T cells were plate in p100 dishes (55,000 cells/cm<sup>2</sup>) coated with 0.1% gelatine.

**Day 1:** Transfection day. We transfected a total amount of 40  $\mu$ g DNA using a total volume of 240  $\mu$ l PEI 10  $\mu$ M *per* each p100 plate.

<b>pLVTHM - Lentiviral transfer plasmid</b>	20 µg
<b>psPAX2- Packaging plasmid</b>	13 µg
<b>pM2 - Envelope plasmid</b>	7 µg

For each plate to transfect, 40 µg of DNA was diluted in 1500 µl of OptiMEM medium (Thermo Fisher) and vortex for 2 minutes. In another tube, 240 µl of PEI was dropwise diluted in 1260 µl of OptiMEM. Then, the PEI solution is slowly added into the DNA mix and rapidly vortex for 5 to 15 seconds to avoid the aggregate formation. The solution was let to rest for 10 minutes at room temperature.

Cells plates were washed once with OptiMEM medium and let them with a final volume of 4 ml of OptiMEM medium. Finally, the PEI-DNA mix was added into each plate slowly. After 1 hour, the medium was changed to 10 ml of complete HEK 293T medium and the cells were reintroduced into the incubator for virus production.

**Day 3:** After 72 hours we collect the supernatant in a 50 ml Falcon tube and centrifuged at 40600g for 5 minutes to precipitate of HEK 293T cells. Then, the supernatant was carefully collected and filtered into a new tube using 0.22 µm filters. Lentivirus containing solution was aliquotted in 2 ml polypropylene cryogenic tubes and stored at -80°C.

Once defrosted, the remaining not-used solution was discarded, since the freeze-thaw process reduces the virus titration by 2 to 3 times.

### 4.3. Virus titration

The virus construction used in our lab contains the GFP sequence that could be used to evaluate the virus efficacy.

1. HEK 293T cells were plated at a concentration of 5,000 cells/cm<sup>2</sup>.
2. 3 hours later, cells were treated with three different volumes of the virus medium (usually 100, 200 or 500 µl).
3. After 72 hours, using ImageJ, we evaluated the percentage of transduced cells (GFP positive) compared to the total number of cells. Biological tites of the viral

preparation were expressed as the number of transducing units (TU) *per ml* (TU/ml) using the following formula:

$$\text{TU/mL} = \frac{(\text{Initial number of cells} \times \text{Percent of transduced cells})}{\text{Virus volume added (in mL)}}$$

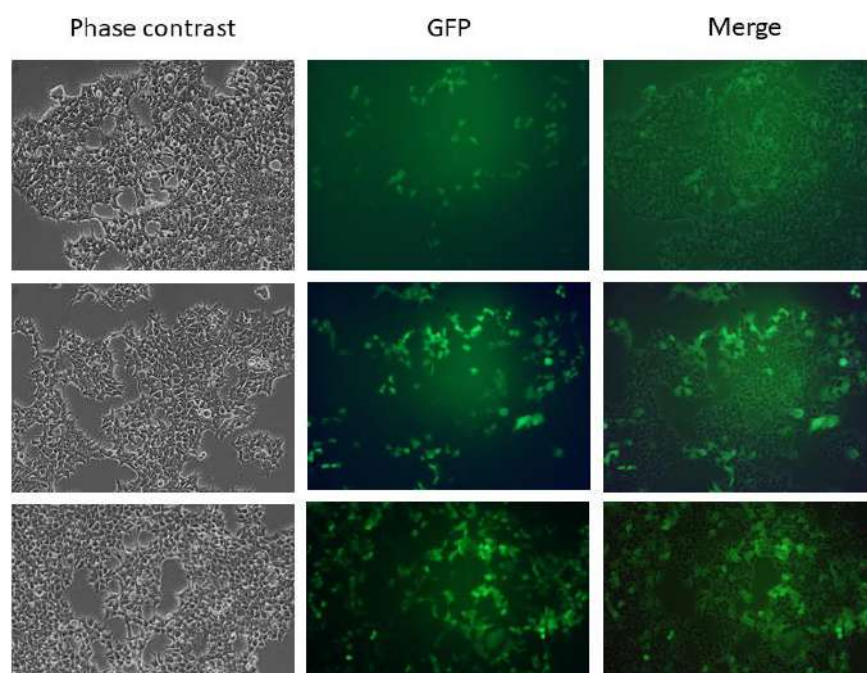


**Figure 48. Representative image of a virus titration using HEK 293T.** Plated cells were transfected with 100, 200 and 500  $\mu\text{l}$  of the virus-containing medium. After 72 phase contrast and fluorescent photos were taken and title was quantified using the formula.

#### 4.4. Lentiviral transduction of primary cell cultures

For our experiments, primary cultured MNs were plated and 2-3 hours later the medium containing the viruses was added. We directly add the virus medium to the cultures in a ratio of 1/3 (3 lentiviral particles for each cell) and incubate overnight. After the 20-24 hours of incubation time, the medium was replaced with fresh NTFs medium supplemented with aphidicolin. The lentivirus transduction efficiency was monitored using the GFP reporter using fluorescence microscopy. Experiments were performed in those cultures that showed a minimum of 90% of positive fluorescence. Final evaluation of the virus effectiveness was done analysing the levels of the shRNA target protein by western blot analysis.



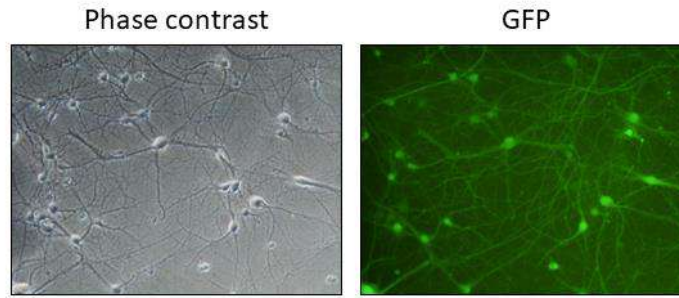


**Figure 49. Representative image of mouse MNs transduced with the lentivirus.** Mouse MNs were isolated and treated with the lentivirus the same day. GFP signal was observable after 6 DIV.

## 5. List of cell cultures drugs

All drugs were prepared in the culture hood, diluted in the appropriate medium, and filtered with 0.22  $\mu\text{m}$  filters, before being added to cell cultures.

Treatment	Description	Dilution medium	Final Concentration	Time of treatment	Supplier
Calpeptin	cell-permeable inhibitor of calpain-1 and calpain-2	DMSO	25 $\mu\text{M}$	3, 6 or 12 hours	Calbiochem
Potassium chloride (KCl)	Metal halide salt	NBM medium	30 mM	3 hours	MERCK
Resveratrol	Phenolic phytoalexin	DMSO	50 nM	12 hours	Sigma
Trehalose	Non-reducing disaccharide	Water	100 mM	6 hours	Sigma
Calpastatin Peptide Ac 184-210	Calpain inhibitory protein	L-15 + 10% HS	100nM	6 hours	Sigma

**Table 14. List of cell cultures drugs.** All treatments were prepared fresh and sterilized before use.

## 6. Evaluation of neuronal viability in culture

The use of isolated primary cells gives us the advantage of evaluating some cellular changes, which otherwise would be very difficult to study. Likewise, cell viability and functionality could be heavily influenced by the effect of a disease or by different treatments and should be taken into consideration in all *in vitro* studies.

For all test of survival and neuronal degeneration, we always carried out three repetitions of each condition and always performed a minimum of 4 independent experiments. All quantifications were analysed with the observer blinded to the condition.

### 6.1. MNs survival

To evaluate MNs survival, cells were isolated and plated at a low density (8,000 cells/cm<sup>2</sup>) to reduce cell-contact signalling, in complete medium containing a cocktail of recombinant NTFs (NTFs medium) or in basal medium with no supplements (NBM). Three hours after purification, NTFs-plated cells were treated with lentivirus following the usual transduction protocol. Twenty hours after transduction, cell medium was replaced and the initial number of cells was counted (Day 0). Photos were taken at 10X in the same initial microscopic areas (four central areas *per* well) at days 3, 6, 9 and 12 days. MN survival was quantified by counting the number of large phase-bright neurons with long axonal processes using the computer program image J (cell-counting plugin.) The results were expressed as the percentage of cells counted each day respect to the initial value at day 0 (considered as 100%).

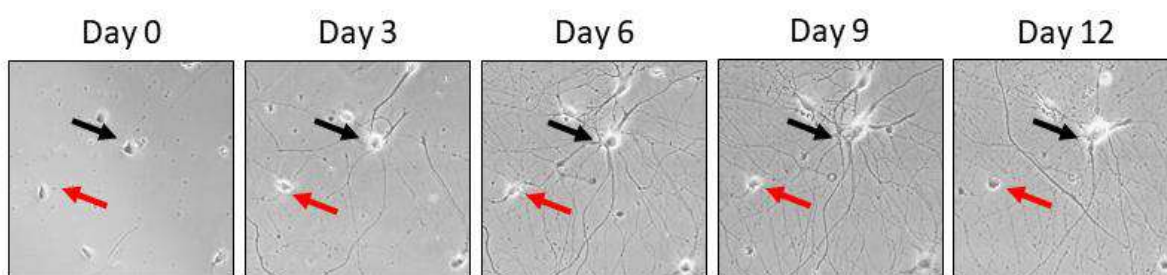


**Figure 50. Example of MNs survival analysis.** For survival analysis, photos are always taken in the same microscopic area as the initial one (Day 0). It can be appreciated in the image how the MNs marked with the black arrow stays alive until the last day of the analysis (Day 12) while the MNs marked with the red arrow end up degenerating.

## 6.2. Neuronal degeneration

Morphometric analysis of neurite degeneration was determined in the primary cultures of MNs. For that, dissociated MNs were cultured at a low-density of 5,000 cells/cm<sup>2</sup> in an M4 cell culture dish, to achieve a neuritic network sufficient but not excessive in density that allows us to efficiently observe the morphology of the neurites.

At days 6, 9 and 12 after plating, phase contrast microscopy images (24 photos *per* well) were obtained with a 40× lens using an inverted microscope.

To analyse the images, we used the imageJ program with NIH ImageJ software. A grid was created over each image using the grid plugin (line area = 50.000) and with the counter, we determine the total number of neurites and the number of neurites that were degenerating in each grid area. Thirty–50 neurites were counted *per* each image. Neurite segments were considered degenerated if they showed evidence of swelling and/or blebbing, reflecting interruptions of the cytoskeleton and accumulations of proteins and organelles.

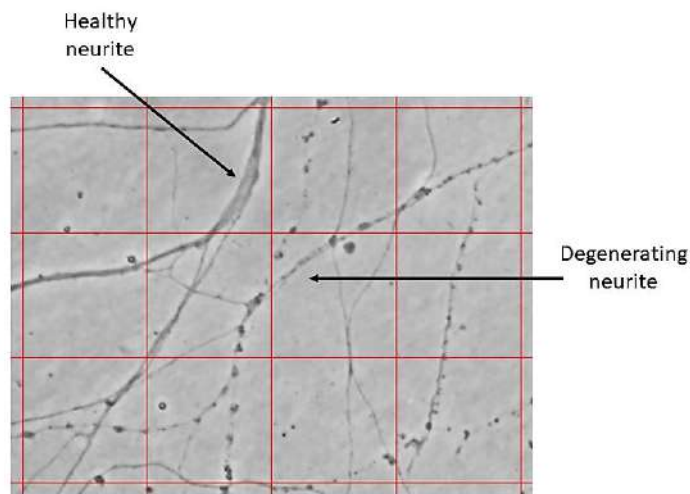


**Figure 51. Example of neuronal degeneration analysis.** For the analysis, the number of degenerated neurites was quantified regarding the total number of neurites in each grid area.

## 6.3. Apoptosis nucleus quantification

Hoechst (Sigma) is part of a group of bis-benzamides, originally developed by Hoechst AG, used to stain DNA. Hoechst enters into the cell and binds to the AT-rich regions of the

double strand of DNA. Once bound, it is excited by ultraviolet light at around 350 nm and emits blue fluorescent light around an emission spectrum of 450 nm. Hoechst is often used to distinguish nuclei that have an apoptotic morphology (condensed pyknotic nucleus and fragmented nucleus), as shown in **Figure 52** and allows us to assess the state of the cell according to the morphology of its nucleus.

For the experiments, MNs were fixed with 4% PFA for 20 minutes and incubated with Hoechst dye at a concentration of 2  $\mu\text{g/ml}$  for 30 minutes. The cells were left in PBS for analysis. The percentage of the apoptotic nuclei was assessed by counting those cells that present a nucleus with apoptotic morphology respect to the total amount of quantified nuclei.

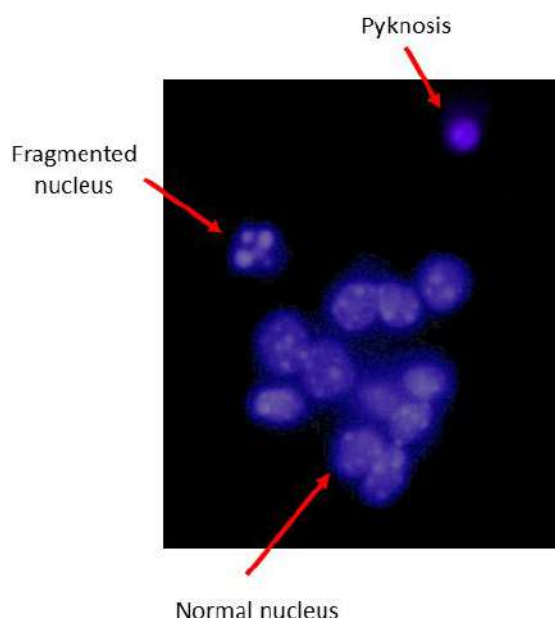


**Figure 52.** *Representative image of MNs nuclei stained with Hoechst dye. Apoptotic nuclei were considered when showing pyknosis and fragmented nucleus.*

## 7. Immunofluorescence technique

In recent years, immunofluorescence has made the transition from a tricky and occasional technique to one of the most common laboratory procedures. Immunofluorescence is based on the use of specific antibodies which have been chemically conjugated to fluorescent dyes, and that can bind directly or indirectly to cellular antigens. The

immunofluorescence technique allows for a visualization of the presence as well as the distribution of target molecules in a sample.

For our experiments, we used the secondary or indirect immunofluorescence approach where the first unlabelled antibody (primary antibody) specifically binds to the target molecule while the second fluorophore-labelled antibody (secondary antibody) recognizes and binds the primary antibody. The use of an indirect immunofluorescence requires a more complex and time-consuming protocol, but it provides more flexibility and amplification of the signal.

We have used two different protocols depending on the origin of the samples. In each experiment all condition were included and were all processed at the same time, so all samples were subjected to the same conditions.

### **7.1. Cell culture immunofluorescence**

For the detection of specific antigens in cultured cells, we have proceeded with the following protocol. On the specified day, MNs were fixed with 4% PFA for 10 min. To avoid alterations in the basal state of the cells with the fixation process, an 8% PFA was added in a 1: 1 ratio directly to the existing volume of culture medium. Then, 3 quick washes were made with PBS 1x and a second fixation with cold methanol (-20 °C) was performed for 10 minutes. the cold methanol also helps with the permeabilization process. To evaluate the autophagy marker LC3 by IF, the step with paraformaldehyde was obviated. After methanol fixation, cells were washed again with PBS 1X.

To block the samples, we used a solution containing BSA (5%) and Triton X-100 (0.2%) in PBS 1X for 2 hours. The incubation with the primary antibody diluted in blocking solution was carried out at 4 °C overnight.

After this incubation period, 3 washes were carried out with blocking solution and the samples were incubated with the appropriate secondary antibody diluted in blocking solution, for 1 hour at room temperature. Finally, after 3 washes with 1X PBS (of 5 minutes each), Hoechst (1:400) stain was performed for 25 minutes at room temperature. Samples were mounted on slides using 15 µl (for 15-mm coverslips) of the water-soluble mucoadhesive, Mowiol (Calbiochem, EMD Millipore, Darmstadt, Germany).

## **7.2. Tissue immunofluorescence**

For antigen immunodetection in tissues, the samples must be pretreated in order to maintain the cellular characteristics and structure of the tissue.

### **7.2.1. Tissue preparation and cryopreservation**

In order to obtain from the same animal, tissue samples for western blot and for immunofluorescence experiments, mice were not perfused intraventricularly.

Instead, mice were sacrificed at given days by decapitation and the lumbar region of the spinal cords was obtained (vertebras included) and quickly submerged in 4% PFA for 24 h. After fixation, tissue was cryopreserved using a sucrose solution (30% sucrose (Sigma), 0.1M Phosphate buffer and 0.02% of sodium azide) for 24-48 h. The purpose of cryopreserving tissues with the sucrose solution is to help prevent ice crystal formation in tissues when water freezes and expands producing holes within cells and loose extracellular matrix (what is called "Swiss Cheese" artefacts). Then spinal cords were dissected and submerged in new sucrose solution for an extra 24 h.

Once dissected and cryopreserved, the samples were embedded using Tissue Freezing Medium (TFM) (Science Services) and preserved at -80 °C. TFM minimizes freeze-fractures by embedding the cellular matrix reducing the water content and allowing the tissue to freeze quickly. It also gives tissue support during cryotomy improving specimen handling. TFM leaves no residue since it is easily washed away during fixation. The lumbar spinal cords were transversely processed using a Leica CM1950 cryostat at 16 µm of thickness. Between 8 and 12 serial slices were placed in each slide (Superfrost plus EV, Thermo Scientific) and let them dry overnight before storing them at -80 °C.

### **7.2.2. Immunofluorescence protocol**

Defreeze the samples for 15-20 minutes and rehydrate them with 2 washes of PBS 1X before permeabilization with a detergent solution (0.3% Triton X-100 in PBS) for 30 minutes. To block unspecific antigens, samples were treated with a 5% BSA solution (in PBS) for 1 hour. After that, the primary antibody was added diluted in PBS 1X+ 0.3% of Triton X-100 overnight at 4 °C.

The secondary antibody was prepared in PBS 1X and incubated for 1 hour a room temperature in darkness, to avoid damaging the fluorescence labelling with the room light. Two fluorescent stainings were also performed; the Hoechst stain and the Nissl stain (NeuroTrace 530/615 Red Fluorescent Nissl Stain/ Life Technologies). We first added the Nissl stain (1:200), just after the secondary antibody, for 30 minutes. This staining is very strong and to be able to continue with the IF, the samples must be washed twice with PBS 1X for 1 hour each time. Finally, we added the Hoescht (Sigma) stain at 1:300 for 30 minutes. After 3 washes with PBS 1X (10 minutes each), samples were embedded in 50  $\mu$ l of Mowiol medium.

### 7.3. List of antibodies

Primary antibody	Host	Dilution	Supplier
<b>SMN</b>	Mouse	1/100	BD Biosciences (Cat. no. 610646)
<b>LC3</b>	Rabbit	1/100	Cell Signalling (Cat. no. 2775)
<b>Calpastatin</b>	Rabbit	1/100	Abcam (Cat. no. ab28252)
<b>Mu-Calpain</b>	Mouse	1/100	Invitrogen (Cat. no. 9A4H8D3)
<b>Islet 1/2</b>	Mouse	1/50	DSHB (University of Iowa) (Cat. no. 39.4D5)
<b>B-III Tubulin</b>	Rabbit	1/150	Cell Signalling (Cat. no. 5568)
<b>Hb9</b>	Rabbit	1/100	Abcam (Cat. no. ab92606)
<b>Synaptophysin 1</b>	Guinea pig	1/500	Synaptic System (Cat. no. 101004)
<b>Choline acetyltransferase (ChAT)</b>	Sheep	1/100	Abcam (Cat. no. ab18736)

**Table 15.** List of the primary antibody used in immunofluorescence analysis. Antibodies were kept at -20 °C and prepare fresh before used.

Secondary antibody	Host/ Isotype	Dilution	Supplier
Alexa Fluor 488 anti-Rabbit	Goat / IgG	1/400	Invitrogen (Cat. no. A11008)
Alexa Fluor 555 anti-Rabbit	Goat / IgG	1/400	Invitrogen (Cat. no. A21428)
Alexa Fluor 555 anti-Mouse	Goat / IgG	1/400	Invitrogen (Cat. no. A21422)
Alexa Fluor 488 anti-Mouse	Goat / IgG	1/400	Jackson ImmunoResearch (Cat. no.715-546-150)
Alexa Fluor 488 anti-Guinea pig	Donkey / IgG	1/400	Jackson ImmunoResearch (Cat. no.706-545-148)
Alexa Fluor 649 anti-Sheep	Donkey / IgG	1/400	Jackson ImmunoResearch (Cat. no.713-496-147)

**Table 16.** List of the secondary antibody used in immunofluorescence analysis. Antibodies were kept at -20 °C and prepare fresh before used.

#### 7.4. Quantification and analysis

All samples were evaluated using a high-resolution Olympus laser scanning inverted confocal microscope (FV1000 and F10) equipped with the Fluoview 500 program. The images were acquired with the immersion oil objective of 60X and analysed using the ImageJ software (National Institute of Health, USA). The same microscope settings were used for the acquisition of digital images.

For all morphometric analysis, a minimum of 50 MNs were imaged for each condition in different areas/sections of the slide and all the experiments were repeated at least 3 times, for mice samples a minimum of three animals *per* condition were included. In spinal cord sections, MN cell bodies were identified in the ventral horn by their characteristic shape and size and Nissl positive stain.

##### 7.4.1. Cell fluorescence measurements

In some experiments, it was important to determine the relative levels of proteins in a specific location or cellular structure and whether treatment could interfere with this localization. In those cases, quantification of the immunofluorescence signal of a specific protein in different structures was necessary.



For the quantification of the fluorescence level of a protein at a specific intracellular location we use the Analyse tool on the NIH ImageJ software. First, using the Nissl, GFP or phase-contrast image, the cell perimeter was determined. Then the selected perimeter was transferred to the corresponding image with the fluorescence to quantify. The integrated intensity was measured only in the specified area of the cell. In the same photo, a surrounded region was selected as a background (BK) measurement. To calculate the fluorescence of the selected area, we used the corrected total cell fluorescence (CTCF) formula:

$$\text{CTCF} = \text{Integrated Density} - (\text{Area of selected cell} \times \text{Mean fluorescence of BK readings})$$

This method is an adaptation of an original protocol from Gavet and Pines, 2010.

#### 7.4.2. Spots number quantification

Inside the cells, there are a large number of proteins that change their cellular localization pattern depending on their activation state. In the present work, we studied the autophagy marker LC3. This protein is normally located in the cytoplasm and goes from a diffuse pattern in its inactive state to a punctured pattern when it is activated and recruited in the autophagic vesicles (Mizushima, 2004). In this situation, quantification of the spots in a determined area is the adequate form to measure LC3.

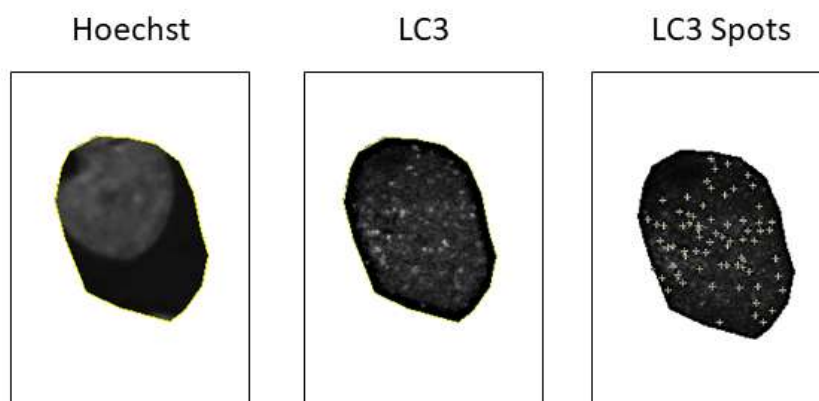


**Figure 53.** Example of LC3 spots quantification using ImageJ software. Cell silhouette was traced and isolated. Spots were automatically identified and quantified by the software.

For quantification, the threshold level of the LC3 digital image was adjusted to highlights all the spots. The threshold value should be the same for all the analysed images. Using the corresponding GFP image, cell perimeter was selected and transferred to the LC3 image. Quantification of the number of spots in the selected area was performed automatically using the “Find Maxima” tool (**Figure 53**).

## **8. Protein analysis technique**

The western blot is a widely used analytical technique in cell and molecular biology that allows the separation and identification of specific proteins from a complex mixture of proteins extracted from cells.

The technique is based on three steps: (1) separation by size, where a sample of tissue homogenate or cellular extract is separated based on protein molecular weight, through a gel electrophoresis; (2) transference to a solid support or membrane producing a band for each protein; and (3) marking target protein using a specific primary and secondary antibody to visualize the protein of interest.

### **8.1. Protein extraction**

#### **8.1.1. Cell culture**

In 4-well tissue culture dishes, after the treatments' times or in the chosen culture times total cell protein lysates were obtained. For that, MNs cultures were first rinsed with ice-cold PBS 1X buffer to stop intracellular reactions and eliminate cell debris and extracellular proteins floating on the cell medium. Then PBS was thoroughly aspirated to avoid dilution of the sample and cells were collected using 27  $\mu$ l of lysis buffer (125mM Tris pH 6.8 and 2% SDS). Lysis buffer was added directly to the centre of the well and using the pipet tip, cells were scraped from the bottom of the plate. The protein samples were collected in a sterile Eppendorf tube, boiled for 5 minutes at 95 °C and stored at -20 °C.

For cell lines grown in bigger cell culture dishes a proportional amount of lysis buffer and a scrapper was used. Sonication of the samples was also performed after the heating step to ensure cells rupture.

### 8.1.2. Tissue

Mice were sacrificed at specific days by decapitation and the thoracic region of the spinal cord was dissected, placed it in a sterile Eppendorf tube and immediately freeze using liquid Nitrogen. Protein extraction was done using Direct Quant 100ST Buffer (DireCt Quant).

Following the product instructions, 25  $\mu$ l of the buffer were added for 1 mg of tissue. For postnatal spinal cord fragments, we used a volume of 150  $\mu$ l of the buffer. Samples were homogenized with a G50 Tissue Grinder (Coyote Bioscience) until the tissue was completely disintegrated. Then tissue disaggregates were heated at 90 °C for 3 minutes while shaking at 750 rpm in a thermoblock (Eppendorf). In this step, the buffer will change from red to orange colour. Before continuing with the protocol, samples must cool down to room temperature (buffer colour will return to red). Once ready, samples were centrifuged at 2000g in an Eppendorf MiniSpin centrifuge for 5 minutes and the supernatant was collected and transferred to a new Eppendorf tube.

To ensure protein solubilisation, we added an extra step of sonication and centrifugation (2000g in an Eppendorf MiniSpin centrifuge for 2 minutes). The supernatant was transferred to a new tube and stored at -20 °C.

### 8.2. Protein concentration quantification

Since MNs are post-mitotic cells and in cultures, we plated the same number of cells in each well, we did not make any quantification of the protein concentration. It was assumed that all the wells had the same number of cells and therefore the same amount of protein (approximately 40  $\mu$ g of protein).

For cell lines and tissue homogenates, protein concentration was quantified using the Bradford method and corroborated with a NanoDrop Spectrophotometer protein quantification. To measure protein concentration with Bradford, we first prepared on ice the Bradford reagent by diluting 1:4 with milliQ sterile water and a BSA protein standard (minimum we use 8 points *per* duplicate to make the standard curve). In a 96-well plate, we loaded the BSA standard dilutions or 1  $\mu$ l of each sample. Using a multi-pipettor, 200  $\mu$ l of the Bradford reagent was added to each well avoiding making bubbles. After that, the plate was set at room temperature for 10-15 minutes and read at 595nm in a SpectraMax

Plate Reader. All values were done *per* duplicate. For each western blot, between 15-20  $\mu$ g of protein was used.

### 8.3. Electrophoresis in SDS-polyacrylamide gel

To detect and characterize proteins, we performed one-dimensional electrophoresis under denaturing conditions on gels formed by a polyacrylamide matrix in the presence of SDS (“Sodiumdodecylsulfate-polyacrylamide gel electrophoresis” or SDS-PAGE) using a mini-PROTEAN® Tetra cell system (Bio-Rad). SDS is an anionic surfactant compound that denatures proteins and binds to polypeptide chains conferring negative charge and allowing samples to separate only according to their molecular weight. To maintain denaturing conditions, SDS must be included in all electrophoresis compounds (gels and buffers).

#### Polyacrylamide gel preparation

For our experiments, we use gels with two differentiated parts: stacking gel and separating gel. The upper, stacking gel is slightly acidic (pH 6.8) and has a lower acrylamide concentration making a porous gel, which separates protein poorly but allows them to form thin, sharply defined bands. The lower gel also called resolving gel, is basic (pH 8.8), and has a higher polyacrylamide content, making the gel's pores narrower. We prepare the gels following the next table:

Stacking gel		Resolving gel	
Tris-HCl (pH=6.8)	125Mm	Tris-HCl (pH=8.8)	375mM
Acrylamimde	3-5% (v/v)	Acrylamimde	7-12% (v/v)
SDS	0.1% (w/v)	SDS	0.1% (w/v)
Ammonium persulfate	0.05% (w/v)	Ammonium persulfate	0.05% (w/v)
TEMED	0.025% (v/v)	TEMED	0.025% (v/v)

**Table 17. Components for stacking and resolving SDS-PAGE gels.** 0.1% of SDS was added to the acrylamide mix to denature proteins and help isolate protein molecules.

### **Samples preparation**

To prepare samples for western blot, 5  $\mu$ l Loading Buffer 5X (LB5X) (10% SDS, 50% Glycerol, 25%  $\beta$ -mercaptoethanol, 0.015% bromophenol blue (Sigma) and 62.5 mM Tris-HCl pH6.8) was added to a final volume of 25  $\mu$ l. Once samples have been prepared with LB5X, we boiled them at 95°C for 5 minutes.

### **Electrophoresis**

Samples, and the Ladder standard (Precision Plus Protein All Blue Standard, Bio-Rad), were loaded to the gel and run at constant amperage of 15 mA/gel (for 11cm gels) when the samples are in the stacking gel, and at 20 mA/gel for the protein separation, using running buffer (25mM pH 8.8 Tris-HCl, 192 mM glycine and 0.1% SDS).

#### **8.4. Protein transference to a PVDF membrane**

When the proteins were separated in the SDS-PAGE we transferred them to polyvinylidene difluoride (PVDF) membranes (0.45  $\mu$ m) (Millipore) using transfer buffer containing SDS (480mM Tris-HCl, glycine 39 mM, 0.0375% SDS 10% methanol) on a semi-dry transfer system (Hoeffer). Before transference, PVDF membranes needed to be activated with methanol for 5 minutes. Blot paper (Albert LabScience) and membrane after methanol were kept in transfer buffer until electrophoresis was finished. Transference was run at constant amperage of 0.8 mA/cm<sup>2</sup>, for 1 hour.

#### **8.5. Protein immunodetection**

Once proteins were transferred to the PVDF membrane, protein unspecific antigens were blocked with a solution of TBST (20 mM Tris-HCl, 150 mM NaCl y 0.1% Tween<sup>®</sup>20 (Sigma)) and 5% of Skim Milk Powder (Sigma) for 2 hours at room temperature. After washing the membrane with TBST to eliminate all the blocking solution, membranes were incubated with a specific primary antibody, for 1 hour at room temperature or overnight at 4 °C. Primary antibodies were diluted in TBST and with 0.02% of sodium azide solution at a concentration described in the table below.

The second incubation was made with secondary antibody conjugated with horseradish peroxidase (HRP) enzyme. We diluted the antibody in TBST with 5% milk and incubated for 1 hour at room temperature. After the incubation, the membrane has to be washed well to completely eliminate the excess of the secondary antibody.

The detection of the protein band was made by a chemical chemiluminescence reaction using a substrate that is specifically recognized by the HRP peroxidase (Luminata™ Forte Western HRP Substrate) (Millipore). For all antibodies, membranes were incubated for 4 minutes (except for tubulin, that was incubated for 1 minute). The image acquisition was made in a ChemiDoc XRS (Bio-Rad) and analyse with the specific for western blot analysis informatics programme Quantity One.

### 8.5.1. List of antibodies

Primary antibody	KDa	Host	Dilution	Gel Percentage	Supplier
<b>SMN</b>	37 and 20	Mouse	1/5000	7 – 17 %	BD Biosciences (Cat. no. 610646)
<b>SMN (2F1)</b>	37 and 17	Mouse	1/1000	17 %	Cell Signaling (Cat. no. 12976)
<b>Calpain-1</b>	80	Mouse	1/1000	7 %	Biomol International Inc. (Cat. no. CG1928)
<b>LC3</b>	14 and 16	Rabbit	1/1000	12 %	Cell Signalling (Cat. no. 2775)
<b>p62</b>	62	Rabbit	1/1000	7 %	Cell Signaling (Cat. no. 5114)
<b>A-Fodrin (Clone AA6)</b>	250, 150, 145 and 120	Mouse	1/4000	7 %	Biomol International Inc. (Cat. no. FG6090)
<b>Calpastatin</b>	100, 70,35 and 25	Rabbit	1/1000	10 %	Abcam (Cat. no. ab28252)
<b>Cleaved Caspase-3</b>	17	Rabbit	1/1000	12 %	Cell Signaling (Cat. no. 9661)
<b>α-Tubulin</b>	50	Mouse	1/50000	7 – 17 %	Sigma (Cat. no. T5168)

**Table 18.** List of the primary antibody used in western blot analysis. Antibodies were kept at -20 °C and prepare fresh before used.

Secondary antibody	Dilution	Supplier
Goat anti-mouse	1/20000	ThermoFisher (Cat. no. 31430)
Goat anti-rabbit	1/20000	ThermoFisher (Cat. no. 31460)

**Table 19.** List of the secondary antibody used in western blot analysis. Antibodies were kept at -20 °C and prepare fresh before used.

## 9. Reverse Transcriptase quantitative PCR

Reverse Transcriptase quantitative polymerase chain reaction (RT-qPCR), is a laboratory technique of molecular biology commonly used to measure gene expression. The key feature of RT-qPCR is that amplification of a targeted DNA is monitored in real-time as PCR is in progress by the use of fluorescent reporter. The fluorescent reporter signal intensity is directly proportional to the number of amplified DNA molecules.

For our experiments, three kits were used in order to ensure fast and high-quality RNA purification and PCR reactions, the RNeasyMini Kit (Qiagen), the SuperScript™ IV One-Step RT-PCR System (Thermo Fisher Scientific) and the iTaq Universal Sybr® green supermix (Biorad).

### 9.1. RNA purification

Before starting the RNA isolation, it is important to adequately prepare the cell culture that will be used. To obtain a good quantity and quality of RNA, it is necessary to start with a minimum number of cells. For our experiments, we cultured 300,000-350,000 CD1 MNs in 35mm cell culture plates (Thermo Fisher Scientific) to ensure an optimum amount of RNA.

Once MNs were treated, RNA was purified following the established protocol of the kit. For that cells were washed with sterile cold PBS 1X and directly lysed with 350 µl of RLT Buffer (RLT Buffer + 1% β-Mercaptoethanol) and a sterile cell scraper (Falcon). Cell lysates were collected into a microcentrifuge tube, vortex and froze at -80 °C to ensure that no cell clumps are visible and that cells were completely lysed.

After defrosted, samples were centrifuged at 4 °C for 3 minutes at maximum speed (8000 g) and the supernatant was collected in a new tube. An equal volume of 70% ethanol was added and accurately mixed with the homogenized lysate. All the lysate-ethanol solution was transferred to an RNeasy spin column placed in a 2 ml collection tube and centrifuged 15 seconds at 8000 g to load the RNA into the column.

Washes and finally elution were performed as follow:

1. 700 µl RW1 Buffer was added to the RNeasy spin column and centrifuged for 15 seconds at 8000 g to wash the spin column membrane. The flow-through was discarded.
2. 500 µl RPE Buffer (RPE Buffer+ 4 volumes of ethanol) was added to the RNeasy spin column and centrifuge for 15 seconds at maximum speed. Flow-through was completely discarded.
3. 500 µl RPE Buffer was added to the RNeasy spin column and centrifuge for 2 minutes at 8000 g. After discarding the flow-through, samples were centrifuged for an additional minute at maximum speed to ensure that o ethanol is carried over during RNA elution. Residual ethanol may interfere with downstream reactions.
4. The RNeasy spin column was then placed in a new 1.5 ml Eppendorf collection tube and 30 µl of RNase-free water was directly added to the spin column membrane and centrifuged for 1 minutes at 8000 g to elute the RNA.

RNA purified samples were quantified using a NanoDrop Spectrophotometer and stored at -80°C.

## **9.2. Reverse transcriptase PCR**

Reverse transcriptase PCR can be performed in two different methods depending on the number of steps, the One-step method and the Two-step method. In the first one, reverse transcriptase reaction is performed in the same tube as the quantitative PCR reaction. The second method involves first the transformation from RNA to a cDNA using a reverse transcription reaction, and then add this cDNA to the PCR reaction.

For our experiments, we used the Two-step method, because although it is more time consuming than the One-step method, is also more sensitive, can be optimized individually



and is usually recommended when the reaction is performed with a limiting amount of starting material.

In that step, two genes were converted to cDNA, the *Smn* gene (gene of interest) and the glyceraldehyde-3-phosphate dehydrogenase or GAPDH gene (housekeeping gene). Quantitative gene expression is often normalized to the expression levels of a control gene ("housekeeping" gene) which expression remains constant in the cells under investigation. We choose to use the GAPDH as a housekeeping gene because is one of the most commonly used. One reaction was individually prepared for each gene.

The primers used for the reverse transcriptase PCR were designed for Dra Ana Garcerá and ordered to Sigma (stock solution 100 $\mu$ M):

- *Smn* Forward (Fwd):

**5' GGGTGAAAGGTTATGTGCTG 3'**

- *Smn* Reverse (Rev):

**5' GTCGGATTCGTGAATGAGCC 3'**

- GAPDH Forward (Fwd):

**5' TGCACCACCAACTGCTTAG 3'**

- GAPDH Reverse (Rev):

**5' GGATGCAGGGATGATGTTC 3'**

The PCR reaction mixture was prepared as:

Reagents	
2X Platinum SuperFi RT-PCR Master Mix	25 µl
Sterile Nuclease free water	x µl (up to the final volume)
<i>Smn</i> / GADPH Fwd primer	2.5 µM
<i>Smn</i> / GADPH Rev primer	2.5 µM
SuperScript IV RT Mix	0.5 µM
DNA Sample	0.01 pg- 1 µg
<b>Total volume: 50 µl</b>	

**Table 20. Reverse transcriptase PCR mix preparation.**

The PCR cycling parameters were:

Step	Temperature	Time	Cycles	
Reverse transcription	50 °C	10 minutes	1	
Retrotranscriptase inhibition / DNA denaturation	98 °C	2 minutes	1	
Amplification	Denaturation	98 °C	10 seconds	40
	Annealing	55 °C	10 seconds	
	Extension	72 °C	1 minutes	
Final Extension	72 °C	5 minutes	1	
Final Hold	4 °C	Indefinitely		

**Table 21. Reverse transcriptase PCR cycling parameters.**

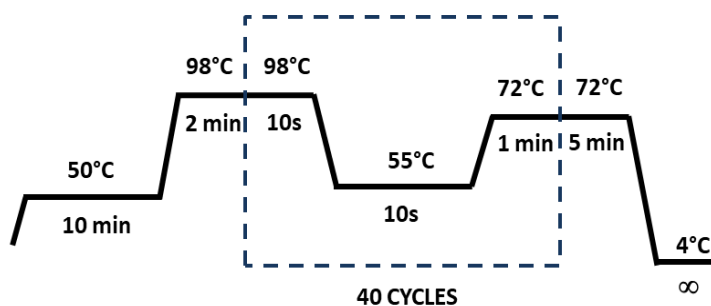


**Figure 54. Schematic representation of PCR cycling parameters.**

After the reaction, cDNA was measured using NanoDrop Spectrophotometer and stored at  $-80^{\circ}\text{C}$ .

### 9.3. Quantitative PCR

The last step was to perform the quantitative PCR (qPCR) where the amplified cDNA is detected between each round of amplification (real-time) instead of doing a detection only at the end of the reaction. Those interreactions measurements allow both qualitative and quantitative result.

Following protocol's instruction, the PCR reaction was prepared in a 96 well plate (BioRad) as:

Reagents	
iTaq universal SYBR Green SuperMix	10 $\mu\text{l}$
Sterile RNase free water	x $\mu\text{l}$ (up to the final volume)
<i>Smn</i> / GADPH Fwd primer	10 $\mu\text{M}$
<i>Smn</i> / GADPH Rev primer	10 $\mu\text{M}$
DNA Sample	100 ng- 100 fg
Total volume: 20 $\mu\text{l}$	

**Table 22. Quantitative PCR mix preparation.**

The qPCR was performed in a CFX96 Real-Time System (BioRad) with the following protocol:

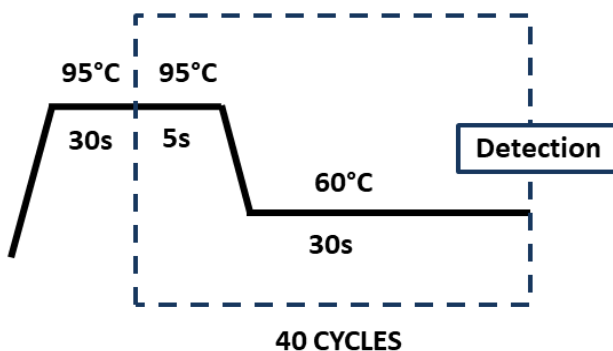


**Figure 55. Schematic representation of PCR cycling parameters.**

Step	Temperature	Time	Cycles
Polimerase activation / DNA denaturation	95 °C	30 seconds	1
Denaturation	95 °C	5 seconds	40
Annealing / Extension	60 °C	30 seconds	
Melt curve analysis	Instrument default settings		

**Table 23. Quantitative PCR cycling parameters.**

## 10. Mouse *in vivo* treatment

The therapeutic effect of Calpeptin (Calbiochem) was tested using the murine models of SMNDelta7 and MutSMA. To this end, mutant mice and WT littermates were divided into 4 experimental groups: WT and mutant mice treated with Calpeptin and WT and mutant mice treated with vehicle.

Calpeptin (Stock solution of 50 mM dissolved in DMSO) was injected at a dose of 6 µg *per* gram of weight in saline solution (6 µg/g/day). Vehicle groups received equal volumes of physiological saline solution with the same amount of DMSO. Treatment was administered through subcutaneous injection (SC, interscapular region) once a day starting from birth (defined as postnatal day 0 (P0) for the experiments) until the end of the experimental time frame or the death of the animals. Drug administration was done using a polypropylene sterile syringe (icogamma plus, 1 mL) and with a 30G needle (BD Mircolance). Survival of animals, as well as body length, weight, and behaviour test (righting reflex and tube test), were analysed.

### 10.1. Physical parameters

To control the possible association between calpeptin administration with changes in pups' growth and development, body length and weight were measured daily, *prior* to behavior tests and calpeptin or sham administration.

Body length was defined in mice as the distance from nose to base of the tail. Measurements were performed by placing the mouse horizontally alongside a metric ruler. Weight was obtained in a kern PCB 2500-2 precision balance with 0.001g of reproducibility.

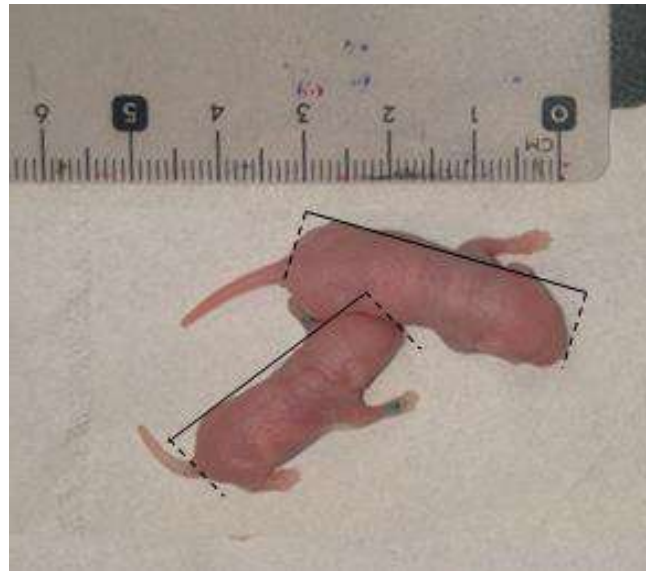


**Figure 56. Body length measurements in SMNDelta7 mice.** Representative image of untreated (Sham) P3 WT (upper) and mutant (Bottom) SMNDelta7 mice. For body length measurements pups were placed horizontally alongside a metric ruler. Body length was defined in mice as the distance from nose to base of the tail.

## 10.2. Motor and behavior test

The two SMA mouse models are characterized by a severe motor function impairment that starts early in their life (Bebée et al., 2012). In order to determine the progression of the disease and the possible functional improvement due to the administrated treatment, two different behaviour test were performed: the righting reflex test and the tube test. These two tests were chosen because both allow evaluation of the motor ability in offspring.

All tests were conducted every day starting from postnatal day 1 (P1), during the light period between 09:00 to 12:00. After measurements, the calpeptin or vehicle administration were performed.

### 10.2.1. Righting Reflex

Neonatal mice normally have the ability to return to their four paws after having been placed in a supine position (righting reflex (RR) response). The RR response can be seen in pups as early as P1-P2 and can be evaluated until P9- P10. The RR can be affected by weakness in limb muscles, trunk muscles and/or generally poor health.

The RR test is a simple and quick test to evaluate the overall body strength and locomotor skills. The test is based on a natural reflex so it does not require *prior* learning or training. Because of its simplicity, it allows the longitudinal study of the progression of a locomotor deterioration, and/or its improvement by therapeutic compounds (Butchbach et al., 2007; Didonato et al., 2011; El-Khodor et al., 2008). It is particularly adapted for mutant mice that are too affected to be tested on other tests.

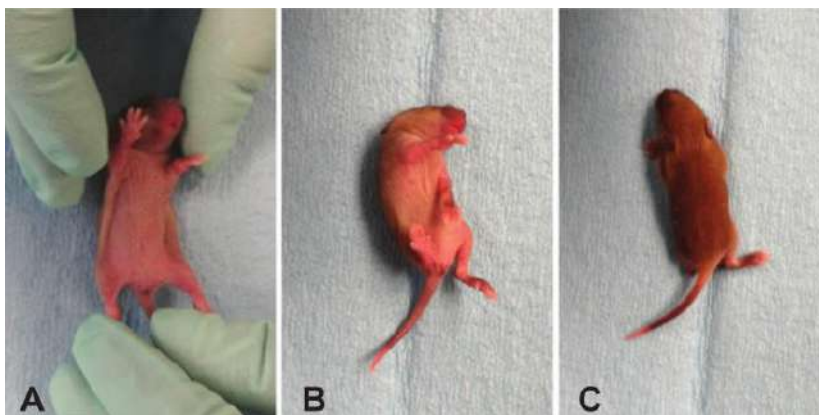


**Figure 57. Example of the righting reflex (RR) test execution. A)** The mouse is placed supine position. **B)** The test requires trunk control and coordination. **C)** The time taken to return to a normal position is measured (four paws position) (Photo from Feather-Schussler and Ferguson, 2016).

The test scores/measure the ability of the mice to return to their four legs after having been placed in the supine position on a flat surface in a maximum time of 30 seconds. The worse the condition of the animal is, the longer it takes to return to a normal position. Normal position was considered when the 4 legs were correctly placed to start walking. Three repetitions were performed for each test with a minimum of 5 minutes of rest between them.

### 10.2.2. Tube test

The tube test (TT), also known as Hind Limb Suspension test, is a non-invasive motor function test specifically designed for neonatal rodents. It evaluates the neuromuscular function, proximal hind-limb muscle strength, weakness and fatigue. The ideal animal age range for this test is from P2 to P8.

In each measurement, mice were placed head down, hanging by the hind limbs in a plastic 50-ml centrifuge tube with a cotton ball cushion at the bottom to protect the animal's head upon its fall. On the TT, two parameters were evaluated: latency to fall from the edge of the tube (express in seconds) assessed over a 30-s period and the Hind-limb score (HLS) which assesses the body posture of the legs and tail adopted during the first 10 seconds of the test.

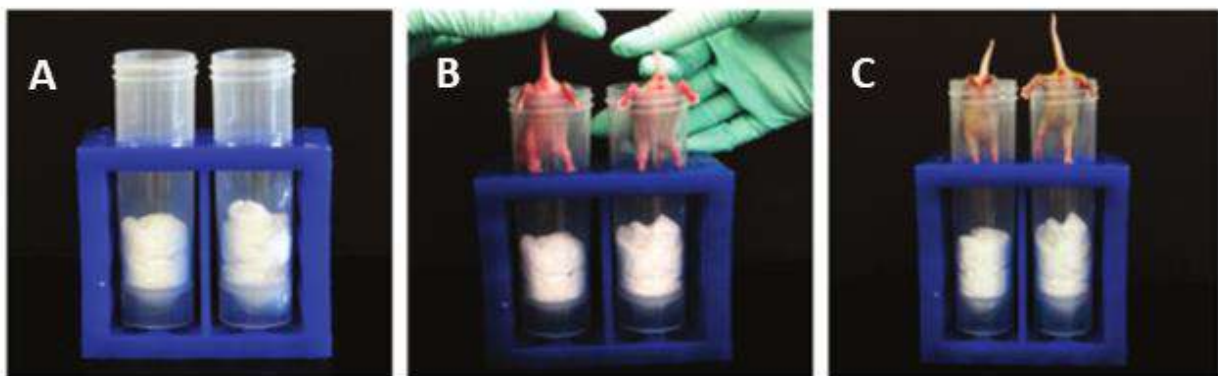


**Figure 58. Example of the tube test (TT) execution. A)** The test consists of a 50mL conical tube held straight up. **B)** Neonatal mouse is placed face down inside a tube, held in the edge by his hind limbs. The test allows evaluation of proximal hind limb muscle strength. **C)** It is measured the maximum time the mouse endures on the edge of the tube before falling inside (Photo from Feather-Schussler and Ferguson, 2016).

As described in El-Khodor et al., 2008, and 2011, the HLS criteria followed were:

- **Score 4:** normal hind-limb separation with tail raised (**Figure 59.A**)
- **Score 3:** slight apparent weakness where hind limbs, are closer together but they seldom touch each other (**Figure 59.B**)
- **Score 2:** hind limbs close to each other and often touching (**Figure 59.C**)

- **Score 1:** weakness where hind limbs are almost always in a clasp position with the tail raised (**Figure 59.D and E**)
- **Score 0:** constant clasp of the hind limbs with the tail lowered. In case the pups failed to hold onto the tube, an HLS score of 0 was given (**Figure 59.F and G**)

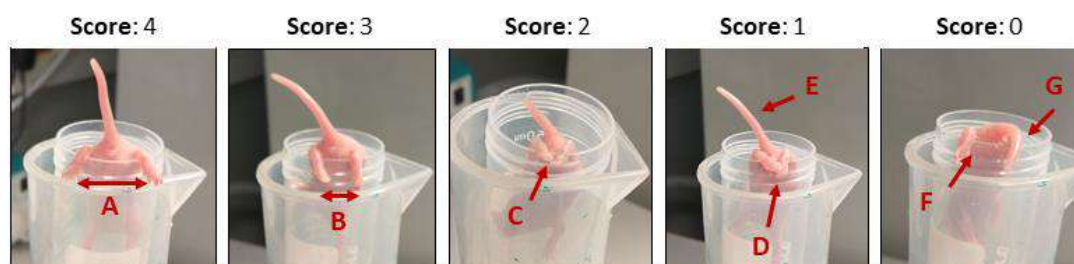


**Figure 59. Scoring criteria for the hind-limb score (HLS).** The adopted posture indicates a specific scored that represent the hind limb muscle strength of the mice.

As a summary in the TT the worse the condition of the animal is, the shorter the time and the lower the score of the HLS. Three repetitions were performed with a minimum of 5 minutes of rest between repetitions.

## 11. Statistics

All the experiments have been carried out *per* duplicate or triplicate in a minimum of three independent experiments. In the case of *in vivo* experiments, the data have been obtained from a minimum of 10 animals *per* group.

The data obtained were analysed with the GraphPad Prism 5 program. In the graphs, the values are shown as the mean  $\pm$  SEM (Standard Error Mean) and the p-value was considered significant when  $p < 0.05$ .

The differences between groups were analysed with the following tests:

- **Students t-test** was used to analyse the differences in a variable between two conditions. In general, if it is not indicated differently, it was assumed that the values follow a Gaussian distribution without assuming equal SD (Standard Deviation).



- **One-way ANOVA** was used to compare differences in the variance in the group means between three or more independent unmatched groups. Gaussian distribution was assumed for all the values. Post-test were used to comparing means of pairs of groups: the Dunnett's test, to compare all columns to a control column, and the Tukey-Kramer test, to compare all pairs of columns.
- **Two-way ANOVA** was used to examine the effect of two categorical factors on a dependent variable. Bonferroni post-test was used to compare differences between columns to a control column.
- **Survival curves** were created with the Kaplan-Meier method to compare survival curves when the outcome was the time until death.

GraphPad Outlier calculator tool with the ESD method (extreme studentized deviate) was used to identify significant outlier values.

## RESULTS

---



# **CHAPTER 1: Autophagy modulators regulate SMN protein stability in Motoneurons.**



**SUMMARY:**

The exact mechanism involved in motoneuron (MNs) degeneration during the development of Spinal Muscular Atrophy (SMA) is still unknown. However, it is known that the deficiency of Survival Motor Neuron (SMN) gene causes axonal defects in the transport and architecture of neurons (Rossoll et al., 2003). MNs function depends upon the maintenance of neurites that extend for great distances from the cell body, and those alterations could be the reason for MNs vulnerability in SMN reduced cells. Autophagy is a highly controlled cell degradation pathway whose precise role within the central nervous system is yet unknown.

Autophagy is important for differentiation, homeostasis and survival in physiological conditions (Mizushima et al., 2008) but, deregulation of the autophagy process has been described in several neurodegenerative disorders such as Huntington disease (Ravikumar et al., 2004), Alzheimer disease (Boland et al., 2008) and spinal cord injury (Kanno et al., 2009) and more recently, autophagy changes have been related to SMA (Custer and Androphy, 2014; Garcera et al., 2013). The accumulation of autophagosomes in neurites observed in those diseases originates and/or exacerbates axonal deficiencies by disruption of axonal transport and interference of intracellular space trafficking suggesting a close relationship between autophagy and neurite collapse.

Previous results from our group have shown that autophagy is already deregulated from early embryonic stages in severe SMA mouse MNs. In addition, the data demonstrate that the modulation of the autophagy process is able to modulate SMN levels. The main objective of this chapter is to analyse the role of autophagy in the development of SMA and its relationship with the mechanisms that regulate SMN protein levels in spinal cord MNs. We will also study the role of the protease calpain, a well-known inhibitor of the autophagy process.

To this aim, we decided to use two different approaches. First, we assessed the basal levels of autophagy in four *in vitro* models of SMA: primary cultures of MNs isolated from the transgenic models MutSMA and SMNDelta7; and two human models obtained from patients with SMA, the cultured fibroblasts and the differentiated MNs from iPSCs. What we have seen is that the autophagy pathway is altered in MNs, but not in other cell types

such as fibroblasts. The second approach was focused on the further characterisation of the link between autophagy, Smn and calpain. To this end, we use an shRNA lentivirus construct to reduce the expression of calpain which resulted in a modulation of autophagy process as well as Smn protein levels in normal CD1 MNs. Parallel experiments showed that Smn regulation by shCalp also occurred in Smn-reduced mouse MNs and this regulation is accompanied to the prevention of neurite degeneration in this model.

## 1. Smn reduction causes an increase of neurite degeneration in cultured MNs

Cultured spinal MNs are a valuable tool to study the basic mechanisms of axon and dendrite growth and to analyse the pathomechanisms underlying MN diseases. Specifically, primary cultures of SMA MNs are useful to study morphological and intracellular MNs specific alterations induced by Smn protein reduction which may be indicative of SMA pathological events.

To date, it is known that deficiency of SMN in MNs does not affect the axonal formation or neurite outgrowth during development (Garcera et al., 2011; Mcgovern et al., 2008), but it causes severe defects in axonal transport and architecture (Rossoll et al., 2003). This suggests that the origin of the neurodegeneration process on MNs during SMA is a consequence of alterations in the maintenance of cellular functions.

In order to further characterize cellular alterations in SMA mouse MNs, we perform a time-course neurite degeneration analysis. For these experiments, MutSMA E12.5 embryos were genotyped and MNs were purified. Cells were plated in NTFs medium at low density to avoid cell contact-mediated effects (approx. 5000 cells/cm<sup>2</sup>). We assessed neurite degeneration at days 6, 9 and 12, by analysing the percentage of the degenerated neurites versus the total number of neurites in an established area of the plate using phase-contrast microscopy. Neurites were considered degenerated when showed evidence of swelling and/or blebbing as described in Press and Milbrandt, 2008. Degenerating and healthy neurites were counted in at least 10 high-power fields *per* image (30–50 neurites), with the observer blinded to the condition. Each condition was done *per* duplicated and experiments were repeated at least three different times.

Starting at day 6, morphometric analysis showed a higher percentage of neurite degeneration in MutSMA MNs compared to WT MNs (Day 6, MutSMA 18.84 ± 12.41% and WT 10.72 ± 6.41%, p=0.0168; Day 9, MutSMA 30.13 ± 13.09% and WT 15.68 ± 6.68%, p= 0.0189). After 12 days in culture MutSMA MNs, showed 43.08 ± 4.71% of degeneration signs whereas WT MNs showed at 24.10± 7.37%, p=0.0002 (**Figure 60**).



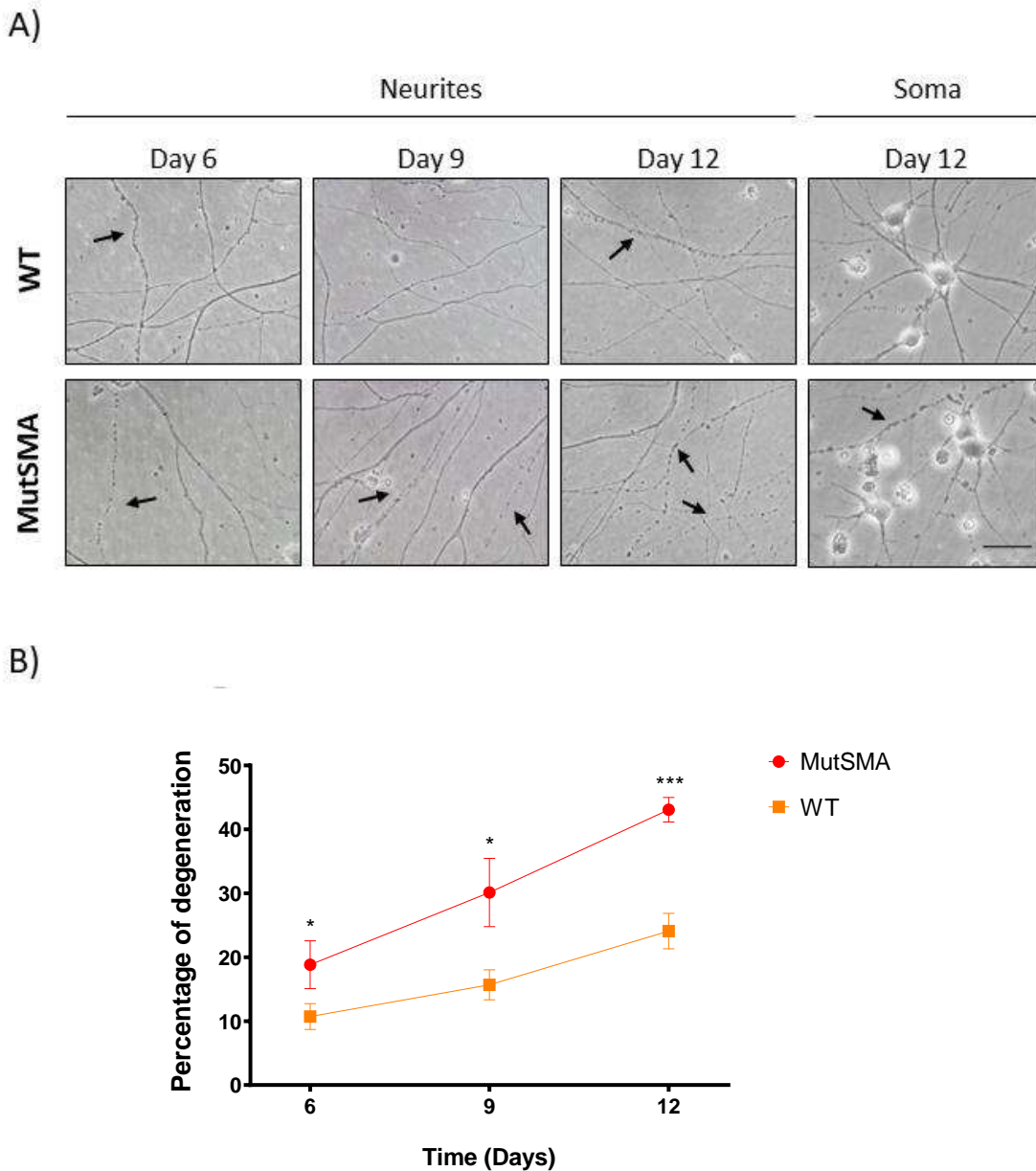


**Figure 60. Neurite degeneration in cultured MNs from a severe SMA mouse model.** E12.5 mutant and WT MNs were isolated from the MutSMA mouse model and cultured in the presence of NTFs. The number of degenerated neurites was evaluated at days 6, 9 and 12. **A)** Representative images of degenerated neurites and soma images at day 12 after cultured. Arrows indicate neurites with swelling and blebbing, signs of degeneration. **B)** Percentages of degenerating neurites. Graph values show mean of the percentage of degenerating neurites for mutant (Red) and WT (Orange)  $\pm$  SEM (Error bars) in each microscopic area. Experiments were done per duplicate in 3 different independent experiments. Asterisks indicate significant differences when comparing the values with the WT using two-way ANOVA test (\*  $p < 0.05$ , \*\*\*  $p < 0.001$ ). Scale bar of 15  $\mu$ m.

Apoptosis was also evaluated at day 12 by counting the number of the apoptotic nuclei and checking the levels of cleaved caspase 3, the active form of caspase 3. The percentage of the apoptotic nuclei (nucleus with pyknosis and blebbing) was assessed using Hoechst stain

and quantified by the number of apoptotic *versus* the total number of nuclei. Results showed no differences between WT ( $23.97 \pm 3.824$  %) and MutSMA MNs ( $19.12 \pm 1.861$  %,  $p=0.2216$ ) (**Figure 61.A**). Likewise, no differences were observed when levels of cleaved caspase 3 were evaluated by western blot (MutSMA  $1.289 \pm 0.1874$ ,  $p=0.1131$ ) (**Figure 61.B**).

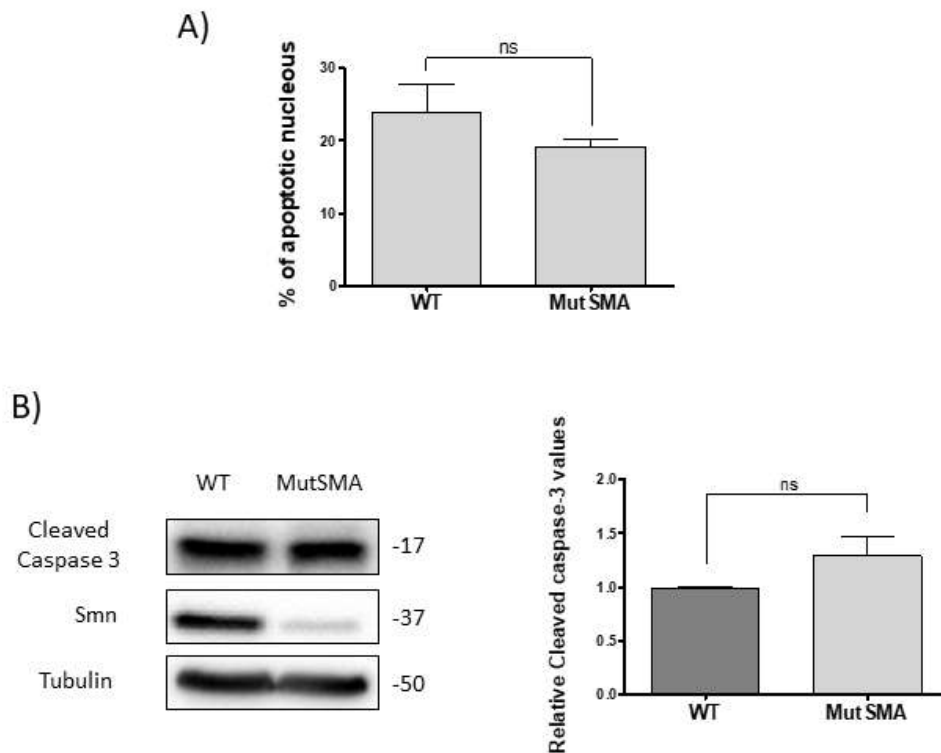


**Figure 61. Apoptosis cell death evaluation in primary cultured SMA mouse MNs.** Mouse MNs from the severe MutSMA mouse model were cultured in the presence of NTFs for 12 DIV and apoptosis parameters were analysed. **A)** The graph shows the percentage of the apoptotic nuclei in MNs cultures after 12 days in culture. Values are the mean  $\pm$  SEM of 3 representative wells from 3 independent experiments. **B)** Protein extracts from MNs cultures were probed with an anti-cleaved caspase 3 by western blot analysis. An anti- $\alpha$  Tubulin antibody was used as a loading control. Graph shows the mean  $\pm$  SEM of cleaved caspase 3 protein level quantification. Differences between groups were analysed using the student t-test (no significant (ns) values were considered when  $p>0.05$ ).

## 2. Increase of autophagy markers expression in SMA mice MNs

Neurites are particularly vulnerable to the accumulation of protein aggregates and damaged organelles. Basal autophagy occurs continuously as a housekeeping function, but insufficient or excessive autophagy could contribute to neurite collapse and degeneration.

Previous results from our group have demonstrated that using a lentiviral RNA interference method to reduce SMN protein level causes dysregulation of the autophagy process in MNs (Garcera et al., 2013). To further study this process in SMA cultured MNs we measured the levels of two autophagy markers, LC3-II and p62.

Microtubule-associated protein light chain 3 (LC3) is a cytosolic protein (LC3-I) that during autophagy, is conjugated to PE to form LC3-PE conjugate or LC3-II, and recruited to autophagosomal membranes. The addition of the PE group increases the rate of band migration in an SDS-PAGE gel, likely due to its hydrophobic nature. As a result, a double band is showed in the western blot, allowing an easy differentiation of LC3-I and LC3-II. Monitoring the conversion of LC3-I to LC3-II by western blotting is considered as a general marker of autophagy initiation (Mizushima, 2004; Tanida and Waguri, 2010). On the other hand, the protein levels of the autophagy receptor p62/SQSTM1 that physically link the autophagic cargo to LC3 is considered as a reporter of the autophagy flux, since p62 exclusively degrades by autophagy (Larsen et al., 2010).

Autophagy was analysed using two severe SMA transgenic mouse models, the MutSMA (**Figure 62**) and the SMNDelta7 (**Figure 63**). Embryos at E12.5 were obtained, genotyped and WT and mutant MNs were isolated and plated in NTFs medium (**Figure 62.A** and **Figure 63.A**). After 6 and 12 days *in vitro* (DIV), protein extracts were obtained and submitted to western blot analysis. Membranes were re probed with an anti-SMN antibody to the examine SMN protein level in mutant MNs and WT (**Figure 62.B** and **Figure 63.B**).

Results in **Figure 62.C** shows that LC3-II significantly increased in MutSMA cells compared to WT at day 6 ( $1.830 \pm 0.3340$ ,  $p=0.014$ ) and 12 ( $1.800 \pm 0.2192$ ,  $p=0.0088$ ). On the other hand, the p62 protein level is not altered at day 6 ( $1.582 \pm 0.7896$ ,  $p=0.5018$ ) but is increased at day 12 ( $2.120 \pm 0.3128$ ,  $p=0.0106$ ) (**Figure 62.D**).

In SMNDelta7 MNs, protein quantification of LC3-II relative levels at day 6 and 12 show an increase in mutant MNs compared to the WT (day 6,  $1.987 \pm 0.6568$ ,  $p=0.0265$ ; day 12,  $1.576 \pm 0.3002$ ,  $p=0.0498$ ) (**Figure 63.C**). Similar to what happens in MutSMA MNs, in this model, it was observed that the level of p62 protein did not change at day 6 ( $1.550 \pm 0.3261$ ,  $p=0.1428$ ) but is increased at day 12 ( $3.308 \pm 1.043$ ,  $p=0.0398$ ) in the mutant compared to WT (**Figure 63.D**). Together these results suggest that in MutSMA and SMNDelta7 MNs, the reduction of Smn causes dysregulation of the autophagy process.

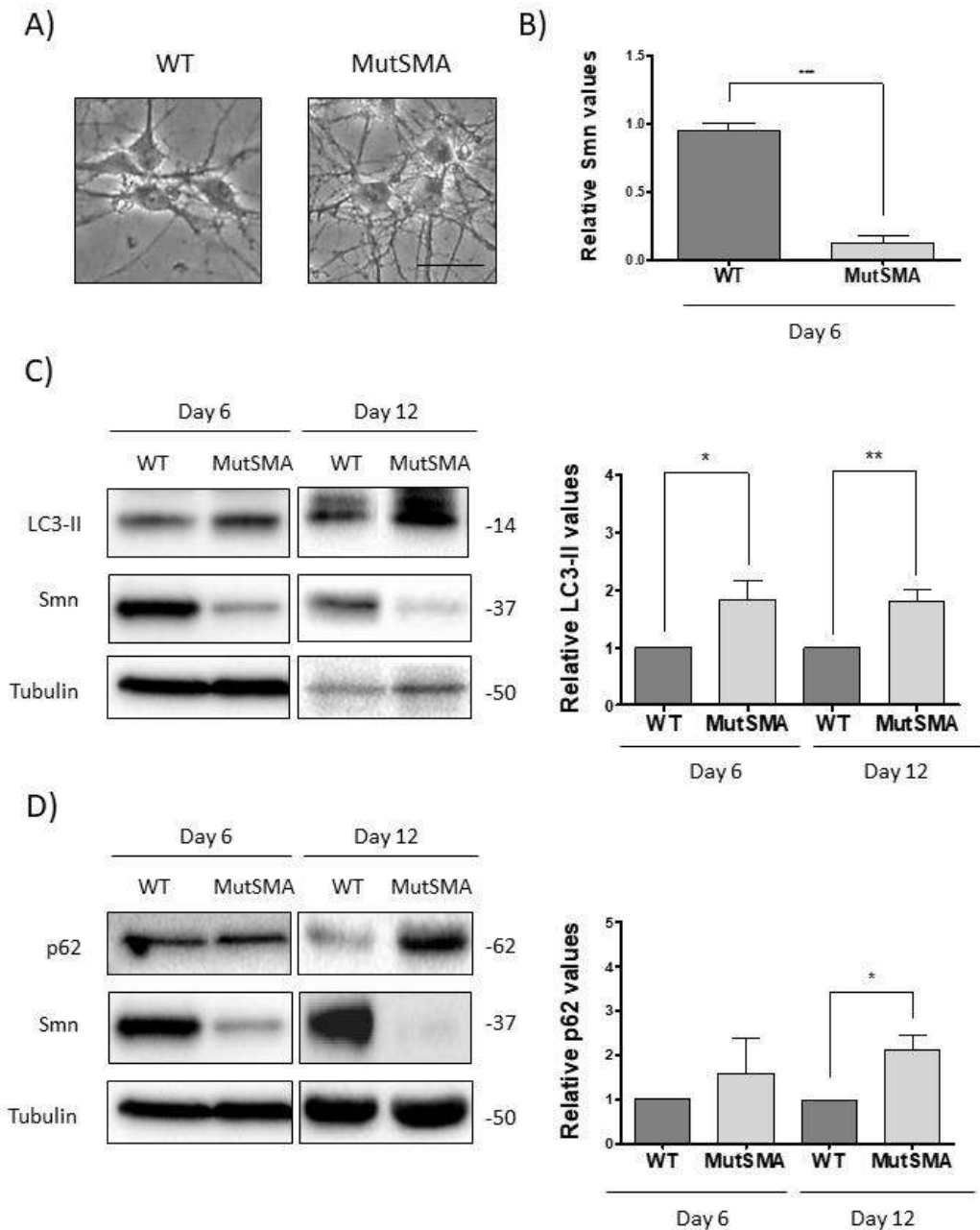


**Figure 62. LC3-II and p62 autophagy markers in spinal cord MNs from the MutSMA mouse model.** MutSMA and WT MNs were purified and cultured for 6 or 12 days in NTFs supplemented medium. **A)** Representative phase-contrast images show MNs cultures on day 6. **B)** Graph shows relative Smn protein levels by western blot in WT and MutSMA after 6 days in culture. **C)** After 6 and 12 DIV protein extracts were obtained and LC3-II levels were analysed by western blot. Membranes were re probed with an anti- $\alpha$  Tubulin antibody as a loading control. Graph represents the expression of LC3-II protein versus tubulin values. **D)** Same experiments were performed to evaluate p62 protein levels. Graph represents p62 levels against tubulin. Graphs show mean  $\pm$  SEM of 3 independent experiments. Values were analysed using the t-test and the two-way ANOVA (\*  $p < 0.05$ , \*\*  $p < 0.01$ , \*\*\*  $p < 0.001$ ). Scale bar of 15  $\mu$ m.

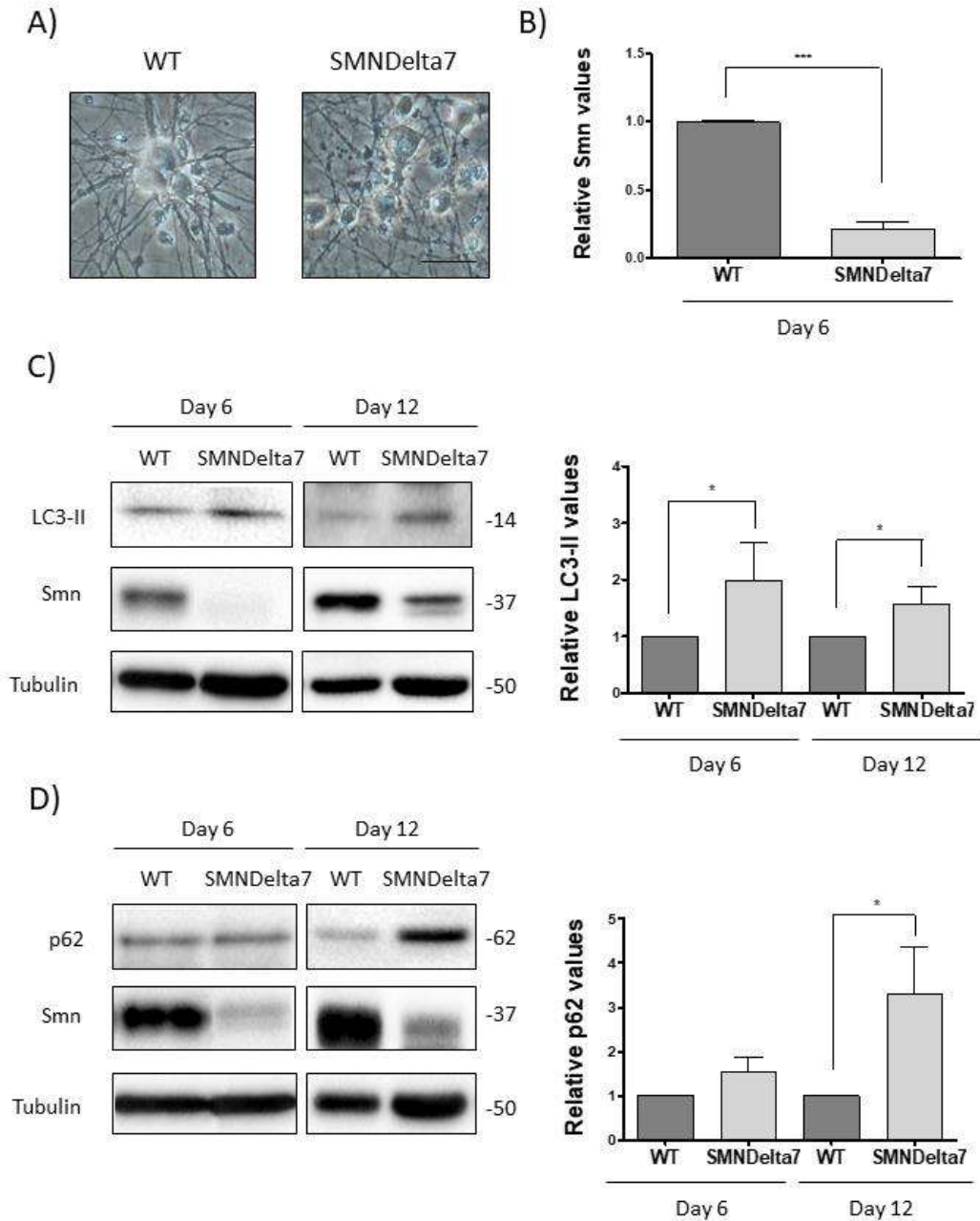


**Figure 63. LC3-II and p62 autophagy markers in spinal cord MNs from the SMNDelta7 mouse model.** SMNDelta7 and WT MNs were purified and cultured for 6 or 12 days in NTFs supplemented medium. **A)** Representative phase-contrast images show MNs cultures on day 6. **B)** Graph shows relative Smn protein levels by western blot in WT and MutSMA after 6 days in culture. **C)** After 6 and 12 DIV protein extracts were obtained and LC3-II levels were analysed by western blot. Membranes were re probed with an anti- $\alpha$  Tubulin antibody as a loading control. Graph represents the expression of LC3-II protein versus tubulin values. **D)** Same experiments were performed to evaluate p62 protein levels. Graph represents p62 levels against tubulin. Graphs show mean  $\pm$  SEM of 3 independent experiments. Values were analysed using the student t-test and the two-way ANOVA (\*  $p < 0.05$ , \*\*  $p < 0.01$ , \*\*\*  $p < 0.001$ ). Scale bar of 15  $\mu$ m.

### 3. Differential autophagy alteration in cultured human fibroblast

To evaluate if the autophagy dysregulation observed in the SMA mice cultures is specific of the MNs or affects other cell types, we cultured 4 untransformed cell lines from primary human skin fibroblasts, 2 from SMA patients (9677 SMA type 1 (SMA 1) and 3813 SMA type 2 (SMA 2)) and 2 from controls (3814 healthy SMA carrier (Control) and 2183 possible Huntington patient (Huntington)).

To characterize these cultured fibroblasts, we performed an immunofluorescence analysis to measure relative SMN levels and to localize LC3-positive structures. By immunofluorescence analysis it can be observed that LC3 undergoes from a diffuse cytosolic pattern to a puncta pattern when LC3-II is recruited at the membrane of the autophagic vesicles (**Figure 64.A**).

Human fibroblasts were cultured on glass coverslips and Fibroblast Growth medium for 2 days. Cells were fixed using cold methanol and SMN and LC3 immunostaining was performed. Measurement of SMN fluorescent intensity was performed using NIH ImageJ software. As expected, fluorescence intensity quantifications showed that SMN protein was reduced in both SMA patients (SMA 2, CTCF  $223.9 \pm 16.05$ ,  $p < 0.0001$  and SMA 1, CTCF  $172.9 \pm 16.75$ ,  $p < 0.0001$ ) compared to the healthy SMA carrier (CTCF  $411.5 \pm 22.42$ ) (**Figure 64.B**). However, contrary to the results observed in mouse MNs, when the number of LC3-positive spots was quantified using ImageJ, we observed a significant reduction in the number of LC3 spots in the SMN reduced cells when compared to the control (Control,  $73.44 \pm 9.972$  puncta; SMA 2,  $22.19 \pm 3.143$  puncta,  $p < 0.0001$  and SMA 1,  $27.12 \pm 2.540$  puncta,  $p < 0.0001$ ) (**Figure 64.C**). Fibroblasts from the possible Huntington patient showed higher levels of SMN (CTCF  $560.8 \pm 60.82$ ,  $p = 0.028$ ) and reduced number of LC3 structures ( $46.08 \pm 7.540$  puncta,  $p = 0.048$ ) (**Figure 64.B and C**).

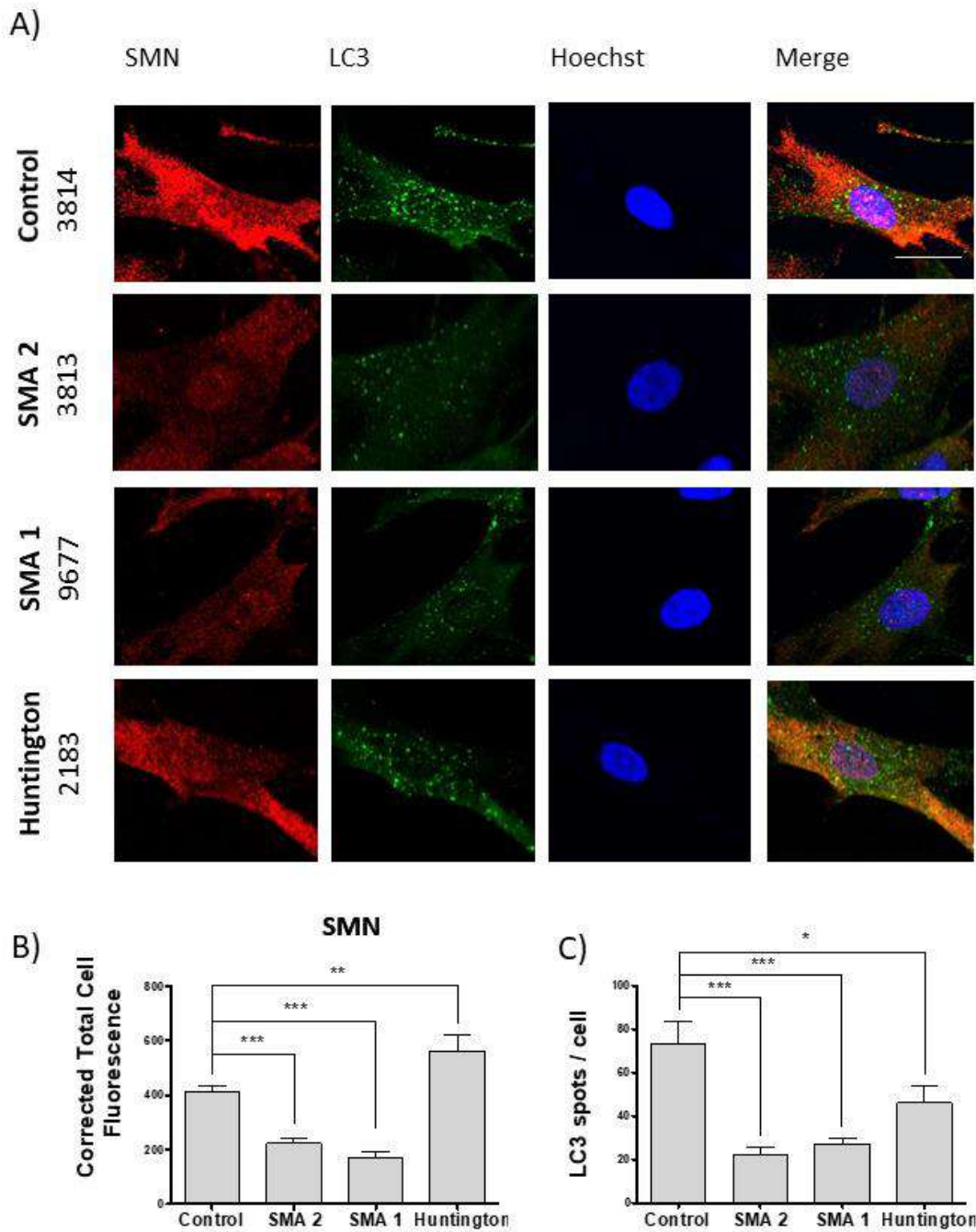


**Figure 64. Measurement of SMN fluorescence level and LC3 spots in human fibroblast.** Human fibroblast from 2 SMA patients (9677 SMA type 1 and 3813 SMA type 2) and 2 controls (3814 healthy SMA carrier and 2183 possible Huntington patient) were cultured in glass-coverslip and processed for immunofluorescence detection using an anti-SMN and anti-LC3 antibodies. Same slides were stained with Hoechst staining to identify the nucleus. **A)** Representative confocal images of immunofluorescent detection of SMN (Red) and LC3 spots (Green) in human fibroblast cultures. Blue indicates Hoechst nuclear staining. **B)** Graph represents the mean  $\pm$  SEM of relative SMN fluorescence measured in cells. **C)** Graph shows the number of LC3 spots in the different cell lines. The mean  $\pm$  SEM corresponds to the quantification of three independent experiments. Values were analysed using the one-way ANOVA with the Dunnett multiple comparison post-test (\*  $p < 0.05$ , \*\*  $p < 0.01$ , \*\*\*  $p < 0.001$ ). Scale bar of 25  $\mu\text{m}$ .



We also measure autophagy markers in these cells using western blot analysis. Cells were cultured for 2 days in Fibroblast Growth medium and then protein extracts were obtained (**Figure 65.A**). Membranes were probed with an anti-LC3 and anti-p62 antibody to examine protein levels of these two autophagy markers.

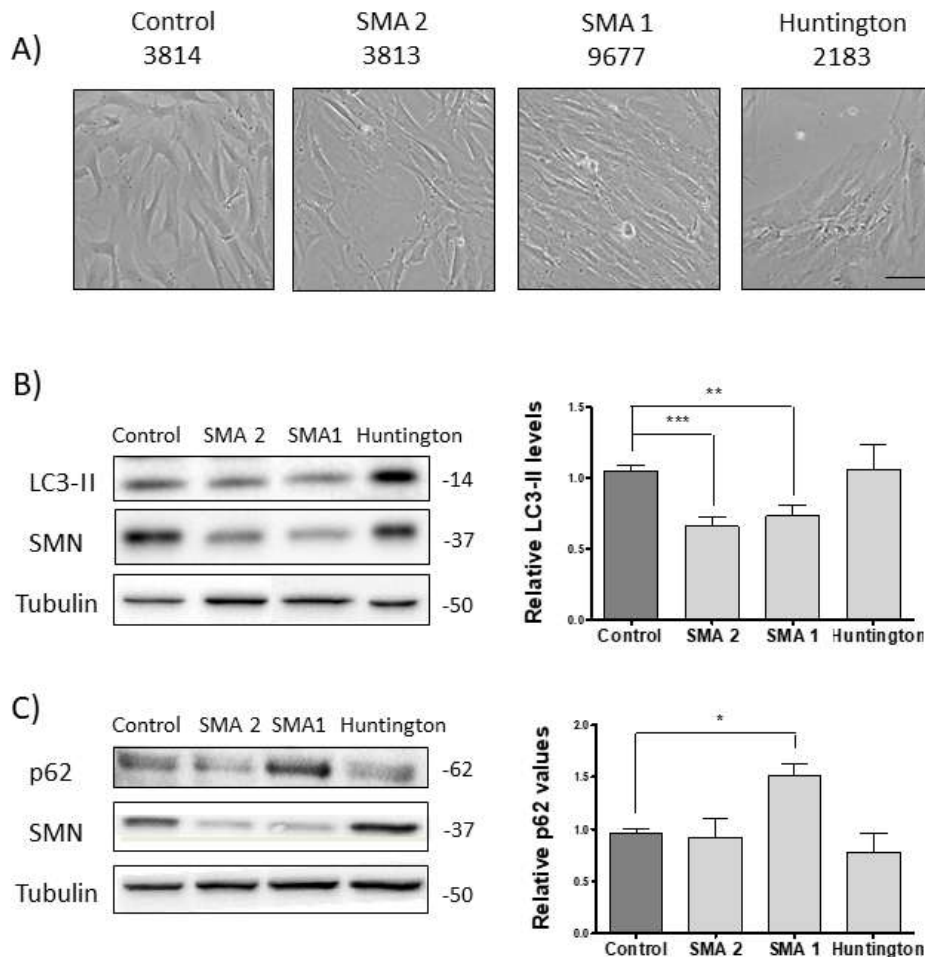


**Figure 65. LC3-II and p62 autophagy markers in human fibroblast cells.** SMA and control human fibroblast cells (9677 SMA type 1, 3813 SMA type 2, 3814 healthy SMA carrier and 2183 possible Huntington patient) were cultured for 2 days and protein extraction was performed and submitted to western blot using an anti-LC3 and anti p62 antibodies. Tubulin was used as protein loading control. **A)** Representative phase-contrast images show fibroblast cultures 2 days after plating. **B)** Western blot analysis of protein extracts probed for LC3-II and SMN. Graph represents mean  $\pm$  SEM of the expression of LC3 protein against tubulin. **C)** Same protein extracts were submitted to western blot analysis using an anti-p62 antibody. Graphs represent the expression of p62  $\pm$  SEM. Values correspond to the quantification of five independent experiments. Values were analysed using the one-way ANOVA with the Dunnett multiple comparison post-test (\*  $p < 0.05$ , \*\*  $p < 0.01$ , \*\*\*  $p < 0.001$ ). Scale bar of 50  $\mu\text{m}$ .



Protein quantification of LC3-II relative levels showed that patient cells had reduced levels of LC3-II when compared with the control (SMA 2,  $0.657 \pm 0.0678$ ,  $p=0.0001$ ; SMA 1,  $0.7325 \pm 0.0791$ ,  $p=0.002$ ) (**Figure 65.B**). Unexpectedly, in this model, it was observed that the level of p62 varies between the SMA patient's cells. Fibroblast from the SMA type 1 patient has a significantly higher level of p62 (SMA 1,  $1.518 \pm 0.1143$ ,  $p=0.0018$ ) while in SMA type 2 cells, levels remain invariable when compare with the control (SMA 2,  $0.9196 \pm 0.1770$ ,  $p=0.8388$ ) (**Figure 65.C**). Regarding the Huntington sample, both LC3 ( $1.059 \pm 0.1814$ ,  $p=0.9773$ ) and p62 protein levels ( $0.7762 \pm 0.1819$ ,  $p=0.3592$ ) remained at the same levels as the control (**Figure 65.B and C**).

#### 4. Autophagy dysregulation in human SMA differentiated MNs

Autophagy alterations observed in the two SMA mouse models suggest a specific autophagy dysregulation in MNs, but not in other cell types as fibroblasts. To further asses if these alterations are specie-specific or cell-specific, we established a differentiated MNs culture from SMA human iPSC (GM23411\*B as control and GM23240\*B from an SMA type 2 patient).

Before we can use the differentiated MNs as a model we needed to perform a molecular characterization using immunofluorescence to ensure that they are mature MNs. To do this, the iPSCs were differentiated following the protocol described in "3.3.2. MNs differentiation protocol" (from "*Materials and Methods*" section). For the last step of differentiation, cells were plated in a coated glass-coverslip in MNs Maturation Medium, and 6 days later, cells were fixed with PFA 4% and cold methanol. For the immunofluorescence analysis we used some of the best-known MNs markers: Islet 1/2 (Insulin related protein 1 and 2), a homeodomain-containing transcription factors expressed in all islet cells in the pancreas and in spinal cord MNs;  $\beta$ -III tubulin, one of the two structural components that form the microtubule network specifically localized in neurons; MN and pancreas homeobox 1 (MNX1), also known as Hb9, a regulator of beta-cell development and MNs differentiation pathways; choline acetyltransferase (ChAT), the transferase enzyme responsible for the synthesis of the neurotransmitter acetylcholine and the most specific indicator for monitoring MNs differentiation; and Synaptophysin;

a synaptic vesicle protein present in neuroendocrine cells and all neurons in the brain and spinal cord. Hoechst stain was used to identify the nucleus.

As shown in **Figure 66** and **Figure 67**, the molecular characterization of the *in vitro* differentiated MNs demonstrate that the obtained cells were positive for all the markers tested suggesting an MNs-like phenotype.

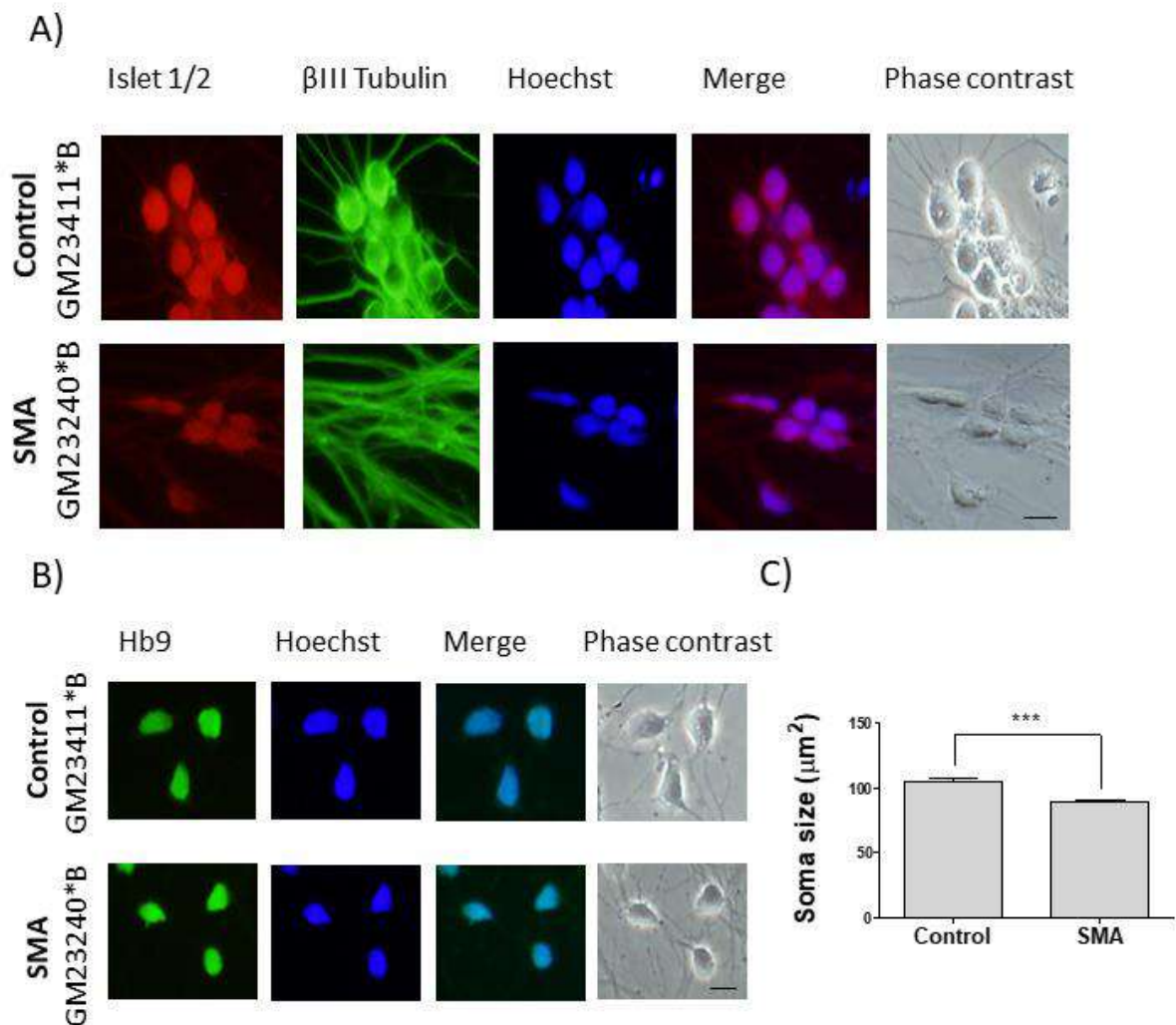


**Figure 66. Characterization of differentiated human MNs using immunofluorescence (1).** Human MNs from an SMA patient (GM23240\*B) and a control (GM23411\*B) were differentiated from iPSC and cultured for 6 days in maturation medium before processing for immunofluorescence. Different MNs markers were analysed (Islet 1/2,  $\beta$ -III Tubulin, and Hb9). Hoechst staining (blue) was performed to identify the nucleus. **A)** Representative microscopy images from hMNs labelled with islet 1/2 (red) and  $\beta$ III Tubulin (green) antibodies. **B)** Microscope immunofluorescence images of hMNs using an anti-Hb9 antibody (green). **C)** Graph shows mean  $\pm$  SEM of the size of the MNs soma. Differences were analysed using the student *t*-test (\*\*\*)  $p < 0.001$ ). Scale bar of 10  $\mu\text{m}$ .

Cell size was also evaluated to identify differences between the control cells and those obtained from the SMA patient. For that, phase-contrast images were obtained and soma was measured using ImageJ software. Results in **Figure 66.C** shows that MNs derived from the SMA patient are significantly smaller than the control cells once differentiated (Control,  $105.2 \pm 3.014 \mu\text{m}^2$  and SMA,  $89.39 \pm 1.593 \mu\text{m}^2$ ,  $p < 0.0001$ ).

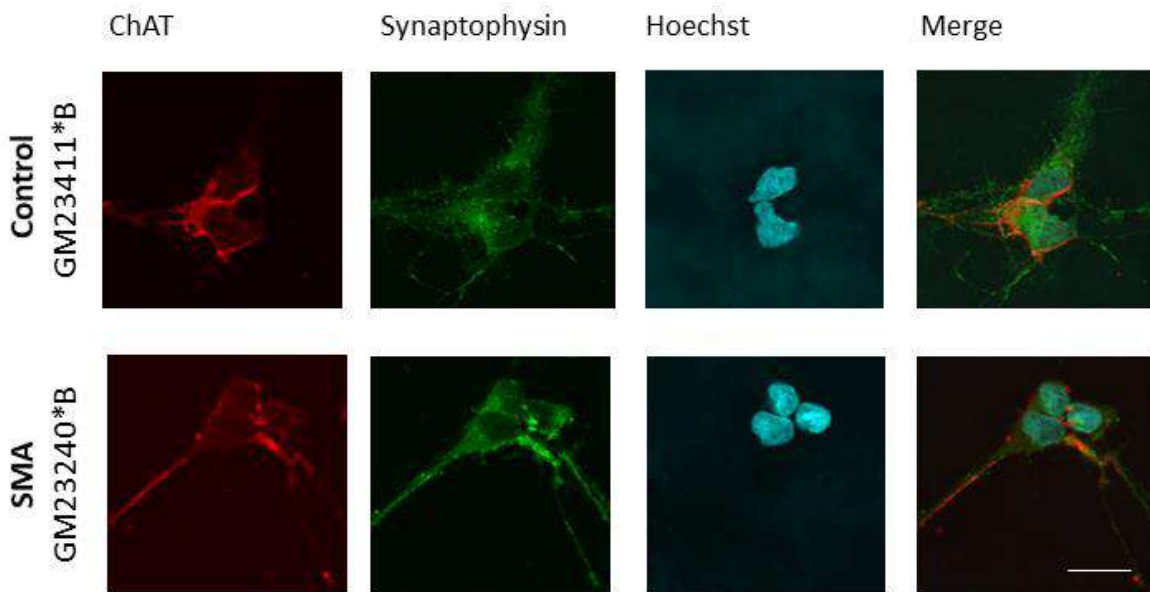


**Figure 67. Characterization of differentiated human MNs using immunofluorescence (2).** Human MNs from an SMA patient (GM23240\*B) and a control (GM23411\*B) were differentiated from iPSC and cultured for 6 days in maturation medium before processing for immunofluorescence. Representative microscopy images from hMNs labelled with Choline acetyltransferase (ChAT) and synaptophysin. Hoechst staining (blue) was performed to identify the nucleus. Scale bar of 12  $\mu\text{m}$ .

We also wanted to know whether SMN protein reduction was maintained in SMA derived MNs after the differentiation process. Thus, we plated the cells in a glass-coverslip and fixed with PFA 4% and cold methanol to perform an immunofluorescence analysis of SMN. Cells were also stained using Hoechst dye. Measurement of protein fluorescent intensity was performed using NIH ImageJ software. As expected, fluorescence intensity quantifications showed that SMN protein was reduced in SMA patient MNs (CTCF  $54.08 \pm 1.926$ ) when compared with the control MNs (CTCF  $113.3 \pm 5.753$ ,  $p < 0.0001$ ) (**Figure 68**).

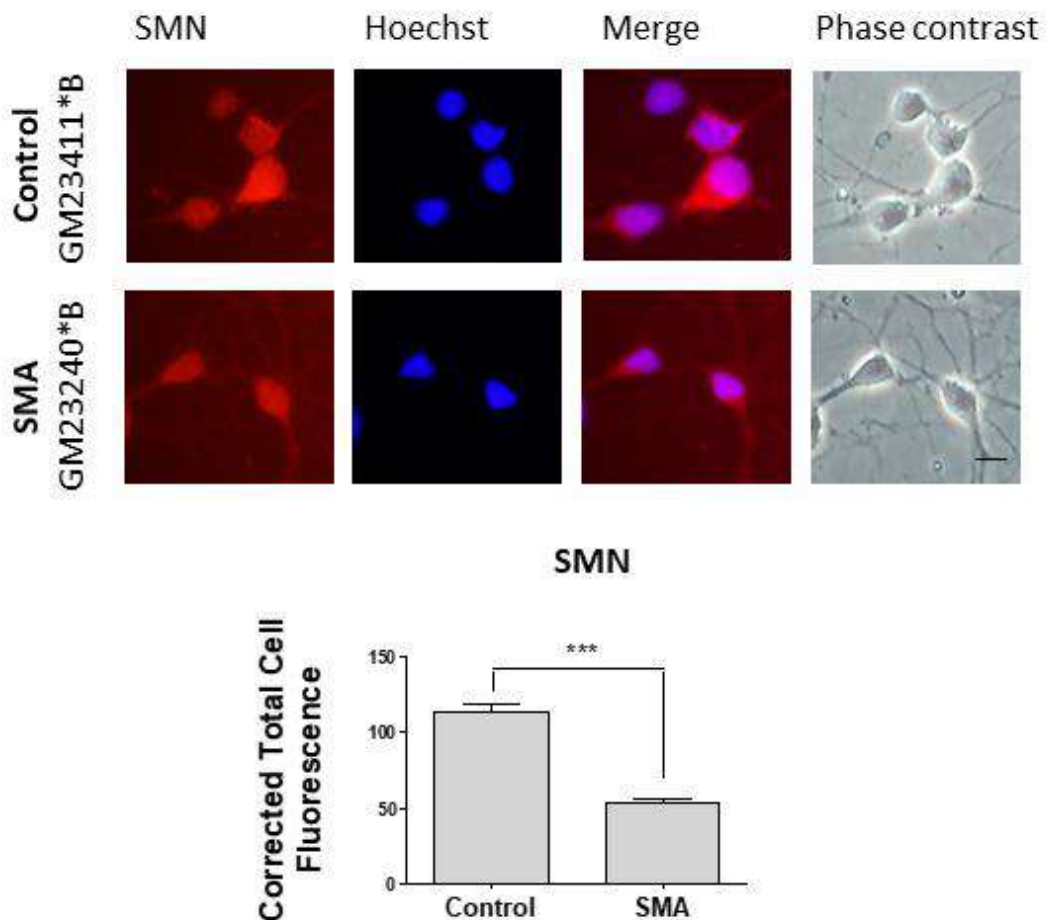


**Figure 68. SMN levels in MNs derived from human iPSCs from an SMA patient and control.** Differentiated human MNs (GM23240\*B and GM23411\*B) were cultured for 6 days and then fixed with PFA. Images of immunofluorescence performed using an anti-SMN antibody (red) in human MNs. Nucleus was stained with Hoechst stain (blue). Graph shows mean  $\pm$  SEM of relative SMN fluorescence levels measured in cells. Differences were analysed using the t-test analysis (\*\*\*)  $p < 0.001$ ). Scale bar of 10  $\mu$ m.

The specific role of autophagy in neurodegenerative diseases remains largely unknown. In particular, it is unclear whether autophagosome accumulation is protective or destructive, but the accumulation of autophagosomes in the neuritic beadings observed in several neurite degeneration models suggests a close relationship between the autophagic process and neurite collapse. To analyse specific changes in autophagy level in soma and neurites of differentiated human SMA MNs, an immunodetection was performed using an antibody against LC3 protein. MNs were grown on glass-coverslips for 6 days before fixation was performed using cold methanol for a few seconds (~10 seconds). Cells were also stained with Hoechst. The number of LC3-positive structures were quantified using ImageJ software. Similar to what we observed in mouse MNs, results showed a significant increase

in the number of LC3 spots in the SMA patient MNs in soma ( $21.72 \pm 1.672$  puncta *per* soma) and in neurite ( $0.2284 \pm 0.0184$  puncta/ $\mu\text{m}$  of neurite) when compared with the control condition (soma,  $4.877 \pm 0.4789$  puncta *per* soma,  $p < 0.0001$ ; neurite,  $0.0612 \pm 0.0129$  puncta/ $\mu\text{m}$  of neurite,  $p < 0.0001$ ) (**Figure 69**).

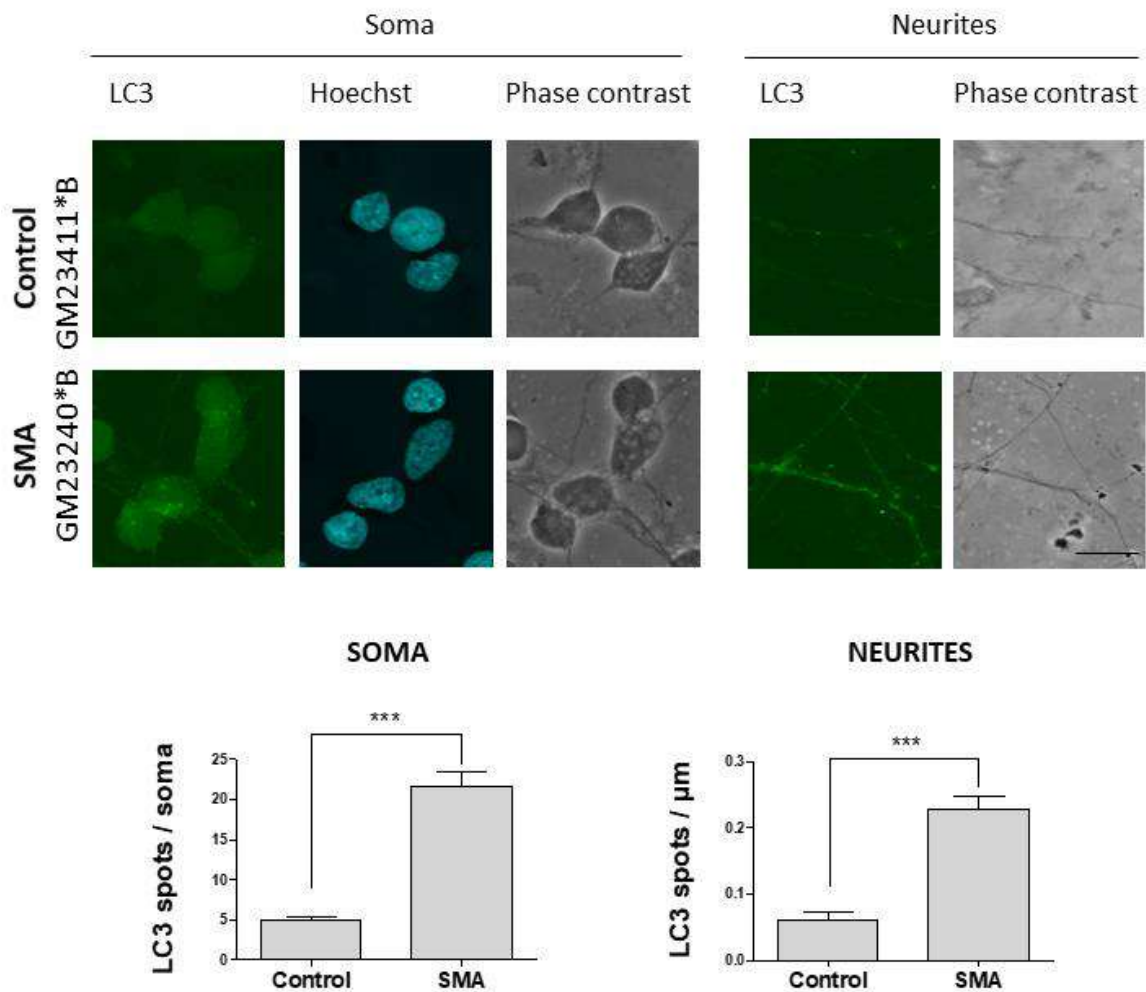


**Figure 69. Measurement of LC3 spots in human MNs using immunofluorescence.** Human MNs (GM23240\*B and GM23411\*B) cultures were fixed and immunofluorescence was performed. Anti-LC3 antibody staining (green) was used to evaluate autophagy vesicles. Fluorescent microscopy images detection shows the number of LC3 spots in control and SMA patient in differentiated MNs after 6 days in culture. Graphs show the number of LC3 spots in soma (**left**) and neurites (**right**) of control and SMA MNs. Values represent mean  $\pm$  SEM. Student *t*-test was used to analyse the statistical differences between groups. Scale bar of  $15 \mu\text{m}$ .

Autophagy markers were also evaluated using western blot analysis. Total cell lysates were collected from SMA patient and control after 6 days from the last differentiation step. LC3-II and p62 protein level were measured using an anti-LC3 and anti-p62 antibody. The results showed an increase of LC3-II ( $1.472 \pm 0.1672$ ,  $p=0.0467$ ) and a reduction of p62 ( $0.4874 \pm 0.0768$ ,  $p=0.0029$ ) in SMA-derived MNs compared to the Control-derived MNs (Figure 70). These results suggest that as occurs in MNs obtained from two transgenic SMA mice models, in human MNs there is also a deregulation of the autophagy process in SMN-reduced cells.

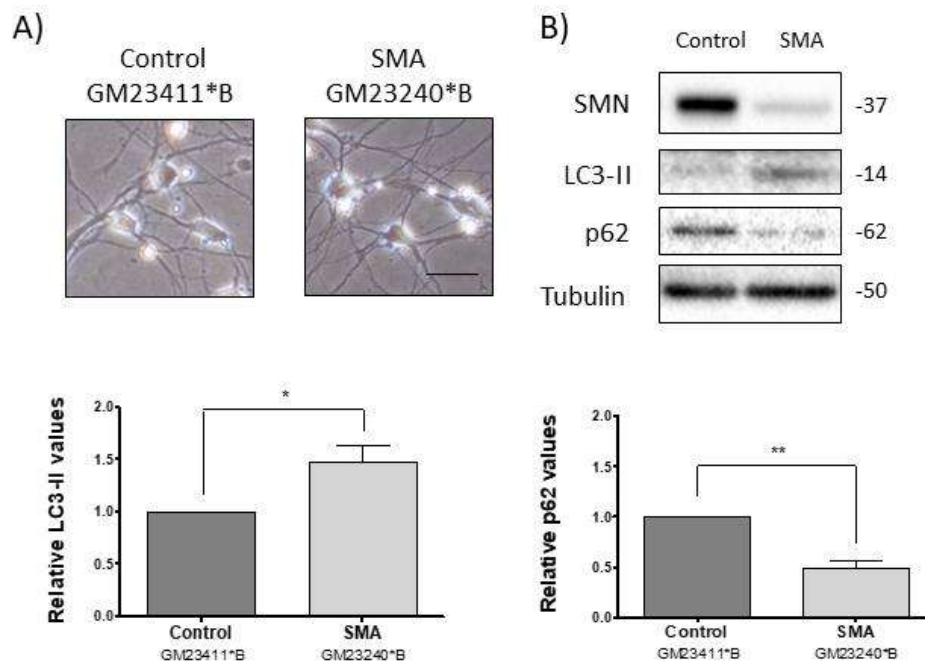


**Figure 70. Analysis of the autophagy markers LC3-II and p62 in differentiated human MNs.** MNs derived from human iPSCs (GM23240\*B and GM23411\*B) were maintained in maturation medium for 6 days. **A)** Representative microscopy images of human MNs after 6 days in culture. **B)** Protein extracts were obtained and submitted to western blot analysis using an anti-LC3 and anti-p62 antibodies. Anti- $\alpha$ -tubulin antibody was used as a loading control. Graphs represent the expression of LC3-II (**left**) and p62 (**right**) and correspond to the quantification of three independent experiments  $\pm$  SEM. Differences were analysed using the student t-test (\*\* $p < 0.01$ , \*\*\*  $p < 0.001$ ). Scale bar of 20  $\mu$ m.

## 5. Effect of Calpain knockdown on autophagy markers and Smn in cultured spinal cord MNs

Calpains are a family of proteases involved in numerous intracellular processes, including neuronal homeostasis (reviewed in Ono and Sorimachi, 2012). Specifically, these non-lysosomal proteases have been described as regulators of autophagy, modulating it through the specific cleavage of substrates essential for the induction of the autophagy process, such as autophagy-related 5 protein (Atg5) (Yousefi et al., 2006) and Beclin 1 (Russo et al., 2011). Moreover, calpain has been directly associated with Smn proteolysis in muscle samples of the severe mouse model of SMA (Fuentes et al., 2010; Walker et al., 2008).

To elucidate whether calpain regulates Smn protein levels and autophagy in our model of cultured MNs we decided to use a downregulation of the endogenous levels of calpain. For that, we used a specifically designed shRNA that targets calpain mRNA, avoiding the production of new protein, and consequently decreasing the protein levels. The used shRNA was introduced into the cultured MNs by a lentiviral vector, that also contains the GFP. The expression of the GFP allows us to control the transfection process by directly observing the GFP-positive cells. Both the shRNA and the lentivirus approach were designed in our lab by Dra Ana Garcera and Dra Myriam Gou-Fabregas as described in “4. shRNA interference by lentiviral transduction” from “*Materials and Methods*” section.

We obtained MNs isolated from CD1 embryos at E12.5, and cultured them in NTFs medium transduced with the empty vector construct (EV) or with the vector containing the shRNA for calpain (shCalp). After 6 days in culture, most of the cells present in the culture were GFP positive (as monitored by fluorescent microscopy) showing a frequency of transduction near 99% (**Figure 71.A**). Protein extracts were obtained and submitted to western blot analysis.

Calpain protein quantification demonstrated shRNA efficiency downregulating calpain protein levels ( $0.6150 \pm 0.054$ -fold reduction,  $p=0.0058$ ). Western blot analysis of Smn and LC3-II protein showed that shCalp significantly increased both proteins (Smn,  $1.595 \pm 0.6447$ ,  $p=0.008$  and LC3-II,  $1.449 \pm 0.1633$ ,  $p=0.0156$ ) compared to EV control, suggesting the role of calpain regulating Smn protein level and autophagy in MNs (**Figure 71.B**).



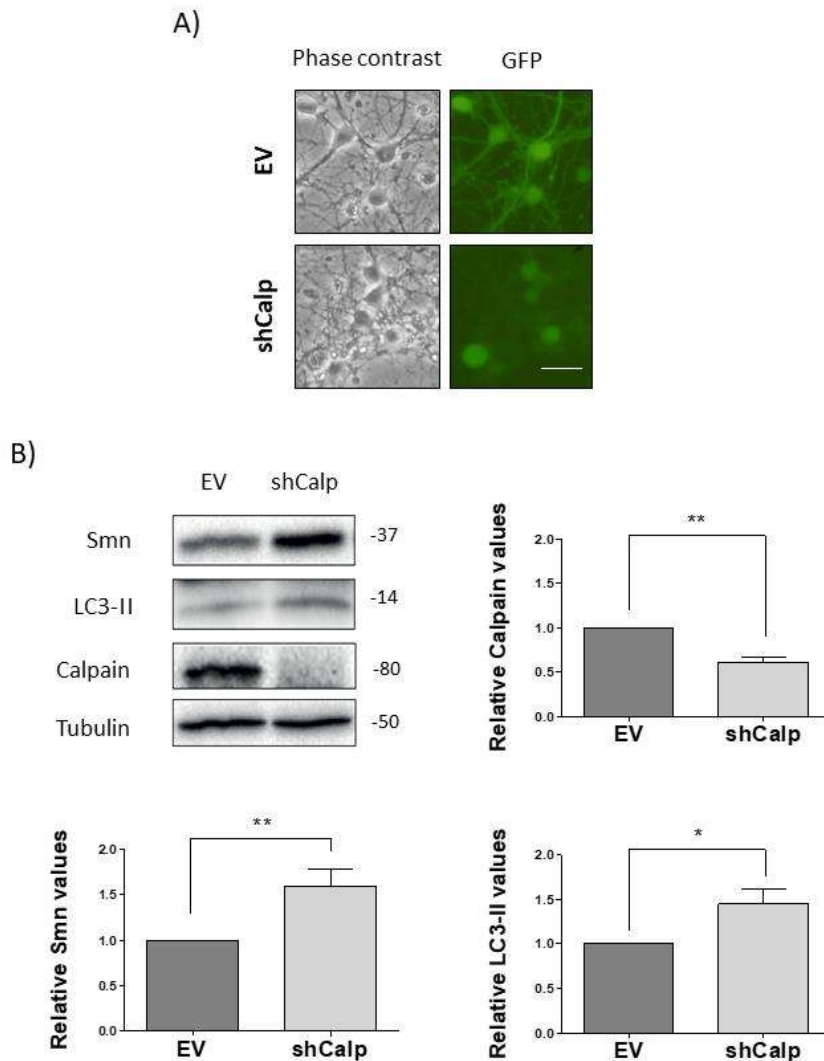


**Figure 71. Effect of endogenous calpain reduction on LC3-II and Smn in CD1 MNs.** CD1 spinal cord isolated MNs were transduced with lentivirus containing the empty vector (EV) or the shCalp construct and cultured for 6 days in the presence of NTFs in the medium. **A)** Representative microscopy images of day 6 MNs cultures. Green fluorescence shows the effective transduction of lentivirus into MNs. **B)** Protein extracts of transduced cultures were probed with anti-SMN, anti-LC3 and anti-calpain antibodies by western blot analysis. Graphs represent the expression of calpain (up right), Smn (bottom left) and LC3-II (bottom right) versus  $\alpha$ -tubulin, corresponding to the quantification of five independent experiments  $\pm$  SEM. Asterisks indicate significant differences using student t-test (\*  $p < 0.05$ , \*\* $p < 0.01$ ). Scale bar of 15  $\mu$ m.

To further examine the increase in the autophagic marker LC3 when calpain protein levels are reduced, we perform an immunofluorescence analysis to measure the intracellular levels of LC3-positive structures. For that CD1 MNs were purified and cultured in glass coverslips coated with Laminin. Three hours after purification the lentivirus containing the EV or the shCalp were added to the culture medium. Six days after transduction, cells were



fixed using cold methanol and LC3 immunostaining was performed. Measurement of LC3-positive spots using ImageJ, showed a significant increase of the number of LC3 spots in the shCalp treated condition compared to the EV in both soma (shCalp  $72.00 \pm 6.770$  puncta *per soma*; EV  $12.92 \pm 2.347$  puncta *per soma*,  $p < 0.0001$ ) and neurites (shCalp  $0.826 \pm 0.093$  puncta/ $\mu\text{m}$  of neurite; EV  $0.423 \pm 0.081$  puncta/ $\mu\text{m}$  of neurite,  $p = 0.0024$ ) (**Figure 72**).

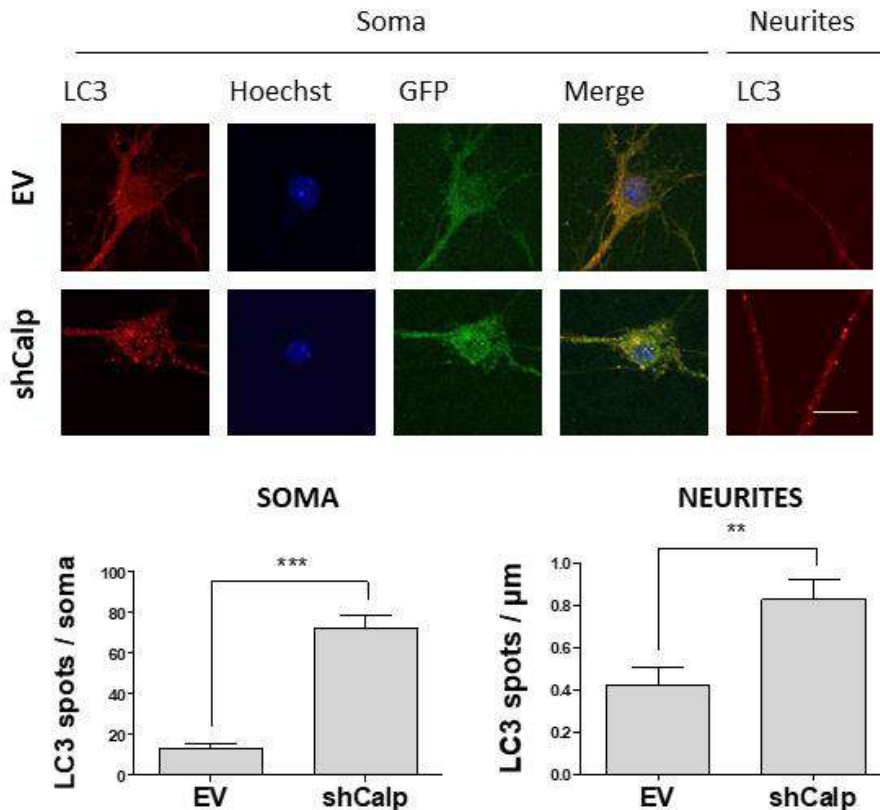


**Figure 72. LC3 autophagy spots levels in CD1 cultured MNs transduced with EV or shCalp using immunofluorescence.** Primary mouse MNs were transduced with lentivirus containing EV or shCalp. Six days after transfection cells were fixed and immunofluorescence was performed. Anti-LC3 antibody staining (red) was used to evaluate autophagy spots. Transfected cells were identified by GFP expression (green) and nuclear localization by Hoechst stain (blue). Graph represents the number of LC3 spots in soma (**left**) and neurites (**right**). Values  $\pm$  SEM correspond to three independent experiments. Differences between EV and shCalp conditions were analysed using the student t-test (\*\* $p < 0.01$ , \*\*\*  $p < 0.001$ ). Scale bar corresponds to  $10 \mu\text{m}$ .

Calpain knockdown had a significant effect on Smn protein level in cultured MNs 6 days after transduction. To further explore this result, we used the calpain specific shRNA to analyse the effect produced by the progressive reduction of calpain on the levels of Smn. For that, MNs were isolated from E12.5 CD1 mouse and maintained in the presence of a

cocktail of NTFs. Three hours later cells were transduced with EV or shCalp lentivirus particles. After 20 hours, medium was replaced with fresh NTFs medium. Protein samples were obtained at days 0, 3, 6, 9 and 12 and Smn and calpain protein levels were evaluated by western blot analysis. Calpain knockdown condition showed the gradual decrease of calpain protein level starting at day 3 up to day 12 (day 3,  $0.655 \pm 0.072$ ,  $p=0.0415$ ; day 6,  $0.531 \pm 0.086$ ,  $p=0.0003$ ; day 9,  $0.149 \pm 0.092$ ,  $p=0.0115$  and day 12,  $0.265 \pm 0.097$ ,  $p=0.0003$ ) compared to the EV control. Correlating with calpain decrease, Smn protein levels gradually increase from day 3 to day 9 (day 3,  $1.301 \pm 0.091$ ,  $p=0.0109$ ; day 6,  $1.694 \pm 0.191$ ,  $p=0.0013$  and day 9,  $1.757 \pm 0.334$ ,  $p=0.040$ ) compared to the EV control (Figure 73).

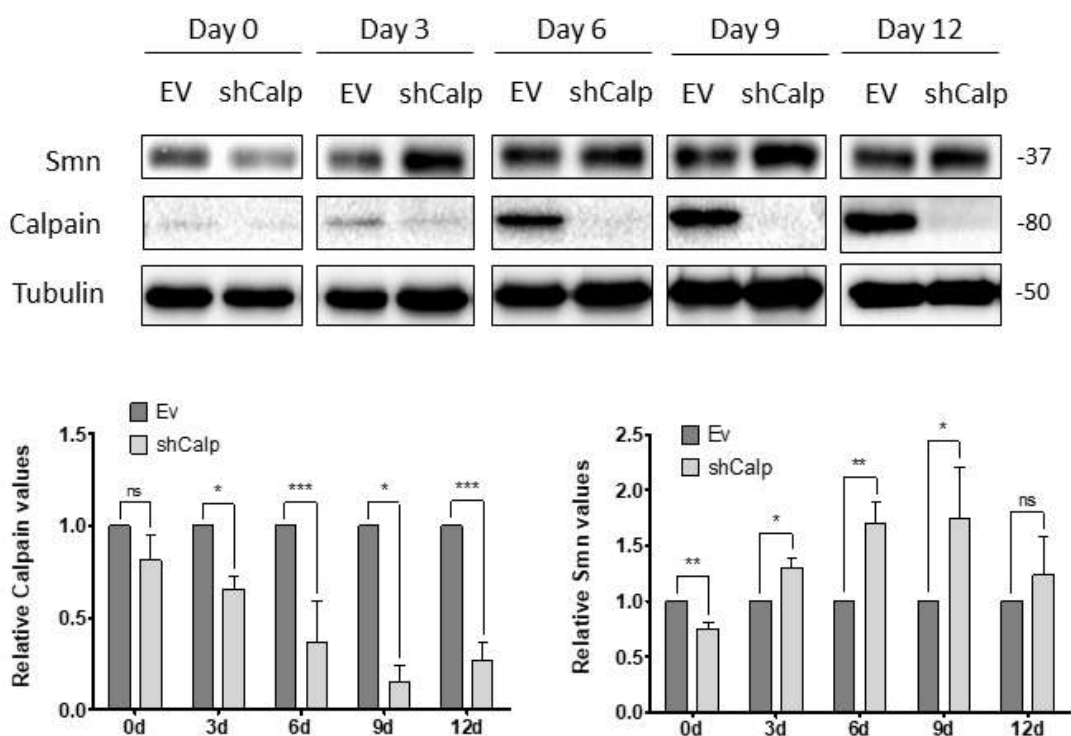


**Figure 73. Effect of endogenous calpain reduction on Smn protein level during different culture period.** CD1 mouse MNs were transduced with lentivirus containing the shCalp or the EV construct and maintained in the presence of neurotrophic factors cocktail (NTFs). Protein extracts from 0, 3, 6, 9 and 12 DIV from EV and shCalp transduced cultures were submitted to western blot analysis and probed with anti-SMN and anti-calpain antibodies. Membranes were re-probed with an anti- $\alpha$ -tubulin antibody, used as a loading control. Graph represents the expression of calpain (left) and Smn (right) over the different periods of time. Values correspond to the quantification of at least five independent experiments  $\pm$  SEM. Significant differences were analysed using two-way ANOVA with the Bonferroni post-test (\*  $p<0.05$ , \*\*  $p<0.01$ , \*\*\*  $p<0.001$  and no significant (ns) when  $p>0.05$ ).

In these cultures, the cell survival percentage was also analysed from day 0 to day 9 following the described protocol (“6.1. MNs survival” section in “*Materials and methods*”). Briefly, isolated MNs were cultured a low density (8,000 cells/cm<sup>2</sup>) to avoid cell contact signalling, and transduced with EV or shCalp lentivirus. Starting from day 0, we counted the number of MNs from four selected areas from each well and followed until the end of the experiment. Results were expressed as a percentage of alive MNs *per day* considering the initial day as 100%. Results in **Figure 74** showed no significant differences between the shCalp and EV treated groups and the control non-transduced NTFs condition (Day 12, NTFs 49.840 ± 9.897, EV 52.960 ± 11.070 and shCalp 48.070 ± 10.030), suggesting that calpain knockdown increase Smn protein level without affecting MNs survival.

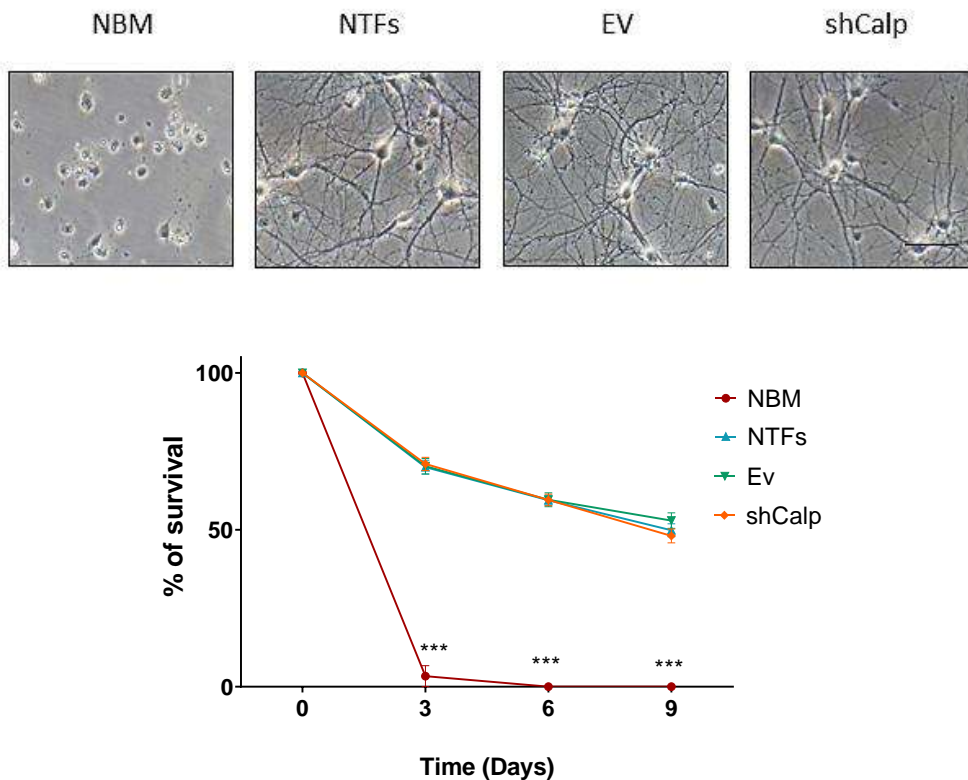


**Figure 74. Influence of shCalp in survival of cultured CD1 spinal cord MNs.** Spinal cord MNs were obtained from CD1 E13 embryos and maintained in the following culture conditions: neurobasal medium (NBM), NBM supplemented with a cocktail of neurotrophic factors (NTFs), NTFs + EV or NTFs+ shCalp. Representative phase-contrast images after 6 DIV of non-transduced MNs cultured (NBM, NTFs), and EV or shCalp transduced cells. Graph represents the percentage of surviving cells after 3, 6, or 9 days in the different culture conditions. The mean ± SEM corresponds to the quantification of five independent experiments. Differences were analysed using two-way ANOVA with the Bonferroni post-test using the NTFs condition as the control condition. Asterisk indicates significant differences of  $p < 0.001$ . Scale bar, 30  $\mu$ m.

In order to clarify whether the increase in Smn produced by the shCalp transfection occurs uniformly in the MNs or differentially in the different areas of the cell, we perform immunofluorescence against SMN. Embryonic MNs were grown in glass coverslips and transduced with the EV or the shRNA constructs. Seven days after transduction, cells were fixed and immunofluorescence analysis was performed using an anti-SMN antibody. Images were obtained using a confocal microscope using the same optical settings.

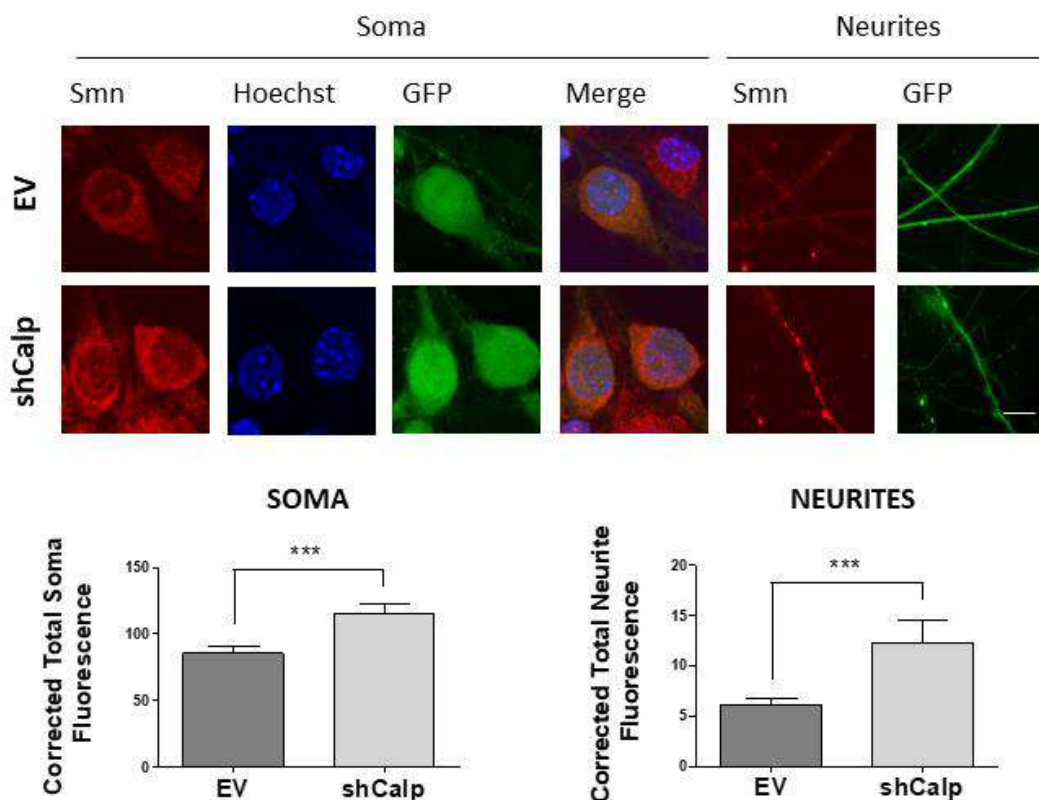


**Figure 75. Effect of shCalp in Smn protein levels in CD1 cultured MNs using immunofluorescence.** Representative confocal images of 6-day EV- and shCalp-transduced cells maintained in the presence of NTFs. Cells were fixed and immunofluorescence was performed with an anti-SMN antibody (red). Blue indicates Hoechst nuclear staining and green indicates GFP expression. Graphs represent the mean of relative Smn fluorescence measured in soma (left) or neurites (right) corresponding to the quantification of five independent experiments  $\pm$  SEM. Scale bar, 5  $\mu$ m. Asterisks indicate significant differences using student t-test (\*\*\*)  $p < 0.001$ .

Images display the normal punctate pattern of Smn throughout the cytosol and nucleus, representative of a functional Smn protein. The intensity of fluorescence generated by the Smn labelling was measured using NIH ImageJ software in two different cellular compartments, soma and neurites. Fluorescence intensity quantifications showed an

increase in Smn protein level in both, soma (CTCF  $115.8 \pm 7.267$ ,  $p=0.0008$ ) and neurites (CTCF  $12.29 \pm 2.214$ ,  $p=0.0002$ ), in the knockdown condition when compared with EV condition (soma, CTCF  $85.43 \pm 5.340$  and neurites,  $6.183 \pm 0.558$ , respectively) (**Figure 75**).

## 6. Calpain Knockdown prevents Smn reduction caused by membrane depolarization

The calpain family consists of cytosolic cysteine proteinases whose enzymatic activities depend on the intracellular  $Ca^{2+}$ . Calpain I and calpain II are the two major isoforms of the calpain family which require  $\mu M$  and  $mM$  of  $Ca^{2+}$  concentrations to initiate their activity (Ono and Sorimachi, 2012).

Alpha-spectrin or also called  $\alpha$ -fodrin is 270 KDa membrane-associated molecule intrinsically linked to membrane/cytoskeleton maintenance, dynamics, remodelling and degradation, especially in the central nervous system. Alpha-fodrin results in the formation of two unique and highly stable breakdown product of 145/150 KDa when processed by calpain (Nath et al., 1996; Yan and Jeromin, 2012). This is the experimental approach used to evaluate calpain activation by measuring the calpain-specific 145/150KDa breakdown products by western blot.

In cell culture is known that addition of high potassium treatment induces a membrane depolarization which in turn activates voltage-gated calcium channels (VGCCs), resulting in an increase in intracellular  $Ca^{2+}$  (Gou-Fabregas et al., 2009; Soler et al., 1998). That elevation of intracellular  $Ca^{2+}$  concentration will trigger a cascade of biochemical processes including calpain activation.

CD1 MNs were plated and cultured with NTFs for 6 days. Then cells were treated with 30mM (30K) or 50 mM (50K) of potassium chloride (KCl) for 3 or 24 hours. Cell lysates were obtained and submitted to western blot using an anti- $\alpha$ -fodrin antibody. After 3 hours of treatment the levels of 145/150 KDa products were significantly increased in 30K ( $1.293 \pm 0.1788$ ,  $p=0.0449$ ) and 50K ( $1.372 \pm 0.2125$ ,  $p=0.0359$ ) conditions compared to NTF control, but no differences were observed after 24 hours of treatment (30K,  $1.118 \pm 0.2162$ ,  $p=0.5897$  and 50K,  $0.9438 \pm 0.1683$ ,  $p=0.7518$ ) (**Figure 76**). These results suggest that calpain is activated after short membrane depolarization in mouse MNs.

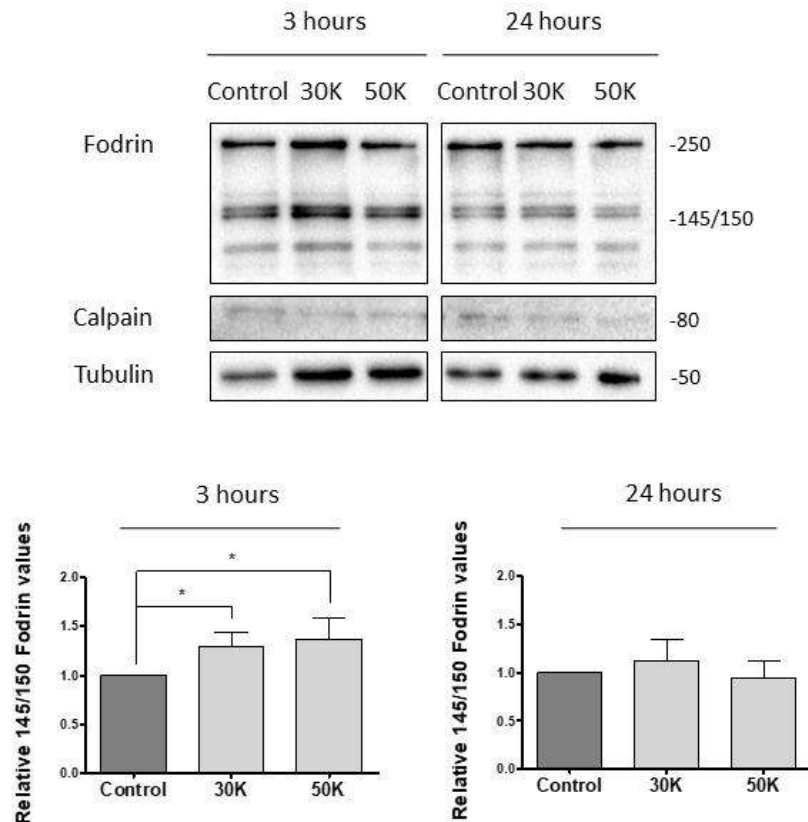


**Figure 76. Effect of high-potassium-induced membrane depolarization on calpain activity.** Calpain activity can be monitored by measuring the specific 145/150 KDa fodrin bands results from calpain cleavage of the 250 KDa full-length form. CD1 spinal cord MNs were cultured and maintained in the presence of NTFs. After 6 DIV cells were treated with 30 (30K) or 50 (50K) mM of potassium chloride (KCl) for 3 or 24 hours. In control condition fresh medium was added without KCl. Total cell lysates were analysed by western blot using an anti-fodrin antibody. Same membranes were also reprobbed with an anti-calpain antibody to check protein levels and with anti- $\alpha$  tubulin as a loading control. Graphs represent the quantification of the 145/150 KDa band fold induction at 3 hours (**left**) and (**right**) from four independent experiments. Values were analysed using the one-way ANOVA with the Dunnett multiple comparison post-test (\*  $p < 0.05$ ).

In this context, we wanted to elucidate whether calpain protein reduction regulates Smn protein in an experimental potassium-induced membrane depolarization. To this end, primary isolated E12.5 CD1 MN cultures were established in the presence of NTFs. Cells were transduced with EV or shCalp constructs. Six days later, cells were treated with NTFs or NTFs+30K for 3 hours and protein extracts were obtained and submitted to western blot using anti-SMN antibody.

As expected, shCalp addition induces an increase of Smn protein level (Control-shCalp,  $1.988 \pm 0.4645$ ,  $p = 0.0421$ ) compared to the EV condition. When potassium treated

condition were evaluated, we observed that in 30K-EV cultures, Smn protein was significantly reduced ( $0.5515 \pm 0.197$ ,  $p < 0.0001$ ) compared to the non-treated EV control condition. However, no significant differences in Smn protein level were observed in 30K shCalp ( $2.391 \pm 1.063$ ,  $p = 0.7286$ ), compared to shCalp condition (**Figure 77**). These results together suggest that high potassium treatment induces Smn protein reduction through calpain in cultured spinal cord MNs.

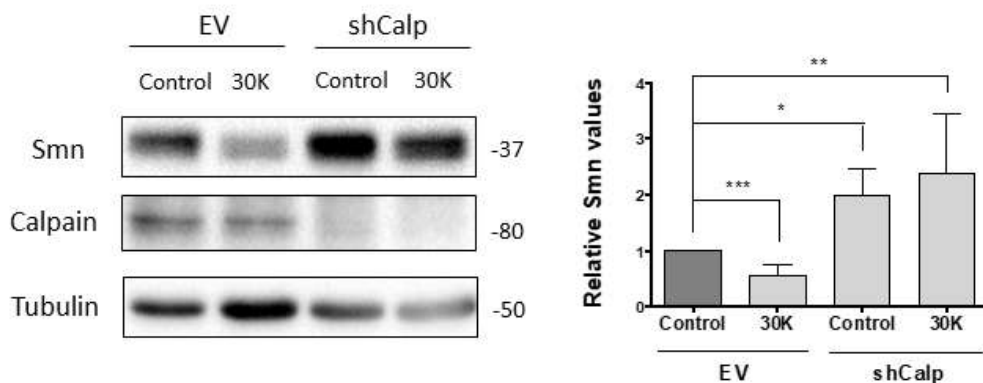


**Figure 77. Effect of calpain knockdown on Smn protein level in high-potassium treatment.** Mouse MNs obtained from CD1 E13 embryos were transduced with lentivirus containing the shCalp or EV constructs and maintained in the presence of NTFs cocktail. Six days after transduction, cells were treated using basal medium with (30 K) or without (Control) 30 mM of KCl during 3 hours. Protein extracts were submitted to western blot using anti-SMN or anti-calpain antibodies. Membranes were reprobbed with an anti- $\alpha$ -tubulin antibody. Graph values represent the expression of Smn versus  $\alpha$ -tubulin and correspond to the quantification of three independent experiments  $\pm$  SEM. Values were analysed using the one-way ANOVA with the Dunnett multiple comparison post-test (\*  $p < 0.05$ , \*\*  $p < 0.01$ , \*\*\*  $p < 0.001$ ).

## 7. Calpain shRNA increases Smn and prevents neurite degeneration in SMA mutant MNs

To determine whether shCalp treatment can also regulate Smn in MNs from a severe SMA transgenic mouse model we cultured WT or MutSMA cells. E12.5 embryos of the severe SMA transgenic mouse were genotyped and the spinal cords of wild-type (WT) and mutant (MutSMA) were dissected. Following the same protocol used for CD1, WT and MutSMA isolated MNs were cultured in the presence of NTFs and transduced with EV or shCalp (**Figure 78.A**). Six days after plating, protein extracts were collected and submitted to western blot analysis using anti-SMN antibody.

Results indicate that Smn is increased in shCalp WT ( $4.057 \pm 1.088$ ,  $p=0.031$ ) compared to control WT condition. Similarly, Smn protein was significantly increased in shCalp MutSMA ( $1.667 \pm 0.1715$ ,  $p=0.0301$ ) compared to the EV. Interestingly no significant differences were found in the Smn levels between the EV-WT cells and the shCalp-treated MutSMA ( $0.5595 \pm 0.236$ ,  $p=0.102$ ) cells indicating that Smn protein levels were restored to the WT levels (**Figure 78.B**).

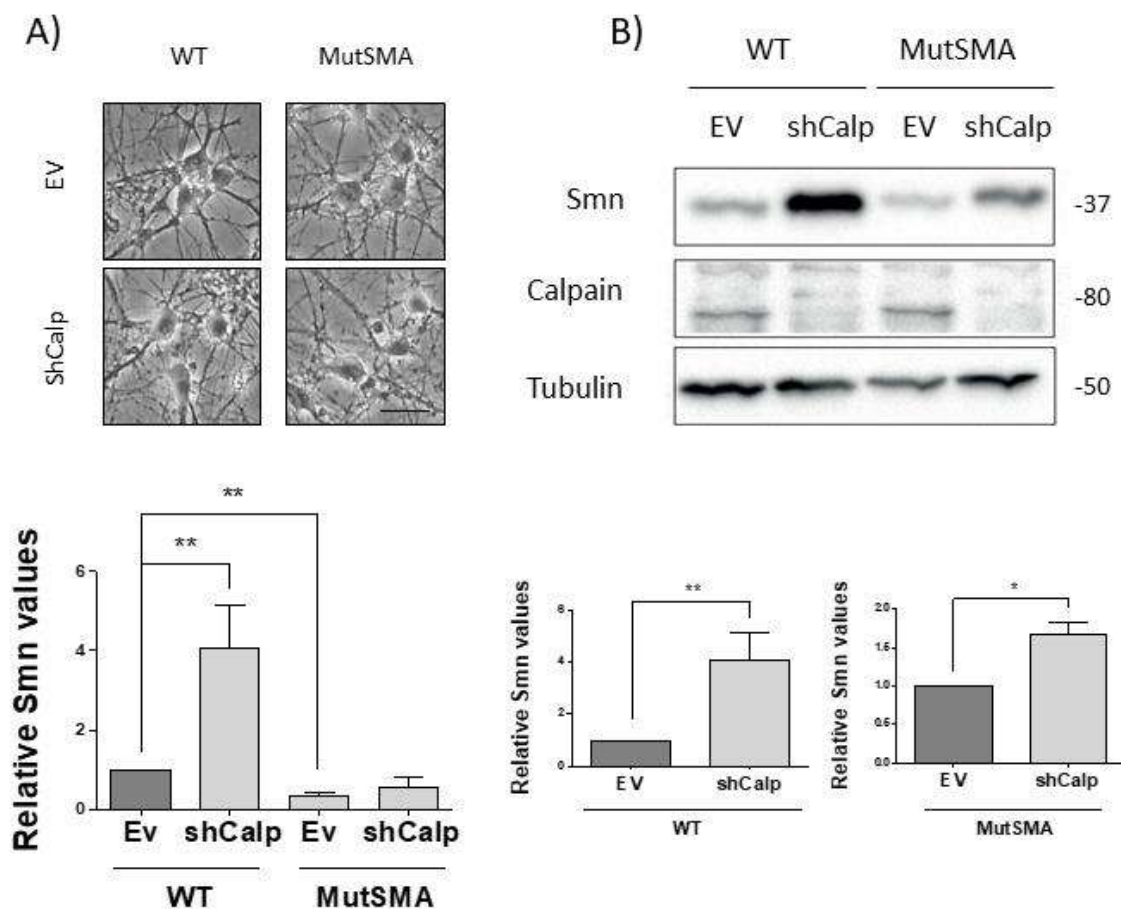


**Figure 78. Endogenous calpain reduction in MutSMA cultured MNs.** MutSMA MNs were transduced with lentivirus containing the EV or shCalp construct for 6 days. A) Representative phase-contrast images show cultured MNs at 6 DIV. B) Protein extracts were probed with anti-SMN antibody using western blot. Same membranes were reprobbed using an anti-calpain to evaluate shRNA effectiveness and anti- $\alpha$  tubulin as a loading control. Graphs represent the expression of Smn versus  $\alpha$ -tubulin comparing to the WT-EV condition (left and centre) or comparing to the MutSMA-EV condition (right). Values correspond to the quantification of four independent experiments  $\pm$  SEM. Significant differences are indicated with asterisks and were determined using the one-way ANOVA with the Dunnett multiple comparison post-test and the student t-test (\*  $p<0.05$ , \*\* $p<0.01$ ). Scale bar of 15  $\mu$ m.



In SMA, SMN deficiency results in neurite degeneration (**Figure 60**). To correlate the increase of Smn in shCalp treated MNs with a phenotypic improvement, we performed a neurite degeneration analysis. Morphometric analysis of neurite degeneration was carried out using MutSMA and WT MNs at a density of 5000 cells/cm<sup>2</sup>. Dissociated MNs were cultured and transduced as described. Neurite degeneration was assessed at 6, 9 and 12 days. At the indicated times, images of phase-contrast microscopy with a 40× lens were obtained and the number of degenerated neurites (swelling and/or blebbing) was counted using ImageJ (**Figure 79**). Fifty and 100 neurites were evaluated *per* condition and experiments were repeated three different times.

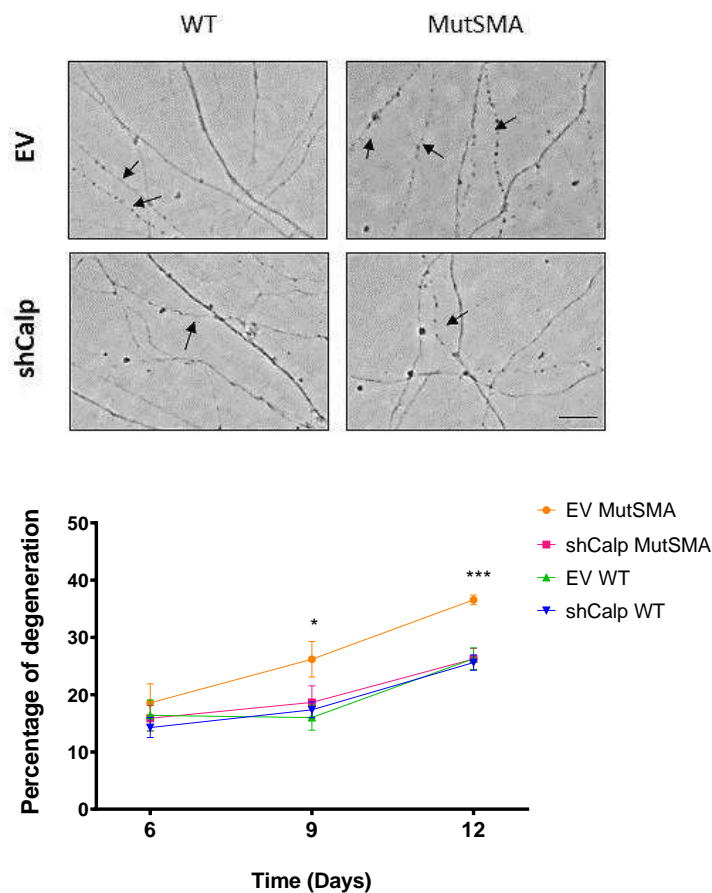


**Figure 79.** *shCalp* treatment in neurite degeneration in MutSMA cultured MNs. MN cultures of WT and MutSMA mice were established at a low-density in the presence of NTFs and transduced with lentivirus containing the *shCalp* construct or the EV construct. Representative images of cells cultured for 9 days after transduction. Arrows indicate neurite degeneration. The percentage of degenerating neurites was measured as described in Material and Methods at 6, 9 and 12 DIV. Graph values are the mean percentages of degenerating neurites per microscopic area for each condition of 12 wells in four independent experiments  $\pm$  SEM. Significant differences were identified using two-way ANOVA test and the Bonferroni post-test (\*  $p < 0.05$ , \*\*  $p < 0.01$ ). Scale bar of 15  $\mu$ m.

As shown in the **Figure 79**, no differences were observed between groups at day 6, but at day 9, the morphometric analysis shows a significantly higher percentage of neurite degeneration in EV-MutSMA ( $26.178 \pm 3.105$  %,  $p=0.0203$ ) cells compared to EV-treated WT ( $16.017 \pm 2.195$  %) MNs. After 12 days, the signs of degeneration increased to  $36.55 \pm 0.865$ % ( $p=0.0003$ ) in EV MutSMA cultures (EV WT,  $26.291 \pm 1.814$  %). Interestingly, MutSMA MNs treated with the calpain shRNA (day 6,  $15.87 \pm 2.253$  %,  $p=0.889$ ; day 9,  $18.64 \pm 2.898$  %,  $p=0.484$  and day 12,  $26.25 \pm 1.849$  %,  $p=0.987$ ) showed no differences with the control WT cells at any of the days (day 6,  $16.37 \pm 2.694$  %; day 9,  $16.02 \pm 2.195$  % and day 12,  $26.29 \pm 1.914$  %), indicating that the endogenous reduction of calpain prevents neurite degeneration.

The number of the apoptotic nuclei were also evaluated after 12 days in culture using Hoechst stain. No significant differences were observed between WT and MutSMA MNs regardless of the treatment (EV-WT,  $22.68 \pm 5.032$  %; shCalp-WT,  $29.38 \pm 3.955$  %; EV-MutSMA,  $31.09 \pm 7.506$  %; shCalp-MutSMA,  $25.52 \pm 4.164$  %;  $p=0.703$ ) (data not shown).



**CHAPTER 2: Calpeptin treatment regulates SMN and has protective effects in mouse models of Spinal Muscular Atrophy.**



## SUMMARY:

In Spinal Muscular Atrophy (SMA) is known that the severity of the disease largely depends on the levels of Survival Motor Neuron (SMN) protein available inside the cells and, that these levels are mainly determined by the number of copies of the *SMN2* gene (Harada et al., 2002; Lefebvre et al., 1997).

Currently, the development of new SMA therapeutic strategies are focused on two main strategies:

- SMN independent strategies: where the improvement of the disease is not a result of the modulation of SMN protein level but an indirect effect, like neuroprotection therapies against motoneuron (MNs) or the development of Stem Cell-based therapies to replace those cells that have been lost during the disease.
- SMN dependent strategies: where the improvement of the disease is due to the specific target of SMN. It can be done by using gene therapy to replace the gene that is lost in SMA, or by targeting the *SMN2* gene.

This second approach seems to be the most interesting one since it, can be achieved by several mechanisms, including upregulation of *SMN2* expression, promoting inclusion of exon 7, stabilization of full-length mRNA and regulation of SMN protein stability (Tariq et al., 2013). Different mechanisms involved in regulating SMN protein stability have been tested in *Smn*-deficient models: the ubiquitin-proteasome system (UPS) (Kwon et al., 2011), histone deacetylase inhibitors (Kernochan et al., 2005), and autophagy (Garcera et al., 2013; Periyakaruppiyah et al., 2016). Moreover, some of those treatments have been already tested to analyse their effect on SMA mice phenotype; showing improvements in survival and motor function (Foran et al., 2016; Kwon et al., 2011; Piras et al., 2017).

Our previous results suggesting that calpain protein might be involved in the regulation of *Smn* protein levels, encourage us to further characterize this effect and test the role of calpain inhibition *in vitro* and *in vivo*. For that, we used calpeptin (Sigma) (Z-Leu-nLeu-H) a pharmacological cell-permeable calpain inhibitor (Tsujinaka et al., 1988). It is one of the most sensitive inhibitors for calpain-1 and it has previously demonstrated neuroprotective effects in stroke disease (Zhou and Cai, 2019) and Multiple Sclerosis (Guyton et al., 2010) models, suggesting the ability of the drug to cross the blood-brain barrier.

Using primary cultures of MNs isolated from the transgenic models MutSMA and SMNDelta7 and two human models obtained from patients with SMA, the cultured fibroblasts and the differentiated MNs from iPSCs, cells were treated with the calpain inhibitor. Our results demonstrate the capacity of calpeptin treatment to inhibit calpain and increase Smn protein even in membrane depolarization conditions. In addition, calpeptin regulates autophagy pathway in MNs' soma and neurites with different effect in each compartment.

To explore the therapeutic potential of calpain inhibition to modify the SMA phenotype, we administered calpeptin to postnatal animals from the severe SMA mouse models MutSMA and SMNDelta7. Calpeptin treatment was able to modify SMA phenotype, significantly improving the lifespan and motor function of these mice. Our observations suggest that calpain regulates SMN level in MNs and calpeptin administration improves SMA phenotype demonstrating the potential utility of calpain inhibitors in SMA therapy.

### 1. Calpeptin treatment increases Smn protein level in cultured spinal cord MNs

In order to further understand how calpain activity could be regulating Smn protein levels in MNs, we tested cell-permeable inhibitor calpeptin treatment in our model of primary MNs culture. We first established a basal culture of CD1 MNs using E12.5 embryos. MNs were isolated and cultured for 6 days. The culture medium was changed to fresh medium containing NTFs (Control) or NTFs plus 25  $\mu$ M of Calpeptin and total cell lysates were obtained at 3, 9, 16, 20 and 24 hours after treatment. Smn protein level was analysed by western blot using an anti-SMN antibody.

As shown in **Figure 80**, Smn protein level was significantly increased after 3, 6, 16 and 20 hours (3h,  $3.335 \pm 0.564$ ,  $p=0.0033$ ; 9h,  $4.401 \pm 0.579$ ,  $p=0.0042$ ; 16h,  $2.892 \pm 0.609$ ,  $p=0.0145$ ; and 20 h,  $2.058 \pm 0.498$ ,  $p=0.0462$ ) of calpeptin treatment compared to their control conditions. No significant differences were observed in the levels of Smn at 24 hours, indicating that calpeptin is effective increasing Smn protein up to 24 hours of treatment.

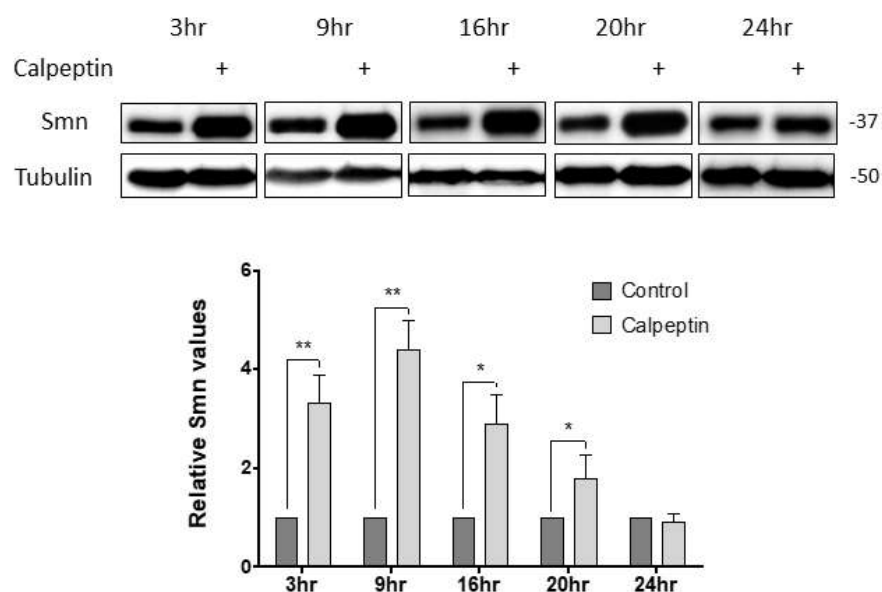


**Figure 80. Effect of calpeptin time-course treatment on Smn protein level in CD1 MNs.** CD1 mouse MNs were isolated and cultured in the presence of NTFs. Six days after plating, cells were treated with 25  $\mu$ M calpeptin and cell lysates were obtained at 3, 9, 16, 20, and 24 hours after treatment. Protein extracts were submitted to western blot analysis using an anti-SMN antibody. Membranes were reprobbed with an anti- $\alpha$ -tubulin antibody as a loading control. Graph values represent the expression of Smn versus  $\alpha$ -tubulin and correspond to the quantification of five independent experiments  $\pm$  SEM. Asterisks indicate significant differences using student t-test (\*  $p<0.05$ , \*\* $p<0.01$ ).



Next we added calpeptin treatment in chronic membrane depolarization conditions to evaluate whether calpain inhibition reverts Smn reduction. First, we establish a CD1 MNs cultures and 6 days later, cells were treated with NTFs (control) or NTFs plus 30K or 25  $\mu$ M calpeptin or 25  $\mu$ M calpeptin+30K. Three hours after treatment, cell lysates were obtained and submitted to western blot using anti- $\alpha$ -fodrin or anti-SMN antibodies. The results obtained showed that 145/150 fodrin fragments were significantly increased in the 30K ( $1.330 \pm 0.125$ ,  $p=0.0005$ ) compared to the control condition, demonstrating that calpain is activated after membrane depolarization in mouse MNs. Nevertheless, the addition of calpeptin (Calpeptin,  $0.6628 \pm 0.05$ ,  $p<0.0001$ ) to the control or the depolarized condition (Calpeptin+30K,  $0.634 \pm 0.07$ ,  $p<0.0001$ ) reduce fodrin cleavage products indicating that in both conditions calpain was inhibited (**Figure 81**).

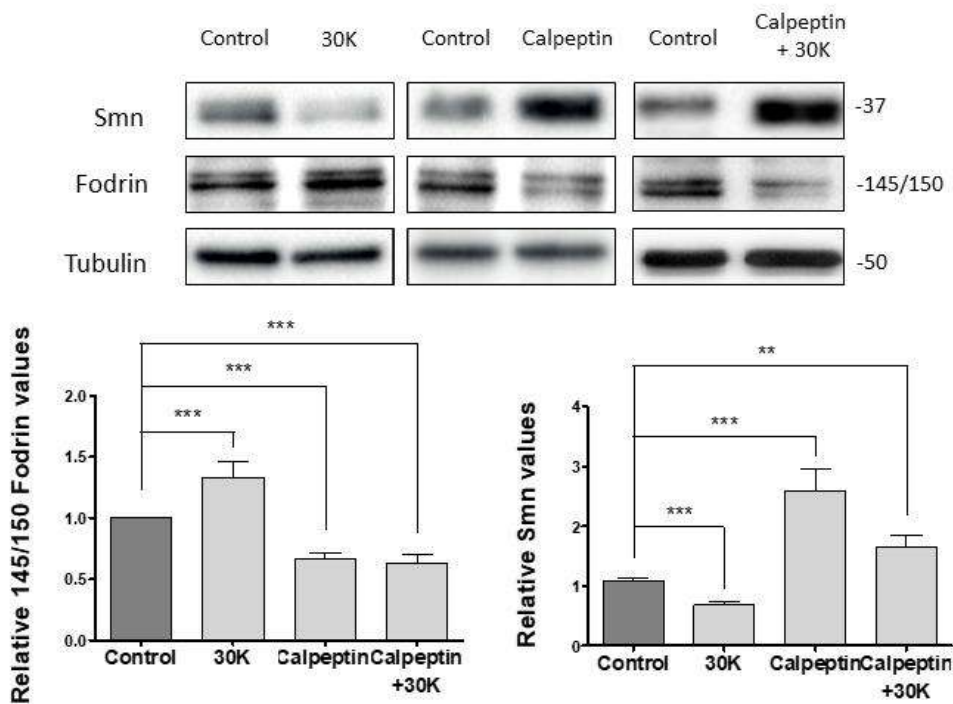


**Figure 81. Effect of calpain activity modulation on Smn protein level in cultured MNs.** CD1 spinal cord were isolated and cultured in NTFs. Six days after plating, cells were treated with 30 K, 25  $\mu$ M calpeptin or 25  $\mu$ M calpeptin+30K. Three hours after treatment, cell lysates were obtained and submitted to western blot using anti-SMN or anti- $\alpha$ -fodrin antibodies. Membranes were reprobbed with an anti- $\alpha$ -tubulin antibody as a loading control. Graph values represent the expression of 145/150 KDa fodrin product (**left**) or Smn (**right**) versus  $\alpha$ -tubulin and correspond to the quantification of at least four independent experiments  $\pm$  SEM. Differences were analysed using the one-way ANOVA with the Dunnett multiple comparison post-test (\*\* $p<0.01$ , \*\*\*  $p<0.001$ ).

When Smn protein level was analysed, we observed inverse results, Smn was reduced in MNs treated with 30K ( $0.685 \pm 0.052$ ,  $p < 0.0001$ ), while calpeptin treatment increased Smn ( $2.583 \pm 0.385$ ,  $p < 0.0001$ ) compared to the control condition. In calpeptin+30K-treated cells, Smn protein level was significantly increased ( $1.652 \pm 0.200$ ,  $p = 0.0015$ ) compared to 30k and control conditions (**Figure 81**). These results together indicate that Smn is reduced in 30K-treated cells and these effects can be prevented by calpeptin treatment.

## 2. High potassium treatment induces direct cleavage of Smn in culture MNs

It is still unclear how Smn protein levels are regulated in cells, but calpain can be one of the mechanism involved in its regulation. In muscle tissue and in U2-OS cell line previous investigations determined that cytosolic, but not nuclear SMN could be processed by calpain leading to the production of 2 fragments, the N- and the C-terminal cleavage products (Fuentes et al., 2010; Walker et al., 2008).

To further assess the relevance of the hypothesis of calpain directly being processing Smn we carried out a CD1 MNs culture (E12.5). Cells were isolated and cultured for 6 days. Then NTFs (Control), 30 mM KCl (30K), 25  $\mu$ M calpeptin or 30K plus 25  $\mu$ M calpeptin treatments, were added for 3 hours. Total lysates were collected and analysed by western blot using two monoclonal antibodies, anti-SMN antibody (Clone 8) (BD Bioscience) and anti-SMN1 antibody (9F2) (Cell Signalling), to detect the cleavage products. Anti-SMN antibody (Clone 8) recognizes full-length and N-terminal fragments, and anti-SMN1 (9F2) antibody recognizes C-terminal fragments.

As expected, quantification of full-length Smn (~37 KDa) using anti-SMN (Clone 8) showed that 30K treatment significantly reduced Smn protein level ( $0.590 \pm 0.075$ ,  $p < 0.0001$ ), whereas calpeptin and calpeptin+30K treatment increased Smn (Calpeptin,  $2.275 \pm 0.551$ ,  $p = 0.0175$ ; Calpeptin+30K,  $1.597 \pm 0.214$ ,  $p = 0.0034$ ), compared to non-treated control (graph not shown).

When the same membranes were overexposed, we were able to detect the N- terminal Smn cleavage product (~20 KDa) band that increase in 30K condition ( $1.980 \pm 0.760$ ,  $p = 0.0431$ ), compared to the untreated control. The addition of 25  $\mu$ M calpeptin to the control NTFs medium or the 30K medium, prevents this increase of the N-terminal

fragment (Calpeptin,  $0.533 \pm 0.243$ ,  $p=0.0172$ ; Calpeptin+30K,  $0.531 \pm 0.197$ ,  $p=0.0054$ ) (Figure 82).

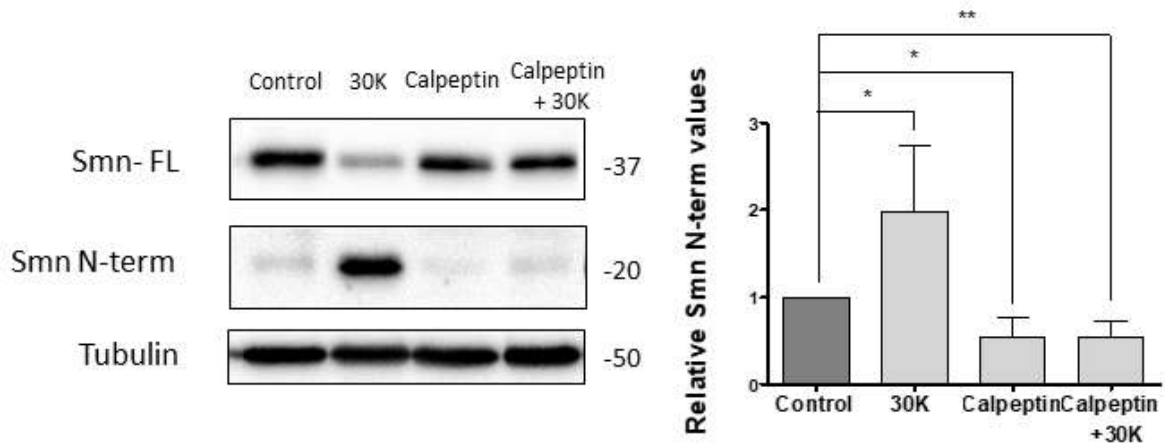


**Figure 82. Effect of high K<sup>+</sup> and calpeptin treatment on SMN cleavage by analysing the Smn N-terminal fragment.** Spinal cord MNs were isolated from E13 CD embryos and cultured in the presence of NTFs. Six days after plating, cells were treated with 30K, 25  $\mu$ M calpeptin or 25  $\mu$ M calpeptin+30K for 3 hours. Cell lysates were obtained and submitted to western blot using an anti-SMN antibody to determine Smn full-length and N-terminal Smn fragment. Membranes were reprobbed with an anti-  $\alpha$ -tubulin antibody. Graph values  $\pm$  SEM represent the expression of N-terminal Smn fragments versus  $\alpha$ -tubulin and correspond to the quantification of at least four independent experiments. Asterisks indicate significant differences assessed by the one-way ANOVA with the Dunnett multiple comparison post-test (\*  $p<0.05$ , \*\* $p<0.01$ ).

Using the anti-SMN1 (9E2) antibody we can detect the C-terminal fragments ( $\sim 17$  kDa) only when membranes were overexposed. As shown in **Figure 83** Smn C-terminal fragments were significantly increased in 30K ( $1.498 \pm 0.291$ ,  $p=0.0410$ ) compared to the control. Conversely, calpeptin treatment significantly reduced C-terminal fragments in control and 30K conditions ( $0.278 \pm 0.043$ ,  $p<0.0001$ , and  $0.221 \pm 0.046$ ,  $p<0.0001$ , respectively). These results together suggest that high K<sup>+</sup> treatment reduces full-length Smn and increases C-terminal fragments what can be prevented with calpeptin treatment, providing an insight into a novel aspect of the post-translation regulation of SMN.

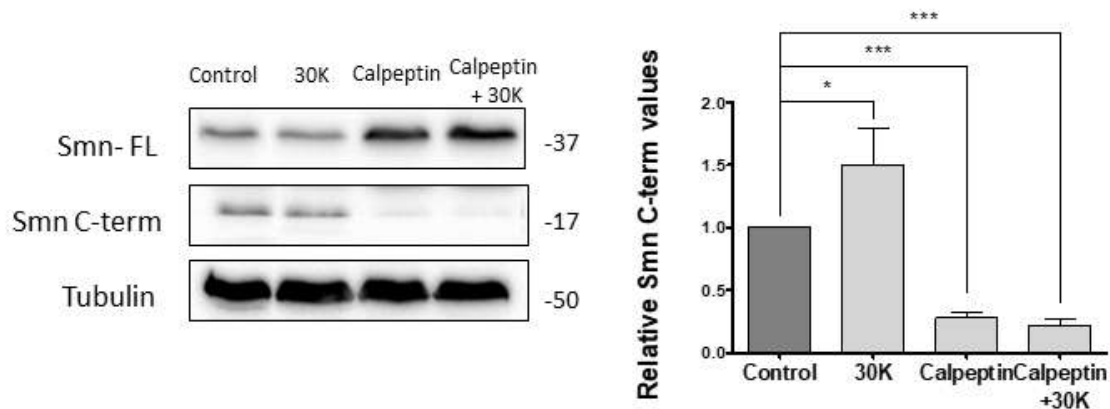


**Figure 83. Effect of high K<sup>+</sup> and calpeptin treatment on SMN cleavage by analysing the Smn C-terminal fragment.** Cultured CD1 mouse MNs were maintained in the presence of NTFs for 6 DIV. Cells were then treated with 30K, 25  $\mu$ M calpeptin or 25  $\mu$ M calpeptin+30K for 3 hours. Cell lysates were obtained and submitted to western blot using an anti-SMN antibody to determine Smn full-length and anti-SMN1 antibody to detect C-terminal Smn fragments. Membranes were reprobed with an anti-  $\alpha$ -tubulin antibody as a loading control. Graph values represent the expression of C-terminal Smn fragments versus  $\alpha$ -tubulin  $\pm$  SEM and correspond to the quantification of at least four independent experiments. Statistical analysis was done using the one-way ANOVA with the Dunnett multiple comparison post-test (\*  $p < 0.05$ , \*\*\*  $p < 0.001$ ).

To confirm that the regulation of Smn by calpain modulation was at the post-transcriptional level, we perform an RT-qPCR. For that, we purify CD1 MNs from E12.5 embryos and cultured them in NTFs supplemented medium for 6 days. Then cells were treated for 3 hours with a control condition or with 25  $\mu$ M calpeptin. RNA extracts were obtained from three independent experiments and processed for RT-qPCR. Results show no differences of Smn mRNA between the control and the treated group, reinforcing the hypothesis that calpain is regulating Smn by directly cleavage at the post-transcriptional level (**Figure 84**).

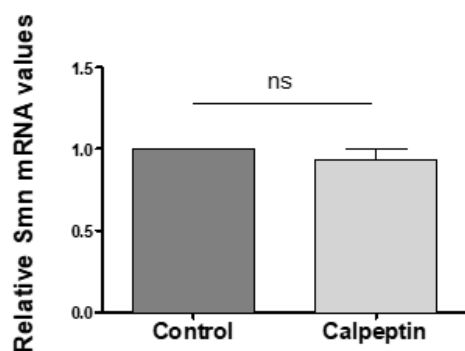


**Figure 84. Smn mRNA levels in calpeptin treated CD1 MNs.** MN cultures of CD1 mice were established in NTFs for 6 days. Cells were treated with 25  $\mu$ M calpeptin for 3 hours. RNA extraction was performed and submitted to RT-qPCR. Graph shows the mean of the relative values of Smn mRNA  $\pm$  SEM. Values were obtained from three independent experiments. Statistical analysis was done with the student t-test (no significant (ns) values were considered when  $p > 0.05$ ).

### 3. Calpeptin treatment increases autophagy markers in mouse MNs

From our previous experiments, we knew that downregulation of calpain protein level using a specific shRNA, increased the level of the autophagy marker LC3-II (**Figure 71**). To further corroborate that calpain activity regulates LC3-II and p62, we evaluate their protein levels in CD1 MNs treated with the calpain inhibitor calpeptin. CD1 MNs were purified and cultured in NTFs medium for 6 days and treated for 3 hours with 30mM of Potassium Chloride (30K), 25  $\mu$ M calpeptin (Calpeptin), or a combination of both (Calpeptin + 30K). Protein extracts were submitted to western blot analysis and LC3-II and p62 were analysed.

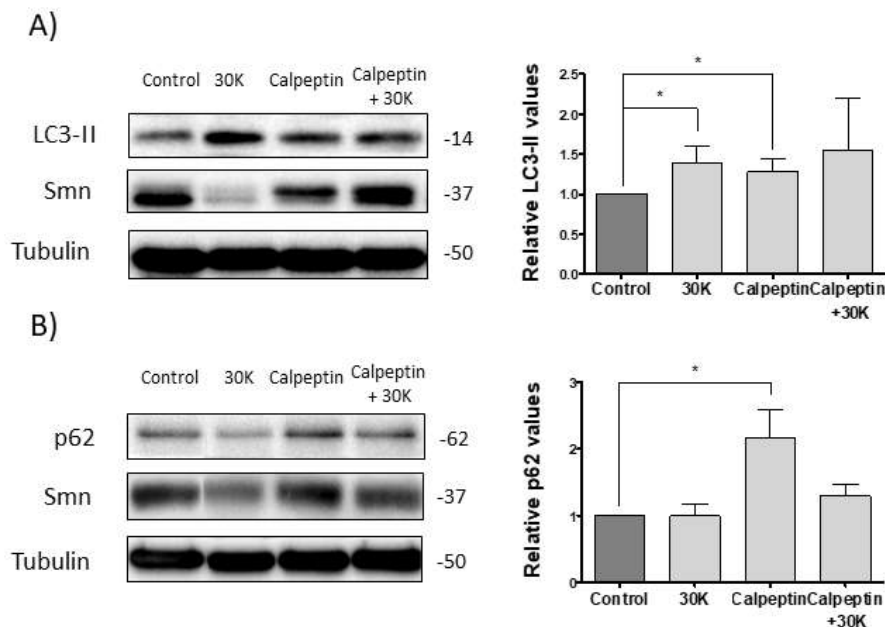


**Figure 85. Changes of autophagy markers in Calpeptin treated CD1 MNs.** Spinal cord MNs were isolated and cultured in the presence of NTFs. After 6 DIV, cells were treated with 30K, 25  $\mu$ M of calpeptin and 25  $\mu$ M of calpeptin+30K for 3 hours. Protein extracts were collected and submitted to western blot analysis. **A)** Membranes were probed with an anti-LC3 and anti-SMN antibodies. Graph shows mean  $\pm$  SEM of the expression of LC3 protein against tubulin. **B)** Levels of p62 protein were also evaluated using an anti-p62 antibody. Graph represent expression of p62 versus  $\alpha$ -tubulin  $\pm$  SEM. Values correspond to the quantification of four independent experiments. Statistical differences were analysed using the one-way ANOVA with the Dunnett multiple comparison post-test (\*  $p < 0.05$ ).

As shown in **Figure 85.A**, the autophagy marker LC3-II was increased in membrane depolarizing conditions (30K) ( $1.388 \pm 0.2177$ ,  $p = 0.0162$ ) as well as in calpain inhibition condition (Calpeptin) ( $1.276 \pm 0.1576$ ,  $p = 0.0495$ ) compared to the control situation.

Interestingly, no differences were observed between the Calpeptin+30K and the Control ( $1.546 \pm 0.6423$ ,  $p=0.203$ ). When p62 was evaluated, only Calpeptin treatment significantly increase its protein level ( $2.156 \pm 0.428$ ,  $p=0.0223$ ) (**Figure 85.B**).

As we have been reporting, soma and neurites are two differentiated structures in MNs and it is important to study the observed differences in both compartments separately. To localize LC3-positive spots in soma and in neurites, we decided to analyse its expression in cultured MNs from the SMNDelta7 mouse model treated with 30 mM potassium chloride (30K) or 25  $\mu$ M of calpeptin (calpeptin). The control condition was left untreated. MNs were plated on glass cover-slips and after 6 days, treatments were added. Fixation was performed using only cold methanol for approximately 10 s, and LC3 immunostaining was performed. Hoechst stain was used to localize the nucleus of MNs cells.

SMNDelta7 MNs showed higher number of LC3 spots in both, soma ( $97.710 \pm 9.103$  puncta *per* soma,  $p<0.0001$ ) and neurites ( $0.641 \pm 0.058$  puncta/ $\mu$ m of neurite,  $p<0.0001$ ), compared to the control WT MNs ( $39.72 \pm 3.244$  puncta *per* soma and  $0.274 \pm 0.037$  puncta/ $\mu$ m of neurite). We observed that in WT MNs, the 30K treatment increased LC3-positive spots in soma and neurites ( $58.42 \pm 7.018$  puncta *per* soma,  $p=0.0081$ , and  $0.552 \pm 0.061$  puncta/ $\mu$ m of neurite,  $p=0.0004$ ) compared to the control condition. However, calpeptin treatment only increased autophagy vesicles in soma ( $64.100 \pm 9.343$  puncta *per* soma,  $p=0.006$  and  $0.249 \pm 0.019$  puncta/ $\mu$ m of neurite,  $p=0.645$ ). Interestingly, SMNDelta7 MNs results showed different responses to the treatments. While 30K treatment significantly decreases the number of autophagy vesicles in the soma ( $65.710 \pm 7.390$  puncta *per* soma,  $p=0.0074$ ) without modifying the number in neurites ( $0.685 \pm 0.043$  puncta/ $\mu$ m of neurite,  $p=0.531$ ), the calpeptin treatment decrease the LC3 spots in the neurites ( $0.406 \pm 0.030$  puncta/ $\mu$ m of neurite,  $p=0.0003$ ) without affecting the soma ( $93.67 \pm 6.301$  puncta *per* soma,  $p=0.708$ ) (**Figure 86**).

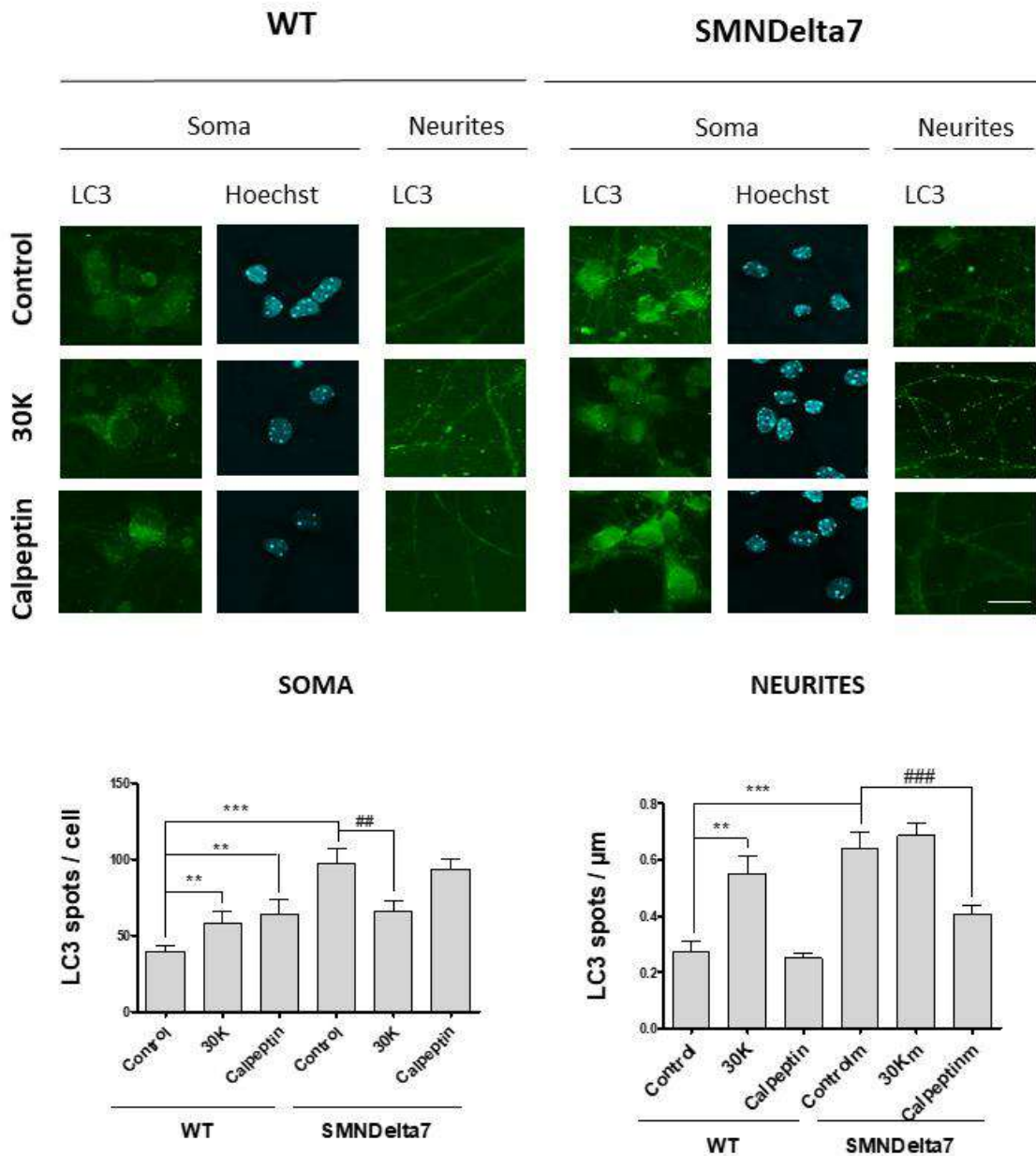


**Figure 86. Effect of calpain activity modulation in LC3 spots levels in SMNDelta7 MNs.** SMNDelta7 and WT MNs were purified and cultured for 6 days in the presence of NTFs medium. Cells were treated with 30K or 25  $\mu\text{M}$  of calpeptin for 3 hours and then fixed with PFA 4%. Immunofluorescence was performed using an anti-LC3 antibody (green) and LC3 spots were quantified in soma and in neurites. Hoechst stain was used to identify the nucleus. Graphs show the number of LC3 spots in soma (**left**) and neurites (**right**) of WT and SMNDelta7 MNs. Values represent mean  $\pm$  SEM. Significant differences were determined using the one-way ANOVA with the Dunnett multiple comparison post-test and the student t-test (\*\*  $p < 0.01$ , \*\*\*  $p < 0.001$ ). Scale bar of 15  $\mu\text{m}$ .

#### 4. Calpeptin treatment increases Smn protein level in SMA mutant MNs

To determine whether calpeptin treatment regulates Smn in SMA MNs, E12.5 embryos from the MutSMA and the SMNDelta7 mouse models were genotyped and MNs were

purified. Mutant and WT isolated MNs were cultured in the presence of NTFs following the same protocols as for CD1 cultures (**Figure 87.A**). Six days after purification, cells were treated for 3 hours with 25  $\mu$ M calpeptin. Protein extracts were collected and submitted to western blot analysis using SMN antibody.

In MutSMA cultured MNs, results in **Figure 87.B** indicates that Smn protein level was increased in calpeptin-treated WT condition ( $2.439 \pm 0.3495$ ,  $p=0.0146$ ) compared to the non-treated control condition. Furthermore, calpeptin treatment of MutSMA cells increased Smn protein ( $5.181 \pm 1.487$ ,  $p=0.0241$ ) compared to the non-treated MutSMA condition.

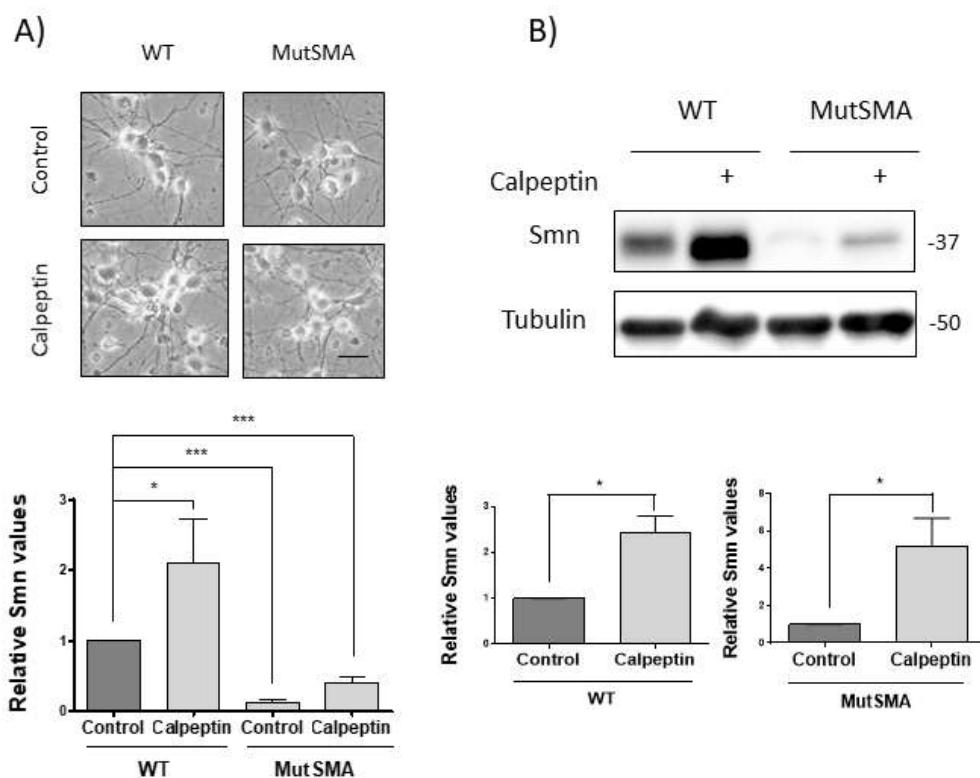


**Figure 87. Effect of calpeptin treatment in Smn protein level in MutSMA MNs.** Isolated MutSMA and WT MNs were cultured for 6 days and treated with or without calpeptin (25  $\mu$ M) for 3 hours. **A)** Representative phase contrast images of MNs cultures after 6 DIV. **B)** Total cell lysates were collected and submitted to western blot analysis using an anti-SMN antibody. Anti- $\alpha$  tubulin was used as a loading control. Graphs values show relative Smn protein levels  $\pm$  SEM comparing to the WT-Control condition (**left and centre**) or comparing to the MutSMA-Control condition (**right**). Values correspond to the quantification of three independent experiments. Significant differences are indicated with asterisks and were determined using the one-way ANOVA with the Dunnett multiple comparison post-test and the student t-test (\*  $p<0.05$ , \*\*\*  $p<0.001$ ). Scale bar of 15  $\mu$ m.



The same experiment was performed using the SMNDelta7 mouse line. E12.5 embryos were genotyped and MNs purified and cultured for 6 days in NTFs medium (**Figure 88.A**). Cells were treated with the calpain inhibitor calpeptin (25  $\mu$ M) for 3 hours, before protein extracts were collected and analysed using western blot technique. Results showed a trend of increase, that did not become significant, in the WT treated condition ( $1.499 \pm 0.2634$ ,  $p=0.0571$ ) versus the WT untreated condition. Like it was observed in the MutSMA MNs, in SMNDelta7 cells, calpeptin treatment increased Smn protein level ( $2.765 \pm 0.5123$ ,  $p=0.0333$ ) compared to the control condition. This increase of Smn in the Calpeptin-SMNDelta7 cells ( $0.7089 \pm 0.3237$ ,  $p=0.4803$ ) was not significantly different from the control-WT cells (**Figure 88.B**), suggesting that protein levels were restored to normal values.

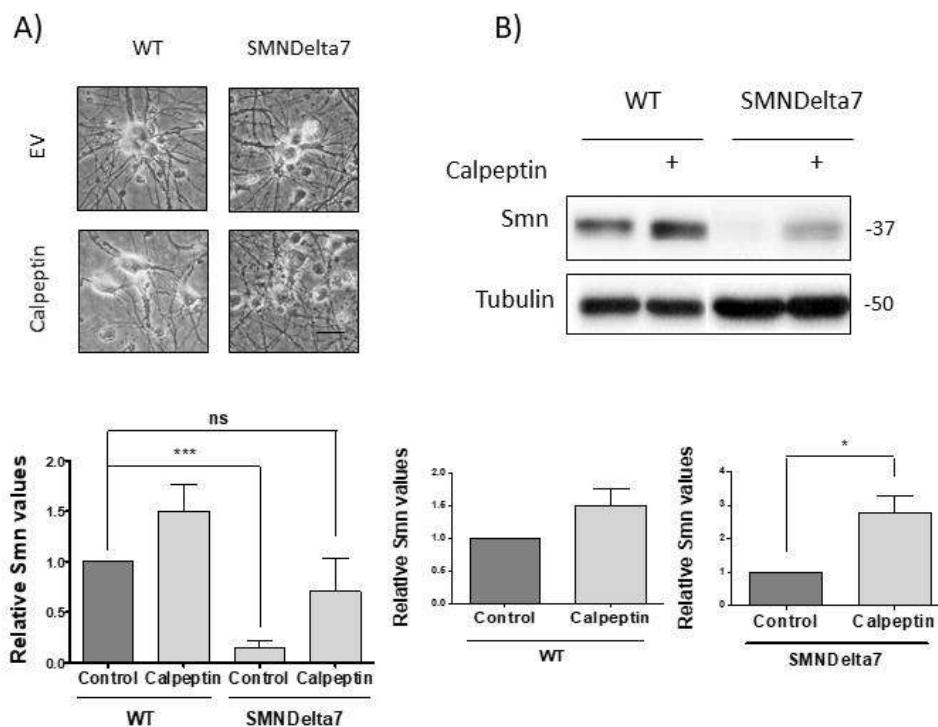


**Figure 88. Effect of calpeptin treatment in Smn protein level in SMNDelta7 MNs.** SMNDelta7 and WT MNs were isolated and cultured in the presence of NTFs. Six days after plating, cells were treated with 25  $\mu$ M calpeptin or left untreated. **A)** Representative microscopic images of MNs at day 6. **B)** Three hours after treatment, protein extracts were obtained and submitted to western blot analysis using an anti-SMN antibody. Membranes were re probed with an anti- $\alpha$ -tubulin antibody. Graphs values represent the expression of Smn versus  $\alpha$ -tubulin in comparing to WT (left and centre) and mutSMA (right) and correspond to the quantification of three independent experiments  $\pm$  SEM. Asterisks indicate significant differences using one-way ANOVA with the Dunnett multiple comparison post-test and the student t-test (\*  $p < 0.05$ , \*\*\*  $p < 0.001$ , no significant (ns)  $p > 0.05$ ). Scale bar of 15  $\mu$ m.

## 5. Calpeptin treatment in human SMN reduced cells

Once it was observed the effect produced by calpeptin treatment in MNs from the two SMA mouse models, we decided to test this treatment in human cells, the fibroblast cell-lines and the differentiated MNs. First, we established the fibroblast cultures of the healthy carrier 3814 cell-line (Control) and the 2 SMA cell – lines, the 9677 and the 3813 (SMA 1 and SMA 2, respectively). Cells were cultured for 2 days (**Figure 89.A**) and then treated 25  $\mu$ M calpeptin or left untreated for 6 hours. Total cell lysates were collected and analysed using anti-SMN and anti-fodrin antibodies in western blot. In any of the cell-lines, we observed no difference in the calpeptin-treated cells compared to their respective untreated controls both in SMN protein levels, and 145/150 fodrin fragments (**Figure 89.B**), suggesting that the treatment did not work in these cells, either because the dose was not enough or the treatment time was not adequate.

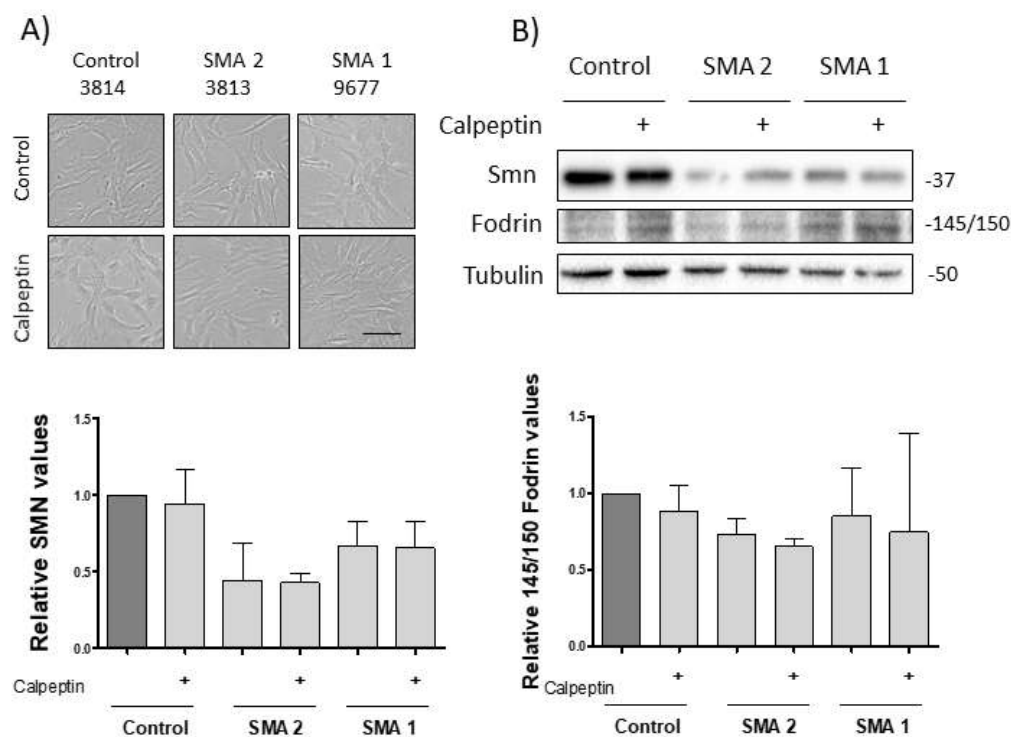


**Figure 89. Effect of calpeptin treatment in SMN levels in human fibroblast cultures.** Control (3814 healthy SMA carrier) and SMA patient derived (9677 SMA type 1, 3813 SMA type 2) fibroblast cell lines were cultured for 2 days and then treated 25  $\mu$ M calpeptin or left untreated for 6 hours. **A)** Representative phase contrast images of cell cultures after 2 DIV. **B)** Total cell lysates were collected and submitted to western blot analysis using an anti-SMN and an anti-fodrin antibodies. Anti- $\alpha$  tubulin was used as a loading control. Graphs values show relative SMN (**left**) and fodrin (**right**) protein levels  $\pm$  SEM. Values correspond a three independent experiments. Scale bar of 100  $\mu$ m.

The same results were observed in the differentiated human MNs. SMA and Control derived MNs were maintained in maturation medium for 6 days (**Figure 90.A**) and then treated with 25  $\mu\text{M}$  calpeptin or left untreated for 6 hours. After the treatment, protein extracts were obtained and submitted to western blot analysis using anti-SMN and anti-fodrin antibodies. As shown in **Figure 90.B**, no changes were observed neither in SMN or 145/150 fodrin fragments compared to their respective control condition, again suggesting that the treatment did not work in these cells. For future experiments, it will be necessary to carry out a time-course and a dose-effect curve to determine the adequate dose and treatment time in these cells to be able to study the effect of *in vitro* calpeptin treatment in human cells.

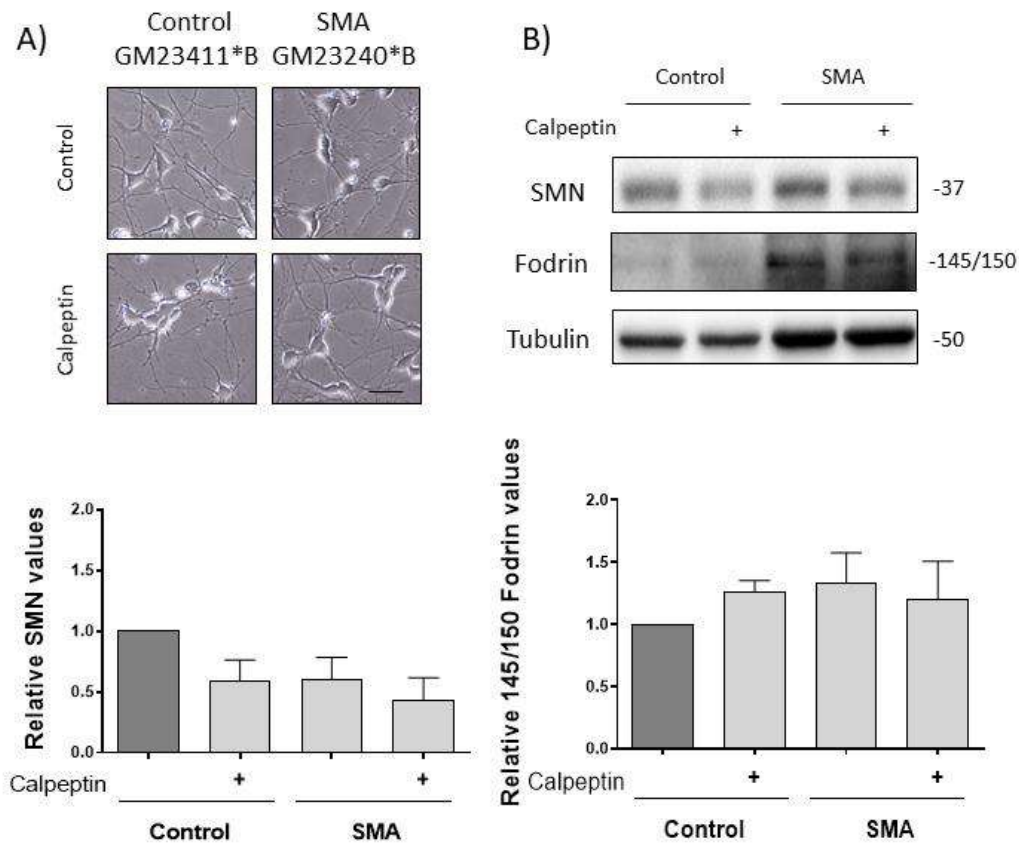


**Figure 90. Effect of calpeptin treatment in SMN levels in human differentiated MNs.** MNs derived from hiPSCs (GM23240\*B and GM23411\*B) were maintained in maturation medium for 6 days and then treated with 25  $\mu\text{M}$  calpeptin or left untreated for 6 hours. **A)** Representative microscopy images of human MNs after 6 days in culture. **B)** Protein extracts were obtained and submitted to western blot analysis using an anti-SMN and anti-fodrin antibodies. Anti- $\alpha$ -tubulin antibody was used as a loading control. Graphs represent the expression of SMN (**left**) and 145/10 fodrin fragments (**right**) and correspond to the quantification of three independent experiments  $\pm$  SEM. Scale bar of 20  $\mu\text{m}$ .

## 6. Effect of calpeptin and mTOR independent autophagy inducers treatment on CD1 MNs

In MNs obtained from SMA mouse models, treatment with is effective increasing the levels of Smn and the autophagy marker LC3-II. Therefore, we wonder if the use of calpeptin in combination with other autophagy regulators could have a synergistic effect increasing Smn protein levels. For that, we selected two autophagy inducers that we had previously tested in the laboratory and that we knew they increased the Smn protein in MNs: resveratrol (mTOR-dependent autophagy inducer) and trehalose (mTOR-independent autophagy inducer).

The first autophagy inducer tested in combination was resveratrol. Resveratrol (3,5,4'-trihydroxy-trans-stilbene), is a natural polyphenol compound found in the roots of plants and in some edible fruits including berries and grapes (skin and seeds). It is postulated to modulate autophagy by directly inhibiting mTOR (resveratrol competes with ATP in the ATP-binding pocket of mTOR) (Park et al., 2016). To measure the effectiveness of the co-treatment we added 25  $\mu$ M of calpeptin (Calpeptin), 50nM of Resveratrol (50Resv) or a combination of calpeptin and resveratrol (Calpeptin+50Resv) to MNs cultures. Twelve hours later, protein extracts were obtained and submitted to western blot analysis using an anti-SMN antibody. Results showed that both treatments individually increase the levels of Smn (Calpeptin,  $3.570 \pm 0.7931$ ,  $p=0.0026$  and 50Resv,  $1.409 \pm 0.1739$ ,  $p=0.0338$ ), but that the combination of both treatments did not have a synergistic effect since it prevails the effect of increase similar to the calpeptin treatment (Calpeptin+50Resv,  $3.175 \pm 0.5707$ ,  $p=0.0119$ ). Fodrin measurement was used as a control of the calpain inhibition by calpeptin. As expected only cells that received calpeptin showed reduced levels in the specific 145/150 fodrin fragments (Calpeptin,  $0.6266 \pm 0.0990$ ,  $p=0.0014$ ; 50Resv,  $0.7895 \pm 0.1432$ ,  $p=0.2318$  and Calpeptin+50Resv,  $0.6679 \pm 0.0878$ ,  $p=0.0071$ ) LC3-II was also measured to evaluate the effect of the treatments in the autophagy pathway. All treatments alone or in combination produced an increase of the levels of LC3-II (Calpeptin,  $1.276 \pm 0.1576$ ,  $p=0.0381$ ; 50Resv,  $1.208 \pm 0.0501$ ,  $p<0.0001$ ; and Calpeptin+50Resv,  $1.116 \pm 0.0673$ ,  $p=0.0073$ ) (**Figure 91**).

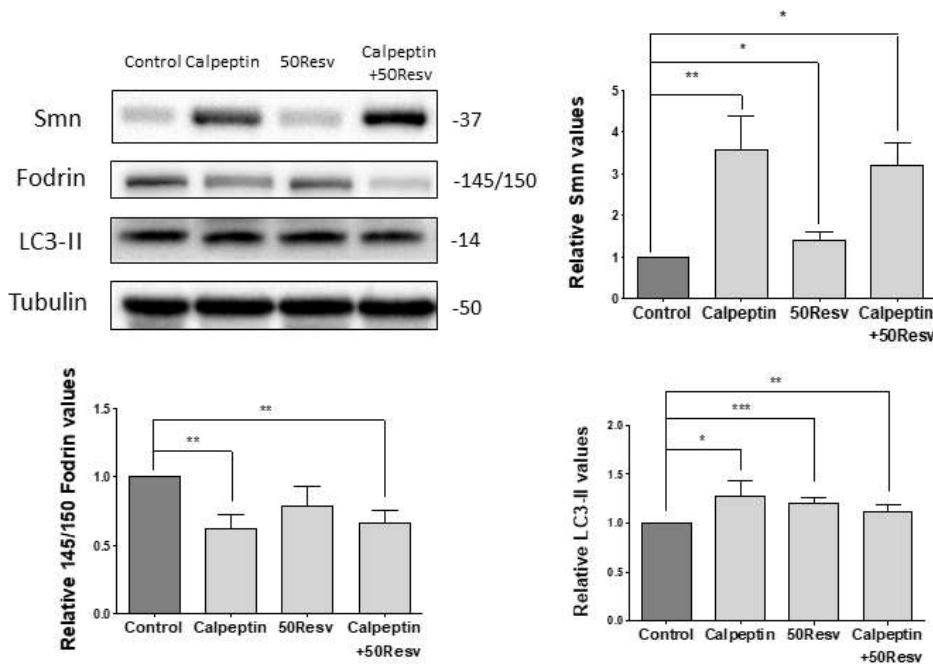


**Figure 91. Combination of calpeptin and resveratrol treatment in CD1 cultured MNs.** Cultured CD1 mouse MNs were maintained in the presence of NTFs. Six days after plating cells were left untreated or treated with 25  $\mu$ M of calpeptin, 50 nM of Resveratrol (50Resv) or a combination of the calpeptin with the resveratrol (Calpeptin+50Resv) for 12 hours. Total cell lysate was submitted to western blot using an anti-SMN, anti-fodrin and anti-LC3 antibodies. Alpha-tubulin was used as a loading control. Graphs represent the relative values of Smn (**left**) or 145/150 fodrin (**right**) versus  $\alpha$ -tubulin  $\pm$  SEM. Values were obtained from three independent experiments and were analysed using the one-way ANOVA with the Dunnett multiple comparison post-test and the student t-test (\*  $p < 0.05$ , \*\*  $p < 0.01$ , \*\*\*  $p < 0.001$ ).

The second autophagy inducer tested was trehalose. Trehalose is a natural disaccharide sugar found extensively in a diverse range of organisms including bacteria, plants, insects, yeast, fungi, and invertebrates but not in mammals. It is not clear the mechanism why trehalose modulates autophagy. It is known that trehalose induces autophagy (measured by the increase in the LC3-I to LC3-II conversion) without affecting mTOR signalling pathway (mTOR- independent) (Chen et al., 2016).

CD1 MNs were cultured in NTFs for 6 days before treatment was added: 25  $\mu$ M of calpeptin, 100 mM of trehalose or a combination of Calpeptin+Trehalose. After 6 hours, protein extracts were obtained and submitted to western blot using an anti-SMN antibody. The results showed that all treatments were able to increase the Smn protein level (Calpeptin,  $1.891 \pm 0.3871$ ,  $p = 0.018$ ; Trehalose,  $1.477 \pm 0.1868$ ,  $p = 0.0005$  and Calpeptin+Trehalose,  $1.887 \pm 0.3616$ ,  $p = 0.0002$ ) compared to the control cells. However, the combination of both

treatments did not have a synergistic effect, since result showed an increase similar to the calpeptin treatment. In Calpeptin+Trehalose condition specific 145/150 fodrin fragments were measured as control of calpain inhibition and only Calpeptin and Calpeptin+Trehalose treated cells showed a reduction of those fragments (Calpeptin,  $0.6924 \pm 0.0451$ ,  $p < 0.0001$ ; Trehalose,  $1.074 \pm 0.0839$ ,  $p = 0.5401$  and Calpeptin+Trehalose,  $0.7541 \pm 0.1799$ ,  $p = 0.0005$ ). Analysis of LC3-II protein level showed that all treatments modulate autophagy by increasing LC3-II (Calpeptin,  $1.455 \pm 0.1982$ ,  $p = 0.0146$ ; Trehalose,  $1.299 \pm 0.2153$ ,  $p = 0.0108$  and Calpeptin+Trehalose,  $1.234 \pm 0.0482$ ,  $p < 0.0001$ ) (**Figure 92**).

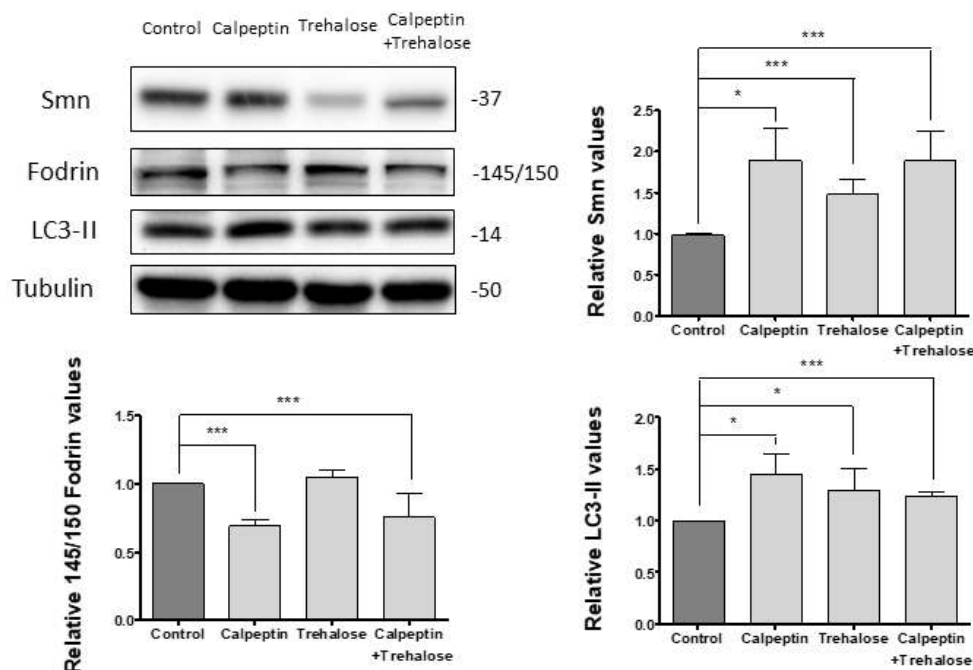


**Figure 92, Combination of calpeptin and trehalose treatment in CD1 cultured MNs.** CD1 MNs were cultured for 6 days in the presence of NTFs before treatment was added: 25  $\mu$ M of calpeptin, 100 mM of trehalose and a combination of calpeptin+trehalose. After 6 hours protein extracts were obtained and probed with the anti-SMN, anti-fodrin and anti-LC3 antibodies. To make sure of protein charge, membranes were reprobed using an anti- $\alpha$  tubulin. Graph represent relative values of Smn, fodrin and LC3  $\pm$  SEM from three independent experiments. Asterisks indicate statistical differences obtained using the one-way ANOVA with the Dunnett multiple comparison post-test and the student t-test (\*  $p < 0.05$ , \*\*\*  $p < 0.001$ ).

## 7. Calpeptin administration extends survival in MutSMA and SMNDelta7 mice

In SMA, SMN protein levels are critical determinants of the disease onset and severity. Moreover, the use of therapies that increase SMN levels has shown to improve symptoms

and survival. Considering that all our results together strongly suggest that calpain inhibition positively regulates Smn protein level in cultured MNs, we decided to test the therapeutic potential of calpeptin treatment in two severe mouse models of SMA, the MutSMA and the SMNDelta7.

In both mouse models, pregnancy development was controlled to accurately determine the birth date, also called postnatal day 0 (P0). Mice were tattooed, genotyped and distributed in the different groups of treatment. WT and mutant littermates began to receive treatment at P1 with a daily dose of 6 $\mu$ g of calpeptin *per* gram of weight (treatment groups) or physiological saline (Sham groups) with a subcutaneous injection. Lifespan, body weight and body size were monitored in order to evaluate the effect of calpeptin *in vivo*.

Results showed that calpeptin administration significantly improved the lifespan of the MutSMA-Calpeptin group (average days  $9 \pm 2.97$ ,  $n=11$ ), compared with the MutSMA-Sham (average days  $4.083 \pm 2.54$ ,  $n=12$ ,  $p<0.0001$ ) (**Figure 93 right**). Likewise, the lifespan of SMNDelta7-Calpeptin group (average days  $14.417 \pm 2.906$ ,  $n= 15$ ) was significantly increased compared to SMNDelta7-Sham (average days  $9.8 \pm 2.898$ ,  $n =10$ ,  $p<0.0001$ ) mice (**Figure 93 left**).

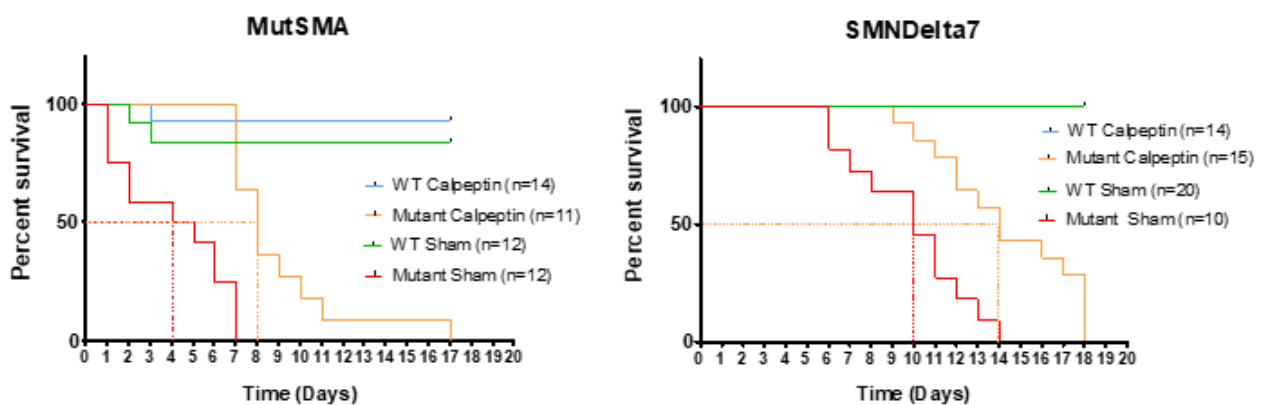


**Figure 93. Effect of calpeptin administration on survival of MutSMA and SMNDelta7 mice.** Postnatal animals from mutSMA and SMNDelta7 mice were treated daily subcutaneous with calpeptin or with physiological saline (Sham). Survival of calpeptin-treated or non-treated in mutSMA (**right**) and in SMNDelta7 (**left**) differences were calculated by the log-rank Mantel-Cox test.

When the weight of the animals was measured, no significant differences were found in Calpeptin-treated mutant compared to non-treated mice in any of the SMA mouse models. When compared to WT groups, the weight of the mutant-calpeptin mice progressively increased with time, but it was always reduced compared to the WT sham and calpeptin treated mice. In contrast, weight was slightly increased in Calpeptin-treated WT groups compared with Sham-treated WT groups from day 13 of treatment to the end of the experiment (**Figure 94.A**). When body size was evaluated and no differences were observed between any of the groups in any off the SMA mouse model (**Figure 94.B**).

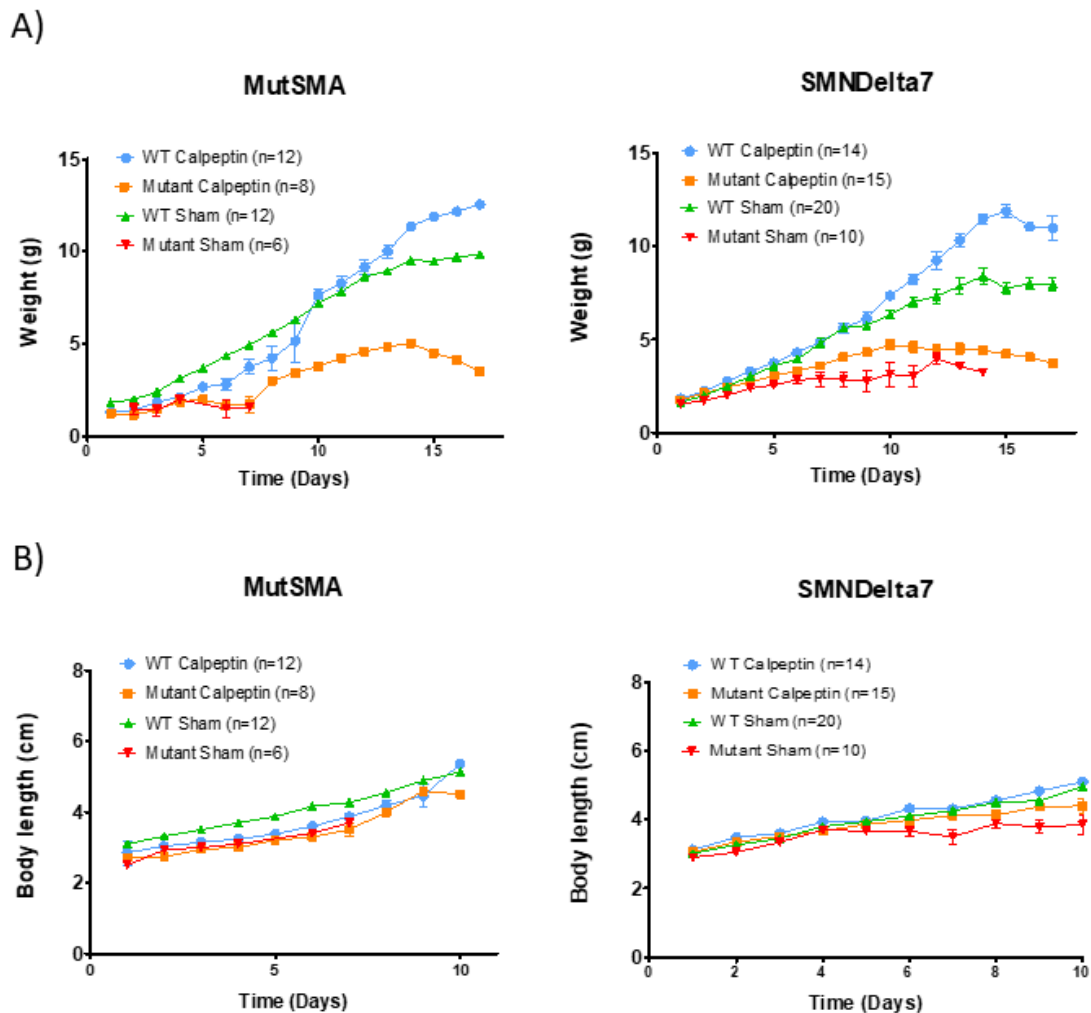


**Figure 94.** Changes in weight in MutSMA and SMNDelta7 mice after calpeptin administration. MutSMA and SMNDelta7 mice were treated subcutaneously with calpeptin or with physiological saline (Sham). **A)** Body weight of WT and mutant mice was evaluated daily from P0 to P18. Data are expressed as mean  $\pm$  SEM ( $n = 6-20$ ). **B)** Body length was also measured from P0 to P10. Results are shown as mean  $\pm$  SEM ( $n = 6-20$ ).



## 8. Calpeptin treatment improves Motor function in SMA mice

MutSMA and SMNDelta7 mouse models are two of the most severe SMA mouse models and are characterized by severe motor function impairment (Bebbee et al., 2012). To further assess the therapeutic potential of calpeptin we analysed whether the enhancement in lifespan observed in both models correlated with a motor functional improvement. For that, two behavioural tests were performed: the Righting Reflex test and the Tube test.

The righting reflex response is a natural reflex that needs no learning. It is made by neonatal mice when they return to their four paws after having been placed in a supine position. The test is ideal for mutant mice with severe motor function impairment to study the progression of locomotor deterioration which is presented as an increase in the time to right. The test was performed on mice in the following groups: Sham and Calpeptin treated WT, and Sham and Calpeptin treated mutant (MutSMA and SMNDelta7) groups. The test was designed with a maximum time of 30 seconds and measures were performed daily before the calpeptin injection from P1 to P10. The test was done in triplicate for each animal with 5 minutes resting time between tests.

Results obtained in WT groups showed that the righting reflex time was consistently faster (~10 s) than in mutant groups (~30 s). In calpeptin-treated MutSMA, there were no significant differences from the beginning of the treatment (P1) to P7 compared to sham-treated MutSMA. However, from P7 to the end of the experiment the righting reflex time progressively decreased in calpeptin-treated MutSMA (**Figure 95 top**) and SMNDelta7 (~20 s) (**Figure 95 bottom**).

## Righting reflex test

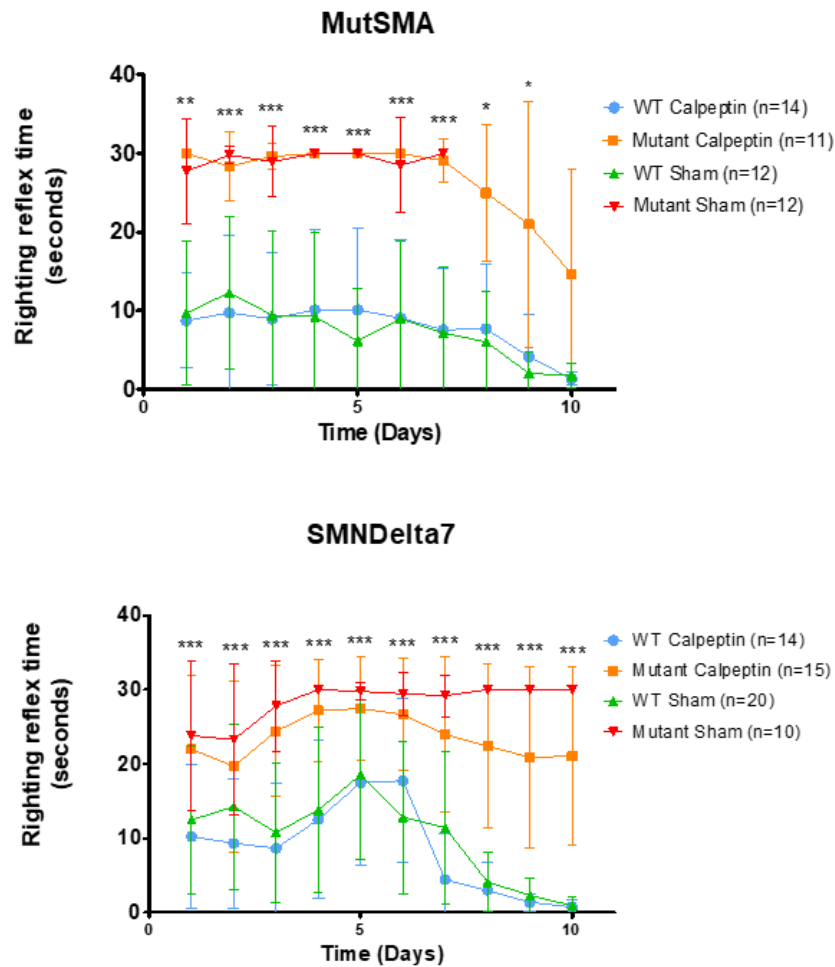


**Figure 95.** Changes in the motor function measured with the righting reflex test in *MutSMA* and *SMNDelta7* mice treated with calpeptin. Mean time to right  $\pm$  SEM between P1 and P10 was measured in *MutSMA* groups (top) or *SMNDelta7* groups (bottom). Two-way ANOVA test and Bonferroni post-test were performed to compare calpeptin-treated and untreated groups. Asterisks indicate significant differences (\*  $p < 0.05$ , \*\*  $p < 0.01$ , \*\*\*  $p < 0.001$ ).

The tube test is a non-invasive motor function test specifically designed for neonatal rodents. It evaluates the proximal hind-limb muscle strength, weakness and fatigue. The ideal animal age range for this test is from P2 to P8 since when they grow up, mice could learn how to “cheat” on the test. In each trial, the mouse was placed head down, hanging by its hind limbs in a tube. Two parameters were evaluated in the present study: latency to fall from the edge of the tube (in seconds) and the Hind-limb score (HLS) which assess the

positioning of the legs and tail during the first 10 seconds of the test. Mice with motor weakness show reduced time to fall and a low score of HLS.

The Tube test was performed in the same sham and treated groups of mice than for the Righting Reflex test. The test was designed with a maximum time of 30 seconds, and measures were performed in triplicate daily after the righting reflex and before the calpeptin injection, from P1 to P8.

When the latency time was analysed in the MutSMA model, we observed no differences in time-to-fall from P1 to P5. Nevertheless, on days 6 (P6) and 7 (P7) Calpeptin-treated MutSMA mice (P6,  $15.619 \pm 10.661$  seconds,  $n=7$ ) showed significantly increased time-to-fall compared to sham-treated MutSMA group (P6,  $3.844 \pm 1.923$  seconds,  $n=3$ ,  $p<0.05$ ) and no significant differences compared to WT groups (P6 WT-Sham,  $19.407 \pm 9.535$ ). In mutant SMNDelta7 mice, Calpeptin treatment significantly increased latency-to-fall compared to Sham-treated controls from P3 to the end of the experiment ( $p<0.05$ ) (**Figure 96.A**).

In both SMA models, HLS measures revealed that calpeptin treatment of mutant mice significantly increased the score compared to Sham mutants (MutSMA P2 to P8,  $p<0.001$ ; SMNDelta7 P6 to P8,  $p<0.05$ ) (**Figure 96.B**). Altogether, the results obtained from the behaviour tests suggested that calpeptin treatment ameliorates motor function of mutant mice in both SMA models analysed.

## Tube test

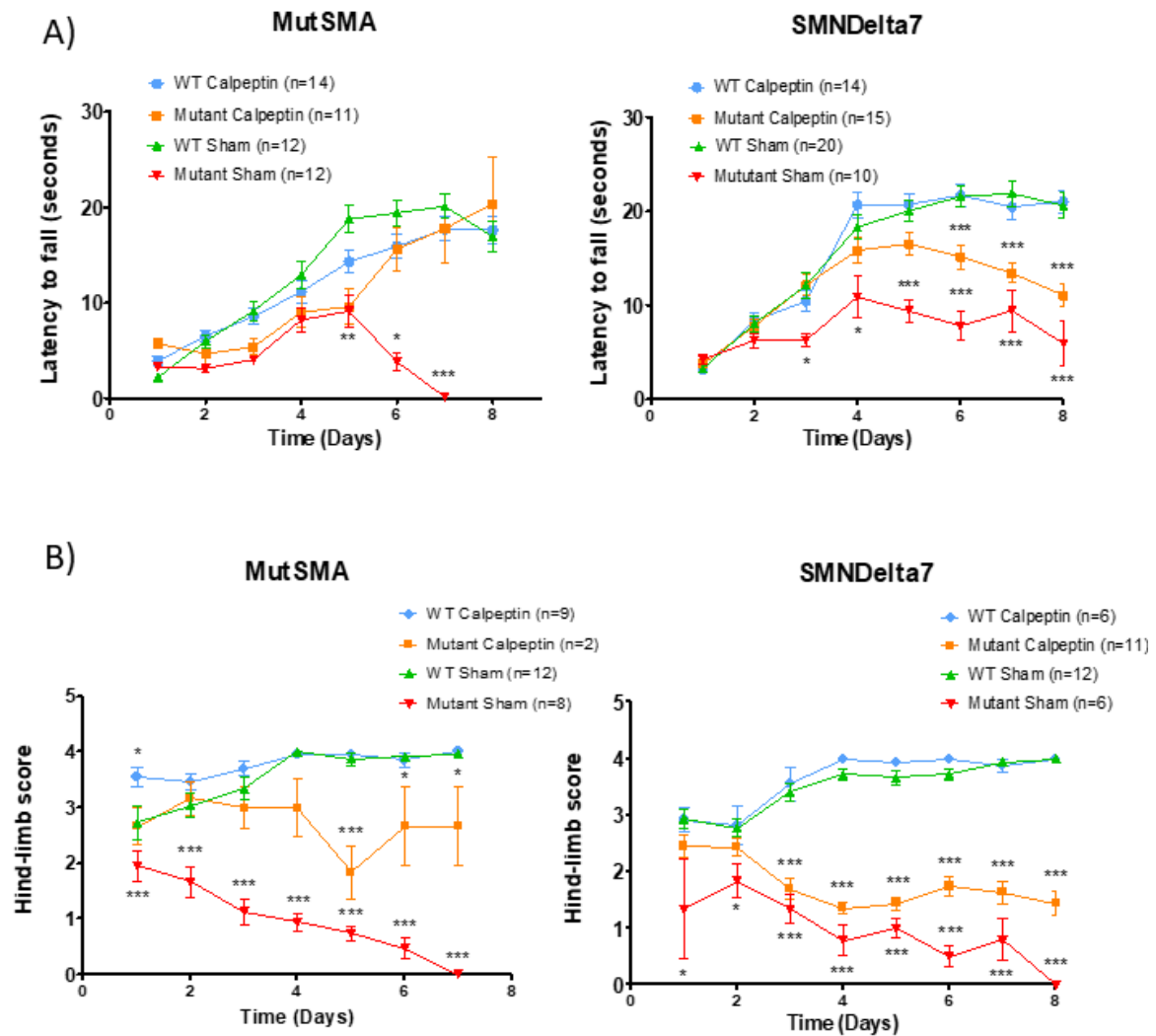


**Figure 96. Motor function changes measured by tube test in MutSMA and SMNDelta7 treated mice. A) Mean of latency to fall  $\pm$  SEM between P1 and P8 was measured in MutSMA groups (left) and SMNDelta7 groups (right), and B) mean of hind-limb score  $\pm$  SEM between P2 and P8 was measured in MutSMA groups (left) and SMNDelta7 groups (right). Two-way ANOVA test and Bonferroni post-test was performed to compare calpeptin-treated and untreated groups. Asterisks indicate significant differences (\*  $p < 0.05$ , \*\*  $p < 0.01$ , \*\*\*  $p < 0.001$ ).**



**CHAPTER 3: Calpain pathway is altered in  
Spinal Muscular Atrophy models.**



**SUMMARY:**

Neurodegeneration is a complex process that usually leads to neuronal death. In Spinal Muscular Atrophy (SMA) the cellular and molecular mechanisms causing motoneuron (MNs) loss of function and degeneration are only partially known. According to the results of numerous studies to date, there is no doubt that abnormal calpain activation triggers activation and progression of apoptotic processes in numerous neurodegenerative pathologies such as Alzheimer Disease (Mahaman et al., 2019), Parkinson Disease (Mouatt-Prigent et al., 1996), Huntington Disease (Gafni and Ellerby, 2002), and Amyotrophic Lateral Sclerosis (Yamashita et al., 2012). Furthermore, in some cases, like in Alzheimer Disease, this calpain overactivation was partially caused by a downregulation of calpastatin, the endogenous calpain inhibitor (Rao et al., 2008).

Our previous *in vitro* results also postulate the role of calpain protease regulating Survival Motor Neuron (SMN) protein and the positive effect on SMA phenotype of treatment with calpain inhibitors. Thus, it is very crucial to untangle all the aspects of calpain-mediated neurodegeneration in order to protect neurons and prevent degeneration minimizing its lethal effects. For that reason, we decided to analyse the calpain pathway in the different models of SMA and assess whether it is altered in the disease.

Using the SMA *in vitro* models, primary cultures of MNs isolated from the transgenic models MutSMA and SMNDelta7; and two human models obtained from patients with SMA, the cultured fibroblasts and the differentiated MNs from iPSCs, we analysed the level of calpain pathway members. *In vitro* results indicate a cell-specific increase of calpain activity in SMN-reduced MNs without alterations on the calpain protein levels. However, this overactivation of calpain was not caused by a downregulation of calpastatin.

Western blot analysis of spinal cord extract from SMA mice treated with the calpain inhibitor, calpeptin, showed an increase of SMN accompanied with a reduction of calpain and its endogenous inhibitor calpastatin. Thus, our results show that calpain activity is increased in SMA MNs and its inhibition may have a beneficial effect on SMA phenotype through the increase of SMN and the downregulation of calpain pathway.





## 1. Calpain activity is increased in mouse SMA MNs

Our previous results demonstrated that both endogenous reduction of calpain levels and inhibition using calpeptin increased Smn levels and improved the severity of the disease, both *in vitro* and *in vivo*. Moreover, although the exact physiological functions of calpains are not fully known, the over-activation of calpains has been implicated in several pathological processes such as HD, AD and spinal cord injury (Gafni and Ellerby, 2002; Mahaman et al., 2019; Vosler et al., 2008). Therefore, we decided to study whether calpain pathway is altered in SMA. We used the four models of SMA that we have in the laboratory: two models of cultured MNs obtained from two transgenic SMA mice (MutSMA and SMNDelta7) and two *in vitro* human models (the fibroblasts cell lines and the differentiated MNs from iPSCs).

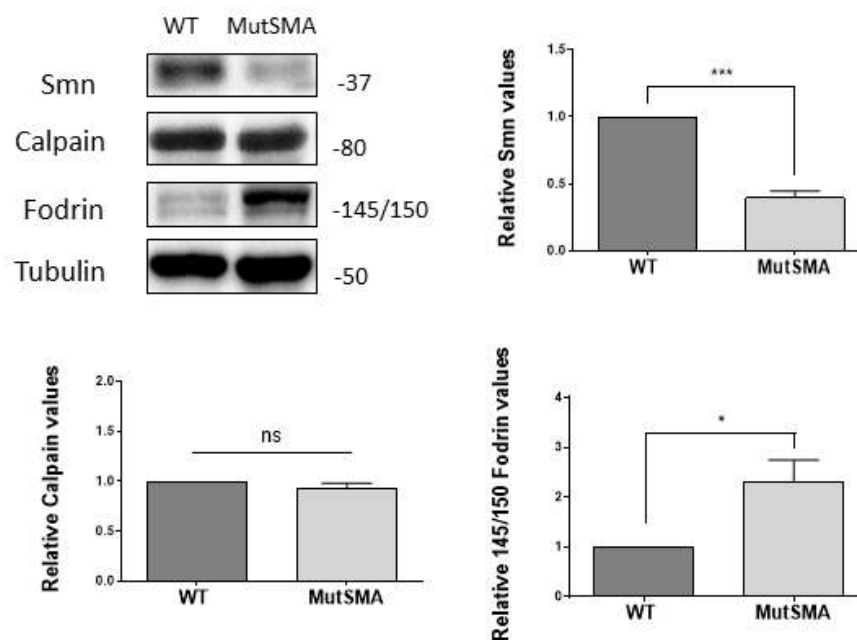


**Figure 97. Analysis by western blot of calpain and calpain activation in MutSMA cultured MNs.** MutSMA and WT MNs were isolated and cultured in the presence of NTFs for 4 DIV. Protein extracts were obtained and submitted to western blot analysis. Anti-calpain and anti-fodrin antibodies were used to analyse calpain levels and activity. Anti-SMN antibody was used to corroborate Smn levels and anti- $\alpha$  tubulin was used as loading control. Graph represent relative levels of Smn (**top**), relative levels of calpain (**left**) and relative levels of 145/150 fodrin fragments (**right**)  $\pm$  SEM obtained from three independent cultures. Asterisks indicate significant differences using the student t-test (\*  $p < 0.05$ , \*\*\*  $p < 0.001$ , no significant (ns)  $p > 0.05$ ).

Starting with the two SMA mouse models, we genotyped E12.5 embryos and isolated the MNs. WT and mutant MNs were cultured in the presence of NTFs for 4 days and total cell lysates were obtained. Using western blot analysis, we evaluated the levels of Smn, calpain and the 145/150 fodrin breakdowns produced specifically by calpain activation.

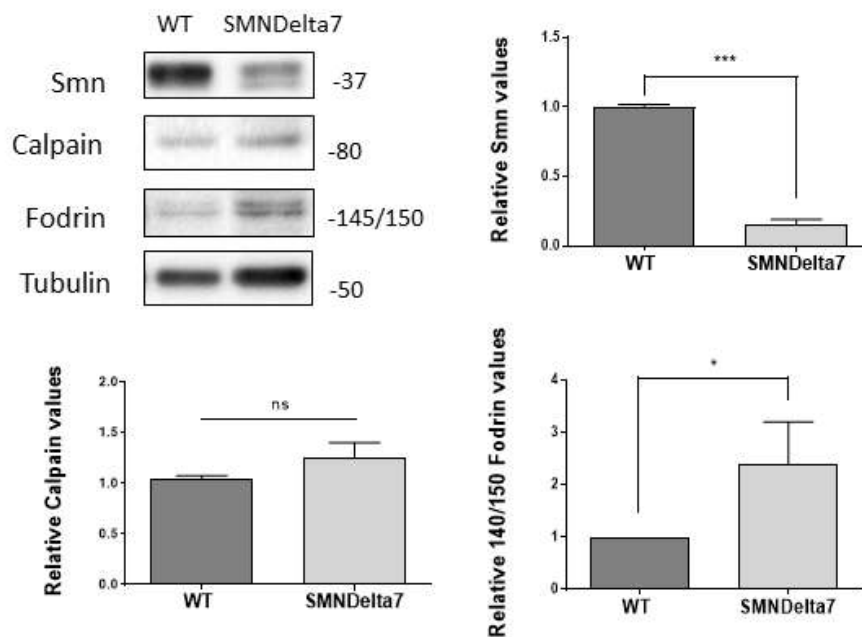


**Figure 98. Analysis by western blot of calpain and calpain activation in SMNDelta7 cultured MNs.** SMNDelta7 and WT MNs were isolated and cultured in the presence of NTFs for 4 DIV. Protein extracts were obtained and submitted to western blot analysis. Anti-calpain and anti-fodrin antibodies were used to analyse calpain levels and activity. Anti-SMN antibody was used to corroborate Smn levels and anti- $\alpha$  tubulin was used as loading control. Graph represent relative levels of Smn (**top**), relative levels of calpain (**left**) and relative levels of 145/150 fodrin fragments (**right**)  $\pm$  SEM obtained from three independent cultures. Asterisks indicate significant differences using the student t-test (\*  $p < 0.05$ , \*\*\*  $p < 0.001$ , no significant (ns)  $p > 0.05$ ).

As expected, MNs from mutant animals of both models (MutSMA and SMNDelta7) have lower levels of Smn than their respective WT (MutSMA,  $0.3944 \pm 0.04912$ ,  $p < 0.0001$  and SMNDelta7,  $0.1559 \pm 0.03615$ ,  $p < 0.0001$ ). Regarding the proteins analysed, we obtained the same results in both SMA models. While the levels of calpain did not show differences in MNs obtained from the mutants and those obtained from the WTs (MutSMA,  $0.9339 \pm$

0.0465,  $p=0.1865$  and SMNDelta7,  $1.253 \pm 0.1477$ ,  $p=0.127$ ), we observed a significant increase in the levels of the 145/150 KDa fodrin fragments (MutSMA,  $2.300 \pm 0.4391$ ,  $p=0.0143$  and SMNDelta7,  $2.376 \pm 0.8238$ ,  $p=0.0294$ ) in mutant MNs compared to the WT controls (**Figure 97** and **Figure 98**). This suggests that although calpain levels are not affected its activity is increased in SMA.

We also measured the protein levels of calpastatin, an endogenous protein that specifically binds to and inhibits calpain (Crawford, 1990), to see whether the over-activation of calpain was due to the loss of the inhibitor in the mutant MNs. SMA mouse models showed the same results: calpastatin protein levels did not change in mutant and their respective WTs (MutSMA,  $0.9628 \pm 0.0851$ ,  $p=0.6777$  and SMNDelta7,  $1.044 \pm 0.2479$ ,  $p=0.9660$ ) (**Figure 99.A** and **B**), suggesting that the deregulation of calpain activity must come from an excess of activation rather than a defect of the inhibition.

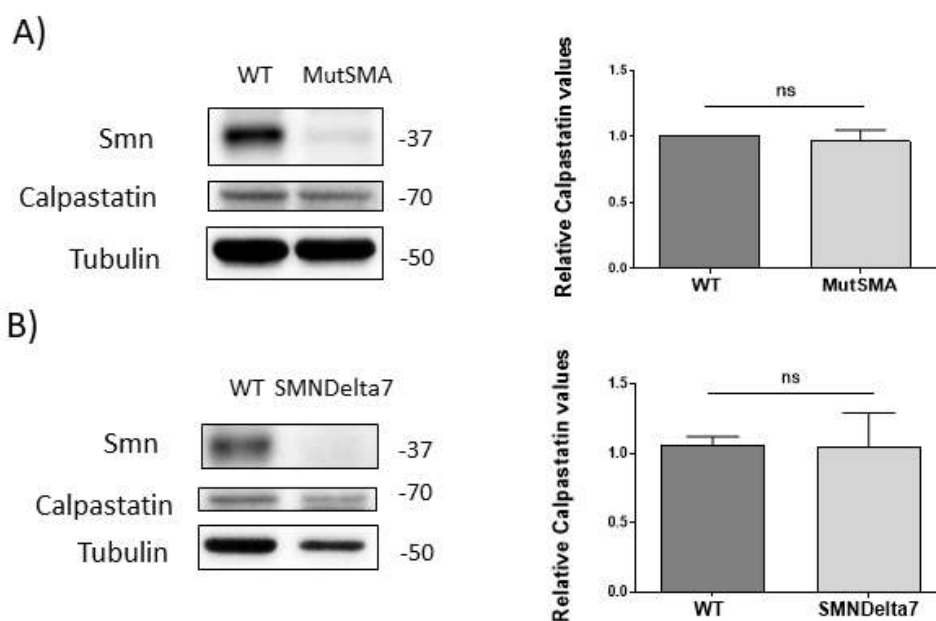


**Figure 99. Analysis of calpastatin protein levels in MutSMA and SMNDelta7 cultured MNs.** Mutant and WT MNs were isolated and cultured in the presence of NTFs for 4 DIV. Protein extracts were obtained and submitted to western blot analysis. Calpastatin protein levels were evaluated using an anti-calpastatin antibody. Anti- $\alpha$  tubulin antibody was used as loading control. **A)** Graph shows relative calpastatin levels vs  $\alpha$  tubulin in MutSMA mouse model. Values were obtained from three independent cultures. **B)** Graph shows relative calpastatin levels vs  $\alpha$  tubulin in SMNDelta7 mouse model. Values were obtained from three independent cultures. Asterisks indicate significant differences using the student t-test (no significant (ns)  $p>0.05$ ).

## 2. Calpain activity is altered in SMA human SMA cells

In order to further evaluate alterations in calpain pathway in human cells, we measured calpain, fodrin specific fragments and calpastatin protein levels in the human *in vitro* models. Fibroblasts cells obtained from 2 controls (3814 healthy SMA carrier (Control) and 2183 possible Huntington patient (Huntington)) and 2 SMA patients (9677 SMA type 1 (SMA 1) and 3813 SMA type 2 (SMA 2)) were plated and cultured for 2 days in Fibroblast Growth medium. Protein extracts were obtained and submitted to western blot analysis using an anti-SMN, an anti-calpain, an anti- $\alpha$  fodrin and anti-calpastatin antibodies.

Results in **Figure 100.A** showed that cells from the SMA patients have a significant reduction in SMN protein level compared to the Control (SMA 2,  $0.4725 \pm 0.0767$ ,  $p=0.0001$ ; SMA 1,  $0.4087 \pm 0.0649$ ,  $p<0.0001$  and Huntington,  $0.7032 \pm 0.0938$ ,  $p=0.0581$ ). As observed in mouse SMA MNs, calpain levels did not change in SMN-reduced cells and the Control (SMA 2,  $0.9011 \pm 0.0908$ ,  $p=0.3179$  and SMA 1,  $0.7272 \pm 0.2261$ ,  $p=0.2729$ ), but surprisingly specific fodrin breakdowns were significantly reduced in those cells (Huntington,  $0.6368 \pm 0.0405$ ,  $p=0.0019$  and SMA 1,  $0.6379 \pm 0.0883$ ,  $p=0.0023$ ).

Interestingly, fibroblasts from the possible Huntington patient present a significant reduction in the calpain levels ( $0.2641 \pm 0.0071$ ,  $p<0.0001$ ) without showing any variation in the 145/150 fodrin fragments ( $0.9370 \pm 0.1503$ ,  $p=0.3877$ ) compared to the SMA carrier (Control).

When calpastatin levels were measured using western blot, we observed no differences in any of the cell lines (SMA 2,  $0.6431 \pm 0.1881$ ,  $p=0.0696$ ; SMA 1,  $0.9405 \pm 0.1267$ ,  $p=0.2365$  and Huntington,  $2.231 \pm 0.8806$ ,  $p=0.3238$ ) (**Figure 100.B**).

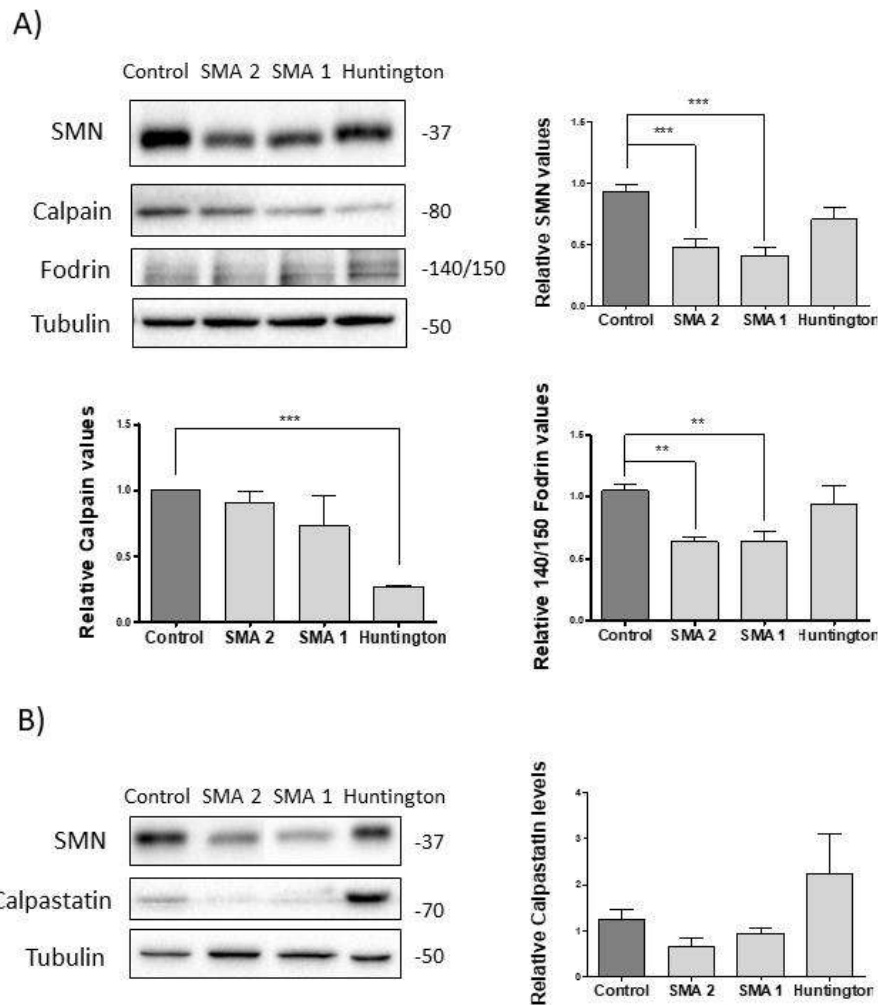


**Figure 100. Analysis by western blot of calpain, calpain activation and calpastatin in human cultured fibroblast.** SMA and control human fibroblast cells (9677 SMA type 1, 3813 SMA type 2, 3814 healthy SMA carrier and 2183 possible Huntington patient) were cultured for 2 days. **A)** protein extraction was performed and submitted to western blot using an anti-calpain and anti-fodrin antibodies. Tubulin was used as protein loading control and anti-SMN antibody was used to evaluate SMN levels. Graph represent relative levels of SMN (**top**), relative levels of calpain (**left**) and relative levels of 145/150 fodrin fragments (**right**)  $\pm$  SEM obtained from three independent cultures. **B)** Western blot analysis of protein extracts probed for calpastatin. Graph represents mean  $\pm$  SEM of the expression of calpastatin protein against  $\alpha$ -tubulin. Values correspond to the quantification of four independent experiments done per duplicate. Differences were analysed using the one-way ANOVA with the Dunnett multiple comparison post-test and the student t-test (\*\* $p < 0.01$ , \*\*\*  $p < 0.001$ ).

Results obtained in human SMA differentiated MNs from iPSCs (GM23240\*B (SMA) and GM23411\*B (Control)) were differentiated. In the last step of differentiation, cells were maintained in the MNs Maturation medium for 6 days and total cell lysates were obtained. Western blot analysis was performed using anti-SMN, anti-calpain, anti- $\alpha$  fodrin and

anti-calpastatin antibodies. SMN protein levels were reduced in the SMA patient MNs ( $0.3226 \pm 0.0598$ ,  $p < 0.0001$ ) compared to the control cells. Human differentiated MNs showed calpain levels were significantly reduced in the SMA cells ( $0.6779 \pm 0.0572$ ,  $p = 0.001$ ), while fodrin 145/150 breakdown products were increased ( $1.287 \pm 0.0963$ ,  $p = 0.0278$ ) (**Figure 101.A**). Calpastatin protein levels were also evaluated and no significant differences were observed in control and SMA MNs ( $1.073 \pm 0.189$ ,  $p = 0.7206$ ) (**Figure 101.B**). All these results together suggest that calpain is over-activated without showing any defect in the levels of the inhibitory protein, calpastatin, in MNs affected with SMA, but not in fibroblasts cells.

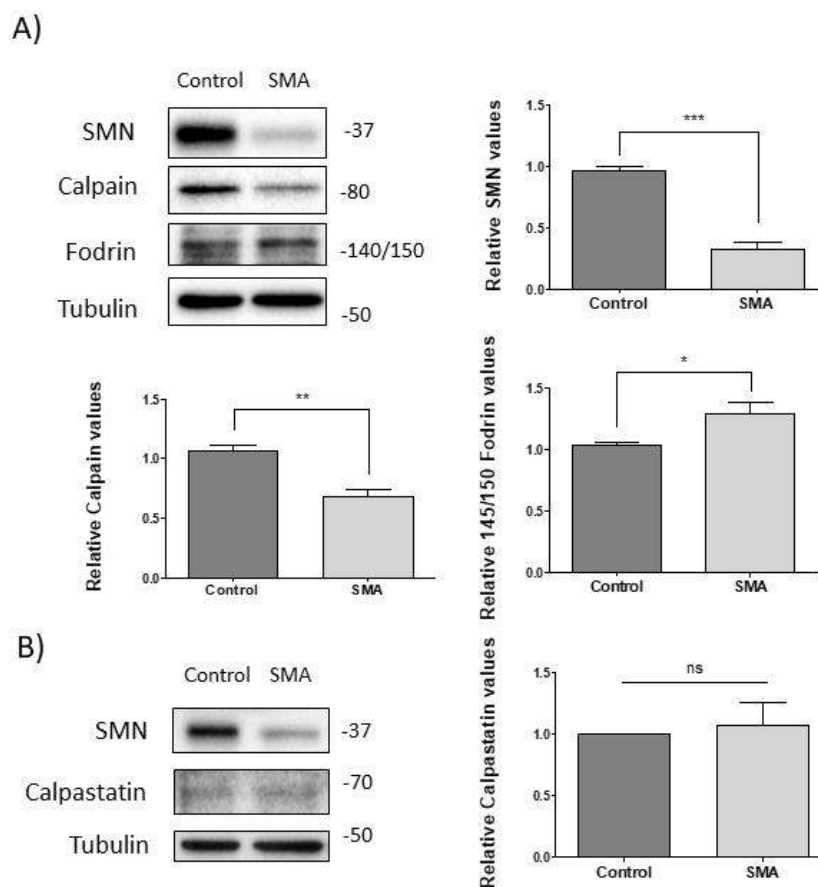


**Figure 101. Analysis by western blot of calpain, calpain activation and calpastatin in human differentiated MNs.** MNs derived from human iPSCs (GM23240\*B and GM23411\*B) were maintained in maturation medium for 6 days. **A)** Protein extracts were obtained and submitted to western blot analysis using an anti-calpain and anti-fodrin antibodies. Anti- $\alpha$ -tubulin antibody was used as a loading control. Anti-SMN antibody was used to analyse SMN protein level each condition. Graphs represent the expression of SMN (**top**), calpain (**left**) and 145/150 fodrin fragments (**right**) vs  $\alpha$ -tubulin **B)** Western blot analysis of protein extracts probed for calpastatin. Graph represents mean  $\pm$  SEM of the expression of calpastatin protein against  $\alpha$ -tubulin. Values correspond to the quantification of three independent experiments  $\pm$  SEM. Differences were analysed using the student t-test (\*  $p < 0.05$ , \*\*  $p < 0.01$ , \*\*\*  $p < 0.001$ , no significant (ns)  $p > 0.05$ ).

### 3. Smn and calpain are modulated with calpeptin treatment in spinal cord of SMNDelta7 mouse model

The results obtained in cultured MNs have the limitations of being an *in vitro* model and that the cells are in the early stages of the disease. In order to study alterations in calpain pathway, we decided to obtain spinal cord samples of calpeptin treated SMNDelta7 at postnatal day 8 (P8).

SMNDelta7 mouse model starts to show progressive muscle weakness at day 5 and progressively gets more pronounced until the moment of death (Mean survival is reported to be ~13 days) (Ie et al 2005). Consequently, we decided to collect samples at P8, to evaluate MNs changes at a symptomatic stage, previous to MNs loss (reported at ~P10). Since we already have tested calpeptin treatment *in vivo*, we also obtained samples from treated animals in order to see if calpeptin effects are due to calpain activity modulation.

SMNDelta7 animals were genotyped and randomly assigned to a sham or treatment group. Calpeptin was administrated daily at a dose of 6 µg of calpeptin *per* gram of weight. Sham animals received the same volume of saline solution. At P8, mice were sacrificed and thoracic spinal cord tissue was obtained and submitted to western blot analysis using an anti-SMN, anti- $\alpha$ -fodrin and anti-calpain antibodies. Lumbar region of the same animals was processed for immunofluorescence analysis.

As shown in **Figure 102**, mutant SMNDelta7 sham mice have significantly lower levels of Smn ( $0.067 \pm 0.032$ ,  $n=8$ ,  $p=0.0002$ ) compared to the WT Sham group ( $n=5$ ). Interestingly, calpeptin treatment partially restores calpain levels in spinal cord tissue ( $0.583 \pm 0.351$ ,  $n=4$ ,  $p=0.2355$ ). No significant differences in protein levels were observed between the WT group regardless of treatment (WT Calpeptin,  $1.345 \pm 0.360$ ,  $n=4$ ,  $p=0.6055$ ). Unexpectedly, when calpain was evaluated, we observed that the SMNDelta7 Sham group had an increase in the levels of the protein ( $2.348 \pm 0.332$ ,  $n=7$ ,  $p=0.0136$ ) compared to the WT Sham group ( $n=7$ ). We also observed that treatment with calpeptin significantly reduced calpain levels, both in WT ( $0.631 \pm 0.060$ ,  $n=4$ ,  $p=0.0100$ ) and in mutant ( $0.789 \pm 0.071$ ,  $n=4$ ,  $p=0.0339$ ). However, despite these alterations in calpain protein levels, only the SMNDelta7 Sham mice showed higher levels of fodrin specific breakdowns (SMNDelta7 Sham,  $2.644 \pm 0.715$ ,



n=7, p=0.0410; SMNDelta7 Calpeptin,  $1.110 \pm 0.299$ , n=4, p=0.6597; WT Calpeptin,  $1.140 \pm 0.244$ , n=3, p=0.7199).

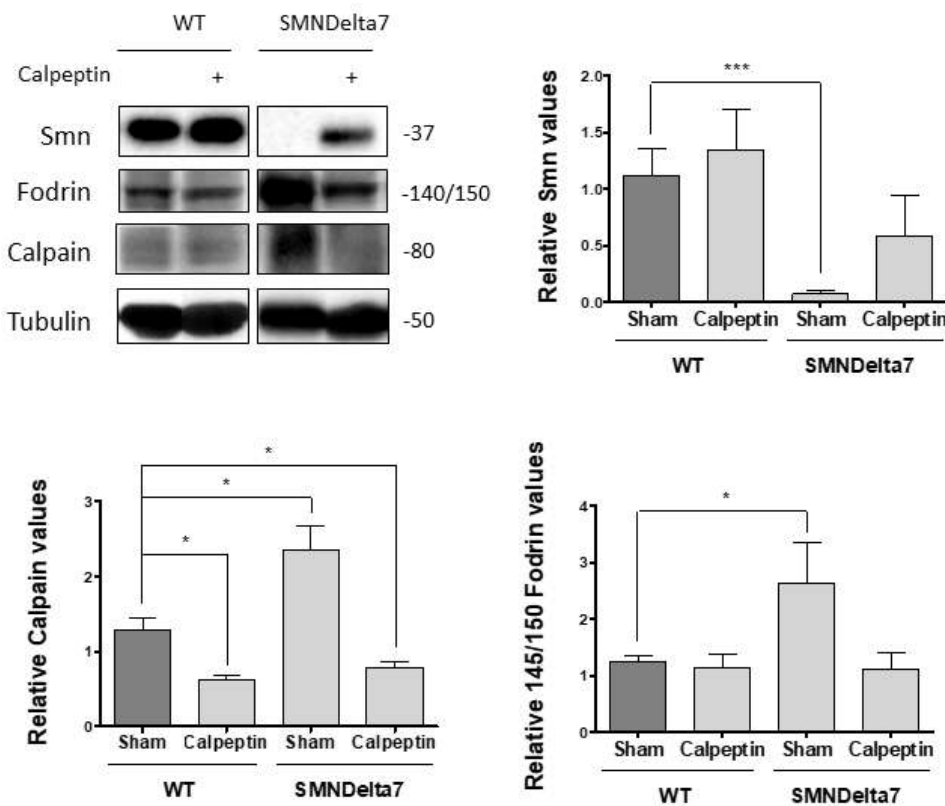


**Figure 102.** *Smn*, *calpain* and *fodrin* protein level measured in spinal cord protein extracts from **SMNdelta7** treated mice. SMNdelta7 and WT mice were treated daily with calpeptin or with physiological saline (Sham) for 8 days. Spinal cord was dissected and processed for western blot analysis. An anti-SMN, anti-calpain and anti-fodrin antibodies were used. Graphs represent the relative values of *Smn* (**top**), *Calpain* (**left**) and 145/150 *fodrin* (**right**) versus  $\alpha$ -tubulin  $\pm$  SEM. Values were obtained from five different spinal cords in each group and were analysed using the one-way ANOVA with the Dunnett multiple comparison post-test and the student t-test (\*  $p < 0.05$ , \*\*\*  $p < 0.001$ ).

When calpastatin levels were evaluated, we observed no differences in any of the conditions (SMNDelta7 Sham,  $1.596 \pm 0.366$ , n=3, p=0.1788; SMNDelta7 Calpeptin,  $2.357 \pm 0.573$ , n=4, p=0.3537; WT Calpeptin,  $2.728 \pm 0.939$ , n=3, p=0.1397) compared to the WT Sham mice (n=3) (**Figure 103**). However, it seems that calpeptin treatment have a tendency to increase calpastatin protein levels, yet these differences are not significant, possibly due to the limited number of animals used.

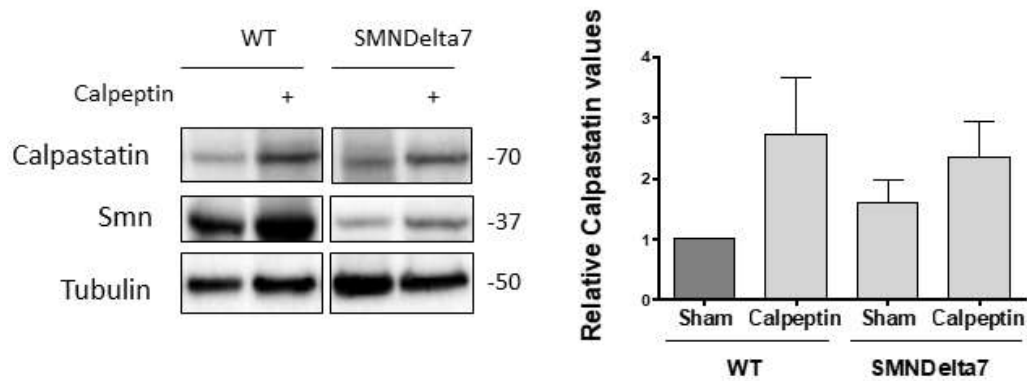


**Figure 103. Calpastatin protein level measured in spinal cord protein extracts from SMNdelta7 treated mice.** SMNdelta7 and WT mice were treated daily with calpeptin or with physiological saline (Sham) for 8 days. Spinal cord was dissected and processed for western blot analysis using an anti-calpastatin antibody. Graph represents mean  $\pm$  SEM of the expression of calpastatin protein against  $\alpha$ -tubulin. Values correspond to the quantification of three independent experiments  $\pm$  SEM. Differences were analysed using the student *t*-test.

#### 4. Smn, calpain and calpastatin immunofluorescence in calpeptin-treated SMNDelta7 MNs

To differentiate whether the alterations of calpain pathway observed using spinal cord lysate are MNs specific or not, we obtained lumbar spinal cord from calpeptin-treated/Sham SMNDelta7 mice and analysed them using immunofluorescence.

For that, genotyped SMNDelta7 animals were and randomly assigned to a sham or treatment group and calpeptin (6  $\mu$ g of *per* gram of weight) or vehicle (saline solution) were administrated daily. At P8, mice were sacrificed and lumbar spinal cord tissue was fixated using PFA 4% and cryopreserved with 20% glucose buffer. Samples were processed using a cryostat at 16  $\mu$ m and immunofluorescence was performed using the specific antibody. Nissl stain was used to identify MNs in the spinal cord tissue (**Figure 104**). Hoechst dye was performed to localize cells' nucleus. Relative fluorescence levels were analysed with ImageJ software as described in "7.4.1. Cell fluorescence measurements" in "Materials and Methods" section.

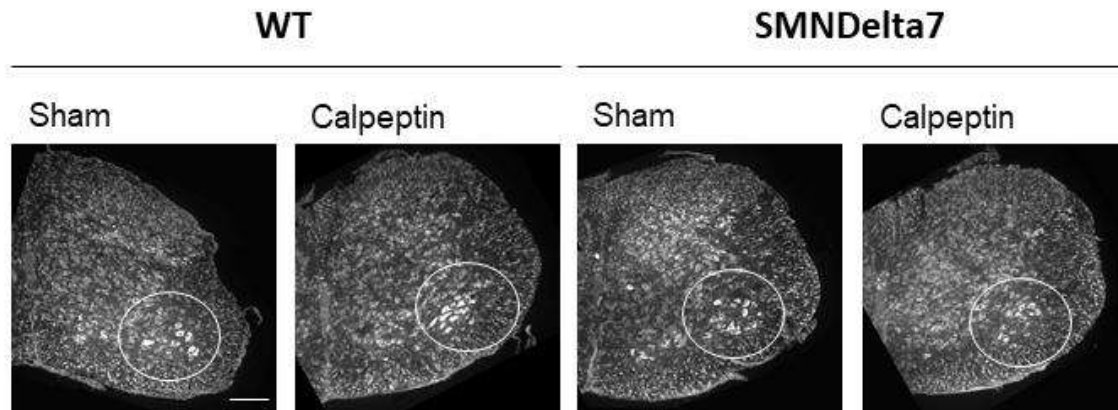


**Figure 104. MNs identification in P8 lumbar spinal cord MNs from SMNDelta7 treated mice.** Using Nissl staining MNs were identified based on cell size and location in the ventral horn of the spinal cord. Images show representative MNs identifications in the different groups. Scale bar of 200  $\mu$ m.

Smn levels were analysed using the anti-SMN antibody in the MNs soma in the ventral horn of the spinal cord. As shown in **Figure 105**, the results obtained confirm that Smn protein levels are reduced in the SMNDelta7 Sham group (WT Sham, CTCF  $222.8 \pm 30.84$ , n=71 MNs and SMNDelta7 Sham, CTCF  $49.11 \pm 3.806$ , n=46 MNs  $p < 0.0001$ ) while treatment with calpeptin significantly increases these levels (SMNDelta7 + Calpeptin, CTCF  $108.2 \pm 9.388$ , n=97 MNs,  $p < 0.0001$ ). Surprisingly, no differences were observed between WT Sham and WT treated conditions (WT + Calpeptin CTCF  $232.2 \pm 38.04$ , n=64 MNs,  $p = 0.8489$ ).

To start analysing calpain pathway, same spinal cord slides were analysed using anti-Calpain and anti-calpastatin antibodies. MNs in the ventral horn of the spinal cord were identified using the Nissl stain and fluorescence level was evaluated.

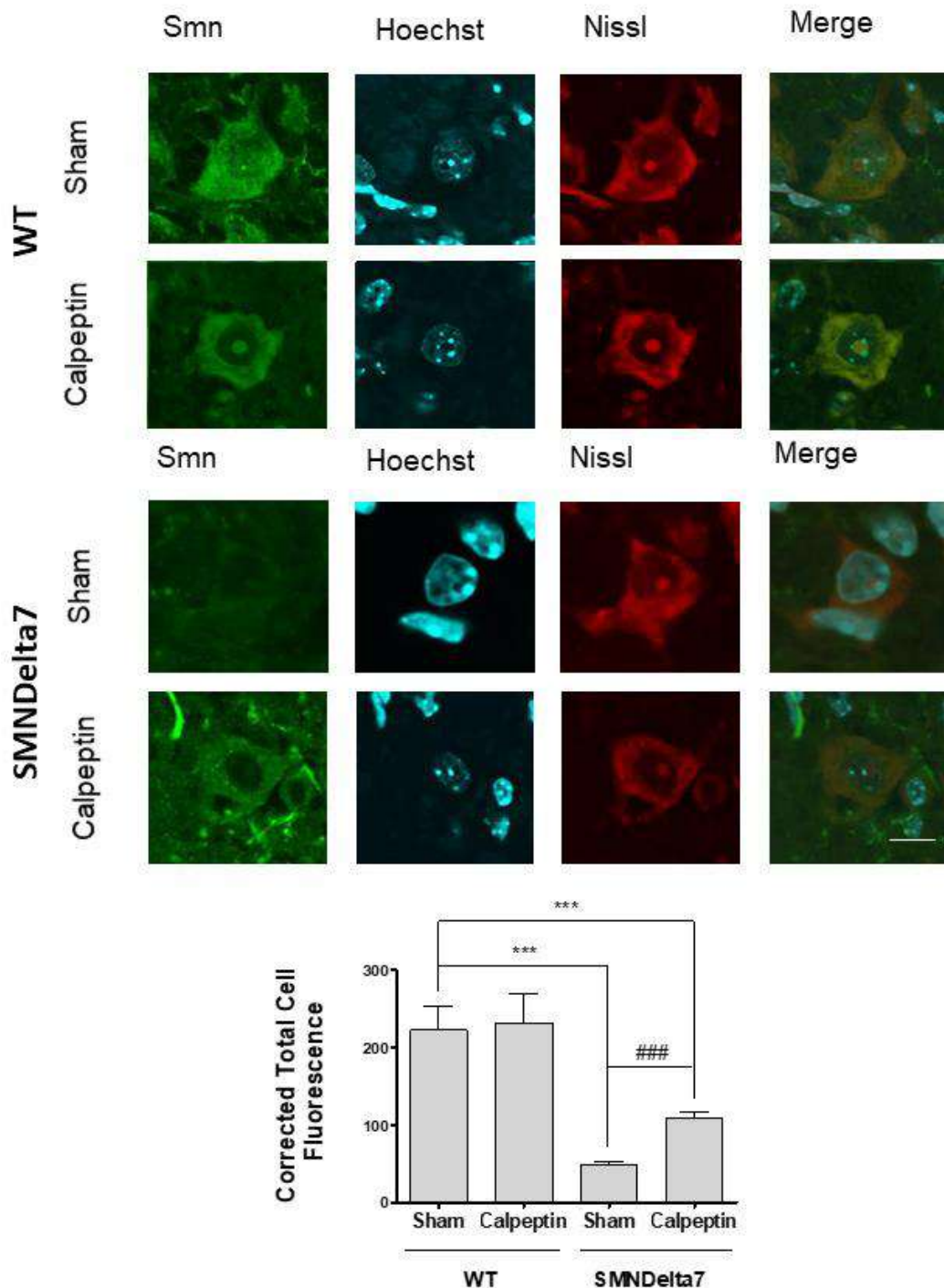


**Figure 105.** *Smn* level measured in P8 spinal cord MNS from SMNdelta7 treated mice using immunofluorescence. Calpeptin treated SMNdelta7 and WT mice were sacrificed at day P8 and spinal cord was fixed to perform and immunofluorescence using an anti-SMN antibody (green). Same slides were stained with Nissl stain (red) for MN specific detection and Hoechst staining (blue) to identify the nucleus. Images show representative MNS fluorescent levels. Graph represent the mean  $\pm$  SEM of relative *Smn* fluorescence measured in MNS. Values were obtained from spinal cord slides from a minimum of three animals per group and were analysed using the one-way ANOVA with the Dunnett multiple comparison post-test (\*\* $p < 0.001$ , and ###  $p < 0.001$  vs the SMNdelta7-Sham values). Scale bar of 5  $\mu$ m.

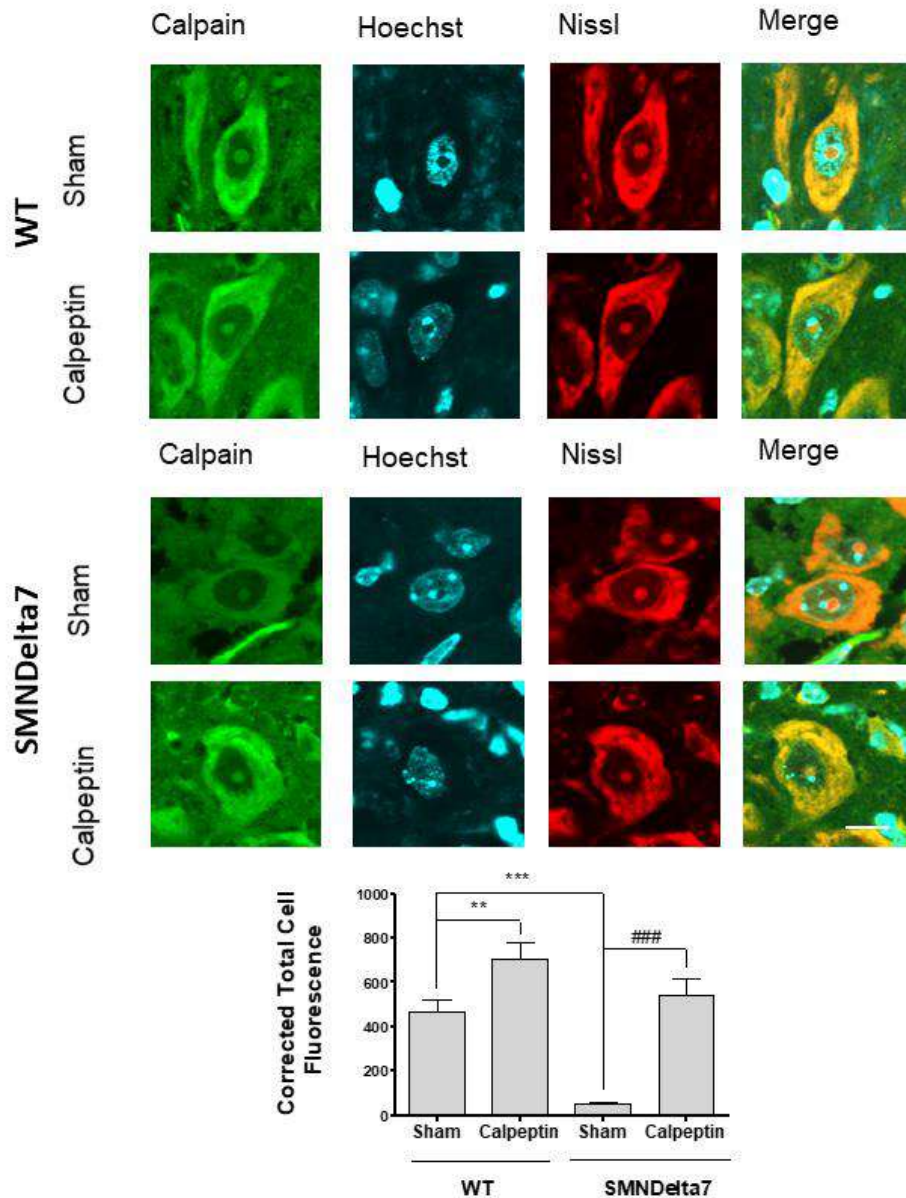


**Figure 106. Calpain protein level measured in P8 spinal cord MNS from SMNdelta7 treated mice using immunofluorescence.** SMNdelta7 and WT mice were treated with calpeptin or physiological saline (Sham) for 8 days. The spinal cord was fixed to perform and immunofluorescence using an anti-calpain antibody (green). Same slides were stained with Nissl stain (red) for MN specific detection and Hoechst staining (blue) to identify the nucleus. Images show representative MNS fluorescent levels. Graph represent the mean  $\pm$  SEM of relative calpain fluorescence measured in MNS. Values were obtained from spinal cord slides from a minimum of three animals per group and were analysed using the one-way ANOVA with the Dunnett multiple comparison post-test (\*\*  $p < 0.01$ , \*\*\*  $p < 0.001$ , and ###  $p < 0.001$  vs the SMNDelta7-Sham values). Scale bar of 5  $\mu$ m.

Results showed that SMNdelta7 Sham mice have reduced calpain levels (CTCF  $47.87 \pm 12.59$ ,  $n=143$  MNS,  $p < 0.0001$ ) compared to WT Sham (CTCF  $469.4 \pm 52.78$ ,  $n=109$  MNS). Regarding the treatment, we observed that calpeptin administration increases calpain

protein levels in both WT (CTCF  $702.7 \pm 74.16$ ,  $n=79$  MNs,  $p=0.0091$ ) and mutant (CTCF  $544.5.0 \pm 72.95$ ,  $n=126$  MNs,  $p<0.0001$ ) compared to their respective Sham groups. No differences were observed between WT Sham group and SMNDelta7 Calpeptin group ( $p=0.4178$ ) (**Figure 106**).

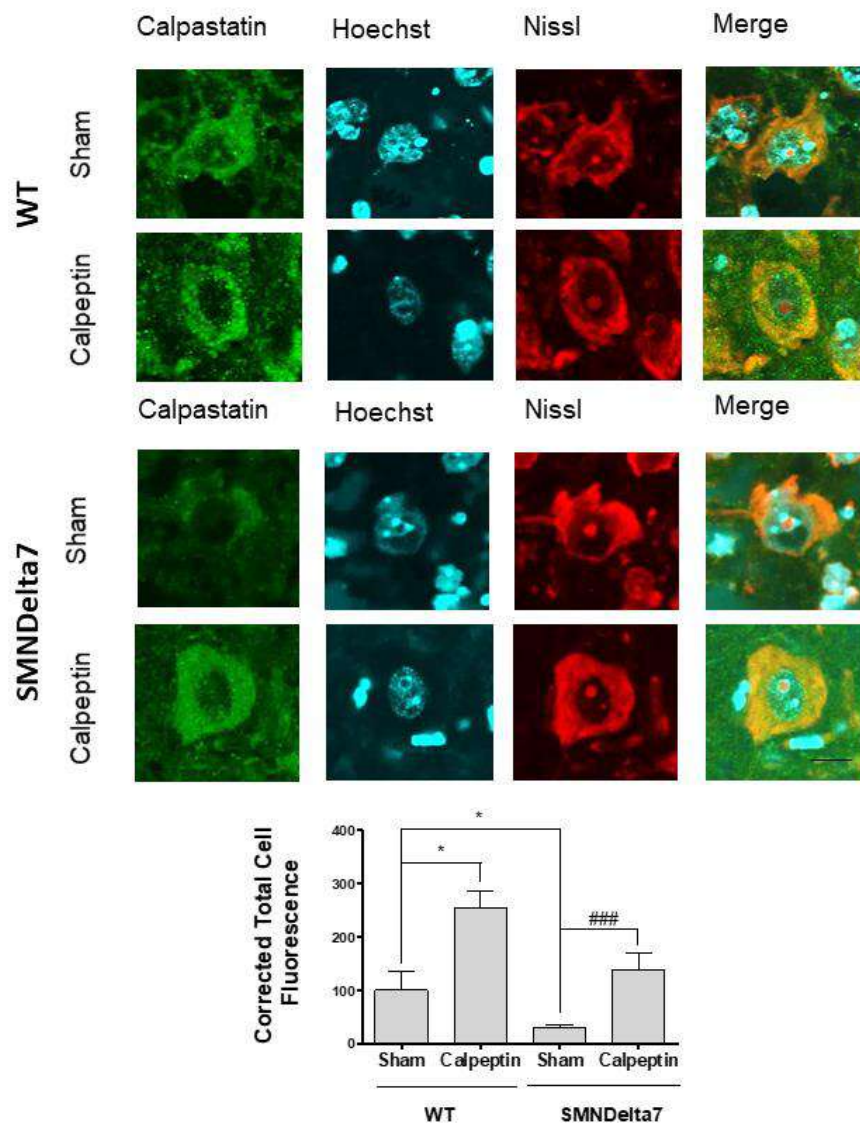


**Figure 107. Calpastatin protein level measured in P8 spinal cord MNS from SMNdelta7 treated mice using immunofluorescence.** Calpeptin treated SMNdelta7 and WT mice were sacrificed at day P8 and spinal cord was fixed to perform and immunofluorescence using an anti-calpastatin antibody (green). Same slides were stained with Nissl stain (red) for MN specific detection and Hoechst staining (blue) to identify the nucleus. Images show representative MNS fluorescent levels. Graph represent the mean  $\pm$  SEM of relative calpastatin fluorescence measured in MNS. Values were obtained from spinal cord slides form a minimum of three animals per group and were analysed using the one-way ANOVA with the Dunnett multiple comparison post-test (\*  $p<0.05$ , and ###  $p<0.001$  vs the SMNDelta7-Sham values). Scale bar of  $5 \mu\text{m}$ .

Measures using an anti-calpastatin antibody showed that mutant non-treated animals had a reduced level of fluorescence (WT Sham, N=33 MNs, CTCF  $100.2 \pm 36.46$  and SMNDelta7 Sham, N=40 MNs, CTCF  $30.23 \pm 4.917$ ,  $p=0.0183$ ). Moreover, treatment with calpeptin increase calpastatin fluorescence in both WT (WT + Calpeptin, N=27 MNs, CTCF  $253.7 \pm 32.96$ ,  $p=0.0208$ ) and mutant mice (SMNDelta7 + Calpeptin, N=29 MNs, CTCF  $137.0 \pm 32.16$ ,  $p=0.0003$  vs SMNDelta7 Sham) compared to their respective Sham conditions. No differences were observed between WT Sham group and SMNDelta7 Calpeptin group ( $p=0.4647$ ) (**Figure 107**).

### 5. Calpastatin peptide as a treatment to inhibit calpain

Calpeptin is considered one of the best and most sensitive calpain inhibitors compared to other inhibitors such as Z-Leu-Met-H and leupeptin (Tsujinaka et al., 1988) but like other inhibitors it can have unknown off-targets. Because of that, we decided to analyse the effect of the Calpastatin inhibitory Peptide Ac 184-210 (Sigma) on MNs since calpastatin protein is the calpain-specific protein that binds to and inhibits calpain knowing that have no inhibitory effect on any other proteases (Crawford, 1990).

We performed a time-course dose-effect experiment to clarify the use of the treatment in our primary cultured MNs model. CD1 MNS were isolated from E12.5 embryos and cultured for 6 days in NTFs medium. Cells were treated with 3 doses of calpastatin peptide (25, 50 and 100 nM) for 3,6,9, 12,16 and 24 hours. Total cell lysates were obtained and submitted to western blot to analyse Smn and fodrin protein levels. Results showed that from all doses and treatment times tested, only 100nM for 6 hours was able to reduce 145/150 fodrin fragments while increasing Smn levels (**Figure 108**).



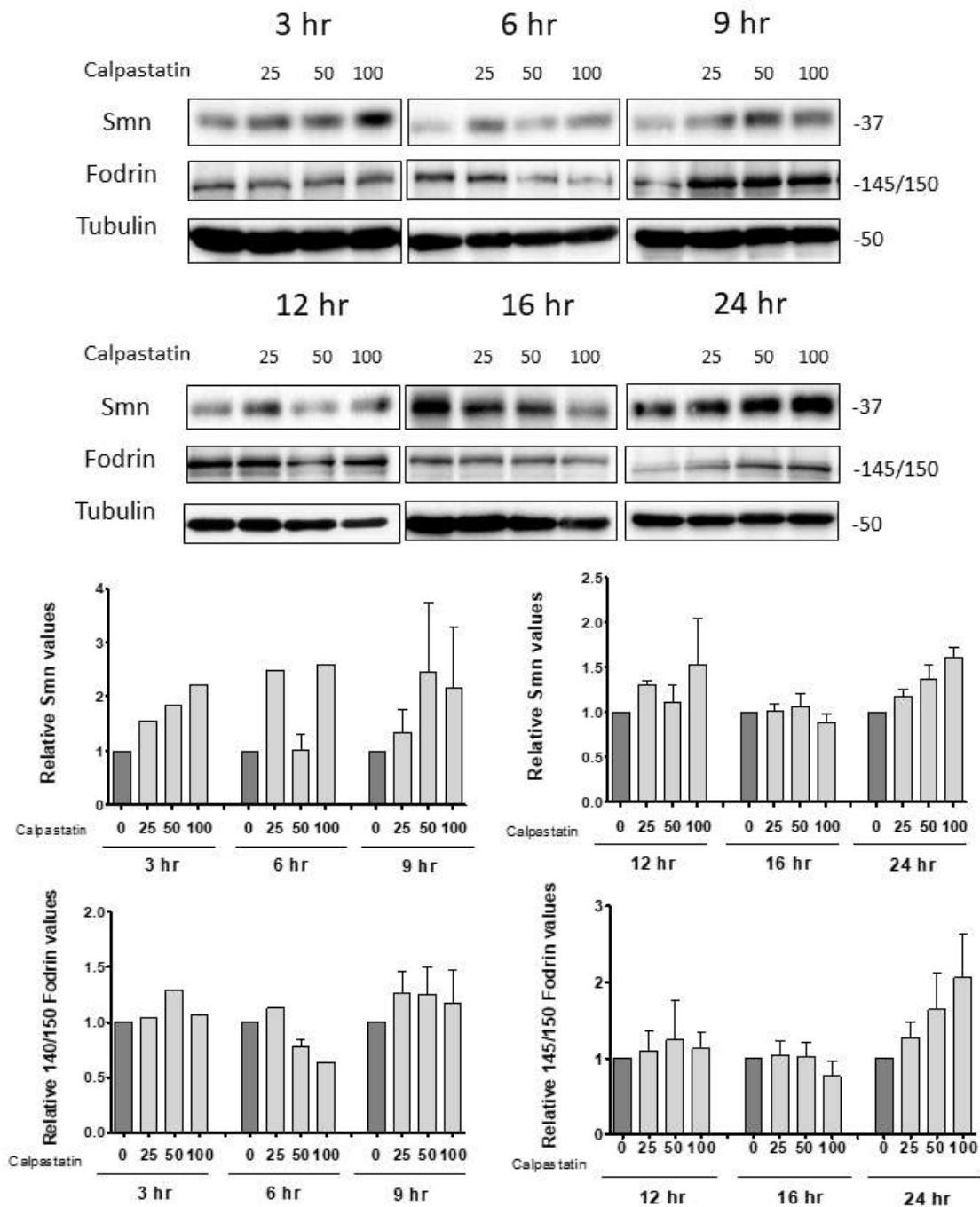


**Figure 108. Effect of calpastatin time-course treatment on Smn protein level in CD1 MNs.** CD1 mouse MNs were isolated and cultured in the presence of NTFs. Six days after plating, cells were treated with 25, 50 or 100nM of calpastatin or left untreated and cell lysates were obtained at 3, 6, 9, 12, 16 and 24 hours after treatment. Protein extracts were submitted to western blot analysis using an anti-SMN and anti-fodrin antibodies. Membranes were reprobbed with an anti- $\alpha$ -tubulin antibody as a loading control. Graph values represent the expression of Smn (**top graphs**) or 145/150 fodrin fragments (**bottom graphs**) vs  $\alpha$ -tubulin and correspond to the quantification of four independent experiments  $\pm$  SEM.



Therefore, considering the 100nM for 6 hours as the satisfactory dose, we decided to evaluate the effect of calpastatin treatment on Smn level in MNs isolated from the MutSMA mouse model. E12.5 embryos were genotyped and MNs purified and cultured for 6 days in the presence of NTFs (**Figure 109.A**). Cells were treated with 100nM of calpastatin peptide for 6 hours and total cell lysate was obtained and submitted to western blot analysis to analyse Smn and fodrin protein levels. Regarding to calpain inhibition measured by fodrin 145/150 breakdown products levels, we observed that, Calpastatin treatment does not have any effect in WT ( $0.835 \pm 0.194$ ,  $p=0.2349$ ) but significantly reduce fragments levels in mutant MNs ( $0.583 \pm 0.0559$ ,  $p<0.0001$ , and  $p=0.0211$  versus Control MutSMA). As it has previously reported earlier in this chapter, MutSMA have higher fodrin 145/150 levels ( $2.041 \pm 0.367$ ,  $p=0.0056$ ) (**Figure 109.B**).

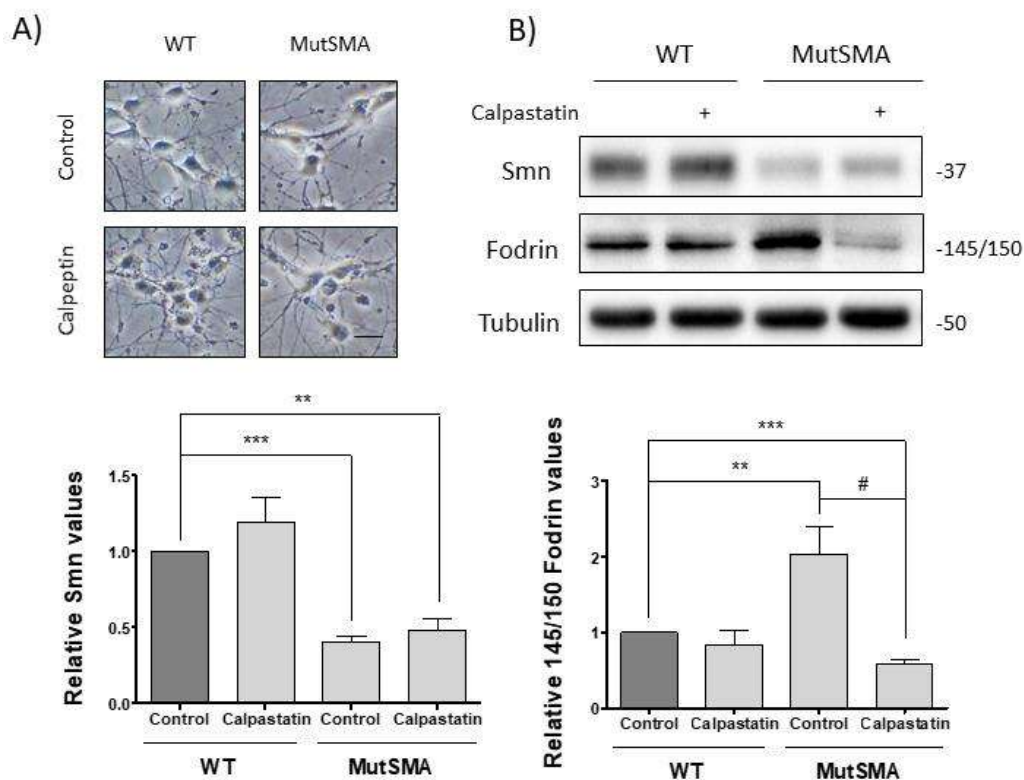


**Figure 109. Effect of calpastatin treatment in MutSMA cultured MNs.** MutSMA and WT MNs were purified and cultured for 6 days in NTFs supplemented medium. MNs were treated with 100 nM of calpastatin for 6 hours. Control condition was left untreated. **A)** Representative phase-contrast images show MNs cultures on day 6. **B)** Total cell lysates were collected and submitted to western blot analysis using an anti-SMN and an anti-fodrin antibodies. Anti- $\alpha$  tubulin was used as a loading control. Graphs values show relative SMN (**left**) and fodrin (**right**) protein levels  $\pm$  SEM. Values correspond a three independent experiments. (\*\* $p<0.01$ , \*\*\*  $p<0.001$ , and #  $p<0.01$  vs the Control MutSMA values). Scale bar of 15  $\mu$ m.

Interestingly, when Smn levels were analysed we observed that, regardless the changes detected in fodrin breakdown, there were no differences in Smn. The only significant differences were in the MutSMA conditions (Control MutSMA,  $0.407 \pm 0.040$ ,  $p < 0.0001$  and Calpastatin MutSMA,  $0.486 \pm 0.074$ ,  $p = 0.0026$ ) compared to the WT Sham (**Figure 109.B**).

In the same way, calpastatin treatment was tested at the same concentration in human fibroblasts grown for 2 days (**Figure 110.A**). As happened with calpeptin treatment, we did not observe any effect of the treatment neither in the Control or SMA affected (SMA 1 and SMA 2) cells when SMN and fodrin protein levels were analysed, suggesting that dose and treatment time is specific and different from the used in the mouse MNs (**Figure 110.B**).

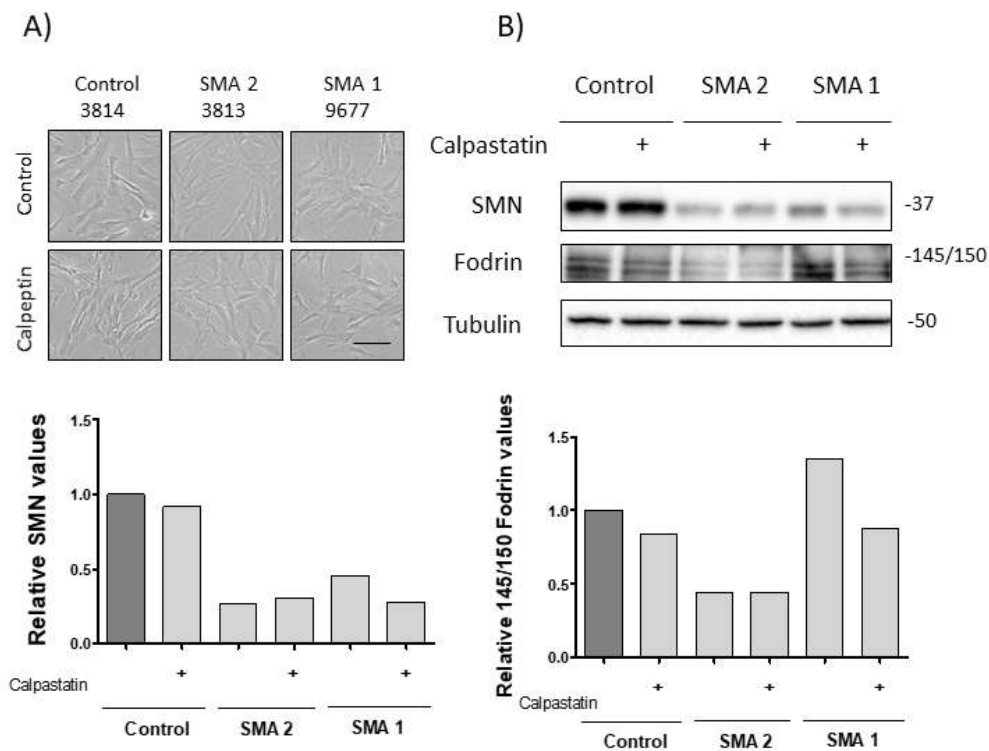


**Figure 110. Effect of calpastatin treatment in human fibroblast cell lines.** Control (3814 healthy SMA carrier) and SMA patient-derived (9677 SMA type 1 (SMA 1), 3813 SMA type 2 (SMA 2)) fibroblast cell lines were cultured for 2 days and then treated 100nM of calpastatin or left untreated for 6 hours. **A)** Representative phase-contrast images of cell cultures after 2 DIV. **B)** Total cell lysates were collected and submitted to western blot analysis using anti-SMN and anti-fodrin antibodies. Anti- $\alpha$  tubulin was used as a charge control. Graphs values show relative SMN (left) and fodrin (right) protein levels  $\pm$  SEM. Values correspond to two independent experiments. Scale bar of 100  $\mu$ m.



## **DISCUSSION**

---



At the present time, it is extensively accepted that SMA is a multisystemic disease where the reduction of the SMN levels, a protein ubiquitously expressed, affects multiple organs and tissues. Even so, the degeneration of  $\alpha$ MN remains the best notable alteration of the disease and is responsible for the most severe symptom, the muscular atrophy. For that reason, the study of the alterations in MNs during SMA remains a priority to understand the disease. Primary cultures of MNs have become a useful tool to study the basic mechanism underlying neuronal degeneration in SMA and therefore can contribute significantly to the development of new therapeutic strategies.

In the present work, we used primary cultured MNs from embryonic spinal cord of CD1 and SMA mouse models, but also two human cultured models as a first approach to validate disease alterations in patients. Rodent MNs were obtained after mechanical and chemical dissociation of the spinal cord and separated from the rest of the cells using a density gradient (at the embryonic stage, MNs have higher size and density). Human *in vitro* models consist of fibroblast cell lines and MNs obtained from the differentiation of iPSCs.

But why are MNs the main affected cells in SMA disease? What makes them so sensitive to the reduction of SMN levels? The final reason is still unknown, but there are several hypotheses. Neurons are highly polarized cells consisting of the cell body (soma) and extensions (axon and dendrites). This polarity is crucial to neuronal function, where the compartmentalization largely relies on the asymmetric subcellular localization of mRNA and proteins. Affection of normal levels of certain transcripts in the distal axon could produce axonal specific alterations related to this specialized structure and induce specific vulnerability of MNs.

Previous results of the group showed that in cultured MNs the reduction of Smn protein using an shRNA caused neurite degeneration, consisting of axonal swelling and blebbing, after 9 days of interference, while cell death was only detectable at later stages (Garcera et al., 2011). These data recapitulate previously described alterations in SMA mice (McGovern et al., 2008) and patients (reviewed by Burghes and Beattie, 2009) suggesting that reduction of Smn levels induced disturbances in axon growth and maintenance that lead to a neurodegenerative response in neurites previous to cell death, although their role in the pathogenesis of SMA is still not fully understood. In order to corroborate that neuronal degeneration occurs previous to cell death, we analysed the neurite degeneration

process in cultured MNs from the severe SMA mouse model, the MutSMA. The results obtained are in agreement with the previous hypothesis, as MutSMA MNs showed a higher percentage of neurite degeneration, starting at 6 DIV, without showing any difference in the number of apoptotic nuclei or in the level of caspase 3 activation at 12 days in culture, again indicating that neurite degeneration occurs *prior* to the detection of apoptotic death alterations in the soma.

Autophagy is a highly regulated process responsible for the degradation of cytosolic proteins and organelles by incorporation into a double-membrane vesicle, called autophagosome, that is delivered to the lysosome for degradation (reviewed in Dikic and Elazar, 2018). Under physiological conditions, autophagy is important for differentiation, homeostasis and survival, however, several studies have related alterations of this process to numerous neurodegenerative disorders (reviewed in Menzies et al., 2015) including SMA (Custer and Androphy, 2014; Garcera et al., 2013).

Whether the process is over-activated in an effort to preserve neuronal function by removing damaged cellular material, or the normal flux slows, resulting in the failure of the clean-up of cell waste organelles or proteins, excessive or insufficient autophagic activity can lead to self-destruction. SMN reduction causes changes in microtubule-associated axonal transport and architecture (Rossoll et al., 2003) that may contribute to autophagy defects (Custer and Androphy, 2014; Garcera et al., 2013) that in turn can compromise axonal traffic and induce cell toxicity, among other effects that can be detrimental to the cells.

Measuring the number of autophagosomes is complicated and there is no perfectly specific assay to do it. The most common methods used are: electron microscopy for assessing autophagosomes, fluorescent microscopy detection of the subcellular localization of LC3 and biochemical detection of the membrane-associated form of LC3 (Mizushima, 2004).

Using electron microscopy is the best way to directly observe the autophagy vesicles, however, the assessment of autophagosome number using this technique requires considerable and specialized technical expertise. Thus, microscopy and biochemistry, are methods more widely used to measure autophagy in order to support electron microscopy observations. In contrast to the cytoplasmic localization of LC3-I, when LC3 is conjugated to PE (forming LC3-II) is recruited into the autophagosomal membranes both in the luminal

and cytosolic surfaces, and maintained until the last step of the autophagic process. The process is visualized by fluorescence microscopy as a change in the pattern distribution, from a diffuse cytoplasmic pattern (LC3-I) to as punctate structures that primarily represent autophagosomes (LC3-II) that can be quantified (Mizushima, 2004).

On the other hand, measuring autophagy levels using western blot technique consists of the detection of the two main endogenous forms of LC3, LC3-I and LC3-II. Using an anti-LC3 antibody, LC3-I and LC3-II can be easily distinguished during SDS-PAGE because of the extreme hydrophobicity of LC3-II makes it migrate faster than LC3-I, showing an apparent molecular weight of 14 and 16 kDa, respectively. Normalized to a loading control, the amount of LC3-II is a good marker of the number of autophagosomes since, once recruited to the outer and inner membrane of the autophagosome, it remains attached until fusion with the lysosome that degrades the luminal pool while the cytosolic side can be dilapidated and recycled (Kabeya et al., 2000; Tanida et al., 2004).

In the group we have previously demonstrated using electron microscopy experiments and immunofluorescence analysis, an increased number of autophagy structures in spinal cord MNs of embryonic and postnatal SMA mouse model when compared to non-mutant samples (Periyakarupiah et al., 2016). In the same way, it has been recently demonstrated that autophagic markers are increased in spinal cord extracts of SMA mouse models (Custer and Androphy, 2014). To confirm autophagy deregulation in SMA pathogenesis and progress specifically in MNs, we have measured LC3-II protein levels using western blot in cultured MNs from the SMA mouse model MutSMA and SMNDelta7 at short and extended culture periods of time. The obtained results showed a significant increase of the autophagy marker in both SMA mouse models. Moreover, we have measured LC3-II protein level and autophagic vesicles in differentiated human SMA MNs. And one more time, we observed an increase of autophagic markers in those cells, strongly suggesting, together with SMA mouse models results, that autophagy is impaired in MNs during SMA disease.

This idea was corroborated with the measurement of LC3-II protein level and LC3-positive puncta in SMA patients cultured fibroblasts in where we did not observe any increase of these markers. The reduction in the number of autophagosomes in human fibroblast results again suggests that autophagy impairment is specific of MNs.



The autophagosome is an intermediate structure in a dynamic pathway and the rise of LC3-II levels can result from either an increase of the autophagosome synthesis or a suppression of autolysosomes conversion steps downstream in the autophagy pathway (fusion with lysosome and degradation). One common alternative method to detect the autophagic flux is by measuring the levels of the autophagy substrate p62. During the autophagic process, p62 is selectively incorporated into autophagosomes through direct binding to LC3 and is efficiently and exclusively degraded by autophagy (Bjørkøy et al., 2005). Therefore, the total cellular expression levels of p62 inversely correlate with autophagic activity.

We have observed an increase of p62 protein level in mice cultured spinal cord MNs at prolonged cultured times (12 DIV) suggesting a decreased autophagic flux in SMN-reduced cells. On the contrary, no differences were observed in differentiated SMA patient MNs. Even it seems contradictory results, we have to consider that, although the human MNs we obtained show the expression of mature MNs markers, like Islet 1/2,  $\beta$ III Tubulin, Hb9 and ChAT, these cells were cultured for a short period of time (6 DIV after MNs differentiation). Previously published results had already demonstrated that SMA neurons display reduced autophagosome clearance and an increase of p62 protein levels when cells were cultured for 14 DIV after MNs differentiation (Rodriguez-Muela et al., 2018). Possibly, as occurs with the SMA mouse MNs, the differences in p62 levels are only clearly increased at long-time cultured cells, so future experiments will be needed to elucidate p62 alterations in human differentiated MNs. Even p62 could be used as a good indicator of autophagy suppression, it also has some potential limitations (Mizushima et al., 2010). The single measurement of the p62 protein level may not be sufficient to estimate the autophagic flux. It would be useful to complement these results with the measurement of other autophagy substrates and use different autophagy modulators, like bafilomycin, 3-methyladenine (3-MA) and ammonium chloride, in order to further establish the autophagy alterations in SMA.

Nevertheless, all of these results strongly suggest that autophagy is impaired in SMA disease even though the role of this deregulation in SMA pathogenesis and progress is still unknown. One of the possibilities is that the increase of autophagy in SMN-reduced MNs can be the consequence of axonal transport disruption produced by the reduction of SMN and it exacerbates the neurodegeneration. In neurons, autophagy process is spatially and

temporally regulated along the axon. Under homeostatic conditions formation of autophagosomes is primarily produced in the distal axon. After, autophagosomes undergo retrograde transport along the axon toward the soma via the microtubule-based molecular motor dynein (Cheng et al., 2015). As autophagosomes move toward the soma, they mature into degradative organelles by merging with late endosomes/lysosomes. Full degradation and recycling of the autophagic cargo is then produced in the soma. Under pathogenic conditions, defects in retrograde transport affects the autophagic flux, resulting in an accumulation of autophagosomes within dystrophic axons by the impossibility of efficiently reaching the soma for degradation. This will produce failed clearance of proteotoxins such as damaged mitochondria that leads to an increase in ROS production and an increase in p62 levels, which will be exacerbated as more severe the axonal degeneration is (Maday et al., 2012).

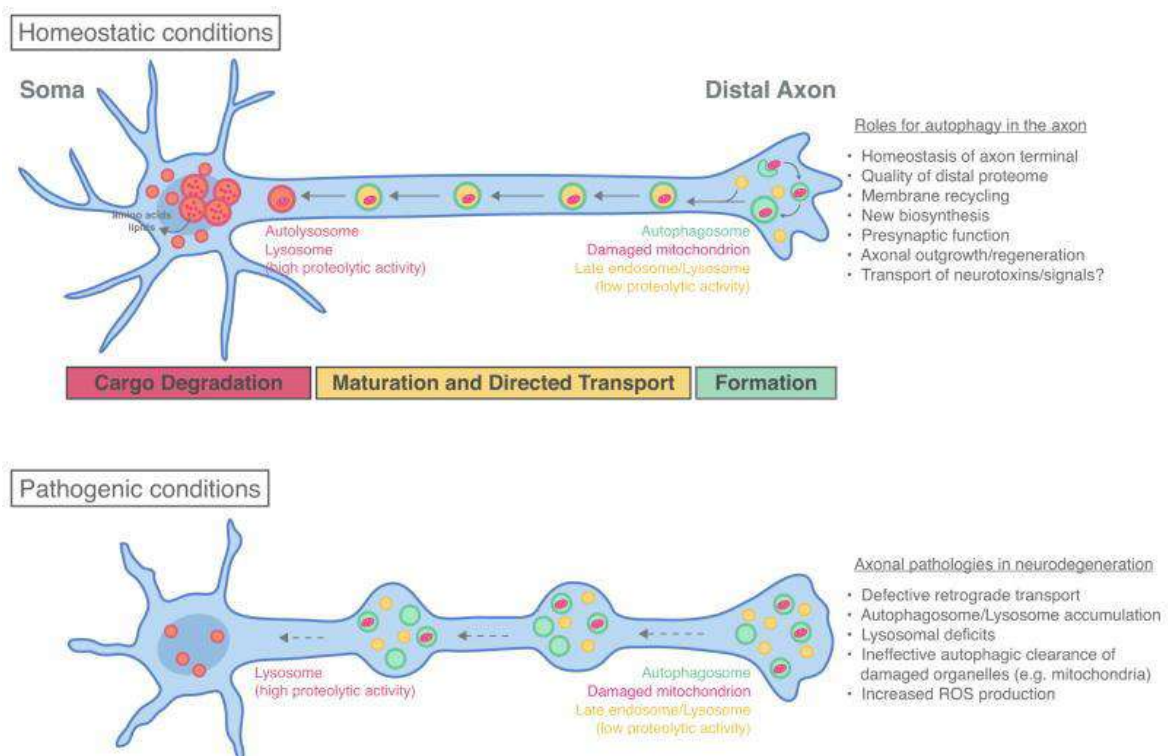


**Figure 111. Autophagy pathway in neurons in homeostatic and pathogenic conditions.** Under homeostatic conditions, autophagosome formation is produced in the distal axon and then undergo retrograde transport toward the soma as they mature into degradative autolysosomes. In pathogenic conditions, defects in retrograde transport results in an accumulation of immature autophagosomes producing axon degeneration (Maday, 2016).

In the process of a pathogenic autophagosomes accumulation in neurites, the axon terminal undergoes a process of swelling and dystrophy, followed by retraction and neuron death. These neurodegenerative alterations correlate with our neurite degeneration results, where swelling and beebbling were the characteristics used to determine a degenerated neurite. We specifically measured LC3-positive spots in soma and in neurites using SMNDelta7 and differentiated human MNs, and we observed that the increase of these structures in both compartments. To strongly conclude that autophagosome accumulation in MNs neurites is related to neurodegeneration in SMA pathogenesis further experiments will be needed.

Whether autophagy is a viable therapeutic target in SMA still remains unclear. Nevertheless, some groups have already started to use autophagy inhibitor, such as 3-MA, in SMA mouse models showing a delay in MN degeneration and extension of mice lifespan (Piras et al., 2017). This supports the hypothesis that autophagy manipulation may be useful in SMA treatment. In this context, future studies focused on the role of proteins involved in autophagy and other intracellular SMA altered mechanisms will be needed to identify potential targets for combinatorial therapeutics.

The calpain family is composed by a group of  $\text{Ca}^{2+}$ -dependent regulatory proteases that share homology in their protease domain. Although the exact function of this protein family is unknown, it is interesting to remark that calpains are considered as modulator proteases due to their limited proteolytic activity and intrinsic substrate specificity. It makes them a good candidate to regulate protein functions and cellular pathways, including the degradational system of autophagy. By cleaving proteins involved in this pathway, calpains have shown to negatively regulate autophagy at multiple levels (Goll et al., 2003; Weber et al., 2019).

Starting at the nucleation step, it has been showed that Beclin 1 is a calpain substrate (Russo et al., 2011). Its proteolytic reduction blocks the formation of the complex responsible to initiate the autophagic pathway downstream of mTORC1. In the same line of evidences, calpain proteolyze the  $\alpha$ -subunit of heterotrimeric G proteins ( $\text{G}\alpha$ ) (Greenwood and Jope, 1994) leading to an increase of I3P and consequently inhibiting the autophagosome synthesis. Once autophagy starts, the pathway is mainly driven by the autophagy-related (Atg) proteins, and nearly all of them can be cleaved by calpains *in vitro*

(Norman et al., 2010). However, the biological relevance of this proteolysis has only been demonstrated for Atg5 (Xia et al., 2010; Yousefi et al., 2006). Calpain cleavage of Atg5 leads to the disturbance of the Atg5-Atg12 complex formation and as a consequence, inhibits the phagophore membrane expansion. Other less known calpain substrates are the Lysosome-associated membrane protein 2 (LAMP2) (Villalpando Rodriguez and Torriglia, 2013) and the autophagy receptors, p62 (Colunga et al., 2014) and OPTN (Kim et al., 2013), compromising lysosomal permeabilization and cargo binding, respectively.

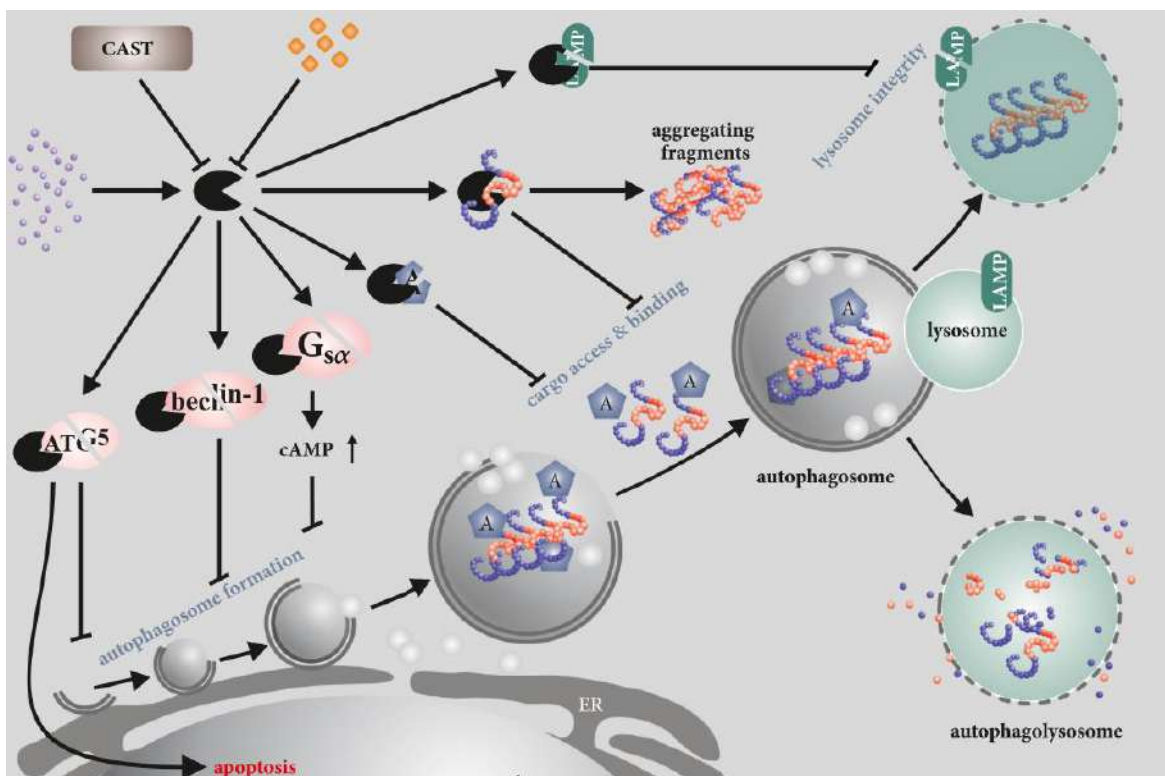


**Figure 112. Calpain proteolytic targets in the autophagy process.** Calpain can act at different levels of the autophagic process causing a defect in cellular homeostasis. Calpain can lead to the inhibition of autophagy induction by cleaving signal transduction molecules or autophagic proteins, like beclin-1 and Atg5. However, it can also change the dynamics of cargo degradation by processing adapter proteins, like optineurin and p62, or lysosome-associated proteins (LAMPs) (Weber et al., 2019).

In many pathological conditions, autophagy and calpain machineries are common players and have been targeted as a therapeutic strategy in experimental systems. However, the exact mechanism on how these two systems interact under specific disease conditions is still unknown and warrants in-depth analysis.

Our results showed that both the calpain-1 knockdown and its pharmacological inhibition induce an increase of the active form of LC3. This increase in LC3-II protein levels was corroborated in the calpain knockdown model using immunofluorescence analysis that showed an increase in the LC3-positive puncta in both soma and neurites. These results are in accordance with previous reports revealing that overexpression of constitutively active calpain inhibits autophagosome synthesis and that calpeptin treatment increases the number of autophagosome-like structures and decreases the number of mitochondria (which are endogenous autophagy substrates) in COS-7 cells (Williams et al., 2008).

Calpain is activated in response to  $\text{Ca}^{2+}$  signals and could be mediating neuronal degeneration in response to toxic  $\text{Ca}^{2+}$  levels (Das et al., 2005; Gou-Fabregas et al., 2009). The addition of high potassium concentrations on the culture medium is a useful tool to induce membrane depolarization and consequently increasing intracellular  $\text{Ca}^{2+}$  levels by activation of the VCCS channels (Malva et al., 1995). Degradation of full-length  $\alpha$ -fodrin to the 150/145 kDa specific fodrin breakdown product has been extensively attributed to the activation of calpain (Nath et al., 1996). In our hands, the addition of 30 and 50 mM of KCl into the cell culture medium results in calpain activation short-time treatment (3 hours) but not in long-time treatment (24 hours) when measured  $\alpha$ -fodrin specific breakdown products.

When autophagy in high potassium condition was analysed in CD1 MNs cultures we surprisingly observed an increase of LC3-II protein level. Although it may seem contradictory, that both, the activation and the inhibition of calpain could increase autophagic vesicles, we have to consider the large amount of proteolytic targets of calpain throughout the entire autophagic process (Weber et al., 2019). Thus, we decided to analyse the autophagic flux by measuring p62, and we observe that, while the treatment with calpeptin significantly increases p62, the protein levels do not change in 30K treatment, indicating that the origin of the autophagic accumulation may be the consequence of different alterations in the pathway.

Moreover, we have to consider that  $\text{Ca}^{2+}$  regulates multiple physiological functions in cells and it is clearly related to autophagy. However, the exact role of  $\text{Ca}^{2+}$  in this process is poorly understood and still under debate. Evidences show that this intracellular second messenger can regulate autophagy in both directions, activation and inhibition. To explain

this  $\text{Ca}^{2+}$  duality, it has been proposed that the role of  $\text{Ca}^{2+}$  in autophagy depends on the cell state and reflects spatiotemporal  $\text{Ca}^{2+}$  signals in unstressed versus stressful situations (reviewed in Sun et al., 2016).

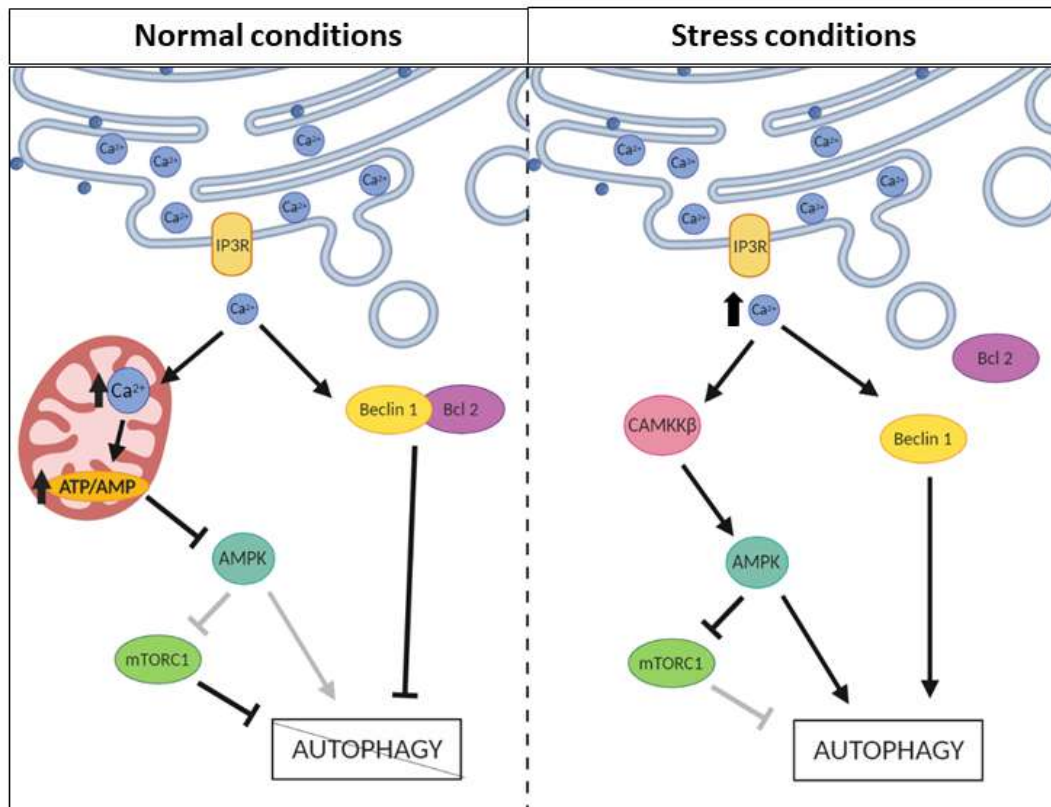


**Figure 113. Calcium regulation of autophagy.** The existing data revealed that intracellular  $\text{Ca}^{2+}$  levels can affect autophagy, both positively and negatively. This bidirectional role of  $\text{Ca}^{2+}$  in the regulation of autophagy can be indicating that it probably depends on the context of the time, and cell state (S de la Fuente).

Under normal conditions, constitutive IP3R induce a  $\text{Ca}^{2+}$  release from the ER that triggers into the mitochondria inhibiting autophagy as a result of the increase of ATP production and the suppression of AMPK. Furthermore, IP3R-mediated  $\text{Ca}^{2+}$  signals could regulate the autophagic pathway by decreasing the release of Beclin 1 from Bcl-2–Beclin 1 complex sequestration and preventing the activation of the autophagy process. As a consequence, unstressed cells shut down the induction of autophagy by specifically targeting mitochondria bioenergetics and blocking autophagy induction signalling, maintaining autophagy at a basal level and reinforcing the crucial role of  $\text{Ca}^{2+}$  release in the controlled microdomains. However, when cells encounter stressful conditions, such as nutrition

deprivation, oxidative stress, high temperatures and accumulation of damaged organelles,  $\text{Ca}^{2+}$  signalling is intensified and not confined to a specialized microdomain, inducing autophagy through a pathway that has not been completely understood. It is speculated that abnormal  $\text{Ca}^{2+}$  can mediate autophagy by its binding with the calmodulin-dependent protein kinase kinase  $\beta$  (CaMKK $\beta$ ) that will activate autophagy by AMPK–mTOR pathway (Sun et al., 2016).

Additional experiments will be needed to establish the differences in the increase in the autophagosome number in 30K and calpeptin treatment conditions. For instance, examining proteins at different steps of the autophagy signalling pathway and analysing the effect on autophagy of these treatments in combination with different autophagy modulators (such as bafilomycin, 3-MA and ammonium chloride) as well as with different  $\text{Ca}^{2+}$  modulators (like BAPTA, Dantrolene, Thapsigargin Nifedipine, Conotoxin and Agatoxin).

Recent results obtained in SMN $\Delta$ 7 MNs showed that, under standard culture conditions, Smn-reduced MNs have a higher number of LC3-positive vesicles in both soma and neurites. However, when calpain inhibition was evaluated we observed that calpeptin increased LC3 spots in MNs soma of WT cells whereas 30K treatment did not induce any change. However, we could not detect the same effect in neurites. LC3 spots in WT neurites did not increase after calpeptin treatment, but after 30K treatment, we observed that LC3 increased in this MNs segment. Interestingly, in SMA cells, calpeptin treatment prevented LC3 increase in SMA neurites, but not in cell soma. Induction of membrane depolarization with 30K in mutant cells have an unexpected effect, decreasing autophagic LC3 spots in soma without any effect in neurites. More experiments will be needed in order to finally clarify the effect of calpain modulation over autophagy regulation. Our results correlate with the idea that an accumulation of autophagosomes in SMA neurites results unfavourable for the cell. Moreover, treatments that prevent autophagosome accumulation and allows outflow to the soma may help to prevent neurite degeneration.

The  $\text{Ca}^{2+}$  concentrations necessary for calpains activation are in the range of micro- to millimolar (Ono and Sorimachi, 2012), which is rather beyond the nanomolar  $\text{Ca}^{2+}$  levels in cells under normal physiological conditions. This apparent contradiction is solved by the compartmentalization of cellular microenvironments, where  $\text{Ca}^{2+}$  increases are tightly

controlled (Friedrich, 2004; Goll et al., 2003). In SMA it has been described  $\text{Ca}^{2+}$  alteration localized in the axonal compartment probably related to a decreased  $\text{Ca}^{2+}$  reuptake by intracellular organelles (Jablonka et al., 2007; Ruiz et al., 2010). These observations postulated that  $\text{Ca}^{2+}$  changes in SMA MNs are located in axons and can contribute to specific axonal alterations, such as the deregulation of calpain activation and the autophagy deregulation. In this context, we have observed that calpeptin treatment may regulate autophagosome accumulation in neurites and consequently, this effect may result beneficial by preventing neurite collapse and MN degeneration.

In several neurodegenerative diseases, the activity of calpain has been implicated in the processing of key proteins such as  $\alpha$ -fodrin (Nath et al., 1996), TDP43 (Yamashita et al., 2012), and CaMKIV (Gou-Fabregas et al., 2014). More recently SMN has also been included in the list of proteolytic targets of calpain by Fuentes et al., 2010 and Walker et al., 2008, where they described and mapped the proteolysis of SMN by calpain in mammalian muscle cell lysates. These two publications provide new evidences of the post-translation regulation of the cytosolic SMN. In the present work, we propose that calpain system may be involved in SMN degradation in MNs and therefore calpain inhibition can be used as a new therapeutic target for SMA. The first approach using the calpain-1 knockdown showed that in a primary culture of isolated CD1 and SMA mice spinal cord MNs, endogenous calpain reduction clearly increased Smn protein level even in membrane depolarization conditions. Likewise, the calpain downregulation of Smn protein level prevents neurite degeneration in SMA mouse MNs.

In recent studies, using NSC34 cells and human fibroblast cell lines, calpeptin treatment did not induce any changes in SMN protein level (Burnett et al., 2009; Locatelli et al., 2015). However, in apparent contradiction, our results showed a significant increase of Smn cultures spinal cord MNs were treated with calpeptin. In this work, Locatelli et al., 2015 only tested 24 hours time-point treatment with calpeptin. However, using a time-course experiment we showed that calpeptin treatment is able to increase Smn levels only until 20 hours in cell culture medium. In their discussion, Locatelli and collaborators also suggest that SMN calpain cleavage could not be excluded from consideration in more physiological conditions. Furthermore, it was described that ALLN (N-Acetyl-Leu-Leu-Norleu-al) calpain inhibitor treatment reduces SMN cleavage in HeLa and C2C12 cells (Walker et al., 2008).



In agreement with previous publications demonstrating that Smn located in the muscle cell is a proteolytic target of calpain (Fuentes et al., 2010; Walker et al., 2008), we observed that Smn protein level in mouse MNs is also modulated by calpain, although the functional implications of this cleavage is not completely understood neither in the muscle cells or neurons.

Similar to the results obtained in Burnett et al., 2009 in SMA patient-derived fibroblasts, when we performed our experiments using human *in vitro* models (fibroblast and differentiated MNs) we observed that calpain inhibitor, calpeptin, had no effect on SMN protein level. In their discussion, the authors suggest that SMN degradation pathways are cell-type dependent and are differentially regulated in cell compartments. However, examining our experiments we suggest that the lack of effect of calpeptin treatment is due to inadequate doses or treatment time periods for human cultured cells, since the results were the same for both fibroblasts and differentiated MNs. More dose-response and time-course experiments should be performed using human SMA differentiated MNs to finally conclude if calpeptin inhibition regulates SMN protein level in these cells.

To specifically identify the proteolytic processing of SMN by calpain, we had measured using western blot analysis the predicted SMN cleavage fragments products (N- and C-terminus) of 20 and 17 KDa, respectively (Fuentes et al., 2010). As expected in cultured MN system membrane depolarization treatment clearly increased both N- and C-terminal Smn protein level, which can be prevented by calpeptin. We have also observed that calpeptin treatment reduced Smn N- and C-terminal fragments and increases full-length Smn without changes in Smn mRNA levels, indicating that the regulation of calpain is by direct effect on Smn protein. Given that we can also measure the N- and C-terminal fragments even in control conditions it suggests that calpain basal activity may be processing Smn and regulating its level in these cells.

In PC12 cells, it has been observed that C-terminal domain of SMN can regulate actin cytoskeletal dynamics by modulating the G- to F-actin ratio, and that the overexpression of this terminal fragment rescues neurite outgrowth defects caused by endogenous Smn depletion (van Bergeijk et al., 2007). In this context, many evidences establish the importance of actin cytoskeletal dynamics in SMN function and SMA pathology (Hensel and

Claus, 2018) and could be an interesting approach to study SMN cleavage products in SMA affected samples.

Together, muscle and MN mice studies strongly suggest a significant role of calpain activity in the control of SMN protein level. Since SMN protein level are critical for disease onset and severity we decided to test calpeptin as a potential therapeutic strategy using two severe SMA mouse models. Based on the *in vitro* time-course performed using calpeptin we decided to implement the daily administration since in culture, calpeptin effect lasts for up to 24 hours. We performed a bibliographic research to identify the doses in where calpeptin has been previously used in *in vivo* experiments. Calpeptin has been largely tested in different animal models as a therapeutic approach in stroke and myocardial infarction in a range of doses from 20  $\mu\text{g/g}$  to 0.4  $\mu\text{g/g}$  of weight (Mani et al., 2009, 2008; Peng et al., 2011). To this end, we decided to adopt the most common dose in the bibliography at 6  $\mu\text{g}$  per g of animal weight.

MutSMA and SMNDelta7 mouse models are catalogued as severe form of SMA characterized by a rapid motor function impairment and a short lifespan (Bebee et al., 2012). Despite the severity of these mice models, a daily dose of calpeptin treatment improved the progression of the disease by ameliorating motor ability and increasing lifespan. However, calpain inhibition does not completely reverse the disease phenotype observed in these mice and other doses will be needed to test.

SMA disease complexity is likely related to several functions of SMN but also to a specific characteristic of the affected cells. To effectively treat SMA it has to be considered the complete SMA pathology and affectation. Calpeptin treatment is based on the increase of Smn protein level by blocking calpain activation. Calpains overactivation has been implicated in many neurodegenerative disorders, such as AD (Mahaman et al., 2019), ALS (Yamashita et al., 2012), PD (Mouatt-Prigent et al., 1996), polyQ disorders HD (Gafni and Ellerby, 2002) and neuronal injury (Wright and Vissel, 2016). But calpain activity is dysregulated in SMA?

To determine calpain activity in different SMA affected cells we measured the 150/145 specific fodrin breakdown products using western blot. We observed that in both mice cultured spinal cord MNs and differentiated human SMA MNs calpain-specific fodrin products were increased, but not in human SMA cultured fibroblasts. These results suggest

that the calpain deregulation in SMN-reduced conditions is cell-type specific. Using western blot to measure calpain protein level we observed that basal level of calpain was not increased in any of the SMA mouse models MNs and was reduced in differentiated human SMA MNs. This confirms that this increase of calpain activity was not the consequence of an increase of calpain protein levels.

The best-characterized calpains the ubiquitous isoforms calpain-1 and calpain-2 both composed by an 80-KDa catalytic subunit (CAPN1 and CAPN2, respectively) and a common 28-KDa regulatory subunit commonly known as calpain small subunit 1 (CAPNS1) (reviewed in Goll et al., 2003). This shared subunit is necessary for calpain-1 and calpain-2 proteolytic activity. Since we only measured the 80-KDa catalytic subunit of calpain-1, it could be that the SMA affected cells had more CAPNS1 and therefore, even these cells did not have more calpain catalytic subunit they could have a more active functional calpain, formed by the two subunits. As a future experiment it would be interesting to also evaluate the CAPNS1 protein level to clearly demonstrate basal functional calpain levels in SMA affected cells.

Calpain overactivation can be caused by an increase of intracellular  $\text{Ca}^{2+}$  concentration or by a reduction of the natural endogenous inhibitor calpastatin. Calpastatin is the only known specific inhibitor for classical calpains in cells, due to the intrinsically unstructured form of calpastatin and the complex formed with calpain (reviewed in Wendt et al., 2004). Depletion of endogenous calpastatin has been previously shown in mouse models of several neurodegenerative disorders (Diepenbroek et al., 2014; F. M. Menzies et al., 2015; Rao et al., 2014). However, western blot analysis of calpastatin levels in cultured SMA MNs, mice and human, showed no changes of this protein in these cells suggesting that calpain overactivation may be the result of other intracellular changes, such as  $\text{Ca}^{2+}$  homeostasis. It may correlate with previously published results showing that  $\text{Ca}^{2+}$  changes localized in some neuronal sections in SMA disease that may contribute to the increase of calpain activity in these particular spaces (Jablonka et al., 2007; Ruiz et al., 2010). It would be interesting to further connect these alterations in SMA pathology, performing basal  $\text{Ca}^{2+}$  measurements in SMN-reduced cells but also using different ion chelators and  $\text{Ca}^{2+}$  modulators, such as BAPTA, Dantrolene, Thapsigargin Nifedipine, Conotoxin and Agatoxin, to establish, if possible, the origin of this  $\text{Ca}^{2+}$  deregulation.

Finally, we also determined calpain activity in spinal cord extracts from sham and calpeptin-treated SMN $\Delta$ 7 mice using western blot analysis. We observed as it happened in the *in vitro* models, the 150/145 specific fodrin breakdown products were increased and no changes in calpastatin were detected in the mutant untreated mice compared to the untreated WT. Nevertheless, calpain protein levels were also increased in mutant sham animals. Because in spinal cord extract we could not distinguish the specific changes in MNs and therefore, we could not determine if calpeptin administration ameliorated SMA pathology by modulating Smn protein level and calpain activity in MNs.

For that reason, we decided to perform a histopathologic analysis of the lumbar region 1 and 2 (L1 and L2) of the spinal cord from P8 SMN $\Delta$ 7 sham calpeptin-treated mice. Immunofluorescence experiments of lumbar spinal cord sections showed that Smn, calpastatin and calpain were reduced in Sham SMN $\Delta$ 7 mutant MNs soma. We also observed that *in vivo* calpeptin treatment significantly increases calpastatin and calpain levels in both mutant and WT MNs, suggesting that calpain can also be regulating the members of the pathway. It is true that some publications propose that calpain proteolytic activity can degrade calpastatin and produce its own autolysis. However, these phenomena have only been detected in *in vitro* systems and have not been demonstrated in *in vivo* models (Doumit and Koochmaraie, 1999; Hanna et al., 2008). Although this hypothesis that calpain modulating its own protein levels cannot be ruled out, more experiments are necessary to conclude that calpeptin produces these increases by blocking calpain activity and not by another pathway, for example inducing transcription.

Interestingly, *in vivo* calpeptin administration increased Smn protein in spinal cord extracts and in MNs soma but only in mutant treated mice. This modest increase of Smn protein in MNs correlates with the moderate effect observed in the disease phenotype observed in these mice. Our results strongly suggest that the beneficial effects of *in vivo* treatment with calpeptin may be mediated to some extent by the increase of Smn protein in MNs, however, SMA disease complexity is related to several functions of Smn in multiple tissues. For example, it is known that calpain regulates the level of Smn in muscle and satellite cells of skeletal muscle on SMA. Consequently, it may be interesting to perform histopathologic analysis of skeletal muscle to further characterize the effect of calpeptin administration in SMA pathogenesis.

Likewise, it will be interesting to test higher doses of calpeptin as well as to test the combined treatment with other therapies for SMA that have previously demonstrated a certain degree of effectiveness, such as Branaplam, Zolgensma, Nusinersen, Valproate and Mestion, in order to find a calpeptin dose and/or treatment combination capable of completely reversing phenotype SMA.

Calpain inhibition has been observed to be beneficial in several neurological diseases, such as ALS (Rao et al., 2016), stroke (Zhou and Cai, 2019) and AD (Wright and Vissel, 2016). Nevertheless, here we demonstrated that calpain inhibition is beneficial in ameliorating a childhood-onset disease but also the relevance of calpain activity as an essential and common mechanism regulating neurodegeneration in several diseases of different origins.

Furthermore, in a moment where most of the SMA therapies are focus on the SMN1 and SMN2 genes, here we provide a new SMN dependent approach for SMA therapeutics directly focus on SMN protein: the calpain inhibition.

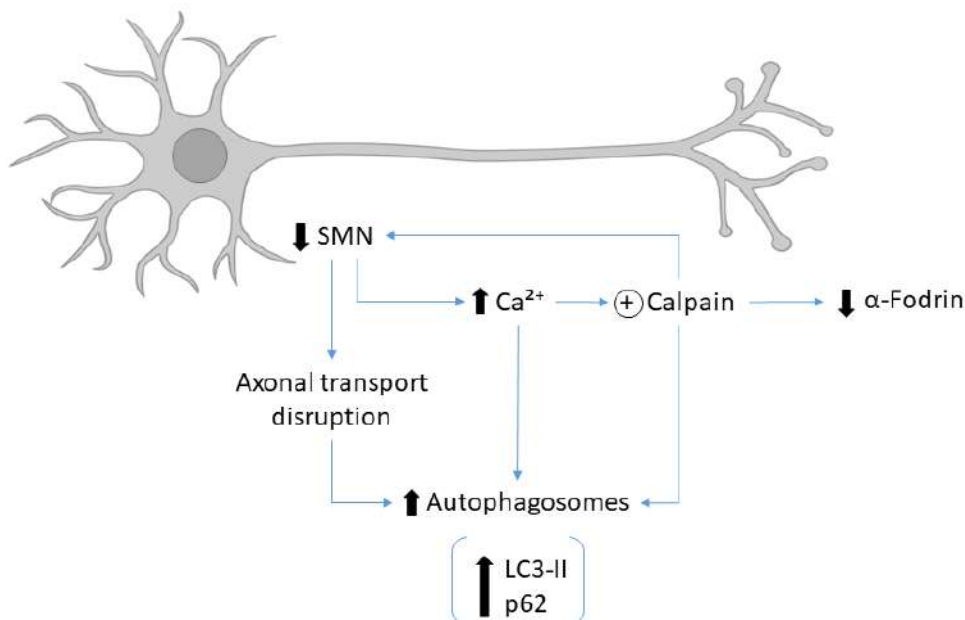


**Figure 114. Schematic representation of calpain involvement in SMA.** The reduction of SMN protein level occurred in SMA may produce alterations in  $\text{Ca}^{2+}$  homeostasis as described in (Ruiz et al., 2010). Increase of  $\text{Ca}^{2+}$  concentration can induce an over-activation of calpain. Simultaneously, these alterations can induce axonal transport causing a deregulation of the autophagy and leading or contributing to the MNs degeneration (S. de la Fuente).

In summary, calpain and autophagy pathways are intracellular proteolytic mechanisms involved in the development of several neurodegenerative disorders. In the present work, we have demonstrated that both calpain activity and autophagy are altered in SMN-reduced cells. We suggest that the positive effect of *in vivo* calpeptin treatment on SMA mice survival and motor phenotype can be the result of SMN and LC3 autophagosome protein regulation in SMA MNs. The analysis of new SMA modifiers belonging to several intracellular regulatory pathways that participate differently to disease progression, may contribute to find new treatment strategies to cover the high variability of clinical courses of SMA patients.



## **CONCLUSIONS**

---





## CONCLUSIONS

- I. Cultured mouse SMA MNs show higher percentage of neurite degeneration than WT cells.
- II. SMN-reduced human and mouse MNs, but not human fibroblasts, show an increase of LC3 autophagy marker.
- III. Calpain knockdown increases Smn and LC3 in cultured CD1 MNs soma and neurites, without altering MNs survival.
- IV. Addition of high potassium medium to cultured CD1 MNs induces calpain activation and reduces Smn levels after short treatment period. The effect can be prevented using lentiviral delivery of calpain shRNA.
- V. Endogenous calpain reduction increases Smn and prevents neurite degeneration in cultured MNs from severe SMA mouse model.
- VI. Treatment with the calpain inhibitor calpeptin increases Smn protein level in cultured CD1 MNs.
- VII. High potassium medium induces Smn proteolysis in CD1 MNs *in vitro*. The addition of calpeptin prevents this effect.
- VIII. Calpain activation with high potassium medium and calpain inhibition with calpeptin increase LC3 II protein levels in cultured CD1 MNs. Calpeptin treatment, but not high potassium increases p62.
- IX. *In vitro* calpeptin treatment increases LC3 spots in WT MNs soma, but not in SMNDelta7 cells. On the contrary, calpeptin treatment reduces LC3 spots in SMNDelta7 MNs neurites, but not in WT cells.
- X. *In vivo* daily calpeptin administration to two severe SMA mouse models extends lifespan and ameliorates motor function.
- XI. Human and mouse SMN-reduced MNs show an increase of calpain activity compared to control. This effect is not associated with the reduction of the endogenous calpain inhibitor calpastatin.
- XII. *In vivo* calpeptin treatment of SMNDelta7 mice increases Smn protein in mutant spinal cord MNs, but not in WT MNs. The same treatment rises calpain and calpastatin level in both WT and mutant.



## REFERENCES

---



- A. Nash, L., K. Burns, J., Warman Chardon, J., Kothary, R., J. Parks, R., 2017. Spinal Muscular Atrophy: More than a Disease of Motor Neurons? *Curr. Mol. Med.* 16, 779–792. <https://doi.org/10.2174/1566524016666161128113338>
- Al-Zaidy, S.A., Kolb, S.J., Lowes, L., Alfano, L.N., Shell, R., Church, K.R., Nagendran, S., Sproule, D.M., Feltner, D.E., Wells, C., Ogrinc, F., Menier, M., L'Italien, J., Arnold, W.D., Kissel, J.T., Kaspar, B.K., Mendell, J.R., 2019a. AVXS-101 (Onasemnogene Apeparovovec) for SMA1: Comparative Study with a Prospective Natural History Cohort. *J. Neuromuscul. Dis.* 6, 307–317. <https://doi.org/10.3233/jnd-190403>
- Al-Zaidy, S.A., Pickard, A.S., Kotha, K., Alfano, L.N., Lowes, L., Paul, G., Church, K., Lehman, K., Sproule, D.M., Dabbous, O., Maru, B., Berry, K., Arnold, W.D., Kissel, J.T., Mendell, J.R., Shell, R., 2019b. Health outcomes in spinal muscular atrophy type 1 following AVXS-101 gene replacement therapy. *Pediatr. Pulmonol.* 54, 179–185. <https://doi.org/10.1002/ppul.24203>
- Andreassi, C., Angelozzi, C., Tiziano, F.D., Vitali, T., De Vincenzi, E., Boninsegna, A., Villanova, M., Bertini, E., Pini, A., Neri, G., Brahe, C., 2004. Phenylbutyrate increases SMN expression in vitro: Relevance for treatment of spinal muscular atrophy. *Eur. J. Hum. Genet.* 12, 59–65. <https://doi.org/10.1038/sj.ejhg.5201102>
- Arce, V., Garces, A., De Bovis, B., Filippi, P., Henderson, C.E., Pettmann, B., DeLapeyrière, O., 1999. Cardiotrophin-1 requires LIFR $\beta$  to promote survival of mouse motoneurons purified by a novel technique. *J. Neurosci. Res.* 55, 119–126. [https://doi.org/10.1002/\(SICI\)1097-4547\(19990101\)55:1<119::AID-JNR13>3.0.CO;2-6](https://doi.org/10.1002/(SICI)1097-4547(19990101)55:1<119::AID-JNR13>3.0.CO;2-6)
- Arnold, A.S., Gueye, M., Guettier-Sigrist, S., Courdier-Fruh, I., Coupin, G., Poindron, P., Gies, J.P., 2004. Reduced expression of nicotinic AChRs in myotubes from spinal muscular atrophy I patients. *Lab. Investig.* 84, 1271–1278. <https://doi.org/10.1038/labinvest.3700163>
- Arthur, J.S.C., Elce, J.S., Hegadorn, C., Williams, K., Greer, P.A., 2000. Disruption of the Murine Calpain Small Subunit Gene, *Capn4*: Calpain Is Essential for Embryonic Development but Not for Cell Growth and Division. *Mol. Cell. Biol.* 20, 4474–4481. <https://doi.org/10.1128/mcb.20.12.4474-4481.2000>
- Aslan, N., Yildizdas, D., Coban, Y., Horoz, O.O., Mert, G.G., Ozcan, N., 2019. A Novel Adverse Event of Nusinersen Treatment: Thrombocytosis. *Indian J. Pediatr.* 86, 1157. <https://doi.org/10.1007/s12098-019-03069-1>
- Axe, E.L., Walker, S.A., Manifava, M., Chandra, P., Roderick, H.L., Habermann, A., Griffiths, G., Ktistakis, N.T., 2008. Autophagosome formation from membrane compartments enriched in phosphatidylinositol 3-phosphate and dynamically connected to the endoplasmic reticulum. *J. Cell Biol.* 182, 685–701. <https://doi.org/10.1083/jcb.200803137>
- Badadani, M., 2012. Autophagy Mechanism, Regulation, Functions, and Disorders. *ISRN Cell Biol.* 2012, 1–11. <https://doi.org/10.5402/2012/927064>
- Baki, A., Tompa, P., Alexa, A., Molnar, O., Friedrich, P., 1996. Autolysis parallels activation of  $\mu$ -calpain. *Biochem. J.* 318, 897–901. <https://doi.org/10.1042/bj3180897>
- Bäumer, D., Lee, S., Nicholson, G., Davies, J.L., Parkinson, N.J., Murray, L.M., Gillingwater, T.H., Ansorge, O., Davies, K.E., Talbot, K., 2009. Alternative splicing events are a late feature of pathology in a mouse model of spinal muscular atrophy. *PLoS Genet.* 5. <https://doi.org/10.1371/journal.pgen.1000773>

- Bebee, T.W., Dominguez, C.E., Chandler, D.S., 2012. Mouse models of SMA: Tools for disease characterization and therapeutic development. *Hum. Genet.* 131, 1277-1293. <https://doi.org/10.1007/s00439-012-1171-5>
- Benuck, M., Banay-Schwartz, M., DeGuzman, T., Lajtha, A., 1996. Changes in Brain Protease Activity in Aging. *J. Neurochem.* 67, 2019–2029. <https://doi.org/10.1046/j.1471-4159.1996.67052019.x>
- Bertini, E., Dessaud, E., Mercuri, E., Muntoni, F., Kirschner, J., Reid, C., Lusakowska, A., Comi, G.P., Cuisset, J.M., Abitbol, J.L., Scherrer, B., Ducray, P.S., Buchbjerg, J., Vianna, E., van der Pol, W.L., Vuillerot, C., Blaettler, T., Fontoura, P., André, C., Bruno, C., Chabrol, B., Deconinck, N., Estournet, B., Fontaine-Carbonnel, S., Goemans, N., Gorni, K., Govoni, A., Guglieri, M., Lochmuller, H., Magri, F., Mayer, M., Müller-Felber, W., Rivier, F., Roper, H., Schara, U., Scoto, M., van den Berg, L., Vita, G., Walter, M.C., 2017. Safety and efficacy of olesoxime in patients with type 2 or non-ambulatory type 3 spinal muscular atrophy: a randomised, double-blind, placebo-controlled phase 2 trial. *Lancet Neurol.* 16, 513–522. [https://doi.org/10.1016/S1474-4422\(17\)30085-6](https://doi.org/10.1016/S1474-4422(17)30085-6)
- Bertrand, S., Burlet, P., Clermont, O., Huber, C., Fondrat, C., Thierry-Mieg, D., Munnich, A., Lefebvre, S., 1999. The RNA-binding properties of SMN: Deletion analysis of the zebrafish orthologue defines domains conserved in evolution. *Hum. Mol. Genet.* 8, 775–782. <https://doi.org/10.1093/hmg/8.5.775>
- Bessou, P., Emonet-Dénand, F., Laporte, Y., 1965. Motor fibres innervating extrafusal and intrafusal muscle fibres in the cat. *J. Physiol.* 180, 649–672. <https://doi.org/10.1113/jphysiol.1965.sp007722>
- Bevan, A.K., Hutchinson, K.R., Foust, K.D., Braun, L., McGovern, V.L., Schmelzer, L., Ward, J.G., Petruska, J.C., Lucchesi, P.A., Burghes, A.H.M., Kaspar, B.K., 2010. Early heart failure in the SMNΔ7 model of spinal muscular atrophy and correction by postnatal scAAV9-SMN delivery. *Hum. Mol. Genet.* 19, 3895–3905. <https://doi.org/10.1093/hmg/ddq300>
- Bezprozvanny, I., 2009. Calcium signaling and neurodegenerative diseases. *Trends Mol. Med.* 15, 89–100. <https://doi.org/10.1016/j.molmed.2009.01.001>
- Bianco, F., Pane, M., D'Amico, A., Messina, S., Delogu, A.B., Soraru, G., Pera, M.C., Mongini, T., Politano, L., Baranello, G., Vita, G., Tiziano, F.D., Morandi, L., Bertini, E., Mercuri, E., 2015. Cardiac function in types II and III spinal muscular atrophy: Should we change standards of care? *Neuropediatrics* 46, 33–36. <https://doi.org/10.1055/s-0034-1395348>
- Bjørkøy, G., Lamark, T., Brech, A., Outzen, H., Perander, M., Øvervatn, A., Stenmark, H., Johansen, T., 2005. p62/SQSTM1 forms protein aggregates degraded by autophagy and has a protective effect on huntingtin-induced cell death. *J. Cell Biol.* 171, 603–614. <https://doi.org/10.1083/jcb.200507002>
- Boido, M., de Amicis, E., Valsecchi, V., Trevisan, M., Ala, U., Rugg, M.A., Hettwer, S., Vercelli, A., 2018. Increasing agrin function antagonizes muscle atrophy and motor impairment in spinal muscular atrophy. *Front. Cell. Neurosci.* 12. <https://doi.org/10.3389/fncel.2018.00017>
- Boido, M., Vercelli, A., 2016. Neuromuscular junctions as key contributors and therapeutic targets in spinal muscular atrophy. *Front. Neuroanat.* 10. <https://doi.org/10.3389/fnana.2016.00006>
- Boland, B., Kumar, A., Lee, S., Platt, F.M., Wegiel, J., Yu, W.H., Nixon, R.A., 2008. Autophagy induction and autophagosome clearance in neurons: Relationship to autophagic pathology in

- Alzheimer's disease. *J. Neurosci.* 28, 6926–6937. <https://doi.org/10.1523/JNEUROSCI.0800-08.2008>
- Boon, K.L., Xiao, S., McWhorter, M.L., Donn, T., Wolf-Saxon, E., Bohnsack, M.T., Moens, C.B., Beattie, C.E., 2009. Zebrafish survival motor neuron mutants exhibit presynaptic neuromuscular junction defects. *Hum. Mol. Genet.* 18, 3615–3625. <https://doi.org/10.1093/hmg/ddp310>
- Bordet, T., Berna, P., Abitbol, J.L., Pruss, R.M., 2010. Olesoxime (TRO19622): A novel mitochondrial-targeted neuroprotective compound. *Pharmaceuticals.* 3, 345–368. <https://doi.org/10.3390/ph3020345>
- Bowerman, M., Michalski, J.-P., Beauvais, A., Murray, L.M., DeRepentigny, Y., Kothary, R., 2014. Defects in pancreatic development and glucose metabolism in SMN-depleted mice independent of canonical spinal muscular atrophy neuromuscular pathology. *Hum. Mol. Genet.* 23, 3432–44. <https://doi.org/10.1093/hmg/ddu052>
- Bowerman, M., Murray, L.M., Beauvais, A., Pinheiro, B., Kothary, R., 2012a. A critical smn threshold in mice dictates onset of an intermediate spinal muscular atrophy phenotype associated with a distinct neuromuscular junction pathology. *Neuromuscul. Disord.* 22, 263–76. <https://doi.org/10.1016/j.nmd.2011.09.007>
- Bowerman, M., Swoboda, K.J., Michalski, J.-P., Wang, G.S., Reeks, C., Beauvais, A., Murphy, K., Woulfe, J., Screaton, R.A., Scott, F.W., Kothary, R., 2012b. Glucose metabolism and pancreatic defects in spinal muscular atrophy. *Ann. Neurol.* 72, 256–268. <https://doi.org/10.1002/ana.23582>
- Boyer, J.G., Murray, L.M., Scott, K., De Repentigny, Y., Renaud, J.M., Kothary, R., 2013. Early onset muscle weakness and disruption of muscle proteins in mouse models of spinal muscular atrophy. *Skelet. Muscle* 3. <https://doi.org/10.1186/2044-5040-3-24>
- Bricceno, K. V., Martinez, T., Leikina, E., Duguez, S., Partridge, T.A., Chernomordik, L. V., Fischbeck, K.H., Sumner, C.J., Burnett, B.G., 2014. Survival motor neuron protein deficiency impairs myotube formation by altering myogenic gene expression and focal adhesion dynamics. *Hum. Mol. Genet.* 23, 4745–4757. <https://doi.org/10.1093/hmg/ddu189>
- Briese, M., Esmaili, B., Fraboulet, S., Burt, E.C., Christodoulou, S., Towers, P.R., Davies, K.E., Sattelle, D.B., 2009. Deletion of smn-1, the *Caenorhabditis elegans* ortholog of the spinal muscular atrophy gene, results in locomotor dysfunction and reduced lifespan. *Hum. Mol. Genet.* 18, 97–104. <https://doi.org/10.1093/hmg/ddn320>
- Briese, M., Esmaili, B., Sattelle, D.B., 2005. Is spinal muscular atrophy the result of defects in motor neuron processes? *BioEssays.* 27, 946–957. <https://doi.org/10.1002/bies.20283>
- Briscoe, J., Pierani, A., Jessell, T.M., Ericson, J., 2000. A homeodomain protein code specifies progenitor cell identity and neuronal fate in the ventral neural tube. *Cell* 101, 435–445. [https://doi.org/10.1016/S0092-8674\(00\)80853-3](https://doi.org/10.1016/S0092-8674(00)80853-3)
- Brown, N., Crawford, C., 1993. Structural modifications associated with the change in Ca<sup>2+</sup> sensitivity on activation of m-calpain. *FEBS Lett.* 322, 65–68. [https://doi.org/10.1016/0014-5793\(93\)81112-D](https://doi.org/10.1016/0014-5793(93)81112-D)
- Burghes, A.H.M., Beattie, C.E., 2009. Spinal muscular atrophy: Why do low levels of survival motor neuron protein make motor neurons sick? *Nat. Rev. Neurosci.* 10, 597–609.



<https://doi.org/10.1038/nrn2670>

- Burke, R.E., Levine, D.N., Tsairis, P., Zajac, F.E., 1973. Physiological types and histochemical profiles in motor units of the cat gastrocnemius. *J. Physiol.* 234, 723–748. <https://doi.org/10.1113/jphysiol.1973.sp010369>
- Burnett, B.G., Munoz, E., Tandon, A., Kwon, D.Y., Sumner, C.J., Fischbeck, K.H., 2009. Regulation of SMN Protein Stability. *Mol. Cell. Biol.* 29, 1107–1115. <https://doi.org/10.1128/mcb.01262-08>
- Butchbach, M.E.R., Edwards, J.D., Burghes, A.H.M., 2007. Abnormal motor phenotype in the SMNΔ7 mouse model of spinal muscular atrophy. *Neurobiol. Dis.* 27, 207–219. <https://doi.org/10.1016/j.nbd.2007.04.009>
- Button, R.W., Roberts, S.L., Willis, T.L., Oliver Hanemann, C., Luo, S., 2017. Accumulation of autophagosomes confers cytotoxicity. *J. Biol. Chem.* 292, 13599–13614. <https://doi.org/10.1074/jbc.M117.782276>
- Calucho, M., Bernal, S., Alías, L., March, F., Venceslá, A., Rodríguez-Álvarez, F.J., Aller, E., Fernández, R.M., Borrego, S., Millán, J.M., Hernández-Chico, C., Cuscó, I., Fuentes-Prior, P., Tizzano, E.F., 2018. Correlation between SMA type and SMN2 copy number revisited: An analysis of 625 unrelated Spanish patients and a compilation of 2834 reported cases. *Neuromuscul. Disord.* 28, 208–215. <https://doi.org/10.1016/j.nmd.2018.01.003>
- Campbell, R.L., Davies, P.L., 2012. Structure-function relationships in calpains. *Biochem. J.* 447, 335–351. <https://doi.org/10.1042/BJ20120921>
- Chan, Y.B., Miguel-Aliaga, I., Franks, C., Thomas, N., Trülzsch, B., Sattelle, D.B., Davies, K.E., van den Heuvel, M., 2003. Neuromuscular defects in a *Drosophila* survival motor neuron gene mutant. *Hum. Mol. Genet.* 12, 1367–1376. <https://doi.org/10.1093/hmg/ddg157>
- Chandrasekhar, A., 2004. Turning Heads: Development of Vertebrate Branchiomotor Neurons. *Dev. Dyn.* 229, 143–161. <https://doi.org/10.1002/dvdy.10444>
- Chang, H.C.H., Dimlich, D.N., Yokokura, T., Mukherjee, A., Kankel, M.W., Sen, A., Sridhar, V., Fulga, T.A., Hart, A.C., Van Vactor, D., Artavanis-Tsakonas, S., 2008. Modeling spinal muscular atrophy in *Drosophila*. *PLoS One* 3, e3209. <https://doi.org/10.1371/journal.pone.0003209>
- Chang, J.G., Hsieh-Li, H.M., Jong, Y.J., Wang, N.M., Tsai, C.H., Li, H., 2001. Treatment of spinal muscular atrophy by sodium butyrate. *Proc. Natl. Acad. Sci. U. S. A.* 98, 9808–9813. <https://doi.org/10.1073/pnas.171105098>
- Charnas, L., Voltz, E., Pfister, C., Peters, T., Hartmann, A., Berghs-Clairmont, C., Praestgaard, J., de Raspide, M., Deconinck, N., Born, A., Baranello, G., Bertini, E., Schara, U., Goemans, N., Roubenoff, R., 2017. Safety and efficacy findings in the first-in-human trial (FIH) of the oral splice modulator branaplam in type 1 spinal muscular atrophy (SMA): interim results. *Neuromuscul. Disord.* 27, S207–S208. <https://doi.org/10.1016/j.nmd.2017.06.411>
- Chaytow, H., Huang, Y.-T., Gillingwater, T.H., Faller, K.M.E., 2018. The role of survival motor neuron protein (SMN) in protein homeostasis. *Cell. Mol. Life Sci.* 75, 3877–3894. <https://doi.org/10.1007/s00018-018-2849-1>
- Chen, K., Yuan, R., Geng, S., Zhang, Y., Ran, T., Kowalski, E., Liu, J., Li, L., 2017. Toll-interacting protein deficiency promotes neurodegeneration via impeding autophagy completion in high-fat diet-fed ApoE<sup>-/-</sup> mouse model. *Brain. Behav. Immun.* 59, 200–210.

<https://doi.org/10.1016/j.bbi.2016.10.002>

- Chen, X., Li, M., Li, L., Xu, S., Huang, D., Ju, M., Huang, J., Chen, K., Gu, H., 2016. Trehalose, sucrose and raffinose are novel activators of autophagy in human keratinocytes through an mTOR-independent pathway. *Sci. Rep.* 6, 28423. <https://doi.org/10.1038/srep28423>
- Cheng, X.T., Zhou, B., Lin, M.Y., Cai, Q., Sheng, Z.H., 2015. Axonal autophagosomes recruit dynein for retrograde transport through fusion with late endosomes. *J. Cell Biol.* 209, 377–386. <https://doi.org/10.1083/jcb.201412046>
- Chia, R., Achilli, F., Festing, M.F.W., Fisher, E.M.C., 2005. The origins and uses of mouse outbred stocks. *Nat. Genet.* 37, 1181–1186. <https://doi.org/10.1038/ng1665>
- Chiriboga, C.A., 2017. Expert Review of Neurotherapeutics Nusinersen for the treatment of spinal muscular atrophy Nusinersen for the treatment of spinal muscular atrophy. *Expert Rev. Neurother.* 17, 955–962. <https://doi.org/10.1080/14737175.2017.1364159>
- Cifuentes-Diaz, C., Frugier, T., Tiziano, F.D., Lacène, E., Roblot, N., Joshi, V., Moreau, M.H., Melki, J., 2001. Deletion of murine SMN exon 7 directed to skeletal muscle leads to severe muscular dystrophy. *J. Cell Biol.* 152, 1107–1114. <https://doi.org/10.1083/jcb.152.5.1107>
- Cifuentes-Diaz, C., Nicole, S., Velasco, M.E., Borra-Cebrian, C., Panozzo, C., Frugier, T., Millet, G., Roblot, N., Joshi, V., Melki, J., 2002. Neurofilament accumulation at the motor endplate and lack of axonal sprouting in a spinal muscular atrophy mouse model. *Hum. Mol. Genet.* 11, 1439–1447. <https://doi.org/10.1093/hmg/11.12.1439>
- Colunga, A., Bollino, D., Schech, A., Aurelian, L., 2014. Calpain-dependent clearance of the autophagy protein p62/SQSTM1 is a contributor to  $\Delta$ pK oncolytic activity in melanoma. *Gene Ther.* 21, 371–378. <https://doi.org/10.1038/gt.2014.6>
- Coover, D.D., Le, T.T., McAndrew, P.E., Strasswimmer, J., Crawford, T.O., Mendell, J.R., Coulson, S.E., Androphy, E.J., Prior, T.W., Burghes, A.H.M., 1997. The survival motor neuron protein in spinal muscular atrophy. *Hum. Mol. Genet.* 6, 1205–1214. <https://doi.org/10.1093/hmg/6.8.1205>
- Corti, S., Nizzardo, M., Nardini, M., Donadoni, C., Salani, S., Del Bo, R., Papadimitriou, D., Locatelli, F., Mezzina, N., Gianni, F., Bresolin, N., Comi, G.P., 2009. Motoneuron transplantation rescues the phenotype of SMARD1 (Spinal Muscular Atrophy with Respiratory Distress type 1). *J. Neurosci.* 29, 11761–11771. <https://doi.org/10.1523/JNEUROSCI.2734-09.2009>
- Corti, S., Nizzardo, M., Nardini, M., Donadoni, C., Salani, S., Ronchi, D., Simone, C., Falcone, M., Papadimitriou, D., Locatelli, F., Mezzina, N., Gianni, F., Bresolin, N., Comi, G.P., 2010. Embryonic stem cell-derived neural stem cells improve spinal muscular atrophy phenotype in mice. *Brain* 133, 465–81. <https://doi.org/10.1093/brain/awp318>
- Crawford, C., 1990. Protein and Peptide Inhibitors of Calpains. In Mellgren RL, Murachi T (eds). In Intracellular Calcium-dependent Proteolysis. Boca Raton, Fla: CRC Press. pp. 75–89.
- Crawford, T.O., Pardo, C.A., 1996. The neurobiology of childhood spinal muscular atrophy. *Neurobiol. Dis.* 3, 97–110. <https://doi.org/10.1006/nbdi.1996.0010>
- Crocker, S.J., Smith, P.D., Jackson-Lewis, V., Lamba, W.R., Hayley, S.P., Grimm, E., Callaghan, S.M., Slack, R.S., Melloni, E., Przedborski, S., Robertson, G.S., Anisman, H., Merali, Z., Park, D.S., 2003. Inhibition of calpains prevents neuronal and behavioral deficits in an MPTP mouse

- model of Parkinson's disease. *J. Neurosci.* 23, 4081–4091. <https://doi.org/10.1523/jneurosci.23-10-04081.2003>
- Cullheim, S., Fleshman, J.W., Glenn, L.L., Burke, R.E., 1987. Membrane area and dendritic structure in type-identified triceps surae alpha motoneurons. *J. Comp. Neurol.* 255, 68–81. <https://doi.org/10.1002/cne.902550106>
- Custer, S.K., Androphy, E.J., 2014. Autophagy dysregulation in cell culture and animals models of spinal muscular atrophy. *Mol. Cell. Neurosci.* 61, 133–40. <https://doi.org/10.1016/j.mcn.2014.06.006>
- Dachs, E., Hereu, M., Piedrafita, L., Casanovas, A., Calderó, J., Esquerda, J.E., 2011. Defective neuromuscular junction organization and postnatal myogenesis in mice with severe spinal muscular atrophy. *J. Neuropathol. Exp. Neurol.* 70, 444–461. <https://doi.org/10.1097/NEN.0b013e31821cbd8b>
- Darbar, I.A., Plaggert, P.G., Resende, M.B.D., Zanoteli, E., Reed, U.C., 2011. Evaluation of muscle strength and motor abilities in children with type II and III spinal muscle atrophy treated with valproic acid. *BMC Neurol.* 11, 36. <https://doi.org/10.1186/1471-2377-11-36>
- Das, A., Sribnick, E.A., Wingrave, J.M., Del Re, A.M., Woodward, J.J., Appel, S.H., Banik, N.L., Ray, S.K., 2005. Calpain activation in apoptosis of ventral spinal cord 4.1 (VSC4.1) motoneurons exposed to glutamate: Calpain inhibition provides functional neuroprotection. *J. Neurosci. Res.* 81, 551–562. <https://doi.org/10.1002/jnr.20581>
- Dasen, J.S., Jessell, T.M., 2009. Hox networks and the origins of motor neuron diversity. *Curr. Top. Dev. Biol.* 88, 169–200. [https://doi.org/10.1016/S0070-2153\(09\)88006-X](https://doi.org/10.1016/S0070-2153(09)88006-X)
- de Lahunta, A., Glass, E., 2009. Lower Motor Neuron, in: *Veterinary Neuroanatomy and Clinical Neurology*. Elsevier, pp. 77–133. <https://doi.org/10.1016/B978-0-7216-6706-5.00005-6>
- Dear, T.N., Boehm, T., 1999. Diverse mRNA expression patterns of the mouse calpain genes *Capn5*, *Capn6* and *Capn11* during development. *Mech. Dev.* 89, 201–9. [https://doi.org/10.1016/S0925-4773\(99\)00214-2](https://doi.org/10.1016/S0925-4773(99)00214-2)
- Dear, T.N., Meier, N.T., Hunn, M., Boehm, T., 2000. Gene structure, chromosomal localization, and expression pattern of *Capn12*, a new member of the calpain large subunit gene family. *Genomics* 68, 152–160. <https://doi.org/10.1006/geno.2000.6289>
- Dear, T.N., Möller, A., Boehm, T., 1999. CAPN11: A calpain with high mRNA levels in testis and located on chromosome 6. *Genomics* 59, 243–247. <https://doi.org/10.1006/geno.1999.5859>
- Dessaud, E., André, C., Scherrer, B., Berna, P., Pruss, R., Cuvier, V., Hauke, W., Bruno, C., Chabrol, B., Comi, G., Cuisset, J.M., Deconinck, N., Goemans, N., Estournet, B., Fontaine-Carbonel, S., Gorni, K., Kirschner, J., Lusakowska, A., Lochmuller, H., Mayer, M., Mercuri, E., Müller-Felber, W., Muntoni, F., Rivier, F., Roper, H., Schara, U., den Berg, L. Van, Vita, G., Walter, M., Bertini, E., 2014. G.O.19: Results of a phase II study to assess safety and efficacy of olesoxime (TRO19622) in 3–25 years old spinal muscular atrophy patients. *Neuromuscul. Disord.* 24, 920–921. <https://doi.org/10.1016/j.nmd.2014.06.418>
- Deter, R.L., De Duve, C., 1967. Influence of glucagon, an inducer of cellular autophagy, on some physical properties of rat liver lysosomes. *J. Cell Biol.* 33, 437–49. <https://doi.org/10.1083/jcb.33.2.437>

- Di Bartolomeo, S., Corazzari, M., Nazio, F., Oliverio, S., Lisi, G., Antonioli, M., Pagliarini, V., Matteoni, S., Fuoco, C., Giunta, L., D'Amelio, M., Nardacci, R., Romagnoli, A., Piacentini, M., Cecconi, F., Fimia, G.M., 2010. The dynamic interaction of AMBRA1 with the dynein motor complex regulates mammalian autophagy. *J. Cell Biol.* 191, 155–168. <https://doi.org/10.1083/jcb.201002100>
- Didonato, C.J., Bogdanik, L., Sumner, C., Burghes, A.H.M., 2011. Behavioral Phenotyping for neonates: Righting reflex SOP (ID) Number MD\_M.2.2.002.
- DiDonato, C.J., Chen, X.N., Noya, D., Korenberg, J.R., Nadeau, J.H., Simard, L.R., 1997. Cloning, characterization, and copy number of the murine survival motor neuron gene homolog of the spinal muscular atrophy-determining gene. *Genome Res.* 7, 339–352. <https://doi.org/10.1101/gr.7.4.339>
- Diepenbroek, M., Casadei, N., Esmer, H., Saido, T.C., Takano, J., Kahle, P.J., Nixon, R.A., Rao, M. V., Melki, R., Pieri, L., Helling, S., Marcus, K., Krueger, R., Masliah, E., Riess, O., Nuber, S., 2014. Over expression of the calpain-specific inhibitor calpastatin reduces human alpha-Synuclein processing, aggregation and synaptic impairment in [A30P]αSyn transgenic mice. *Hum. Mol. Genet.* 23, 3975–3989. <https://doi.org/10.1093/hmg/ddu112>
- Dikic, I., 2017. Proteasomal and Autophagic Degradation Systems. *Annu. Rev. Biochem.* 86, 193–224. <https://doi.org/10.1146/annurev-biochem-061516-044908>
- Dikic, I., Elazar, Z., 2018. Mechanism and medical implications of mammalian autophagy. *Nat. Rev. Mol. Cell Biol.* 19, 349–364. <https://doi.org/10.1038/s41580-018-0003-4>
- Dimitriadi, M., Derdowski, A., Kalloo, G., Maginnis, M.S., O'herm, P., Bliska, B., Sorkaç, A., Nguyen, K.C.Q., Cook, S.J., Poulogiannis, G., Atwood, W.J., Hall, D.H., Hart, A.C., 2016. Decreased function of survival motor neuron protein impairs endocytic pathways. *Proc. Natl. Acad. Sci. U. S. A.* 113, E4377-4386. <https://doi.org/10.1073/pnas.1600015113>
- Dimitriadi, M., Kye, M.J., Kalloo, G., Yersak, J.M., Sahin, M., Hart, A.C., 2013. The neuroprotective drug riluzole acts via small conductance Ca<sup>2+</sup>-activated K<sup>+</sup> supchannels to ameliorate defects in spinal muscular atrophy models. *J. Neurosci.* 33, 6557–6562. <https://doi.org/10.1523/JNEUROSCI.1536-12.2013>
- Dimitriadi, M., Sleigh, J.N., Walker, A., Chang, H.C., Sen, A., Kalloo, G., Harris, J., Barsby, T., Walsh, M.B., Satterlee, J.S., Li, C., van Vactor, D., Artavanis-Tsakonas, S., Hart, A.C., 2010. Conserved genes act as modifiers of invertebrate SMN loss of function defects. *PLoS Genet.* 6, 1–16. <https://doi.org/10.1371/journal.pgen.1001172>
- Doumit, M.E., Koohmaraie, M., 1999. Immunoblot analysis of calpastatin degradation: Evidence for cleavage by calpain in postmortem muscle. *J. Anim. Sci.* 77, 1467–1473. <https://doi.org/10.2527/1999.7761467x>
- Du, Z.-W., Chen, H., Liu, H., Lu, J., Qian, K., Huang, C.-L., Zhong, X., Fan, F., Zhang, S.-C., 2015. Generation and expansion of highly pure motor neuron progenitors from human pluripotent stem cells. *Nat. Commun.* 6, 6626. <https://doi.org/10.1038/ncomms7626>
- Dubowitz, V., 1999. Very severe spinal muscular atrophy (SMA type 0): An expanding clinical phenotype. *Eur. J. Paediatr. Neurol.* 3, 49–51. [https://doi.org/10.1016/S1090-3798\(99\)80012-9](https://doi.org/10.1016/S1090-3798(99)80012-9)
- Dufty, B.M., Warner, L.R., Hou, S.T., Jiang, S.X., Gomez-Isla, T., Leenhouts, K.M., Oxford, J.T., Feany,

- M.B., Masliah, E., Rohn, T.T., 2007. Calpain-cleavage of  $\alpha$ -synuclein: Connecting proteolytic processing to disease-linked aggregation. *Am. J. Pathol.* 170, 1725–1738. <https://doi.org/10.2353/ajpath.2007.061232>
- Durmus, H., Yilmaz, R., Gulsen-Parman, Y., Oflazer-Serdaroglu, P., Cuttini, M., Dursun, M.M. uh, Deymeer, F., 2017. Muscle magnetic resonance imaging in spinal muscular atrophy type 3: Selective and progressive involvement. *Muscle and Nerve* 55, 651–656. <https://doi.org/10.1002/mus.25385>
- duVerle, D., Takigawa, I., Ono, Y., Sorimachi, H., Mamitsuka, H., 2010. CaMPDB: a resource for calpain and modulatory proteolysis. *Genome Inform.* 22, 202–13. [https://doi.org/10.1142/9781848165786\\_0017](https://doi.org/10.1142/9781848165786_0017)
- Eccles, J.C., Eccles, R.M., Iggo, A., Lundberg, A., 1960. Electrophysiological Studies on Gamma Motoneurons. *Acta Physiol. Scand.* 50, 32–40. <https://doi.org/10.1111/j.1748-1716.1960.tb02070.x>
- Edens, B.M., Ajroud-Driss, S., Ma, L., Ma, Y.C., 2015. Molecular mechanisms and animal models of spinal muscular atrophy. *Biochim. Biophys. Acta - Mol. Basis Dis.* 1852, 685–692 <https://doi.org/10.1016/j.bbadis.2014.07.024>
- Edinger, A.L., Thompson, C.B., 2004. Death by design: apoptosis, necrosis and autophagy. *Curr. Opin. Cell Biol.* 16, 663–9. <https://doi.org/10.1016/j.ceb.2004.09.011>
- El-Khodor, B.F., Edgar, N., Chen, A., Winberg, M.L., Joyce, C., Brunner, D., Suárez-Fariñas, M., Heyes, M.P., 2008. Identification of a battery of tests for drug candidate evaluation in the SMN $\Delta$ 7 neonate model of spinal muscular atrophy. *Exp. Neurol.* 212, 29–43. <https://doi.org/10.1016/j.expneurol.2008.02.025>
- El-Khodor, B.F., Sumner, C., Hopkins, J., 2011. Behavioral Phenotyping for Neonates: Hind Limb Suspension Test (a.k.a. Tube Test) SOP (ID) Number SMA\_M.2.2.001.
- Emori, Y., Kawasaki, H., Imajoh, S., Imahori, K., Suzuki, K., 1987. Endogenous inhibitor for calcium-dependent cysteine protease contains four internal repeats that could be responsible for its multiple reactive sites. *Proc. Natl. Acad. Sci. U. S. A.* 84, 3590–3594. <https://doi.org/10.1073/pnas.84.11.3590>
- English, L., Chemali, M., Duron, J., Rondeau, C., Laplante, A., Gingras, D., Alexander, D., Leib, D., Norbury, C., Lippé, R., Desjardins, M., 2009. Autophagy enhances the presentation of endogenous viral antigens on MHC class I molecules during HSV-1 infection. *Nat. Immunol.* 10, 480–7. <https://doi.org/10.1038/ni.1720>
- Eskelinen, E.L., 2005. Maturation of autophagic vacuoles in Mammalian cells. *Autophagy.* 1, 1–10. <https://doi.org/10.4161/auto.1.1.1270>
- Fallini, C., Bassell, G.J., Rossoll, W., 2012. Spinal muscular atrophy: the role of SMN in axonal mRNA regulation. *Brain Res.* 1462, 81–92. <https://doi.org/10.1016/j.brainres.2012.01.044>
- Fallini, C., Bassell, G.J., Rossoll, W., 2010. High-efficiency transfection of cultured primary motor neurons to study protein localization, trafficking, and function. *Mol. Neurodegener.* 5, 17. <https://doi.org/10.1186/1750-1326-5-17>
- Fallini, C., Donlin-Asp, P.G., Rouanet, J.P., Bassell, G.J., Rossoll, W., 2016. Deficiency of the Survival of Motor Neuron Protein Impairs mRNA Localization and Local Translation in the Growth Cone

- of Motor Neurons. *J. Neurosci.* 36, 3811–20. <https://doi.org/10.1523/JNEUROSCI.2396-15.2016>
- Fallini, C., Rouanet, J.P., Donlin-Asp, P.G., Guo, P., Zhang, H., Singer, R.H., Rossoll, W., Bassell, G.J., 2014. Dynamics of survival of motor neuron (SMN) protein interaction with the mRNA-binding protein IMP1 facilitates its trafficking into motor neuron axons. *Dev. Neurobiol.* 74, 319–332. <https://doi.org/10.1002/dneu.22111>
- Farooq, F., Balabanian, S., Liu, X., Holcik, M., MacKenzie, A., 2009. p38 Mitogen-activated protein kinase stabilizes SMN mRNA through RNA binding protein HuR. *Hum. Mol. Genet.* 18, 4035–45. <https://doi.org/10.1093/hmg/ddp352>
- Farooq, F., Molina, F.A., Hadwen, J., MacKenzie, D., Witherspoon, L., Osmond, M., Holcik, M., MacKenzie, A., 2011. Prolactin increases SMN expression and survival in a mouse model of severe spinal muscular atrophy via the STAT5 pathway. *J. Clin. Invest.* 121, 3042–50. <https://doi.org/10.1172/JCI46276>
- Feather-Schussler, D.N., Ferguson, T.S., 2016. A battery of motor tests in a neonatal mouse model of cerebral palsy. *J. Vis. Exp.* 2016. <https://doi.org/10.3791/53569>
- Ferreira, A., 2012. Calpain Dysregulation in Alzheimer's Disease. *ISRN Biochem.* 2012, 1–12. <https://doi.org/10.5402/2012/728571>
- Finkel, R.S., McDermott, M.P., Kaufmann, P., Darras, B.T., Chung, W.K., Sproule, D.M., Kang, P.B., Reghan Foley, A., Yang, M.L., Martens, W.B., Oskoui, M., Glanzman, A.M., Flickinger, J., Montes, J., Dunaway, S., O'Hagen, J., Quigley, J., Riley, S., Benton, M., Ryan, P.A., Montgomery, M., Marra, J., Gooch, C., De Vivo, D.C., 2014. Observational study of spinal muscular atrophy type I and implications for clinical trials. *Neurology* 83, 810–817. <https://doi.org/10.1212/WNL.0000000000000741>
- Finkel, R.S., Mercuri, E., Darras, B.T., Connolly, A.M., Kuntz, N.L., Kirschner, J., Chiriboga, C.A., Saito, K., Servais, L., Tizzano, E., Topaloglu, H., Tulinius, M., Montes, J., Glanzman, A.M., Bishop, K., Zhong, Z.J., Gheuens, S., Bennett, C.F., Schneider, E., Farwell, W., De Vivo, D.C., 2017. Nusinersen versus Sham Control in Infantile-Onset Spinal Muscular Atrophy. *N. Engl. J. Med.* 377, 1723–1732. <https://doi.org/10.1056/NEJMoa1702752>
- Finkel, R.S., Mercuri, E., Meyer, O.H., Simonds, A.K., Schroth, M.K., Graham, R.J., Kirschner, J., Iannaccone, S.T., Crawford, T.O., Woods, S., Muntoni, F., Wirth, B., Montes, J., Main, M., Mazzone, E.S., Vitale, M., Snyder, B., Quijano-Roy, S., Bertini, E., Davis, R.H., Qian, Y., Sejersen, T., 2018. Diagnosis and management of spinal muscular atrophy: Part 2: Pulmonary and acute care; medications, supplements and immunizations; other organ systems; and ethics. *Neuromuscul. Disord.* 28, 197–207. <https://doi.org/10.1016/j.nmd.2017.11.004>
- Fischer, U., Liu, Q., Dreyfuss, G., 1997. The SMN-SIP1 complex has an essential role in spliceosomal snRNP biogenesis. *Cell* 90, 1023–1029. [https://doi.org/10.1016/S0092-8674\(00\)80368-2](https://doi.org/10.1016/S0092-8674(00)80368-2)
- Fletcher, E. V., Simon, C.M., Pagiazitis, J.G., Chalif, J.I., Vukojicic, A., Drobac, E., Wang, X., Mentis, G.Z., 2017. Reduced sensory synaptic excitation impairs motor neuron function via Kv2.1 in spinal muscular atrophy. *Nat. Neurosci.* 20, 905–916. <https://doi.org/10.1038/nn.4561>
- Foran, E., Kwon, D.Y., Nofziger, J.H., Arnold, E.S., Hall, M.D., Fischbeck, K.H., Burnett, B.G., 2016. CNS uptake of bortezomib is enhanced by P-glycoprotein inhibition: implications for spinal muscular atrophy. *Neurobiol. Dis.* 88, 118–24. <https://doi.org/10.1016/j.nbd.2016.01.008>

- Foust, K.D., Wang, X., McGovern, V.L., Braun, L., Bevan, A.K., Haidet, A.M., Le, T.T., Morales, P.R., Rich, M.M., Burghes, A.H.M., Kaspar, B.K., 2010. Rescue of the spinal muscular atrophy phenotype in a mouse model by early postnatal delivery of SMN. *Nat. Biotechnol.* 28, 271–274. <https://doi.org/10.1038/nbt.1610>
- Friedrich, P., 2004. The intriguing Ca<sup>2+</sup> requirement of calpain activation. *Biochem. Biophys. Res. Commun.* 323, 1131–1133. <https://doi.org/10.1016/j.bbrc.2004.08.194>
- Frugier, T., Tiziano, F.D., Cifuentes-Diaz, C., Miniou, P., Roblot, N., Dierich, A., Le Meur, M., Melki, J., 2000. Nuclear targeting defect of SMN lacking the C-terminus in a mouse model of spinal muscular atrophy. *Hum. Mol. Genet.* 9, 849–858. <https://doi.org/10.1093/hmg/9.5.849>
- Fuentes, J.L., Strayer, M.S., Matera, A.G., 2010. Molecular determinants of survival motor neuron (SMN) protein cleavage by the calcium-activated protease, calpain. *PLoS One* 5, e15769. <https://doi.org/10.1371/journal.pone.0015769>
- Fujikake, N., Shin, M., Shimizu, S., 2018. Association between autophagy and neurodegenerative diseases. *Front. Neurosci.* 12. <https://doi.org/10.3389/fnins.2018.00255>
- Gabanella, F., Butchbach, M.E.R., Saieva, L., Carissimi, C., Burghes, A.H.M., Pellizzoni, L., 2007. Ribonucleoprotein assembly defects correlate with spinal muscular atrophy severity and preferentially affect a subset of spliceosomal snRNPs. *PLoS One.* 2, e921. <https://doi.org/10.1371/journal.pone.0000921>
- Gafni, J., Ellerby, L.M., 2002. Calpain Activation in Huntington's Disease. *J. Neurosci.* 22, 4842–4849. <https://doi.org/10.1523/jneurosci.22-12-04842.2002>
- Gafni, J., Hermel, E., Young, J.E., Wellington, C.L., Hayden, M.R., Ellerby, L.M., 2004. Inhibition of calpain cleavage of Huntingtin reduces toxicity: Accumulation of calpain/caspase fragments in the nucleus. *J. Biol. Chem.* 279, 20211–20220. <https://doi.org/10.1074/jbc.M401267200>
- Gal, J., Ström, A.-L., Kwinter, D.M., Kilty, R., Zhang, J., Shi, P., Fu, W., Wooten, M.W., Zhu, H., 2009. Sequestosome 1/p62 links familial ALS mutant SOD1 to LC3 via an ubiquitin-independent mechanism. *J. Neurochem.* 111, 1062–73. <https://doi.org/10.1111/j.1471-4159.2009.06388.x>
- Ganley, I.G., Lam, D.H., Wang, J., Ding, X., Chen, S., Jiang, X., 2009. ULK1.ATG13.FIP200 complex mediates mTOR signaling and is essential for autophagy. *J. Biol. Chem.* 284, 12297–305. <https://doi.org/10.1074/jbc.M900573200>
- Garbes, L., Heesen, L., Hölker, I., Bauer, T., Schreml, J., Zimmermann, K., Thoenes, M., Walter, M., Dimos, J., Peitz, M., Brüstle, O., Heller, R., Wirth, B., 2013. VPA response in SMA is suppressed by the fatty acid translocase CD36. *Hum. Mol. Genet.* 22, 398–407. <https://doi.org/10.1093/hmg/dds437>
- Garcera, A., Bahi, N., Periyakaruppiyah, A., Arumugam, S., Soler, R.M., 2013. Survival motor neuron protein reduction deregulates autophagy in spinal cord motoneurons in vitro. *Cell Death Dis.* 4, e686(2013) ..<https://doi.org/10.1038/cddis.2013.209>
- Garcera, A., Mincheva, S., Gou-Fabregas, M., Caraballo-Miralles, V., Lladó, J., Comella, J.X., Soler, R.M., 2011. A new model to study spinal muscular atrophy: neurite degeneration and cell death is counteracted by BCL-X(L) Overexpression in motoneurons. *Neurobiol. Dis.* 42, 415–26. <https://doi.org/10.1016/j.nbd.2011.02.003>
- Gavet, O., Pines, J., 2010. Progressive Activation of CyclinB1-Cdk1 Coordinates Entry to Mitosis. *Dev.*

- Cell 18, 533–543. <https://doi.org/10.1016/j.devcel.2010.02.013>
- Gavrilina, T.O., McGovern, V.L., Workman, E., Crawford, T.O., Gogliotti, R.G., Didonato, C.J., Monani, U.R., Morris, G.E., Burghes, A.H.M., 2008. Neuronal SMN expression corrects spinal muscular atrophy in severe SMA mice while muscle-specific SMN expression has no phenotypic effect. *Hum. Mol. Genet.* 17, 1063–1075. <https://doi.org/10.1093/hmg/ddm379>
- Ge, L., Melville, D., Zhang, M., Schekman, R., 2013. The ER–Golgi intermediate compartment is a key membrane source for the LC3 lipidation step of autophagosome biogenesis. *Elife* 2, e00947. <https://doi.org/10.7554/eLife.00947>
- Giesemann, T., Rathke-Hartlieb, S., Rothkegel, M., Bartsch, J.W., Buchmeier, S., Jockusch, B.M., Jockusch, H., 1999. A role for polyproline motifs in the spinal muscular atrophy protein SMN. Profilins bind to and colocalize with SMN in nuclear gems. *J. Biol. Chem.* 274, 37908–37914. <https://doi.org/10.1074/jbc.274.53.37908>
- Glick, D., Barth, S., Macleod, K.F., 2010. Autophagy: Cellular and molecular mechanisms. *J. Pathol.* 221, 3–12. <https://doi.org/10.1002/path.2697>
- Glock, C., Heumüller, M., Schuman, E.M., 2017. mRNA transport & local translation in neurons. *Curr. Opin. Neurobiol.* 45, 169–177. <https://doi.org/10.1016/j.conb.2017.05.005>
- Goll, D.E., Thompson, V.F., Li, H., Wei, W., Cong, J., 2003. The calpain system. *Physiol. Rev.* 83, 731–801. <https://doi.org/10.1152/physrev.00029.2002>
- Gombash, S.E., Cowley, C.J., Fitzgerald, J.A., Iyer, C.C., Fried, D., McGovern, V.L., Williams, K.C., Burghes, A.H.M., Christofi, F.L., Gulbransen, B.D., Foust, K.D., 2015. SMN deficiency disrupts gastrointestinal and enteric nervous system function in mice. *Hum. Mol. Genet.* 24, 3847–3860. <https://doi.org/10.1093/hmg/ddv127>
- Gorecka, J., Kostiuk, V., Fereydooni, A., Gonzalez, L., Luo, J., Dash, B., Isaji, T., Ono, S., Liu, S., Lee, S.R., Xu, J., Liu, J., Taniguchi, R., Yastula, B., Hsia, H.C., Qyang, Y., Dardik, A., 2019. The potential and limitations of induced pluripotent stem cells to achieve wound healing. *Stem Cell Res. Ther.* 10, 87. <https://doi.org/10.1186/s13287-019-1185-1>
- Gou-Fabregas, M., Garcera, A., Mincheva, S., Perez-Garcia, M.J., Comella, J.X., Soler, R.M., 2009. Specific vulnerability of mouse spinal cord motoneurons to membrane depolarization. *J. Neurochem.* 110, 1842–54. <https://doi.org/10.1111/j.1471-4159.2009.06278.x>
- Gou-Fabregas, M., Ramírez-Núñez, O., Cacabelos, D., Bahi, N., Portero, M., Garcera, A., Soler, R.M., 2014. Calpain activation and CaMKIV reduction in spinal cords from hSOD1G93A mouse model. *Mol. Cell. Neurosci.* 61, 219–225. <https://doi.org/10.1016/j.mcn.2014.07.002>
- Greensmith, L., Vrbová, G., 1997. Disturbances of neuromuscular interaction may contribute to muscle weakness in spinal muscular atrophy. *Neuromuscul. Disord.* 7, 369–372. [https://doi.org/10.1016/S0960-8966\(97\)00047-3](https://doi.org/10.1016/S0960-8966(97)00047-3)
- Greenwood, A.F., Jope, R.S., 1994. Brain G-protein proteolysis by calpain: enhancement by lithium. *Brain Res.* 636, 320–326. [https://doi.org/10.1016/0006-8993\(94\)91031-6](https://doi.org/10.1016/0006-8993(94)91031-6)
- Groen, E.J.N., Fumoto, K., Blokhuis, A.M., Engelen-Lee, J., Zhou, Y., van den Heuvel, D.M.A., Koppers, M., van Diggelen, F., van Heest, J., Demmers, J.A.A., Kirby, J., Shaw, P.J., Aronica, E., Spliet, W.G.M., Veldink, J.H., van den Berg, L.H., Pasterkamp, R.J., 2013. ALS-associated mutations in FUS disrupt the axonal distribution and function of SMN. *Hum. Mol. Genet.* 22,



- 3690–704. <https://doi.org/10.1093/hmg/ddt222>
- Guo, F., Liu, X., Cai, H., Le, W., 2018. Autophagy in neurodegenerative diseases: pathogenesis and therapy. *Brain Pathol.* 28, 3-13. <https://doi.org/10.1111/bpa.12545>
- Guroff, G., 1964. A Neutral, Calcium-activated Proteinase from the Soluble Fraction of Rat Brain, *The Journal of biological chemistry.* 239, 149–155. ISSN: 00219258
- Gutierrez, M.G., Munafó, D.B., Berón, W., Colombo, M.I., 2004. Rab7 is required for the normal progression of the autophagic pathway in mammalian cells. *J. Cell Sci.* 117, 2687–97. <https://doi.org/10.1242/jcs.01114>
- Guyton, M.K., Das, A., Samantaray, S., Wallace IV, G.C., Butler, J.T., Ray, S.K., Banik, N.L., 2010. Calpeptin attenuated inflammation, cell death, and axonal damage in animal model of multiple sclerosis. *J. Neurosci. Res.* 88, 2398–2408. <https://doi.org/10.1002/jnr.22408>
- Hailey, D.W., Rambold, A.S., Satpute-Krishnan, P., Mitra, K., Sougrat, R., Kim, P.K., Lippincott-Schwartz, J., 2010. Mitochondria supply membranes for autophagosome biogenesis during starvation. *Cell* 141, 656–67. <https://doi.org/10.1016/j.cell.2010.04.009>
- Hamasaki, M., Furuta, N., Matsuda, A., Nezu, A., Yamamoto, A., Fujita, N., Oomori, H., Noda, T., Haraguchi, T., Hiraoka, Y., Amano, A., Yoshimori, T., 2013. Autophagosomes form at ER-mitochondria contact sites. *Nature* 495, 389–393. <https://doi.org/10.1038/nature11910>
- Hambley, B., Caimi, P.F., William, B.M., 2016. Bortezomib for the treatment of mantle cell lymphoma: an update. *Ther. Adv. Hematol.* 7, 196–208. <https://doi.org/10.1177/2040620716648566>
- Hamilton, G., Gillingwater, T.H., 2013. Spinal muscular atrophy: going beyond the motor neuron. *Trends Mol. Med.* 19, 40–50. <https://doi.org/10.1016/j.molmed.2012.11.002>
- Hammond, S.M., Gogliotti, R.G., Rao, V., Beauvais, A., Kothary, R., DiDonato, C.J., 2010. Mouse survival motor neuron alleles that mimic SMN2 splicing and are inducible rescue embryonic lethality early in development but not late. *PLoS One* 5, e15887. <https://doi.org/10.1371/journal.pone.0015887>
- Hanna, R.A., Campbell, R.L., Davies, P.L., 2008. Calcium-bound structure of calpain and its mechanism of inhibition by calpastatin. *Nature* 456, 409–412. <https://doi.org/10.1038/nature07451>
- Hanna, R.A., Garcia-Diaz, B.E., Davies, P.L., 2007. Calpastatin simultaneously binds four calpains with different kinetic constants. *FEBS Lett.* 581, 2894–2898. <https://doi.org/10.1016/j.febslet.2007.05.035>
- Hannon, G.J., Rossi, J.J., 2004. Unlocking the potential of the human genome with RNA interference. *Nature.* 431, 371-378. <https://doi.org/10.1038/nature02870>
- Hao, L.T., Burghes, A.H.M., Beattie, C.E., 2011. Generation and Characterization of a genetic zebrafish model of SMA carrying the human SMN2 gene. *Mol. Neurodegener.* 6, 24. <https://doi.org/10.1186/1750-1326-6-24>
- Hao, L.T., Duy, P.Q., Jontes, J.D., Beattie, C.E., 2015. Motoneuron development influences dorsal root ganglia survival and Schwann cell development in a vertebrate model of spinal muscular atrophy. *Hum. Mol. Genet.* 24, 346–360. <https://doi.org/10.1093/hmg/ddu447>

- Hao, L.T., Wolman, M., Granato, M., Beattie, C.E., 2012. Survival motor neuron affects plastin 3 protein levels leading to motor defects. *J. Neurosci.* 32, 5074–5084. <https://doi.org/10.1523/JNEUROSCI.5808-11.2012>
- Hara, T., Nakamura, K., Matsui, M., Yamamoto, A., Nakahara, Y., Suzuki-Migishima, R., Yokoyama, M., Mishima, K., Saito, I., Okano, H., Mizushima, N., 2006. Suppression of basal autophagy in neural cells causes neurodegenerative disease in mice. *Nature* 441, 885–9. <https://doi.org/10.1038/nature04724>
- Harada, Y., Sutomo, R., Sadewa, A.H., Akutsu, T., Takeshima, Y., Wada, H., Matsuo, M., Nishio, H., 2002. Correlation between SMN2 copy number and clinical phenotype of spinal muscular atrophy: three SMN2 copies fail to rescue some patients from the disease severity. *J. Neurol.* 249, 1211–9. <https://doi.org/10.1007/s00415-002-0811-4>
- Hayashi-Nishino, M., Fujita, N., Noda, T., Yamaguchi, A., Yoshimori, T., Yamamoto, A., 2009. A subdomain of the endoplasmic reticulum forms a cradle for autophagosome formation. *Nat. Cell Biol.* 11, 1433–1437. <https://doi.org/10.1038/ncb1991>
- Hayat, M.A., 2017. Overview of Autophagy, in: *Autophagy: Cancer, Other Pathologies, Inflammation, Immunity, Infection, and Aging*. Elsevier, pp. 1–122. <https://doi.org/10.1016/B978-0-12-812146-7.00001-9>
- Hayhurst, M., Wagner, A.K., Cerletti, M., Wagers, A.J., Rubin, L.L., 2012. A cell-autonomous defect in skeletal muscle satellite cells expressing low levels of survival of motor neuron protein. *Dev. Biol.* 368, 323–334. <https://doi.org/10.1016/j.ydbio.2012.05.037>
- He, C., Klionsky, D.J., 2009. Regulation Mechanisms and Signaling Pathways of Autophagy. *Annu. Rev. Genet.* 43, 67–93. <https://doi.org/10.1146/annurev-genet-102808-114910>
- Heier, C.R., Satta, R., Lutz, C., Didonato, C.J., 2010. Arrhythmia and cardiac defects are a feature of spinal muscular atrophy model mice. *Hum. Mol. Genet.* 19, 3906–3918. <https://doi.org/10.1093/hmg/ddq330>
- Hensel, N., Claus, P., 2018. The Actin Cytoskeleton in SMA and ALS: How Does It Contribute to Motoneuron Degeneration? *Neuroscientist.* 24, 54–72. <https://doi.org/10.1177/1073858417705059>
- Hosokawa, N., Hara, T., Kaizuka, T., Kishi, C., Takamura, A., Miura, Y., Iemura, S.I., Natsume, T., Takehana, K., Yamada, N., Guan, J.L., Oshiro, N., Mizushima, N., 2009. Nutrient-dependent mTORC1 association with the ULK1-Atg13-FIP200 complex required for autophagy. *Mol. Biol. Cell* 20, 1981–1991. <https://doi.org/10.1091/mbc.E08-12-1248>
- Hsieh-Li, H.M., Chang, J.G., Jong, Y.J., Wu, M.H., Wang, N.M., Tsai, C.H., Li, H., 2000. A mouse model for spinal muscular atrophy. *Nat. Genet.* 24, 66–70. <https://doi.org/10.1038/71709>
- Hubers, L., Valderrama-Carvajal, H., Laframboise, J., Timbers, J., Sanchez, G., Côté, J., 2011. HuD interacts with survival motor neuron protein and can rescue spinal muscular atrophy-like neuronal defects. *Hum. Mol. Genet.* 20, 553–79. <https://doi.org/10.1093/hmg/ddq500>
- Hurley, J.H., Young, L.N., 2017. Mechanisms of Autophagy Initiation. *Annu. Rev. Biochem.* 86, 225–244. <https://doi.org/10.1146/annurev-biochem-061516-044820>
- Husedzinovic, A., Oppermann, F., Draeger-Meurer, S., Chari, A., Fischer, U., Daub, H., Gruss, O.J., 2014. Phosphoregulation of the human SMN complex. *Eur. J. Cell Biol.* 93, 106–17.

<https://doi.org/10.1016/j.ejcb.2014.01.006>

- Ivanhoe, C.B., Reistetter, T.A., 2004. Spasticity: the misunderstood part of the upper motor neuron syndrome. *Am. J. Phys. Med. Rehabil.* 83, S3-9. <https://doi.org/10.1097/01.phm.0000141125.28611.3e>
- Jablonka, S., Beck, M., Lechner, B.D., Mayer, C., Sendtner, M., 2007. Defective Ca<sup>2+</sup> channel clustering in axon terminals disturbs excitability in motoneurons in spinal muscular atrophy. *J. Cell Biol.* 179, 139–149. <https://doi.org/10.1083/jcb.200703187>
- Jäger, S., Bucci, C., Tanida, I., Ueno, T., Kominami, E., Saftig, P., Eskelinen, E.-L., 2004. Role for Rab7 in maturation of late autophagic vacuoles. *J. Cell Sci.* 117, 4837–48. <https://doi.org/10.1242/jcs.01370>
- Jessell, T.M., 2000. Neuronal specification in the spinal cord: Inductive signals and transcriptional codes. *Nat. Rev. Genet.* 1, 20–29. <https://doi.org/10.1038/35049541>
- Jung, C.H., Jun, C.B., Ro, S.H., Kim, Y.M., Otto, N.M., Cao, J., Kundu, M., Kim, D.H., 2009. ULK-Atg13-FIP200 complexes mediate mTOR signaling to the autophagy machinery. *Mol. Biol. Cell* 20, 1992–2003. <https://doi.org/10.1091/mbc.E08-12-1249>
- Kabeya, Y., Mizushima, N., Ueno, T., Yamamoto, A., Kirisako, T., Noda, T., Kominami, E., Ohsumi, Y., Yoshimori, T., 2000. LC3, a mammalian homologue of yeast Apg8p, is localized in autophagosomal membranes after processing. *EMBO J.* 19, 5720–5728. <https://doi.org/10.1093/emboj/19.21.5720>
- Kania, A., 2014. Spinal motor neuron migration and the significance of topographic organization in the nervous system. *Adv. Exp. Med. Biol.* 800, 133–48. [https://doi.org/10.1007/978-94-007-7687-6\\_8](https://doi.org/10.1007/978-94-007-7687-6_8)
- Kanning, K.C., Kaplan, A., Henderson, C.E., 2010. Motor neuron diversity in development and disease. *Annu. Rev. Neurosci.* 33, 409–40. <https://doi.org/10.1146/annurev.neuro.051508.135722>
- Kanno, H., Ozawa, H., Sekiguchi, A., Itoi, E., 2009. The role of autophagy in spinal cord injury. *Autophagy* 5, 390–2. <https://doi.org/10.4161/auto.5.3.7724>
- Kariya, S., Park, G.H., Maeno-Hikichi, Y., Leykekhman, O., Lutz, C., Arkovitz, M.S., Landmesser, L.T., Monani, U.R., 2008. Reduced SMN protein impairs maturation of the neuromuscular junctions in mouse models of spinal muscular atrophy. *Hum. Mol. Genet.* 17, 2552–2569. <https://doi.org/10.1093/hmg/ddn156>
- Kashima, T., Manley, J.L., 2003. A negative element in SMN2 exon 7 inhibits splicing in spinal muscular atrophy. *Nat. Genet.* 34, 460–3. <https://doi.org/10.1038/ng1207>
- Kernochan, L.E., Russo, M.L., Woodling, N.S., Huynh, T.N., Avila, A.M., Fischbeck, K.H., Sumner, C.J., 2005. The role of histone acetylation in SMN gene expression. *Hum. Mol. Genet.* 14, 1171–82. <https://doi.org/10.1093/hmg/ddi130>
- Khatri, I.A., Chaudhry, U.S., Seikaly, M.G., Browne, R.H., Iannaccone, S.T., 2008. Low bone mineral density in spinal muscular atrophy. *J. Clin. Neuromuscul. Dis.* 10, 11–17. <https://doi.org/10.1097/CND.0b013e318183e0fa>
- Kim, C., Yun, N., Lee, Y.M., Jeong, J.Y., Baek, J.Y., Song, H.Y., Ju, C., Youdim, M.B.H., Jin, B.K., Kim,

- W.K., Oh, Y.J., 2013. Gel-Based protease proteomics for identifying the novel calpain substrates in dopaminergic neuronal cell. *J. Biol. Chem.* 288, 36717–36732. <https://doi.org/10.1074/jbc.M113.492876>
- Kim, Y.C., Guan, K.L., 2015. mTOR: A pharmacologic target for autophagy regulation. *J. Clin. Invest.* 125, 25–32. <https://doi.org/10.1172/JCI73939>
- King, J.S., 2012. Autophagy across the eukaryotes: Is *S. cerevisiae* the odd one out? *Autophagy.* 8, 1159–1162. <https://doi.org/10.4161/auto.20527>
- Kirkin, V., McEwan, D.G., Novak, I., Dikic, I., 2009. A role for ubiquitin in selective autophagy. *Mol. Cell* 34, 259–69. <https://doi.org/10.1016/j.molcel.2009.04.026>
- Klionsky, D.J., Eskelinen, E.L., Deretic, V., 2014. Autophagosomes, phagosomes, autolysosomes, phagolysosomes, autophagolysosomes... Wait, I'm confused. *Autophagy.* 10, 549–551. <https://doi.org/10.4161/auto.28448>
- Koike, M., Shibata, M., Waguri, S., Yoshimura, K., Tanida, I., Kominami, E., Gotow, T., Peters, C., von Figura, K., Mizushima, N., Saftig, P., Uchiyama, Y., 2005. Participation of autophagy in storage of lysosomes in neurons from mouse models of neuronal ceroid-lipofuscinoses (Batten disease). *Am. J. Pathol.* 167, 1713–28. [https://doi.org/10.1016/S0002-9440\(10\)61253-9](https://doi.org/10.1016/S0002-9440(10)61253-9)
- Kolb, S.J., Kissel, J.T., 2015. Spinal Muscular Atrophy. *Neurol. Clin.* 33, 831–846. <https://doi.org/10.1016/j.ncl.2015.07.004>
- Kolobkova, Y.A., Vigont, V.A., Shalygin, A. V., Kaznacheyeva, E. V., 2017. Huntington's disease: Calcium dyshomeostasis and pathology models. *Acta Naturae.* 9, 34–46. <https://doi.org/10.32607/20758251-2017-9-2-34-46>
- Komatsu, M., Qing, J.W., Holstein, G.R., Friedrich, V.L., Iwata, J.I., Kominami, E., Chait, B.T., Tanaka, K., Yue, Z., 2007. Essential role for autophagy protein Atg7 in the maintenance of axonal homeostasis and the prevention of axonal degeneration. *Proc. Natl. Acad. Sci. U. S. A.* 104, 14489–14494. <https://doi.org/10.1073/pnas.0701311104>
- Komatsu, M., Waguri, S., Chiba, T., Murata, S., Iwata, J., Tanida, I., Ueno, T., Koike, M., Uchiyama, Y., Kominami, E., Tanaka, K., 2006. Loss of autophagy in the central nervous system causes neurodegeneration in mice. *Nature.* 441, 880–4. <https://doi.org/10.1038/nature04723>
- Kong, L., Wang, X., Choe, D.W., Polley, M., Burnett, B.G., Bosch-Marcé, M., Griffin, J.W., Rich, M.M., Sumner, C.J., 2009. Impaired synaptic vesicle release and immaturity of neuromuscular junctions in spinal muscular atrophy mice. *J. Neurosci.* 29, 842–851. <https://doi.org/10.1523/JNEUROSCI.4434-08.2009>
- Krosschell, K.J., Kissel, J.T., Townsend, E.L., Simeone, S.D., Zhang, R.Z., Reyna, S.P., Crawford, T.O., Schroth, M.K., Acsadi, G., Kishnani, P.S., Von Kleist-Retzow, J.-C., Hero, B., D'Anjou, G., Smith, E.C., Elsheikh, B., Simard, L.R., Prior, T.W., Scott, C.B., Lasalle, B., Sakonju, A., Wirth, B., Swoboda, K.J., Project Cure SMA Investigator's Network, 2018. Clinical trial of L-Carnitine and valproic acid in spinal muscular atrophy type I. *Muscle Nerve.* 57, 193–199. <https://doi.org/10.1002/mus.25776>
- Kumagai, T., Hashizume, Y., 1982. Morphological and morphometric studies on the spinal cord lesion in Werdnig-Hoffmann disease. *Brain Dev.* 4, 87–96. [https://doi.org/10.1016/S0387-7604\(82\)80002-8](https://doi.org/10.1016/S0387-7604(82)80002-8)

- Kwon, D.Y., Motley, W.W., Fischbeck, K.H., Burnett, B.G., 2011. Increasing expression and decreasing degradation of SMN ameliorate the spinal muscular atrophy phenotype in mice. *Hum. Mol. Genet.* 20, 3667–77. <https://doi.org/10.1093/hmg/ddr288>
- Lafarga, V., Tapia, O., Sharma, S., Bengoechea, R., Stoecklin, G., Lafarga, M., Berciano, M.T., 2018. CBP-mediated SMN acetylation modulates Cajal body biogenesis and the cytoplasmic targeting of SMN. *Cell. Mol. Life Sci.* 75, 527–546. <https://doi.org/10.1007/s00018-017-2638-2>
- Laplante, M., Sabatini, D.M., 2012. mTOR signaling in growth control and disease. *Cell.* 149, 274–293. <https://doi.org/10.1016/j.cell.2012.03.017>
- Larsen, K.B., Lamark, T., Øvervatn, A., Harneshaug, I., Johansen, T., Bjørkøy, G., 2010. A reporter cell system to monitor autophagy based on p62/SQSTM1. *Autophagy* 6, 784–93. <https://doi.org/10.4161/auto.6.6.12510>
- Le, T.T., Covert, D.D., Monani, U.R., Morris, G.E., Burghes, A.H.M., 2000. The survival motor neuron (SMN) protein: effect of exon loss and mutation on protein localization. *Neurogenetics* 3, 7–16. <https://doi.org/10.1007/s100480000090>
- Le, T.T., Pham, L.T., Butchbach, M.E.R., Zhang, H.L., Monani, U.R., Covert, D.D., Gavriliina, T.O., Xing, L., Bassell, G.J., Burghes, A.H.M., 2005. SMN $\Delta$ 7, the major product of the centromeric survival motor neuron (SMN2) gene, extends survival in mice with spinal muscular atrophy and associates with full-length SMN. *Hum. Mol. Genet.* 14, 845–857. <https://doi.org/10.1093/hmg/ddi078>
- Lee, R.H., Heckman, C.J., 1998. Bistability in spinal motoneurons in vivo: Systematic variations in persistent inward currents. *J. Neurophysiol.* 80, 583–593. <https://doi.org/10.1152/jn.1998.80.2.583>
- Lefebvre, S., Bürglen, L., Reboullet, S., Clermont, O., Burlet, P., Viollet, L., Benichou, B., Cruaud, C., Millasseau, P., Zeviani, M., Le Paslier, D., Frézal, J., Cohen, D., Weissenbach, J., Munnich, A., Melki, J., 1995. Identification and characterization of a spinal muscular atrophy-determining gene. *Cell* 80, 155–165. [https://doi.org/10.1016/0092-8674\(95\)90460-3](https://doi.org/10.1016/0092-8674(95)90460-3)
- Lefebvre, S., Burlet, P., Liu, Q., Bertrand, S., Clermont, O., Munnich, A., Dreyfuss, G., Melki, J., 1997. Correlation between severity and SMN protein level in spinal muscular atrophy. *Nat. Genet.* 16, 265–9. <https://doi.org/10.1038/ng0797-265>
- Liu, Q., Dreyfuss, G., 1996. A novel nuclear structure containing the survival of motor neurons protein. *EMBO J.* 15, 3555–3565. <https://doi.org/10.1002/j.1460-2075.1996.tb00725.x>
- Liu, W.J., Ye, L., Huang, W.F., Guo, L.J., Xu, Z.G., Wu, H.L., Yang, C., Liu, H.F., 2016. p62 links the autophagy pathway and the ubiquitin-proteasome system upon ubiquitinated protein degradation. *Cell. Mol. Biol. Lett.* 21, 29. <https://doi.org/10.1186/s11658-016-0031-z>
- Locatelli, D., Terao, M., Kurosaki, M., Zanellati, M.C., Pletto, D.R., Finardi, A., Colciaghi, F., Garattini, E., Battaglia, G.S., 2015. Different stability and proteasome-mediated degradation rate of SMN protein isoforms. *PLoS One* 10. <https://doi.org/10.1371/journal.pone.0134163>
- Long, K.K., O’Shea, K.M., Khairallah, R.J., Howell, K., Paushkin, S., Chen, K.S., Cote, S.M., Webster, M.T., Stains, J.P., Treece, E., Buckler, A., Donovan, A., 2019. Specific inhibition of myostatin activation is beneficial in mouse models of SMA therapy. *Hum. Mol. Genet.* 28, 1076–1089. <https://doi.org/10.1093/hmg/ddy382>

- Lorson, C.L., 2000. An exonic enhancer is required for inclusion of an essential exon in the SMA-determining gene SMN. *Hum. Mol. Genet.* 9, 259–265. <https://doi.org/10.1093/hmg/9.2.259>
- Lorson, C.L., Hahnen, E., Androphy, E.J., Wirth, B., 1999. A single nucleotide in the SMN gene regulates splicing and is responsible for spinal muscular atrophy. *Proc. Natl. Acad. Sci. U. S. A.* 96, 6307–6311. <https://doi.org/10.1073/pnas.96.11.6307>
- Lorson, C.L., Strasswimmer, J., Yao, J.M., Baleja, J.D., Hahnen, E., Wirth, B., Le, T.T., Burghes, A.H.M., Androphy, E.J., 1998. SMN oligomerization defect correlates with spinal muscular atrophy severity. *Nat. Genet.* 19, 63–6. <https://doi.org/10.1038/ng0598-63>
- Lu, D.C., Niu, T., Alaynick, W.A., 2015. Molecular and cellular development of spinal cord locomotor circuitry. *Front. Mol. Neurosci.* 8, 25. <https://doi.org/10.3389/fnmol.2015.00025>
- Lu, K., Psakhye, I., Jentsch, S., 2014. Autophagic clearance of polyQ proteins mediated by ubiquitin-Atg8 adaptors of the conserved CUET protein family. *Cell.* 158, 549–63. <https://doi.org/10.1016/j.cell.2014.05.048>
- MacKenzie, A., 2010. Genetic therapy for spinal muscular atrophy. *Nat. Biotechnol.* 28, 235–237. <https://doi.org/10.1038/nbt0310-235>
- Macleod, M.J., Taylor, J.E., Lunt, P.W., Mathew, C.G., Robb, S.A., 1999. Prenatal onset spinal muscular atrophy. *Eur. J. Paediatr. Neurol.* 3, 65–72. [https://doi.org/10.1016/S1090-3798\(99\)80015-4](https://doi.org/10.1016/S1090-3798(99)80015-4)
- Maday, S., 2016. Mechanisms of neuronal homeostasis: Autophagy in the axon. *Brain Res.* 1649, 143–150. <https://doi.org/10.1016/j.brainres.2016.03.047>
- Maday, S., Wallace, K.E., Holzbaur, E.L.F., 2012. Autophagosomes initiate distally and mature during transport toward the cell soma in primary neurons. *J. Cell Biol.* 196, 407–417. <https://doi.org/10.1083/jcb.201106120>
- Maden, M., 2007. Retinoic acid in the development, regeneration and maintenance of the nervous system. *Nat. Rev. Neurosci.* 8, 755–65. <https://doi.org/10.1038/nrn2212>
- Maggi, L., Mantegazza, R., 2011. Treatment of myasthenia gravis: Focus on pyridostigmine. *Clin. Drug Investig.* 31, 691–701. <https://doi.org/10.2165/11593300-000000000-00000>
- Mahajan, V.B., Skeie, J.M., Bassuk, A.G., Fingert, J.H., Braun, T.A., Daggett, H.T., Folk, J.C., Sheffield, V.C., Stone, E.M., 2012. Calpain-5 Mutations Cause Autoimmune Uveitis, Retinal Neovascularization, and Photoreceptor Degeneration. *PLoS Genet.* 8, e1003001. <https://doi.org/10.1371/journal.pgen.1003001>
- Mahaman, Y.A.R., Huang, F., Kessete Afewerky, H., Maibouge, Tanko Mahamane Salissou, Ghose, B., Wang, X., 2019. Involvement of calpain in the neuropathogenesis of Alzheimer's disease. *Med. Res. Rev.* 39, 608–630. <https://doi.org/10.1002/med.21534>
- Mailman, M.D., Heinz, J.W., Papp, A.C., Snyder, P.J., Sedra, M.S., Wirth, B., Burghes, A.H.M., Prior, T.W., 2002. Molecular analysis of spinal muscular atrophy and modification of the phenotype by SMN2. *Genet. Med.* 4, 20–26. <https://doi.org/10.1097/00125817-200201000-00004>
- Maki, M., Kitaura, Y., Satoh, H., Ohkouchi, S., Shibata, H., 2002. Structures, functions and molecular evolution of the penta-EF-hand Ca<sup>2+</sup>-binding proteins. *Biochim. Biophys. Acta* 1600, 51–60. [https://doi.org/10.1016/s1570-9639\(02\)00444-2](https://doi.org/10.1016/s1570-9639(02)00444-2)

- Maki, M., Takano, E., Mori, H., Kannagi, R., Murachi, T., Hatanaka, M., 1987a. Repetitive region of calpastatin is a functional unit of the proteinase inhibitor. *Biochem. Biophys. Res. Commun.* 143, 300–308. [https://doi.org/10.1016/0006-291X\(87\)90665-6](https://doi.org/10.1016/0006-291X(87)90665-6)
- Maki, M., Takano, E., Mori, H., Sato, A., Murachi, T., Hatanaka, M., 1987b. All four internally repetitive domains of pig calpastatin possess inhibitory activities against calpains I and II. *FEBS Lett.* 223, 174–180. [https://doi.org/10.1016/0014-5793\(87\)80531-8](https://doi.org/10.1016/0014-5793(87)80531-8)
- Malone, D.C., Dean, R., Arjunji, R., Jensen, I., Cyr, P., Miller, B., Maru, B., Sproule, D.M., Feltner, D.E., Dabbous, O., 2019. Cost-effectiveness analysis of using onasemnogene abeparvocec (AVXS-101) in spinal muscular atrophy type 1 patients. *J. Mark. Access Heal. Policy* 7, 1601484. <https://doi.org/10.1080/20016689.2019.1601484>
- Malva, J.˜o O., Ambrósio, A.F., Carvalho, A.P., Duarte, C.B., Carvalho, C.M., 1995. Involvement of class A calcium channels in the KCl induced Ca<sup>2+</sup> influx in hippocampal synaptosomes. *Brain Res.* 696, 242–245. [https://doi.org/10.1016/0006-8993\(95\)00816-9](https://doi.org/10.1016/0006-8993(95)00816-9)
- Mani, S.K., Balasubramanian, S., Zavadzkas, J.A., Jeffords, L.B., Rivers, W.T., Zile, M.R., Mukherjee, R., Spinale, F.G., Kuppuswamy, D., 2009. Calpain inhibition preserves myocardial structure and function following myocardial infarction. *Am. J. Physiol. - Hear. Circ. Physiol.* 297, H1744. <https://doi.org/10.1152/ajpheart.00338.2009>
- Mani, S.K., Shiraishi, H., Balasubramanian, S., Yamane, K., Chellaiah, M., Cooper, G., Banik, N., Zile, M.R., Kuppuswamy, D., 2008. In vivo administration of calpeptin attenuates calpain activation and cardiomyocyte loss in pressure-overloaded feline myocardium. *Am. J. Physiol. - Hear. Circ. Physiol.* 295, H314. <https://doi.org/10.1152/ajpheart.00085.2008>
- Marchler-Bauer, A., Anderson, J.B., Chitsaz, F., Derbyshire, M.K., Deweese-Scott, C., Fong, J.H., Geer, L.Y., Geer, R.C., Gonzales, N.R., Gwadz, M., He, S., Hurwitz, D.I., Jackson, J.D., Ke, Z., Lanczycki, C.J., Liebert, C.A., Liu, C., Lu, F., Lu, S., Marchler, G.H., Mullokandov, M., Song, J.S., Tasneem, A., Thanki, N., Yamashita, R.A., Zhang, D., Zhang, N., Bryant, S.H., 2009. CDD: Specific functional annotation with the Conserved Domain Database. *Nucleic Acids Res.* 37, D205–210. <https://doi.org/10.1093/nar/gkn845>
- Maria Fimia, G., Stoykova, A., Romagnoli, A., Giunta, L., Di Bartolomeo, S., Nardacci, R., Corazzari, M., Fuoco, C., Ucar, A., Schwartz, P., Gruss, P., Piacentini, M., Chowdhury, K., Cecconi, F., 2007. Ambra1 regulates autophagy and development of the nervous system. *Nature.* 447, 1121–1125. <https://doi.org/10.1038/nature05925>
- Marshall, R.S., Li, F., Gemperline, D.C., Book, A.J., Vierstra, R.D., 2015. Autophagic Degradation of the 26S Proteasome Is Mediated by the Dual ATG8/Ubiquitin Receptor RPN10 in Arabidopsis. *Mol. Cell.* 58, 1053–66. <https://doi.org/10.1016/j.molcel.2015.04.023>
- Martínez-Hernández, R., Soler-Botija, C., Also, E., Alias, L., Caselles, L., Gich, I., Bernal, S., Tizzano, E.F., 2009. The developmental pattern of myotubes in spinal muscular atrophy indicates prenatal delay of muscle maturation. *J. Neuropathol. Exp. Neurol.* 68, 474–481. <https://doi.org/10.1097/NEN.0b013e3181a10ea1>
- Martinez-Vicente, M., Tallozy, Z., Wong, E., Tang, G., Koga, H., Kaushik, S., De Vries, R., Arias, E., Harris, S., Sulzer, D., Cuervo, A.M., 2010. Cargo recognition failure is responsible for inefficient autophagy in Huntington's disease. *Nat. Neurosci.* 13, 567–576. <https://doi.org/10.1038/nn.2528>
- Matera, A.G., Wang, Z., 2014. A day in the life of the spliceosome. *Nat. Rev. Mol. Cell Biol.* 15, 108–

21. <https://doi.org/10.1038/nrm3742>
- McGovern, V.L., Gavrilina, T.O., Beattie, C.E., Burghes, A.H.M., 2008. Embryonic motor axon development in the severe SMA mouse. *Hum. Mol. Genet.* 17, 2900–2909. <https://doi.org/10.1093/hmg/ddn189>
- McWhorter, M.L., Monani, U.R., Burghes, A.H.M., Beattie, C.E., 2003. Knockdown of the survival motor neuron (Smn) protein in zebrafish causes defects in motor axon outgrowth and pathfinding. *J. Cell Biol.* 162, 919–931. <https://doi.org/10.1083/jcb.200303168>
- Mealer, R.G., Murray, A.J., Shahani, N., Subramaniam, S., Snyder, S.H., 2014. Rhes, a striatal-selective protein implicated in Huntington disease, binds beclin-1 and activates autophagy. *J. Biol. Chem.* 289, 3547–54. <https://doi.org/10.1074/jbc.M113.536912>
- Medeiros, R., Kitazawa, M., Chabrier, M.A., Cheng, D., Baglietto-Vargas, D., Kling, A., Moeller, A., Green, K.N., Laferla, F.M., 2012. Calpain inhibitor A-705253 mitigates Alzheimer's disease-like pathology and cognitive decline in aged 3xTgAD mice. *Am. J. Pathol.* 181, 616–625. <https://doi.org/10.1016/j.ajpath.2012.04.020>
- Mehler, M.F., Mabie, P.C., Zhang, D., Kessler, J.A., 1997. Bone morphogenetic proteins in the nervous system. *Trends Neurosci.* 20, 309–317. [https://doi.org/10.1016/S0166-2236\(96\)01046-6](https://doi.org/10.1016/S0166-2236(96)01046-6)
- Melki, J., Abdelhak, S., Sheth, P., Bachelot, M.F., Burlet, P., Marcadet, A., Aicardi, J., Barois, A., Carriere, J.P., Fardeau, M., 1990. Gene for chronic proximal spinal muscular atrophies maps to chromosome 5q. *Nature* 344, 767–8. <https://doi.org/10.1038/344767a0>
- Melki, J., Lefebvre, S., Burglen, L., Burlet, P., Clermont, O., Millasseau, P., Reboullet, S., Bénichou, B., Zeviani, M., Le Paslier, D., 1994. De novo and inherited deletions of the 5q13 region in spinal muscular atrophies. *Science* 264, 1474–7. <https://doi.org/10.1126/science.7910982>
- Melloni, E., Averna, M., Stifanese, R., De Tullio, R., Defranchi, E., Salamino, F., Pontremoli, S., 2006. Association of calpastatin with inactive calpain: A novel mechanism to control the activation of the protease? *J. Biol. Chem.* 281, 24945–24954. <https://doi.org/10.1074/jbc.M601449200>
- Mentis, G.Z., Blivis, D., Liu, W., Drobac, E., Crowder, M.E., Kong, L., Alvarez, F.J., Sumner, C.J., O'Donovan, M.J., 2011. Early Functional Impairment of Sensory-Motor Connectivity in a Mouse Model of Spinal Muscular Atrophy. *Neuron* 69, 453–467. <https://doi.org/10.1016/j.neuron.2010.12.032>
- Menzies, Fiona M., Fleming, A., Rubinsztein, D.C., 2015. Compromised autophagy and neurodegenerative diseases. *Nat. Rev. Neurosci.* 16, 345–57. <https://doi.org/10.1038/nrn3961>
- Menzies, F. M., Garcia-Arencibia, M., Imarisio, S., O'Sullivan, N.C., Ricketts, T., Kent, B.A., Rao, M. V., Lam, W., Green-Thompson, Z.W., Nixon, R.A., Saksida, L.M., Bussey, T.J., O 'Kane, C.J., Rubinsztein, D.C., 2015. Calpain inhibition mediates autophagy-dependent protection against polyglutamine toxicity. *Cell Death Differ.* 22, 433–444. <https://doi.org/10.1038/cdd.2014.151>
- Mercuri, E., Bertini, E., Messina, S., Solari, A., D'Amico, A., Angelozzi, C., Battini, R., Berardinelli, A., Boffi, P., Bruno, C., Cini, C., Colitto, F., Kinali, M., Minetti, C., Mongini, T., Morandi, L., Neri, G., Orcesi, S., Pane, M., Pelliccioni, M., Pini, A., Tiziano, F.D., Villanova, M., Vita, G., Brahe, C., 2007. Randomized, double-blind, placebo-controlled trial of phenylbutyrate in spinal muscular atrophy. *Neurology* 68, 51–55.



<https://doi.org/10.1212/01.wnl.0000249142.82285.d6>

- Mercuri, E., Finkel, R.S., Montes, J., Mazzone, E.S., Sormani, M.P., Main, M., Ramsey, D., Mayhew, A., Glanzman, A.M., Dunaway, S., Salazar, R., Pasternak, A., Quigley, J., Pane, M., Pera, M.C., Scoto, M., Messina, S., Sframeli, M., Vita, G.L., D'Amico, A., van den Hauwe, M., Sivo, S., Goemans, N., Kaufmann, P., Darras, B.T., Bertini, E., Muntoni, F., de Vivo, D.C., 2016. Patterns of disease progression in type 2 and 3 SMA: Implications for clinical trials. *Neuromuscul. Disord.* 26, 126–131. <https://doi.org/10.1016/j.nmd.2015.10.006>
- Mercuri, E., Finkel, R.S., Muntoni, F., Wirth, B., Montes, J., Main, M., Mazzone, E., Vitale, M., Snyder, B., Quijano-Roy, S., Bertini, E., Davis, R.H., Meyer, O.H., Simonds, A.K., Schroth, M.K., Graham, R.J., Kirschner, J., Iannaccone, S.T., Crawford, T.O., Woods, S., Qian, Y., Sejersen, T., Tiziano, F.D., Tizzano, E., Swoboda, Kathryn, Swoboda, Kathy, Laing, N., Kayoko, S., Prior, T., Chung, W.K., Wu, S.M., Coleman, C., Gee, R., Glanzman, A., Kroksmark, A.K., Krosschell, K., Nelson, L., Rose, K., Stępień, A., Vuillerot, C., Dubousset, J., Farrington, D., Flynn, J., Halanski, M., Hasler, C., Miladi, L., Reilly, C., Roye, B., Sponseller, P., Hurst, R., Tarrant, S., Barja, S., Foust, K., Kyle, B., Rodan, L., Roper, H., Seffrood, E., Szlagatys-Sidorkiewicz, A., 2018. Diagnosis and management of spinal muscular atrophy: Part 1: Recommendations for diagnosis, rehabilitation, orthopedic and nutritional care. *Neuromuscul. Disord.* 28, 103–115. <https://doi.org/10.1016/j.nmd.2017.11.005>
- Mercuri, E., Kirschner, J., Baranello, G., Servais, L., Goemans, N., Pera, M., Marquet, A., Seabrook, T., Sturm, S., Armstrong, G., Kletzl, H., Czech, C., Kraus, D., Abdallah, H., Mueller, L., Gorni, K., Khwaja, O., 2017. Clinical studies of RG7916 in patients with spinal muscular atrophy: SUNFISH part 1 study update. *Neuromuscul. Disord.* 27, S209. <https://doi.org/10.1016/j.nmd.2017.06.415>
- Miguel-Aliaga, I., Chan, Y.B., Davies, K.E., Van Den Heuvel, M., 2000. Disruption of SMN function by ectopic expression of the human SMN gene in *Drosophila*. *FEBS Lett.* 486, 99–102. [https://doi.org/10.1016/S0014-5793\(00\)02243-2](https://doi.org/10.1016/S0014-5793(00)02243-2)
- Mizushima, N., 2004. Methods for monitoring autophagy. *Int. J. Biochem. Cell Biol.* 36, 2491–2502 <https://doi.org/10.1016/j.biocel.2004.02.005>
- Mizushima, N., Levine, B., Cuervo, A.M., Klionsky, D.J., 2008. Autophagy fights disease through cellular self-digestion. *Nature.* 451, 1069–1075. <https://doi.org/10.1038/nature06639>
- Mizushima, N., Yoshimori, T., Levine, B., 2010. Methods in Mammalian Autophagy Research. *Cell.* 140, 313–326. <https://doi.org/10.1016/j.cell.2010.01.028>
- Moldoveanu, T., Gehring, K., Green, D.R., 2008. Concerted multi-pronged attack by calpastatin to occlude the catalytic cleft of heterodimeric calpains. *Nature* 456, 404–408. <https://doi.org/10.1038/nature07353>
- Moldoveanu, T., Hosfield, C.M., Lim, D., Elce, J.S., Jia, Z., Davies, P.L., 2002. A Ca<sup>2+</sup> switch aligns the active site of calpain. *Cell.* 108, 649–660. [https://doi.org/10.1016/S0092-8674\(02\)00659-1](https://doi.org/10.1016/S0092-8674(02)00659-1)
- Monani, U.R., De Vivo, D.C., 2014. Neurodegeneration in spinal muscular atrophy: From disease phenotype and animal models to therapeutic strategies and beyond. *Future Neurol.* 9, 49–65. <https://doi.org/10.2217/fnl.13.58>
- Monani, U.R., Sendtner, M., Coover, D.D., Parsons, D.W., Andreassi, C., Le, T.T., Jablonka, S., Schrank, B., Rossoll, W., Prior, T.W., Morris, G.E., Burghes, A.H.M., 2000. The human centromeric survival motor neuron gene (SMN2) rescues embryonic lethality in *Smn*<sup>-/-</sup> mice

- and results in a mouse with spinal muscular atrophy. *Hum. Mol. Genet.* 9, 333–339. <https://doi.org/10.1093/hmg/9.3.333>
- Moreau, K., Fleming, A., Imarisio, S., Lopez Ramirez, A., Mercer, J.L., Jimenez-Sanchez, M., Bento, C.F., Puri, C., Zavodszky, E., Siddiqi, F., Lavau, C.P., Betton, M., O’Kane, C.J., Wechsler, D.S., Rubinsztein, D.C., 2014. PICALM modulates autophagy activity and tau accumulation. *Nat. Commun.* 5, 4998. <https://doi.org/10.1038/ncomms5998>
- Mouatt-Prigent, A., Karlsson, J.O., Agid, Y., Hirsch, E.C., 1996. Increased M-calpain expression in the mesencephalon of patients with Parkinson’s disease but not in other neurodegenerative disorders involving the mesencephalon: A role in nerve cell death? *Neuroscience* 73, 979–987. [https://doi.org/10.1016/0306-4522\(96\)00100-5](https://doi.org/10.1016/0306-4522(96)00100-5)
- Murachi, T., 1989. Intracellular regulatory system involving calpain and calpastatin. *Biochem. Int.* 18, 263–294. ISSN: 01585231
- Murray, L.M., Comley, L.H., Thomson, D., Parkinson, N., Talbot, K., Gillingwater, T.H., 2008. Selective vulnerability of motor neurons and dissociation of pre- and post-synaptic pathology at the neuromuscular junction in mouse models of spinal muscular atrophy. *Hum. Mol. Genet.* 17, 949–962. <https://doi.org/10.1093/hmg/ddm367>
- Nakatogawa, H., Suzuki, K., Kamada, Y., Ohsumi, Y., 2009. Dynamics and diversity in autophagy mechanisms: lessons from yeast. *Nat. Rev. Mol. Cell Biol.* 10, 458–67. <https://doi.org/10.1038/nrm2708>
- Naryshkin, N.A., Weetall, M., Dakka, A., Narasimhan, J., Zhao, X., Feng, Z., Ling, K.K.Y., Karp, G.M., Qi, H., Woll, M.G., Chen, G., Zhang, N., Gabbeta, V., Vazirani, P., Bhattacharyya, A., Furia, B., Risher, N., Sheedy, J., Kong, R., Ma, J., Turpoff, A., Lee, C.-S., Zhang, X., Moon, Y.-C., Trifillis, P., Welch, E.M., Colacino, J.M., Babiak, J., Almstead, N.G., Peltz, S.W., Eng, L.A., Chen, K.S., Mull, J.L., Lynes, M.S., Rubin, L.L., Fontoura, P., Santarelli, L., Haehnke, D., McCarthy, K.D., Schmucki, R., Ebeling, M., Sivaramakrishnan, M., Ko, C.-P., Paushkin, S. V., Ratni, H., Gerlach, I., Ghosh, A., Metzger, F., 2014. Motor neuron disease. SMN2 splicing modifiers improve motor function and longevity in mice with spinal muscular atrophy. *Science* 345, 688–93. <https://doi.org/10.1126/science.1250127>
- Nascimbeni, A.C., Codogno, P., Morel, E., 2017. Phosphatidylinositol-3-phosphate in the regulation of autophagy membrane dynamics. *FEBS J.* 284, 1267–1278. <https://doi.org/10.1111/febs.13987>
- Nath, R., Raser, K.J., Stafford, D., Hajimohammadreza, I., Posner, A., Allen, H., Talanian, R. V., Yuen, P., Gilbertsen, R.B., Wang, K.K., 1996. Non-erythroid alpha-spectrin breakdown by calpain and interleukin 1 beta-converting-enzyme-like protease(s) in apoptotic cells: contributory roles of both protease families in neuronal apoptosis. *Biochem. J.* 319, 683–90. <https://doi.org/10.1042/bj3190683>
- Neil, E.E., Bisaccia, E.K., 2019. Nusinersen: A novel antisense oligonucleotide for the treatment of spinal muscular atrophy. *J. Pediatr. Pharmacol. Ther.* 24, 194–203. <https://doi.org/10.5863/1551-6776-24.3.194>
- Newman, A.C., Scholefield, C.L., Kemp, A.J., Newman, M., McIver, E.G., Kamal, A., Wilkinson, S., 2012. TBK1 Kinase Addiction in Lung Cancer Cells Is Mediated via Autophagy of Tax1bp1/Ndp52 and Non-Canonical NF- $\kappa$ B Signalling. *PLoS One.* 7, e50672. <https://doi.org/10.1371/journal.pone.0050672>

- Niederreither, K., McCaffery, P., Dräger, U.C., Chambon, P., Dollé, P., 1997. Restricted expression and retinoic acid-induced downregulation of the retinaldehyde dehydrogenase type 2 (RALDH-2) gene during mouse development. *Mech. Dev.* 62, 67–78. [https://doi.org/10.1016/S0925-4773\(96\)00653-3](https://doi.org/10.1016/S0925-4773(96)00653-3)
- Nieuwenhuys, R., Voogd, J., Van Huijzen, C., 2008. The human central nervous system, *The Human Central Nervous System*. Springer-Verlag Berlin Heidelberg. pp, 1-967 <https://doi.org/10.1007/978-3-540-34686-9>
- Nixon, R.A., Wegiel, J., Kumar, A., Yu, W.H., Peterhoff, C., Cataldo, A., Cuervo, A.M., 2005. Extensive involvement of autophagy in Alzheimer disease: An immuno-electron microscopy study. *J. Neuropathol. Exp. Neurol.* 64, 113–122. <https://doi.org/10.1093/jnen/64.2.113>
- Noda, T., Ohsumi, Y., 1998. Tor, a phosphatidylinositol kinase homologue, controls autophagy in yeast. *J. Biol. Chem.* 273, 3963–3966. <https://doi.org/10.1074/jbc.273.7.3963>
- Noda, T., Suzuki, K., Ohsumi, Y., 2002. Yeast autophagosomes: de novo formation of a membrane structure. *Trends Cell Biol.* 12, 231–5. [https://doi.org/10.1016/s0962-8924\(02\)02278-x](https://doi.org/10.1016/s0962-8924(02)02278-x)
- Nölle, A., Zeug, A., van Bergeijk, J., Tönges, L., Gerhard, R., Brinkmann, H., Al Rayes, S., Hensel, N., Schill, Y., Apkhazava, D., Jablonka, S., O’mer, J., Srivastav, R.K., Baasner, A., Lingor, P., Wirth, B., Ponimaskin, E., Niedenthal, R., Grothe, C., Claus, P., 2011. The spinal muscular atrophy disease protein SMN is linked to the Rho-kinase pathway via profilin. *Hum. Mol. Genet.* 20, 4865–78. <https://doi.org/10.1093/hmg/ddr425>
- Norman, J.M., Cohen, G.M., Bampton, E.T.W., 2010. The in vitro cleavage of the hAtg proteins by cell death proteases. *Autophagy.* 6, 1042–1056. <https://doi.org/10.4161/auto.6.8.13337>
- Oh, W.J., Wu, C., Kim, S.J., Facchinetti, V., Julien, L.-A., Finlan, M., Roux, P.P., Su, B., Jacinto, E., 2010. mTORC2 can associate with ribosomes to promote cotranslational phosphorylation and stability of nascent Akt polypeptide. *EMBO J.* 29, 3939–51. <https://doi.org/10.1038/emboj.2010.271>
- Ono, Y., Kakinuma, K., Torii, F., Irie, A., Nakagawa, K., Labeit, S., Abe, K., Suzuki, K., Sorimachi, H., 2004. Possible Regulation of the Conventional Calpain System by Skeletal Muscle-specific Calpain, p94/Calpain 3. *J. Biol. Chem.* 279, 2761–2771. <https://doi.org/10.1074/jbc.M308789200>
- Ono, Y., Ojima, K., Shinkai-Ouchi, F., Hata, S., Sorimachi, H., 2016a. An eccentric calpain, CAPN3/p94/calpain-3. *Biochimie.* 122, 169-187. <https://doi.org/10.1016/j.biochi.2015.09.010>
- Ono, Y., Saido, T.C., Sorimachi, H., 2016b. Calpain research for drug discovery: Challenges and potential. *Nat. Rev. Drug Discov.* 15, 854-876. <https://doi.org/10.1038/nrd.2016.212>
- Ono, Y., Sorimachi, H., 2012. Calpains: an elaborate proteolytic system. *Biochim. Biophys. Acta.* 1824, 224–36. <https://doi.org/10.1016/j.bbapap.2011.08.005>
- Oprea, G.E., Kröber, S., McWhorter, M.L., Rossoll, W., Müller, S., Krawczak, M., Bassell, G.J., Beattie, C.E., Wirth, B., 2008. Plastin 3 is a protective modifier of autosomal recessive spinal muscular atrophy. *Science* 320, 524–7. <https://doi.org/10.1126/science.1155085>
- Orsi, A., Razi, M., Dooley, H.C., Robinson, D., Weston, A.E., Collinson, L.M., Tooze, S.A., 2012. Dynamic and transient interactions of Atg9 with autophagosomes, but not membrane integration, are required for autophagy. *Mol. Biol. Cell* 23, 1860–73.

<https://doi.org/10.1091/mbc.E11-09-0746>

- Otomo, C., Metlagel, Z., Takaesu, G., Otomo, T., 2013. Structure of the human ATG12~ATG5 conjugate required for LC3 lipidation in autophagy. *Nat. Struct. Mol. Biol.* 20, 59–66. <https://doi.org/10.1038/nsmb.2431>
- Ottesen, E.W., Howell, M.D., Singh, N.N., Seo, J., Whitley, E.M., Singh, R.N., 2016. Severe impairment of male reproductive organ development in a low SMN expressing mouse model of spinal muscular atrophy. *Sci. Rep.* 6, 20193. <https://doi.org/10.1038/srep20193>
- Owen, N., Doe, C.L., Mellor, J., Davies, K.E., 2000. Characterization of the *Schizosaccharomyces pombe* orthologue of the human survival motor neuron (SMN) protein. *Hum. Mol. Genet.* 9, 675–684. <https://doi.org/10.1093/hmg/9.5.675>
- Pagliardini, S., Giavazzi, A., Setola, V., Lizier, C., Di Luca, M., DeBiasi, S., Battaglia, G., 2000. Subcellular localization and axonal transport of the survival motor neuron (SMN) protein in the developing rat spinal cord. *Hum. Mol. Genet.* 9, 47–56. <https://doi.org/10.1093/hmg/9.1.47>
- Pankiv, S., Clausen, T.H., Lamark, T., Brech, A., Bruun, J.-A., Outzen, H., Øvervatn, A., Bjørkøy, G., Johansen, T., 2007. p62/SQSTM1 binds directly to Atg8/LC3 to facilitate degradation of ubiquitinated protein aggregates by autophagy. *J. Biol. Chem.* 282, 24131–45. <https://doi.org/10.1074/jbc.M702824200>
- Paoletti, P., Vila, I., Rifé, M., Lizcano, J.M., Alberch, J., Ginés, S., 2008. Dopaminergic and glutamatergic signaling crosstalk in Huntington's disease neurodegeneration: The role of p25/cyclin-dependent kinase 5. *J. Neurosci.* 28, 10090–10101. <https://doi.org/10.1523/JNEUROSCI.3237-08.2008>
- Paquette, M., El-Houjeiri, L., Pause, A., 2018. mTOR pathways in cancer and autophagy. *Cancers.* 10. <https://doi.org/10.3390/cancers10010018>
- Parente, V., Corti, S., 2018. Advances in spinal muscular atrophy therapeutics. *Ther. Adv. Neurol. Disord.* 11, 1-13. <https://doi.org/10.1177/1756285618754501>
- Park, D., Jeong, H., Lee, M.N., Koh, A., Kwon, O., Yang, Y.R., Noh, J., Suh, P.G., Park, H., Ryu, S.H., 2016. Resveratrol induces autophagy by directly inhibiting mTOR through ATP competition. *Sci. Rep.* 6, 21772. <https://doi.org/10.1038/srep21772>
- Park, G.H., Kariya, S., Monani, U.R., 2010. Spinal muscular atrophy: New and emerging insights from model mice. *Curr. Neurol. Neurosci. Rep.* 10, 108-117. <https://doi.org/10.1007/s11910-010-0095-5>
- Passini, M.A., Bu, J., Roskelley, E.M., Richards, A.M., Sardi, S.P., O'Riordan, C.R., Klinger, K.W., Shihabuddin, L.S., Cheng, S.H., 2010. CNS-targeted gene therapy improves survival and motor function in a mouse model of spinal muscular atrophy. *J. Clin. Invest.* 120, 1253–1264. <https://doi.org/10.1172/JCI41615>
- Paushkin, S., Charroux, B., Abel, L., Perkinson, R.A., Pellizzoni, L., Dreyfuss, G., 2000. The survival motor neuron protein of *Schizosaccharomyces pombe*: Conservation of survival motor neuron interaction domains in divergent organisms. *J. Biol. Chem.* 275, 23841–23846. <https://doi.org/10.1074/jbc.M001441200>
- Pearn, J., 1978. Incidence, prevalence, and gene frequency studies of chronic childhood spinal

- muscular atrophy. *J. Med. Genet.* 15, 409–413. <https://doi.org/10.1136/jmg.15.6.409>
- Pellizzoni, L., 2007. Chaperoning ribonucleoprotein biogenesis in health and disease. *EMBO Rep.* 8, 340–5. <https://doi.org/10.1038/sj.embor.7400941>
- Pellizzoni, L., Baccon, J., Charroux, B., Dreyfuss, G., 2001. The survival of motor neurons (SMN) protein interacts with the snoRNP proteins fibrillarin and GAR1. *Curr. Biol.* 11, 1079–88. [https://doi.org/10.1016/s0960-9822\(01\)00316-5](https://doi.org/10.1016/s0960-9822(01)00316-5)
- Pellizzoni, L., Kataoka, N., Charroux, B., Dreyfuss, G., 1998. A novel function for SMN, the spinal muscular atrophy disease gene product, in pre-mRNA splicing. *Cell.* 95, 615–24. [https://doi.org/10.1016/s0092-8674\(00\)81632-3](https://doi.org/10.1016/s0092-8674(00)81632-3)
- Pellizzoni, L., Yong, J., Dreyfuss, G., 2002. Essential role for the SMN complex in the specificity of snRNP assembly. *Science.* 298, 1775–9. <https://doi.org/10.1126/science.1074962>
- Peng, S., Kuang, Z., Zhang, Y., Xu, H., Cheng, Q., 2011. The protective effects and potential mechanism of Calpain inhibitor Calpeptin against focal cerebral ischemia-reperfusion injury in rats. *Mol. Biol. Rep.* 38, 905–912. <https://doi.org/10.1007/s11033-010-0183-2>
- Periyakaruppiyah, A., de la Fuente, S., Arumugam, S., Bahi, N., Garcera, A., Soler, R.M., 2016. Autophagy modulators regulate survival motor neuron protein stability in motoneurons. *Exp. Neurol.* 283, 287–97. <https://doi.org/10.1016/j.expneurol.2016.06.032>
- Peter, C.J., Evans, M., Thayanithy, V., Taniguchi-Ishigaki, N., Bach, I., Kolpak, A., Bassell, G.J., Rossoll, W., Lorson, C.L., Bao, Z.-Z., Androphy, E.J., 2011. The COPI vesicle complex binds and moves with survival motor neuron within axons. *Hum. Mol. Genet.* 20, 1701–11. <https://doi.org/10.1093/hmg/ddr046>
- Piazzon, N., Rage, F., Schlotter, F., Moine, H., Branlant, C., Massenet, S., 2008. In vitro and in cellulo evidences for association of the survival of motor neuron complex with the fragile X mental retardation protein. *J. Biol. Chem.* 283, 5598–610. <https://doi.org/10.1074/jbc.M707304200>
- Pickford, F., Masliah, E., Britschgi, M., Lucin, K., Narasimhan, R., Jaeger, P.A., Small, S., Spencer, B., Rockenstein, E., Levine, B., Wyss-Coray, T., 2008. The autophagy-related protein beclin 1 shows reduced expression in early Alzheimer disease and regulates amyloid  $\beta$  accumulation in mice. *J. Clin. Invest.* 118, 2190–2199. <https://doi.org/10.1172/JCI33585>
- Piepers, S., van den Berg, L.H., Brugman, F., Scheffer, H., Ruitkamp-Versteeg, M., van Engelen, B.G., Faber, C.G., de Visser, M., van der Pol, W.-L., Wokke, J.H.J., 2008. A natural history study of late onset spinal muscular atrophy types 3b and 4. *J. Neurol.* 255, 1400–4. <https://doi.org/10.1007/s00415-008-0929-0>
- Pierani, A., Brenner-Morton, S., Chiang, C., Jessell, T.M., 1999. A Sonic hedgehog-independent, retinoid-activated pathway of neurogenesis in the ventral spinal cord. *Cell* 97, 903–915. [https://doi.org/10.1016/S0092-8674\(00\)80802-8](https://doi.org/10.1016/S0092-8674(00)80802-8)
- Pierrot, N., Ferrao Santos, S., Feyt, C., Morel, M., Brion, J.P., Octave, J.N., 2006. Calcium-mediated transient phosphorylation of tau and amyloid precursor protein followed by intraneuronal amyloid- $\beta$  accumulation. *J. Biol. Chem.* 281, 39907–39914. <https://doi.org/10.1074/jbc.M606015200>
- Piras, A., Schiaffino, L., Boido, M., Valsecchi, V., Guglielmotto, M., De Amicis, E., Puyal, J., Garcera, A., Tamagno, E., Soler, R.M., Vercelli, A., 2017. Inhibition of autophagy delays motoneuron

- degeneration and extends lifespan in a mouse model of spinal muscular atrophy. *Cell Death Dis.* 8, 3223. <https://doi.org/10.1038/s41419-017-0086-4>
- Powe, C.E., Allen, M., Puopolo, K.M., Merewood, A., Worden, S., Johnson, L.C., Fleischman, A., Welt, C.K., 2010. Recombinant human prolactin for the treatment of lactation insufficiency. *Clin. Endocrinol. (Oxf)*. 73, 645–53. <https://doi.org/10.1111/j.1365-2265.2010.03850.x>
- Press, C., Milbrandt, J., 2008. Nmnat delays axonal degeneration caused by mitochondrial and oxidative stress. *J. Neurosci.* 28, 4861–71. <https://doi.org/10.1523/JNEUROSCI.0525-08.2008>
- Puri, C., Renna, M., Bento, C.F., Moreau, K., Rubinsztein, D.C., 2013. Diverse autophagosome membrane sources coalesce in recycling endosomes. *Cell* 154, 1285–99. <https://doi.org/10.1016/j.cell.2013.08.044>
- Purves, D., Augustine, G.J., Fitzpatrick, D., Katz, L.C., Anthony-Samuel, L., McNamara, J.O., Williams, S.M., 2003. *Neurosciences*, 2nd edition. de boeck. ISBN-10: 9780878936953
- Purves, D., Augustine, G.J., Fitzpatrick, D., Katz, L.C., LaMantia, A.-S., McNamara, J.O., Williams, S.M., 2001a. Chapter 17: Upper Motor Neuron Control of the Brainstem and Spinal Cord. ISBN-10: 9780878936953
- Purves, D., Augustine, G.J., Fitzpatrick, D., Katz, L.C., LaMantia, A.-S., McNamara, J.O., Williams, S.M., 2001b. The Lower Motor Neuron Syndrome. ISBN-10: 9780878936953
- Purves, D., Augustine, G.J., Fitzpatrick, D., Katz, L.C., LaMantia, A.-S., McNamara, J.O., Williams, S.M., 2001c. Chapter 21: The Visceral Motor System. ISBN-10: 9780878936953
- Rajendra, T.K., Gonsalvez, G.B., Walker, M.P., Shpargel, K.B., Salz, H.K., Matera, A.G., 2007. A *Drosophila melanogaster* model of spinal muscular atrophy reveals a function for SMN in striated muscle. *J. Cell Biol.* 176, 831–841. <https://doi.org/10.1083/jcb.200610053>
- Raker, V.A., Hartmuth, K., Kastner, B., Lührmann, R., 1999. Spliceosomal U snRNP Core Assembly: Sm Proteins Assemble onto an Sm Site RNA Nonanucleotide in a Specific and Thermodynamically Stable Manner. *Mol. Cell. Biol.* 19, 6554–6565. <https://doi.org/10.1128/mcb.19.10.6554>
- Rao, M. V., Campbell, J., Palaniappan, A., Kumar, A., Nixon, R.A., 2016. Calpastatin inhibits motor neuron death and increases survival of hSOD1G93A mice. *J. Neurochem.* 137, 253–265. <https://doi.org/10.1111/jnc.13536>
- Rao, M. V., McBrayer, M.K., Campbell, J., Kumar, A., Hashim, A., Sershen, H., Stavrides, P.H., Ohno, M., Hutton, M., Nixon, R.A., 2014. Specific calpain inhibition by calpastatin prevents tauopathy and neurodegeneration and restores normal lifespan in tau P301L Mice. *J. Neurosci.* 34, 9222–9234. <https://doi.org/10.1523/JNEUROSCI.1132-14.2014>
- Rao, M. V., Mohan, P.S., Peterhoff, C.M., Yang, D.S., Schmidt, S.D., Stavrides, P.H., Campbell, J., Chen, Y., Jiang, Y., Paskevich, P.A., Cataldo, A.M., Haroutunian, V., Nixon, R.A., 2008. Marked calpastatin (CAST) depletion in Alzheimer’s disease accelerates cytoskeleton disruption and neurodegeneration: Neuroprotection by CAST overexpression. *J. Neurosci.* 28, 12241–12254. <https://doi.org/10.1523/JNEUROSCI.4119-08.2008>
- Rao, V.K., Kapp, D., Schroth, M., 2018. Gene Therapy for Spinal Muscular Atrophy: An Emerging Treatment Option for a Devastating Disease. *J. Manag. care Spec. Pharm.* 24, S3-S16. <https://doi.org/10.18553/jmcp.2018.24.12-a.s3>

- Ravanan, P., Srikumar, I.F., Talwar, P., 2017. Autophagy: The spotlight for cellular stress responses. *Life Sci.* 188, 53–67. <https://doi.org/10.1016/j.lfs.2017.08.029>
- Ravikumar, B., Duden, R., Rubinsztein, D.C., 2002. Aggregate-prone proteins with polyglutamine and polyalanine expansions are degraded by autophagy. *Hum. Mol. Genet.* 11, 1107–1117. <https://doi.org/10.1093/hmg/11.9.1107>
- Ravikumar, B., Vacher, C., Berger, Z., Davies, J.E., Luo, S., Oroz, L.G., Scaravilli, F., Easton, D.F., Duden, R., O’Kane, C.J., Rubinsztein, D.C., 2004. Inhibition of mTOR induces autophagy and reduces toxicity of polyglutamine expansions in fly and mouse models of Huntington disease. *Nat. Genet.* 36, 585–595. <https://doi.org/10.1038/ng1362>
- Rice, M.C., O’Brien, S.J., 1980. Genetic variance of laboratory outbred Swiss mice. *Nature.* 283, 157–161. <https://doi.org/10.1038/283157a0>
- Richter, B., Sliter, D.A., Herhaus, L., Stolz, A., Wang, C., Beli, P., Zaffagnini, G., Wild, P., Martens, S., Wagner, S.A., Youle, R.J., Dikic, I., 2016. Phosphorylation of OPTN by TBK1 enhances its binding to Ub chains and promotes selective autophagy of damaged mitochondria. *Proc. Natl. Acad. Sci. U. S. A.* 113, 4039–44. <https://doi.org/10.1073/pnas.1523926113>
- Rindt, H., Feng, Z., Mazzasette, C., Glascock, J.J., Valdivia, D., Pyles, N., Crawford, T.O., Swoboda, K.J., Patitucci, T.N., Ebert, A.D., Sumner, C.J., Ko, C.P., Lorson, C.L., 2015. Astrocytes influence the severity of spinal muscular atrophy. *Hum. Mol. Genet.* 24, 4094–4102. <https://doi.org/10.1093/hmg/ddv148>
- Rodriguez-Muela, N., Parkhitko, A., Grass, T., Gibbs, R.M., Norabuena, E.M., Perrimon, N., Singh, R., Rubin, L.L., 2018. Blocking p62-dependent SMN degradation ameliorates spinal muscular atrophy disease phenotypes. *J. Clin. Invest.* 128, 3008–3023. <https://doi.org/10.1172/JCI95231>
- Rossoll, W., Bassell, G.J., 2009. Spinal muscular atrophy and a model for survival of motor neuron protein function in axonal ribonucleoprotein complexes. *Results Probl. Cell Differ.* 48, 289–326. [https://doi.org/10.1007/400\\_2009\\_4](https://doi.org/10.1007/400_2009_4)
- Rossoll, W., Jablonka, S., Andreassi, C., Kröning, A.-K., Karle, K., Monani, U.R., Sendtner, M., 2003. Smn, the spinal muscular atrophy-determining gene product, modulates axon growth and localization of beta-actin mRNA in growth cones of motoneurons. *J. Cell Biol.* 163, 801–12. <https://doi.org/10.1083/jcb.200304128>
- Roy, N., Mahadevan, M.S., McLean, M., Shutter, G., Yaraghi, Z., Farahani, R., Baird, S., Besner-Johnston, A., Lefebvre, C., Kang, X., Salih, M., Aubry, H., Tamai, K., Guan, X., Ioannou, P., Crawford, T.O., de Jong, P.J., Surh, L., Ikeda, J.E., Korneluk, R.G., MacKenzie, A., 1995. The gene for neuronal apoptosis inhibitory protein is partially deleted in individuals with spinal muscular atrophy. *Cell* 80, 167–178. [https://doi.org/10.1016/0092-8674\(95\)90461-1](https://doi.org/10.1016/0092-8674(95)90461-1)
- Rudnik-Schöneborn, S., Heller, R., Berg, C., Betzler, C., Grimm, T., Eggermann, T., Eggermann, K., Wirth, R., Wirth, B., Zerres, K., 2008. Congenital heart disease is a feature of severe infantile spinal muscular atrophy. *J. Med. Genet.* 45, 635–638. <https://doi.org/10.1136/jmg.2008.057950>
- Ruiz, R., Casañas, J.J., Torres-Benito, L., Cano, R., Tabares, L., 2010. Altered intracellular Ca<sup>2+</sup> homeostasis in nerve terminals of severe spinal muscular atrophy mice. *J. Neurosci.* 30, 849–857. <https://doi.org/10.1523/JNEUROSCI.4496-09.2010>

- Russman, B.S., 2007. Spinal muscular atrophy: clinical classification and disease heterogeneity. *J. Child Neurol.* 22, 946–51. <https://doi.org/10.1177/0883073807305673>
- Russo, R., Berliocchi, L., Adornetto, A., Varano, G.P., Cavaliere, F., Nucci, C., Rotiroti, D., Morrone, L.A., Bagetta, G., Corasaniti, M.T., 2011. Calpain-mediated cleavage of Beclin-1 and autophagy deregulation following retinal ischemic injury in vivo. *Cell Death Dis.* 2, e144(2011). <https://doi.org/10.1038/cddis.2011.29>
- Sagné, C., Agulhon, C., Ravassard, P., Darmon, M., Hamon, M., El Mestikawy, S., Gasnier, B., Giros, B., 2001. Identification and characterization of a lysosomal transporter for small neutral amino acids. *Proc. Natl. Acad. Sci. U. S. A.* 98, 7206–7211. <https://doi.org/10.1073/pnas.121183498>
- Sánchez-Danés, A., Richaud-Patin, Y., Carballo-Carbajal, I., Jiménez-Delgado, S., Caig, C., Mora, S., Di Guglielmo, C., Ezquerro, M., Patel, B., Giralt, A., Canals, J.M., Memo, M., Alberch, J., López-Barneo, J., Vila, M., Cuervo, A.M., Tolosa, E., Consiglio, A., Raya, A., 2012. Disease-specific phenotypes in dopamine neurons from human iPS-based models of genetic and sporadic Parkinson's disease. *EMBO Mol. Med.* 4, 380–395. <https://doi.org/10.1002/emmm.201200215>
- Sanchez, G., Dury, A.Y., Murray, L.M., Biondi, O., Tadesse, H., El Fatimy, R., Kothary, R., Charbonnier, F., Khandjian, E.W., Côté, J., 2013. A novel function for the survival motoneuron protein as a translational regulator. *Hum. Mol. Genet.* 22, 668–84. <https://doi.org/10.1093/hmg/dd5474>
- Sarkar, S., 2013. Regulation of autophagy by mTOR-dependent and mTOR-independent pathways: autophagy dysfunction in neurodegenerative diseases and therapeutic application of autophagy enhancers. *Biochem. Soc. Trans.* 41, 1103–30. <https://doi.org/10.1042/BST20130134>
- Sarkar, S., Floto, R.A., Berger, Z., Imarisio, S., Cordenier, A., Pasco, M., Cook, L.J., Rubinsztein, D.C., 2005. Lithium induces autophagy by inhibiting inositol monophosphatase. *J. Cell Biol.* 170, 1101–1111. <https://doi.org/10.1083/jcb.200504035>
- Sarkar, S., Rubinsztein, D.C., 2008. Huntington's disease: Degradation of mutant huntingtin by autophagy. *FEBS J.* 275, 4263–4270. <https://doi.org/10.1111/j.1742-4658.2008.06562.x>
- Schád, É., Farkas, A., Jékely, G., Tompa, P., Friedrich, P., 2002. A novel human small subunit of calpains. *Biochem. J.* 362, 383–388. <https://doi.org/10.1042/0264-6021:3620383>
- Schmid, A., DiDonato, C.J., 2007. Animal models of spinal muscular atrophy. *J. Child Neurol.* 22, 1004–1012. <https://doi.org/10.1177/0883073807305667>
- Schrank, B., Götz, R., Gunnensen, J.M., Ure, J.M., Toyka, K. V., Smith, A.G., Sendtner, M., 1997. Inactivation of the survival motor neuron gene, a candidate gene for human spinal muscular atrophy, leads to massive cell death in early mouse embryos. *Proc. Natl. Acad. Sci. U. S. A.* 94, 9920–9925. <https://doi.org/10.1073/pnas.94.18.9920>
- Schreml, J., Riessland, M., Paterno, M., Garbes, L., Robach, K., Ackermann, B., Krämer, J., Somers, E., Parson, S.H., Heller, R., Berkessel, A., Sterner-Kock, A., Wirth, B., 2013. Severe SMA mice show organ impairment that cannot be rescued by therapy with the HDACi JNJ-26481585. *Eur. J. Hum. Genet.* 21, 643–652. <https://doi.org/10.1038/ejhg.2012.222>
- Schuster, D.J., Dykstra, J.A., Riedl, M.S., Kitto, K.F., Belur, L.R., Scott Mclvor, R., Elde, R.P., Fairbanks, C.A., Vulchanova, L., 2014. Biodistribution of adeno-associated virus serotype 9 (AAV9) vector after intrathecal and intravenous delivery in mouse. *Front. Neuroanat.* 8.



<https://doi.org/10.3389/fnana.2014.00042>

- Selenko, P., Sprangers, R., Stier, G., Bühler, D., Fischer, U., Sattler, M., 2001. SMN tudor domain structure and its interaction with the Sm proteins. *Nat. Struct. Biol.* 8, 27–31. <https://doi.org/10.1038/83014>
- Sen, A., Dimlich, D.N., Guruharsha, K.G., Kankel, M.W., Hori, K., Yokokura, T., Brachat, S., Richardson, D., Loureiro, J., Sivasankaran, R., Curtis, D., Davidow, L.S., Rubin, L.L., Hart, A.C., Van Vactor, D., Artavanis-Tsakonas, S., 2013. Genetic circuitry of Survival motor neuron, the gene underlying spinal muscular atrophy. *Proc. Natl. Acad. Sci. U. S. A.* 110, E2371–E2380. <https://doi.org/10.1073/pnas.1301738110>
- Shababi, M., Lorson, C.L., Rudnik-Schöneborn, S.S., 2014. Spinal muscular atrophy: A motor neuron disorder or a multi-organ disease? *J. Anat.* 224, 15–28. <https://doi.org/10.1111/joa.12083>
- Shafey, D., Côté, P.D., Kothary, R., 2005. Hypomorphic Smn knockdown C2C12 myoblasts reveal intrinsic defects in myoblast fusion and myotube morphology. *Exp. Cell Res.* 311, 49–61. <https://doi.org/10.1016/j.yexcr.2005.08.019>
- Sharma, A., Lambrechts, A., Hao, L.T., Le, T.T., Sewry, C.A., Ampe, C., Burghes, A.H.M., Morris, G.E., 2005. A role for complexes of survival of motor neurons (SMN) protein with gemins and profilin in neurite-like cytoplasmic extensions of cultured nerve cells. *Exp. Cell Res.* 309, 185–97. <https://doi.org/10.1016/j.yexcr.2005.05.014>
- Shorrock, H.K., Gillingwater, T.H., Groen, E.J.N., 2018. Overview of Current Drugs and Molecules in Development for Spinal Muscular Atrophy Therapy. *Drugs* 78, 293–305. <https://doi.org/10.1007/s40265-018-0868-8>
- Shpargel, K.B., Matera, A.G., 2005. Gemin proteins are required for efficient assembly of Sm-class ribonucleoproteins. *Proc. Natl. Acad. Sci. U. S. A.* 102, 17372–17377. <https://doi.org/10.1073/pnas.0508947102>
- Simic, G., 2008. Pathogenesis of proximal autosomal recessive spinal muscular atrophy. *Acta Neuropathol.* 116, 223–234. <https://doi.org/10.1007/s00401-008-0411-1>
- Simic, G., Mladinov, M., Seso Simic, D., Jovanov Milosevic, N., Islam, A., Pajtak, A., Barisic, N., Sertic, J., Lucassen, P.J., Hof, P.R., Kruslin, B., 2008. Abnormal motoneuron migration, differentiation, and axon outgrowth in spinal muscular atrophy. *Acta Neuropathol.* 115, 313–26. <https://doi.org/10.1007/s00401-007-0327-1>
- Simone, C., Nizzardo, M., Rizzo, F., Ruggieri, M., Riboldi, G., Salani, S., Bucchia, M., Bresolin, N., Comi, G.P., Corti, S., 2014. iPSC-derived neural stem cells act via kinase inhibition to exert neuroprotective effects in spinal muscular atrophy with respiratory distress type 1. *Stem Cell Reports* 3, 297–311. <https://doi.org/10.1016/j.stemcr.2014.06.004>
- Singh, J., Salcius, M., Liu, S.-W., Staker, B.L., Mishra, R., Thurmond, J., Michaud, G., Mattoon, D.R., Printen, J., Christensen, J., Bjornsson, J.M., Pollok, B.A., Kiledjian, M., Stewart, L., Jarecki, J., Gurney, M.E., 2008. DcpS as a therapeutic target for spinal muscular atrophy. *ACS Chem. Biol.* 3, 711–22. <https://doi.org/10.1021/cb800120t>
- Singh, N.N., Shishimorova, M., Cao, L.C., Gangwani, L., Singh, R.N., 2009. A short antisense oligonucleotide masking a unique intronic motif prevents skipping of a critical exon in spinal muscular atrophy. *RNA Biol.* 6, 341–50. <https://doi.org/10.4161/rna.6.3.8723>

- Singh, R.N., Howell, M.D., Ottesen, E.W., Singh, N.N., 2017. Diverse role of survival motor neuron protein. *Biochim. Biophys. Acta - Gene Regul. Mech.* 1860, 299-315. <https://doi.org/10.1016/j.bbagr.2016.12.008>
- Sivaramakrishnan, M., McCarthy, K.D., Campagne, S., Huber, S., Meier, S., Augustin, A., Heckel, T., Meistermann, H., Hug, M.N., Birrer, P., Moursy, A., Khawaja, S., Schmucki, R., Berntenis, N., Giroud, N., Golling, S., Tzouros, M., Banfai, B., Duran-Pacheco, G., Lamerz, J., Hsiu Liu, Y., Luebbers, T., Ratni, H., Ebeling, M., Cléry, A., Paushkin, S., Krainer, A.R., Allain, F.H.-T., Metzger, F., 2017. Binding to SMN2 pre-mRNA-protein complex elicits specificity for small molecule splicing modifiers. *Nat. Commun.* 8, 1476. <https://doi.org/10.1038/s41467-017-01559-4>
- Sleigh, J.N., Buckingham, S.D., Esmaeili, B., Viswanathan, M., Cuppen, E., Westlund, B.M., Sattelle, D.B., 2011a. A novel *Caenorhabditis elegans* allele, *smn-1(cb131)*, mimicking a mild form of spinal muscular atrophy, provides a convenient drug screening platform highlighting new and pre-approved compounds. *Hum. Mol. Genet.* 20, 245–260. <https://doi.org/10.1093/hmg/ddq459>
- Sleigh, J.N., Gillingwater, T.H., Talbot, K., 2011b. The contribution of mouse models to understanding the pathogenesis of spinal muscular atrophy. *Dis. Model. Mech.* 4, 457–67. <https://doi.org/10.1242/dmm.007245>
- Sokol, S.Y., 1999. Wnt signaling and dorso-ventral axis specification in vertebrates. *Curr. Opin. Genet. Dev.* 9, 405–410. [https://doi.org/10.1016/S0959-437X\(99\)80061-6](https://doi.org/10.1016/S0959-437X(99)80061-6)
- Soler, R.M., Egea, J., Mintenig, G.M., Sanz-Rodriguez, C., Iglesias, M., Comella, J.X., 1998. Calmodulin is involved in membrane depolarization-mediated survival of motoneurons by phosphatidylinositol-3 kinase- and MAPK-independent pathways. *J. Neurosci.* 18, 1230–9. <https://doi.org/10.1523/jneurosci.18-04-01230.1998>
- Somers, E., Stencel, Z., Wishart, T.M., Gillingwater, T.H., Parson, S.H., 2012. Density, calibre and ramification of muscle capillaries are altered in a mouse model of severe spinal muscular atrophy. *Neuromuscul. Disord.* 22, 435–442. <https://doi.org/10.1016/j.nmd.2011.10.021>
- Sonneveld, P., Broijl, A., 2016. Treatment of relapsed and refractory multiple myeloma. *Haematologica.* 101, 396-406. <https://doi.org/10.3324/haematol.2015.129189>
- Sorimachi, H., Hata, S., Ono, Y., 2013. Calpain-1/ $\mu$ -Calpain, in: *Handbook of Proteolytic Enzymes*. Elsevier Ltd, pp. 1995–2007. <https://doi.org/10.1016/B978-0-12-382219-2.00453-1>
- Sorimachi, H., Hata, S., Ono, Y., 2011. Impact of genetic insights into calpain biology. *J. Biochem.* 150, 23-37. <https://doi.org/10.1093/jb/mvr070>
- Sorimachi, H., Imajoh-Ohmi, S., Emori, Y., Kawasaki, H., Ohno, S., Minami, Y., Suzuki, K., 1989. Molecular cloning of a novel mammalian calcium-dependent protease distinct from both m- and  $\mu$ -types. Specific expression of the mRNA in skeletal muscle. *J. Biol. Chem.* 264, 20106-20111. ISSN: 00219258
- Sorimachi, H., Ishiura, S., Suzuki, K., 1993. A Novel Tissue-specific Calpain Species Expressed Predominantly in the Stomach Comprises Two Alternative Splicing Products with and without Ca<sup>2+</sup>-binding Domain. *J. Biol. Chem.* 268, 19476–19482. ISSN: 00219258
- Stam, M., Wadman, R.I., Wijngaarde, C.A., Bartels, B., Asselman, F.L., Otto, L.A.M., Goedee, H.S., Habets, L.E., De Groot, J.F., Schoenmakers, M.A.G.C., Cuppen, I., Van Den Berg, L.H., Van Der

- Pol, W.L., 2018. Protocol for a phase II, monocentre, double-blind, placebo-controlled, cross-over trial to assess efficacy of pyridostigmine in patients with spinal muscular atrophy types 2-4 (SPACE trial). *BMJ Open* 8, e019932. <https://doi.org/10.1136/bmjopen-2017-019932>
- Steinbeck, J.A., Studer, L., 2015. Moving stem cells to the clinic: Potential and limitations for brain repair. *Neuron*. 86, 187-206. <https://doi.org/10.1016/j.neuron.2015.03.002>
- Stifani, N., 2014. Motor neurons and the generation of spinal motor neuron diversity. *Front. Cell. Neurosci.* 8, 293. <https://doi.org/10.3389/fncel.2014.00293>
- Stolz, A., Ernst, A., Dikic, I., 2014. Cargo recognition and trafficking in selective autophagy. *Nat. Cell Biol.* 16, 495–501. <https://doi.org/10.1038/ncb2979>
- Stone, D.M., Hynes, M., Armanini, M., Swanson, T.A., Gu, Q., Johnson, R.L., Scott, M.P., Pennica, D., Goddard, A., Phillips, H., Noll, M., Hooper, J.E., de Sauvage, F., Rosenthal, A., 1996. The tumour-suppressor gene patched encodes a candidate receptor for Sonic hedgehog. *Nature*. 384, 129–34. <https://doi.org/10.1038/384129a0>
- Streit, A., Lee, K.J., Woo, I., Roberts, C., Jessell, T.M., Stern, C.D., 1998. Chordin regulates primitive streak development and the stability of induced neural cells, but is not sufficient for neural induction in the chick embryo. *Development*. 125, 507–519. ISSN: 09501991
- Sun, F., Xu, X., Wang, X., Zhang, B., 2016. Regulation of autophagy by Ca<sup>2+</sup>. *Tumor Biol.* 37, 15467-15476. <https://doi.org/10.1007/s13277-016-5353-y>
- Suzuki, K., 1991. Nomenclature of calcium dependent proteinase. *Biomed. Biochim. Acta* 50, 483–4. ISSN: 0232766X
- Suzuki, K., Hata, S., Kawabata, Y., Sorimachi, H., 2004. Structure, Activation, and Biology of Calpain, in: *Diabetes*. 53(SUPPL. 1). <https://doi.org/10.2337/diabetes.53.2007.s12>
- Swoboda, K.J., Scott, C.B., Reyna, S.P., Prior, T.W., LaSalle, B., Sorenson, S.L., Wood, J., Acsadi, G., Crawford, T.O., Kissel, J.T., Krosschell, K.J., D'Anjou, G., Bromberg, M.B., Schroth, M.K., Chan, G.M., Elsheikh, B., Simard, L.R., 2009. Phase II open label study of valproic acid in spinal muscular atrophy. *PLoS One* 4, e5268. <https://doi.org/10.1371/journal.pone.0005268>
- Tadesse, H., Deschênes-Furry, J., Boisvenue, S., Côté, J., 2008. KH-type splicing regulatory protein interacts with survival motor neuron protein and is misregulated in spinal muscular atrophy. *Hum. Mol. Genet.* 17, 506–24. <https://doi.org/10.1093/hmg/ddm327>
- Takano, J., Kawamura, T., Murase, M., Hitomi, K., Maki, M., 1999. Structure of mouse calpastatin isoforms: Implications of species-common and species-specific alternative splicing. *Biochem. Biophys. Res. Commun.* 260, 339–345. <https://doi.org/10.1006/bbrc.1999.0903>
- Talbot, K., Ponting, C.P., Theodosiou, A.M., Rodrigues, N.R., Surtees, R., Mountford, R., Davies, K.E., 1997. Missense mutation clustering in the survival motor neuron gene: A role for a conserved tyrosine and glycine rich region of the protein in RNA metabolism? *Hum. Mol. Genet.* 6, 497–500. <https://doi.org/10.1093/hmg/6.3.497>
- Tan, Y., Dourdin, N., Wu, C., De Veyra, T., Elce, J.S., Greer, P.A., 2006. Conditional disruption of ubiquitous calpains in the mouse. *Genesis* 44, 297–303. <https://doi.org/10.1002/dvg.20216>
- Tanaka, Y., Guhde, G., Suter, A., Eskelinen, E.L., Hartmann, D., Lüllmann-Rauch, R., Janssen, P.M.L., Blanz, J., Von Figura, K., Saftig, P., 2000. Accumulation of autophagic vacuoles and

- cardiomyopathy LAMP-2-deficient mice. *Nature*. 406, 902–906. <https://doi.org/10.1038/35022595>
- Tanida, I., Ueno, T., Kominami, E., 2008. LC3 and autophagy. *Methods Mol. Biol.* 445, 77–88. [https://doi.org/10.1007/978-1-59745-157-4\\_4](https://doi.org/10.1007/978-1-59745-157-4_4)
- Tanida, I., Ueno, T., Kominami, E., 2004. Human light chain 3/MAP1LC3B Is cleaved at its carboxyl-terminal Met 121 to expose Gly120 for lipidation and targeting to autophagosomal membranes. *J. Biol. Chem.* 279, 47704–47710. <https://doi.org/10.1074/jbc.M407016200>
- Tanida, I., Waguri, S., 2010. Measurement of autophagy in cells and tissues. *Methods Mol. Biol.* 648, 193–214. [https://doi.org/10.1007/978-1-60761-756-3\\_13](https://doi.org/10.1007/978-1-60761-756-3_13)
- Tanik, S.A., Schultheiss, C.E., Volpicelli-Daley, L.A., Brunden, K.R., Lee, V.M.Y., 2013. Lewy body-like  $\alpha$ -synuclein aggregates resist degradation and impair macroautophagy. *J. Biol. Chem.* 288, 15194–15210. <https://doi.org/10.1074/jbc.M113.457408>
- Tarabal, O., Caraballo-Miralles, V., Cardona-Rossinyol, A., Correa, F.J., Olmos, G., Lladó, J., Esquerda, J.E., Calderó, J., 2014. Mechanisms involved in spinal cord central synapse loss in a mouse model of spinal muscular atrophy. *J. Neuropathol. Exp. Neurol.* 73, 519–535. <https://doi.org/10.1097/NEN.0000000000000074>
- Tariq, F., Holcik, M., MacKenzie, A., 2013. Spinal Muscular Atrophy: Classification, Diagnosis, Background, Molecular Mechanism and Development of Therapeutics, in: *Neurodegenerative Diseases*. InTech. Chapter 23. <https://doi.org/10.5772/53800>
- Teyssou, E., Takeda, T., Lebon, V., Boillée, S., Doukouré, B., Bataillon, G., Sazdovitch, V., Cazeneuve, C., Meininger, V., LeGuern, E., Salachas, F., Seilhean, D., Millecamps, S., 2013. Mutations in SQSTM1 encoding p62 in amyotrophic lateral sclerosis: genetics and neuropathology. *Acta Neuropathol.* 125, 511–22. <https://doi.org/10.1007/s00401-013-1090-0>
- Thomas, N.H., Dubowitz, V., 1994. The natural history of type I (severe) spinal muscular atrophy. *Neuromuscul. Disord.* 4, 497–502. [https://doi.org/10.1016/0960-8966\(94\)90090-6](https://doi.org/10.1016/0960-8966(94)90090-6)
- Tisdale, S., Pellizzoni, L., 2015. Disease mechanisms and therapeutic approaches in spinal muscular atrophy. *J. Neurosci.* 35, 8691–8700. <https://doi.org/10.1523/JNEUROSCI.0417-15.2015>
- Todd, A.G., Lin, H., Ebert, A.D., Liu, Y., Androphy, E.J., 2013. COPI transport complexes bind to specific RNAs in neuronal cells. *Hum. Mol. Genet.* 22, 729–36. <https://doi.org/10.1093/hmg/dds480>
- Tompa, P., Buzder-Lantos, P., Tantos, A., Farkas, A., Szilágyi, A., Bánóczy, Z., Hudecz, F., Friedrich, P., 2004. On the sequential determinants of calpain cleavage. *J. Biol. Chem.* 279, 20775–20785. <https://doi.org/10.1074/jbc.M313873200>
- Tooze, J., Hollinshead, M., Ludwig, T., Howell, K., Hoflack, B., Kern, H., 1990. In exocrine pancreas, the basolateral endocytic pathway converges with the autophagic pathway immediately after the early endosome. *J. Cell Biol.* 111, 329–345. <https://doi.org/10.1083/jcb.111.2.329>
- Tooze, S.A., Yoshimori, T., 2010. The origin of the autophagosomal membrane, *Nature Publishing Group*. 12, 831–835. <https://doi.org/10.1038/ncb0910-831>
- Tsai, L.K., Tsai, M.S., Ting, C.H., Li, H., 2008. Multiple therapeutic effects of valproic acid in spinal muscular atrophy model mice. *J. Mol. Med.* 86, 1243–1254. <https://doi.org/10.1007/s00109->

008-0388-1

- Tsujinaka, T., Kajiwara, Y., Kambayashi, J., Sakon, M., Higuchi, N., Tanaka, T., Mori, T., 1988. Synthesis of a new cell penetrating calpain inhibitor (calpeptin). *Biochem. Biophys. Res. Commun.* 153, 1201–8. [https://doi.org/10.1016/s0006-291x\(88\)81355-x](https://doi.org/10.1016/s0006-291x(88)81355-x)
- Vai, S., Bianchi, M.L., Moroni, I., Mastella, C., Broggi, F., Morandi, L., Arnoldi, M.T., Bussolino, C., Baranello, G., 2015. Bone and Spinal Muscular Atrophy. *Bone* 79, 116–120. <https://doi.org/10.1016/j.bone.2015.05.039>
- Valori, C.F., Ning, K., Wyles, M., Mead, R.J., Grierson, A.J., Shaw, P.J., Azzouz, M., 2010. Systemic delivery of scAAV9 expressing SMN prolongs survival in a model of spinal muscular atrophy. *Sci. Transl. Med.* 2, 35-42. <https://doi.org/10.1126/scitranslmed.3000830>
- van Bergeijk, J., Rydel-Könecke, K., Grothe, C., Claus, P., 2007. The spinal muscular atrophy gene product regulates neurite outgrowth: importance of the C terminus. *FASEB J.* 21, 1492–1502. <https://doi.org/10.1096/fj.06-7136com>
- Van Meerbeke, J.P., Gibbs, R.M., Plasterer, H.L., Miao, W., Feng, Z., Lin, M.Y., Rucki, A.A., Wee, C.D., Xia, B., Sharma, S., Jacques, V., Li, D.K., Pellizzoni, L., Rusche, J.R., Ko, C.P., Sumner, C.J., 2013. The DcpS inhibitor RG3039 improves motor function in SMA mice. *Hum. Mol. Genet.* 22, 4074–4083. <https://doi.org/10.1093/hmg/ddt257>
- Vancha, A.R., Govindaraju, S., Parsa, K.V.L., Jasti, M., González-García, M., Ballesteros, R.P., 2004. Use of polyethyleneimine polymer in cell culture as attachment factor and lipofection enhancer. *BMC Biotechnol.* 4. <https://doi.org/10.1186/1472-6750-4-23>
- Verhaart, I.E.C., Robertson, A., Wilson, I.J., Aartsma-Rus, A., Cameron, S., Jones, C.C., Cook, S.F., Lochmüller, H., 2017. Prevalence, incidence and carrier frequency of 5q-linked spinal muscular atrophy - A literature review. *Orphanet J. Rare Dis.* 12, 124. <https://doi.org/10.1186/s13023-017-0671-8>
- Vestergaard, P., Glerup, H., Steffensen, B.F., Rejnmark, L., Rahbek, J., Mosekilde, L., 2001. Fracture risk in patients with muscular dystrophy and spinal muscular atrophy. *J. Rehabil. Med.* 33, 150–155. <https://doi.org/10.1080/165019701750300609>
- Villalpando Rodriguez, G.E., Torriglia, A., 2013. Calpain 1 induce lysosomal permeabilization by cleavage of lysosomal associated membrane protein 2. *Biochim. Biophys. Acta - Mol. Cell Res.* 1833, 2244–2253. <https://doi.org/10.1016/j.bbamcr.2013.05.019>
- Vitte, J.M., Davoult, B., Roblot, N., Mayer, M., Joshi, V., Courageot, S., Tronche, F., Vadrot, J., Moreau, M.H., Kemeny, F., Melki, J., 2004. Deletion of murine Smn exon 7 directed to liver leads to severe defect of liver development associated with iron overload. *Am. J. Pathol.* 165, 1731–1741. [https://doi.org/10.1016/S0002-9440\(10\)63428-1](https://doi.org/10.1016/S0002-9440(10)63428-1)
- Vosler, P.S., Brennan, C.S., Chen, J., 2008. Calpain-mediated signaling mechanisms in neuronal injury and neurodegeneration. *Mol. Neurobiol.* 38, 78–100. <https://doi.org/10.1007/s12035-008-8036-x>
- Waldrop, M.A., Kolb, S.J., 2019. Current Treatment Options in Neurology—SMA Therapeutics. *Curr. Treat. Options Neurol.* 21, 25. <https://doi.org/10.1007/s11940-019-0568-z>
- Walker, M.P., Rajendra, T.K., Saieva, L., Fuentes, J.L., Pellizzoni, L., Matera, A.G., 2008. SMN complex localizes to the sarcomeric Z-disc and is a proteolytic target of calpain. *Hum. Mol. Genet.* 17,

- 3399–410. <https://doi.org/10.1093/hmg/ddn234>
- Wan, L., Battle, D.J., Yong, J., Gubitz, A.K., Kolb, S.J., Wang, J., Dreyfuss, G., 2005. The Survival of Motor Neurons Protein Determines the Capacity for snRNP Assembly: Biochemical Deficiency in Spinal Muscular Atrophy. *Mol. Cell. Biol.* 25, 5543–5551. <https://doi.org/10.1128/mcb.25.13.5543-5551.2005>
- Wang, C., Liang, C.C., Bian, Z.C., Zhu, Y., Guan, J.L., 2013. FIP200 is required for maintenance and differentiation of postnatal neural stem cells. *Nat. Neurosci.* 16, 532–542. <https://doi.org/10.1038/nn.3365>
- Wang, Y., Hersheson, J., Lopez, D., Hammer, M., Liu, Y., Lee, K.H., Pinto, V., Seinfeld, J., Wiethoff, S., Sun, J., Amouri, R., Hentati, F., Baudry, N., Tran, J., Singleton, A.B., Coutelier, M., Brice, A., Stevanin, G., Durr, A., Bi, X., Houlden, H., Baudry, M., 2016. Defects in the CAPN1 Gene Result in Alterations in Cerebellar Development and Cerebellar Ataxia in Mice and Humans. *Cell Rep.* 16, 79–91. <https://doi.org/10.1016/j.celrep.2016.05.044>
- Webb, J.L., Ravikumar, B., Rubinsztein, D.C., 2004. Microtubule disruption inhibits autophagosome-lysosome fusion: implications for studying the roles of aggresomes in polyglutamine diseases. *Int. J. Biochem. Cell Biol.* 36, 2541–50. <https://doi.org/10.1016/j.biocel.2004.02.003>
- Weber, J.J., Pereira Sena, P., Singer, E., Nguyen, H.P., 2019. Killing Two Angry Birds with One Stone: Autophagy Activation by Inhibiting Calpains in Neurodegenerative Diseases and beyond. *Biomed Res. Int.* <https://doi.org/10.1155/2019/4741252>
- Weeraratne, S.D., Amani, V., Teider, N., Pierre-Francois, J., Winter, D., Kye, M.J., Sengupta, S., Archer, T., Remke, M., Bai, A.H.C., Warren, P., Pfister, S.M., Steen, J.A.J., Pomeroy, S.L., Cho, Y.-J., 2012. Pleiotropic effects of miR-183~96~182 converge to regulate cell survival, proliferation and migration in medulloblastoma. *Acta Neuropathol.* 123, 539–52. <https://doi.org/10.1007/s00401-012-0969-5>
- Wendt, A., Thompson, V.F., Goll, D.E., 2004. Interaction of calpastatin with calpain: A review. *Biol. Chem.* 385, 465–472. <https://doi.org/10.1515/BC.2004.054>
- Whitehouse, L.L., 2012. Repligen Reports Positive Results from Phase 1 Clinical Trial of RG3039 for Spinal Muscular Atrophy | Business Wire [WWW Document]. URL <https://www.businesswire.com/news/home/20120425005275/en/Repligen-Reports-Positive-Results-Phase-1-Clinical> (accessed 11.4.19).
- Wiese, S., Herrmann, T., Drepper, C., Jablonka, S., Funk, N., Klausmeyer, A., Rogers, M.L., Rush, R., Sendtner, M., 2010. Isolation and enrichment of embryonic mouse motoneurons from the lumbar spinal cord of individual mouse embryos. *Nat. Protoc.* 5, 31–38. <https://doi.org/10.1038/nprot.2009.193>
- Wild, P., Farhan, H., McEwan, D.G., Wagner, S., Rogov, V. V., Brady, N.R., Richter, B., Korac, J., Waidmann, O., Choudhary, C., Dötsch, V., Bumann, D., Dikic, I., 2011. Phosphorylation of the autophagy receptor optineurin restricts Salmonella growth. *Science.* 333, 228–33. <https://doi.org/10.1126/science.1205405>
- Williams, A., Sarkar, S., Cuddon, P., Ttofi, E.K., Saiki, S., Siddiqi, F.H., Jahreiss, L., Fleming, A., Pask, D., Goldsmith, P., O’Kane, C.J., Floto, R.A., Rubinsztein, D.C., 2008. Novel targets for Huntington’s disease in an mTOR-independent autophagy pathway. *Nat. Chem. Biol.* 4, 295–305. <https://doi.org/10.1038/nchembio.79>

- Wirth, B., 2000. An update of the mutation spectrum of the survival motor neuron gene (SMN1) in autosomal recessive spinal muscular atrophy (SMA). *Hum. Mutat.* 15, 228–37. [https://doi.org/10.1002/\(SICI\)1098-1004\(200003\)15:3<228::AID-HUMU3>3.0.CO;2-9](https://doi.org/10.1002/(SICI)1098-1004(200003)15:3<228::AID-HUMU3>3.0.CO;2-9)
- Wirth, B., Mendoza-Ferreira, N., Torres-Benito, L., 2017. Spinal Muscular Atrophy Disease Modifiers, in: *Spinal Muscular Atrophy: Disease Mechanisms and Therapy*. Elsevier Inc., pp. 191–210. <https://doi.org/10.1016/B978-0-12-803685-3.00012-4>
- Witzemann, V., 2006. Development of the neuromuscular junction. *Cell Tissue Res.* 326, 263–271. <https://doi.org/10.1007/s00441-006-0237-x>
- Wright, A.L., Vissel, B., 2016. CAST your vote: Is calpain inhibition the answer to ALS? *J. Neurochem.* 137, 140–141. <https://doi.org/10.1111/jnc.13296>
- Xia, H.G., Zhang, L., Chen, G., Zhang, T., Liu, J., Jin, M., Xiuquan, M., Dawei, M., Yuan, J., 2010. Control of basal autophagy by calpain1 mediated cleavage of ATG5. *Autophagy.* 6, 61–66. <https://doi.org/10.4161/auto.6.1.10326>
- Yamada, T., Placzek, M., Tanaka, H., Dodd, J., Jessell, T.M., 1991. Control of cell pattern in the developing nervous system: polarizing activity of the floor plate and notochord. *Cell.* 64, 635–47. [https://doi.org/10.1016/0092-8674\(91\)90247-v](https://doi.org/10.1016/0092-8674(91)90247-v)
- Yamamoto, Y., Henderson, C.E., 1999. Patterns of programmed cell death in populations of developing spinal motoneurons in chicken, mouse, and rat. *Dev. Biol.* 214, 60–71. <https://doi.org/10.1006/dbio.1999.9413>
- Yamashita, T., Hideyama, T., Hachiga, K., Teramoto, S., Takano, J., Iwata, N., Saido, T.C., Kwak, S., 2012. A role for calpain-dependent cleavage of TDP-43 in amyotrophic lateral sclerosis pathology. *Nat. Commun.* 3, 1307. <https://doi.org/10.1038/ncomms2303>
- Yan, X.-X., Jeromin, A., 2012. Spectrin Breakdown Products (SBDPs) as Potential Biomarkers for Neurodegenerative Diseases. *Curr. Transl. Geriatr. Exp. Gerontol. Rep.* 1, 85–93. <https://doi.org/10.1007/s13670-012-0009-2>
- Ylä-Anttila, P., Vihinen, H., Jokitalo, E., Eskelinen, E.-L., 2009. 3D tomography reveals connections between the phagophore and endoplasmic reticulum. *Autophagy* 5, 1180–5. <https://doi.org/10.4161/auto.5.8.10274>
- Young, P.J., Le, T.T., thi Man, N., Burghes, A.H.M., Morris, G.E., 2000. The relationship between SMN, the spinal muscular atrophy protein, and nuclear coiled bodies in differentiated tissues and cultured cells. *Exp. Cell Res.* 256, 365–74. <https://doi.org/10.1006/excr.2000.4858>
- Yousefi, S., Perozzo, R., Schmid, I., Ziemiecki, A., Schaffner, T., Scapozza, L., Brunner, T., Simon, H.U., 2006. Calpain-mediated cleavage of Atg5 switches autophagy to apoptosis. *Nat. Cell Biol.* 8, 1124–1132. <https://doi.org/10.1038/ncb1482>
- Yu, W.H., Cuervo, A.M., Kumar, A., Peterhoff, C.M., Schmidt, S.D., Lee, J.-H., Mohan, P.S., Mercken, M., Farmery, M.R., Tjernberg, L.O., Jiang, Y., Duff, K., Uchiyama, Y., Näslund, J., Mathews, P.M., Cataldo, A.M., Nixon, R.A., 2005. Macroautophagy--a novel Beta-amyloid peptide-generating pathway activated in Alzheimer's disease. *J. Cell Biol.* 171, 87–98. <https://doi.org/10.1083/jcb.200505082>
- Zerres, K., Rudnik-Schöneborn, S., Forrest, E., Lusakowska, A., Borkowska, J., Hausmanowa-Petrusewicz, I., 1997. A collaborative study on the natural history of childhood and juvenile

- onset proximal spinal muscular atrophy (type II and III SMA): 569 patients. *J. Neurol. Sci.* 146, 67–72. [https://doi.org/10.1016/s0022-510x\(96\)00284-5](https://doi.org/10.1016/s0022-510x(96)00284-5)
- Zhang, H.L., Pan, F., Hong, D., Shenoy, S.M., Singer, R.H., Bassell, G.J., 2003. Active transport of the survival motor neuron protein and the role of exon-7 in cytoplasmic localization. *J. Neurosci.* 23, 6627–37. <https://doi.org/10.1523/jneurosci.23-16-06627.2003>
- Zhang, Z., Pinto, A.M., Wan, L., Wang, W., Berg, M.G., Oliva, I., Singh, L.N., Dengler, C., Wei, Z., Dreyfuss, G., 2013. Dysregulation of synaptogenesis genes antecedes motor neuron pathology in spinal muscular atrophy. *Proc. Natl. Acad. Sci. U. S. A.* 110, 19348–19353. <https://doi.org/10.1073/pnas.1319280110>
- Zhou, Y.-D., Cai, L., 2019. Calpeptin Reduces Neurobehavioral Deficits and Neuronal Apoptosis Following Subarachnoid Hemorrhage in Rats. *J. Stroke Cerebrovasc. Dis.* 28, 125–132. <https://doi.org/10.1016/j.jstrokecerebrovasdis.2018.09.026>
- Zimmerman, L.B., De Jesús-Escobar, J.M., Harland, R.M., 1996. The Spemann organizer signal noggin binds and inactivates bone morphogenetic protein 4. *Cell.* 86, 599–606. [https://doi.org/10.1016/S0092-8674\(00\)80133-6](https://doi.org/10.1016/S0092-8674(00)80133-6)
- Zinzalla, V., Stracka, D., Oppliger, W., Hall, M.N., 2011. Activation of mTORC2 by association with the ribosome. *Cell.* 144, 757–68. <https://doi.org/10.1016/j.cell.2011.02.014>





## **PUBLICATIONS**

---



## **ARTICLES**

Ambika Periyakaruppiah, **Sandra de la Fuente**, Saravanan Arumugam, Núria Bahí, Ana Garcera and Rosa M Soler. *Autophagy modulators regulate survival motor neuron protein stability in motoneuron*. *Experimental Neurology*. (2016) Sep;283(Pt A):287-97. doi: 10.1016/j.expneurol.2016.06.032.

Saravanan Arumugam, Stefka Mincheva-Tasheva, Ambika Periyakaruppiah, **Sandra de la Fuente**, Ana Garcera and Rosa M Soler. *Regulation of Survival Motor Neuron Protein by the Nuclear Factor-Kappa B Pathway in Mouse Spinal Cord Motoneurons*. *Molecular Neurobiology*. (2018) Jun;55(6):5019-5030. doi: 10.1007/s12035-017-0710-4.

**Sandra de la Fuente**, Alba Sansa, Ambika Periyakaruppiah, Ana Garcera and Rosa M Soler. *Calpain Inhibition Increases SMN Protein in Spinal Cord Motoneurons and Ameliorates the Spinal Muscular Atrophy Phenotype in Mice*. *Molecular Neurobiology*. (2019) Jun;56(6):4414-4427. doi: 10.1007/s12035-018-1379-z.

**Sandra de la Fuente**, Alba Sansa, Iván Hidalgo, Nuria Vivancos, Ricardo Romero-Guevara, Ana Garcera and Rosa M Soler. *Calpain system is altered in Survival Motor Neuron- reduced cells from in vitro and in vivo Spinal Muscular Atrophy models*. *Cell Death & Disease*. (2020). Jun; 11, 487. doi: 10.1038/s41419-020-2688-5.

## **PATENTS**

Patent “Tratamiento para la atrofia muscular espinal” Soler Tatche RM; Garcera Teruel A; de la Fuente Ruiz S; PCT/ES2018/070177; 09/03/2018

## **NATIONAL AND INTERNATIONAL CONFERENCES**

· **FENS Forum of Neuroscience**, July 2-6th 2016; Copenhagen, Denmark; Abstract and poster presentation “*Autophagy changes in spinal cord motoneurons of SMA mouse model. Role of autophagy modulators in the regulation of Survival Motor Neuron protein*”. A. Garcera, S. De la Fuente, A. Periyakaruppiah, O. Narcis, R. M. Soler.

- **FENS Forum of Neuroscience**, July 2-6 2016; Copenhagen, Denmark; Abstract and poster presentation "*Survival Motor Neuron protein is regulated by calpain in spinal cord motoneurons*". A. Garcera, S. De la Fuente, A. Periyakauppiiah, D. Nogal, A. Sansa, R.M. Soler.
- **X Simposi de Neurobiologia**, October 6-7th 2016; Barcelona, Spain; Abstract and oral presentation "*Calcium-dependent protease Calpain regulates Survival Motor Neuron protein in cultured mouse motoneurons*". S. de la Fuente, A. Sansa, A. Garcerá and R. M. Soler.
- **I Congreso Interdisciplinar de Neurologia y Neurociencia**, March 10-11th 2017; Lleida, Spain; Abstract and oral presentation "*Calcium-dependent protease Calpain regulates Survival Motor Neuron protein in cultured mouse motoneurons*". S. de la Fuente, A. Sansa, A. Garcerá and R. M. Soler.
- **I Congreso Interdisciplinar de Neurologia y Neurociencia**, March 10-11th 2017; Lleida, Spain; Abstract and poster presentation "*Autophagy changes in spinal cord motoneurons of SMA mouse model. Role of autophagy modulators in the regulation of Survival Motor Neuron protein*". A. Garcera, S. De la Fuente, A. Periyakaruppiiah, O. Narcis, R. M. Soler.
- **17th National Congress of the Spanish Society of Neuroscience**, September 27-30 th, 2017; Alicante, Spain; Abstract and poster presentation "*Autophagy regulates survival motor neuron protein in spinal muscular atrophy mouse model*". S. De la Fuente, A. Periyakaruppiiah, S. Arumugam, A. Garcera, R. M. Soler.
- **FENS Forum of Neuroscience**, July 7-11 th, 2018; Berlin, Germany; Abstract and poster presentation "*Calpain knockdown increases survival motor neuron protein in spinal cord motoneurons*". S. De la Fuente, A. Sansa, A. Quinn, A. Garcera, R.M. Soler.
- **FENS Forum of Neuroscience**, July 7-11 th, 2018; Berlin, Germany; Abstract and poster presentation "*Study of autophagy markers and NF-kappaB pathway in muscle cells of a spinal muscular atrophy mouse model*". A. Garcera, S. Arumugam, S. Alba, I. Hidalgo, S. De la Fuente, R.M. Soler.
- **FENS Forum of Neuroscience**, July 7-11 th, 2018; Berlin, Germany; Abstract and poster presentation "*Nuclear factor-Kappa B and apoptosis pathways are altered in cultured motoneurons of a spinal muscular atrophy mouse model*". A. Sansa, S. Arumugam, S. De la Fuente, N. Vivancos, M. J. Perez-Garcia, J.X. Comella, A. Garcera, R.M. Soler.

- **II Congreso Interdisciplinar de Neurología y Neurociencia**, March 8-9th 2019; Lleida, Spain; Abstract and oral presentation “*Protective effects of Calpain inhibition on Spinal Muscular Atrophy mouse model*”. S. De la Fuente, A. Sansa, A. Garcera, R. M. Soler.
- **II Congreso Interdisciplinar de Neurología y Neurociencia**, March 8-9th 2019; Lleida, Spain; Abstract and poster presentation “*Autophagy regulates Survival Motor Neuron protein in Spinal Muscular Atrophy mouse model*”. S. De la Fuente, A. Periyakaruppiyah, S. Arumugam, A. Garcera, R. M. Soler.
- **2nd International Scientific congress SMA Europe**, February 5-7th 2020; Evry, France; Abstract and poster presentation “*Calpeptin Treatment Increases SMN Protein in Spinal Cord Motoneurons and Ameliorates the SMA Phenotype in Mice*”. S. de la Fuente, A. Sansa, I. Hidalgo, A. Garcerá and R. M. Soler.
- **2nd International Scientific congress SMA Europe**, February 5-7th 2020; Evry, France; Abstract and poster presentation “*Characterisation of survival signalling pathways in motoneurons from an in vitro model of human SMA iPS Cells*”. A. Sansa, N. Vivancos, S. de la Fuente, A. Garcerá and R. M. Soler.



## INDEX OF FIGURES

<b>Figure 1.</b> Diagram showing the organization of the vertebrate nervous system _____	9
<b>Figure 2.</b> Classification of the Somatic MNs according to the type of muscle they innervate ____	13
<b>Figure 3.</b> Spinal cord developmental _____	14
<b>Figure 4.</b> Spinal cord differentiation axis and MNs specification _____	15
<b>Figure 5.</b> Segmental organization of motor columns on the spinal cord and innervation target _	18
<b>Figure 6.</b> Neuromuscular milestones and trajectories from birth to adult life in SMA types ____	21
<b>Figure 7.</b> Duplicated chromosomal region 5q11.2-13.3 containing the SMA locus _____	24
<b>Figure 8.</b> Transcription of the SMN1 and SMN2 genes _____	25
<b>Figure 9.</b> Percentage of patients' number of copies for each SMA type _____	27
<b>Figure 10.</b> Structure of SMN protein _____	28
<b>Figure 11.</b> SMN function in the snRNPs assembly _____	30
<b>Figure 12.</b> SMN function in the transport of mRNA at the axon terminal _____	31
<b>Figure 13.</b> Summary of the described cellular functions of SMN in neuronal cells _____	33
<b>Figure 14.</b> Hypotheses proposed to explain how reduced SMN levels cause MNs affectation ____	36
<b>Figure 15.</b> Representative scheme of the threshold hypothesis in the SMA _____	38
<b>Figure 16.</b> Overview of the systemic alterations known to be affected in SMA _____	42
<b>Figure 17.</b> Mechanism of action of Nusinersen _____	45
<b>Figure 18.</b> Strategies in the development of new therapies for SMA _____	47
<b>Figure 19.</b> Autophagy types in mammalian cells _____	69
<b>Figure 20.</b> Steps during the autophagy process _____	70
<b>Figure 21.</b> Initiation of autophagy via the mTOR pathway _____	72
<b>Figure 22.</b> Autophagosome nucleation signalling pathway _____	74
<b>Figure 23.</b> Potential phagophore membrane sources _____	75
<b>Figure 24.</b> Phagophore elongation signalling pathway _____	77
<b>Figure 25.</b> Cargo selection in the autophagy vesicles in mammals _____	78
<b>Figure 26.</b> Structure and classification of catalytic subunits of human calpains _____	82
<b>Figure 27.</b> Phylogenetic tree of human calpains and their classification _____	83
<b>Figure 28.</b> Three-dimensional structures of the inactive and active form of human calpain CysPc domain _____	85
<b>Figure 29.</b> Structure of the longest isoform of human calpastatin _____	88
<b>Figure 30.</b> Mechanism of calpain inhibition by calpastatin _____	88
<b>Figure 31.</b> Severe SMA mouse model <i>Smn</i> <sup>-/-</sup> ; <i>SMN2</i> <sup>+/+</sup> or <i>MutSMA</i> photographed at postnatal day 4 (P4) with a normal littermate _____	98
<b>Figure 32.</b> SMA mutant mouse <i>Smn</i> <sup>-/-</sup> ; <i>SMN2</i> <sup>+/+</sup> ; <i>SMNΔ7</i> <sup>+/+</sup> or <i>SMNΔ7</i> together with a normal littermate photographed at postnatal day 10 (P10) _____	99
<b>Figure 33.</b> Timeline of major cellular and symptomatic events in <i>MutSMA</i> ( <i>Smn</i> <sup>-/-</sup> ; <i>SMN2</i> <sup>+/+</sup> ) and <i>SMNΔ7</i> ( <i>Smn</i> <sup>-/-</sup> ; <i>SMN2</i> <sup>+/+</sup> ; <i>SMNΔ7</i> <sup>+/+</sup> ) mouse models of SMA _____	100
<b>Figure 34.</b> Schematic representation of genotype PCR cycling parameters _____	102
<b>Figure 35.</b> Genotypes in a 1% agarose gel _____	103
<b>Figure 36.</b> Dissection of mouse embryos spinal cord _____	106
<b>Figure 37.</b> Detail of the separation of the meninges from the spinal cord _____	107
<b>Figure 38.</b> Graphic representation of the centrifugation step of the cells in a 4% BSA gradient _____	108
<b>Figure 39.</b> Graphic representation of the Optiprep™ gradient centrifugation step _____	108
<b>Figure 40.</b> Immunofluorescence of MNs markers in mouse isolated MNs _____	109



<b>Figure 41.</b> Representative culture of HEK 293T cells _____	111
<b>Figure 42.</b> Representative culture of the human fibroblast cell line (GM03814) _____	113
<b>Figure 43.</b> Differentiation process from hiPSCs to mature MNs _____	116
<b>Figure 44.</b> Mechanism of shRNA induced gene silencing _____	118
<b>Figure 45.</b> pLVTHM lentiviral transfer plasmid structure _____	120
<b>Figure 46.</b> psPAX2 packaging plasmid structure _____	120
<b>Figure 47.</b> pM2 envelope plasmid structure _____	121
<b>Figure 48.</b> Representative image of a virus titration using HEK 293T _____	123
<b>Figure 49.</b> Representative image of mouse MNs transduced with the lentivirus _____	124
<b>Figure 50.</b> Example of MNs survival analysis _____	125
<b>Figure 51.</b> Example of neuronal degeneration analysis _____	126
<b>Figure 52.</b> Representative image of MNs nuclei stained with Hoechst dye _____	127
<b>Figure 53.</b> Example of LC3 spots quantification using ImageJ software _____	132
<b>Figure 54.</b> Schematic representation of PCR cycling parameters _____	141
<b>Figure 55.</b> Schematic representation of PCR cycling parameters _____	142
<b>Figure 56.</b> Body length measurements in SMNDelta7 mice _____	144
<b>Figure 57.</b> Example of the righting reflex (RR) test execution _____	145
<b>Figure 58.</b> Example of the tube test (TT) execution _____	146
<b>Figure 59.</b> Scoring criteria for the hind-limb score (HLS) _____	147
<b>Figure 60.</b> Neurite degeneration in cultured MNs from a severe SMA mouse model _____	156
<b>Figure 61.</b> Apoptosis cell death evaluation in primary cultured SMA mouse MNs _____	157
<b>Figure 62.</b> LC3-II and p62 autophagy markers in spinal cord MNs from the MutSMA mouse model _____	159
<b>Figure 63.</b> LC3-II and p62 autophagy markers in spinal cord MNs from the SMNDelta7 mouse model _____	160
<b>Figure 64.</b> Measurement of SMN fluorescence level and LC3 spots in human fibroblast _____	162
<b>Figure 65.</b> LC3-II and p62 autophagy markers in human fibroblast cells _____	163
<b>Figure 66.</b> Characterization of differentiated human MNs using immunofluorescence (1) _____	165
<b>Figure 67.</b> Characterization of differentiated human MNs using immunofluorescence (2) _____	166
<b>Figure 68.</b> SMN levels in MNs derived from human iPSCs from an SMA patient and control _____	167
<b>Figure 69.</b> Measurement of LC3 spots in human MNs using immunofluorescence _____	168
<b>Figure 70.</b> Analysis of the autophagy markers LC3-II and p62 in differentiated human MNs _____	169
<b>Figure 71.</b> Effect of endogenous calpain reduction on LC3-II and Smn in CD1 MNs _____	171
<b>Figure 72.</b> LC3 autophagy spots levels in CD1 cultured MNs transduced with EV or shCalp using immunofluorescence _____	172
<b>Figure 73.</b> Effect of endogenous calpain reduction on Smn protein level during different culture period _____	173
<b>Figure 74.</b> Influence of shCalp in survival of cultured CD1 spinal cord MNs _____	174
<b>Figure 75.</b> Effect of shCalp in Smn protein levels in CD1 cultured MNs using immunofluorescence _____	175
<b>Figure 76.</b> Effect of high-potassium-induced membrane depolarization on calpain activity _____	177
<b>Figure 77.</b> Effect of calpain knockdown on Smn protein level in high-potassium treatment _____	178
<b>Figure 78.</b> Endogenous calpain reduction in MutSMA cultured MNs _____	179
<b>Figure 79.</b> shCalp treatment in neurite degeneration in MutSMA cultured MNs _____	180
<b>Figure 80.</b> Effect of calpeptin time-course treatment on Smn protein level in CD1 MNs _____	187
<b>Figure 81.</b> Effect of calpain activity modulation on Smn protein level in cultured MNs _____	188

<b>Figure 82.</b> Effect of high K <sup>+</sup> and calpeptin treatment on SMN cleavage by analysing the Smn N-terminal fragment _____	190
<b>Figure 83.</b> Effect of high K <sup>+</sup> and calpeptin treatment on SMN cleavage by analysing the Smn C-terminal fragment _____	191
<b>Figure 84.</b> Smn mRNA levels in calpeptin treated CD1 MNs _____	191
<b>Figure 85.</b> Changes of autophagy markers in Calpeptin treated CD1 MNs _____	192
<b>Figure 86.</b> Effect of calpain activity modulation in LC3 spots levels in SMNDelta7 MNs _____	194
<b>Figure 87.</b> Effect of calpeptin treatment in Smn protein level in MutSMA MNs _____	195
<b>Figure 88.</b> Effect of calpeptin treatment in Smn protein level in SMNDelta7 MNs _____	196
<b>Figure 89.</b> Effect of calpeptin treatment in SMN levels in human fibroblast cultures _____	197
<b>Figure 90.</b> Effect of calpeptin treatment in SMN levels in human differentiated MNs _____	198
<b>Figure 91.</b> Combination of calpeptin and resveratrol treatment in CD1 cultured MNs _____	200
<b>Figure 92.</b> Combination of calpeptin and trehalose treatment in CD1 cultured MNs _____	201
<b>Figure 93.</b> Effect of calpeptin administration on survival of MutSMA and SMNDelta7 mice ____	202
<b>Figure 94.</b> Changes in weight in MutSMA and SMNDelta7 mice after calpeptin administration _	203
<b>Figure 95.</b> Changes in the motor function measured with the righting reflex test in MutSMA and SMNDelta7 mice treated with calpeptin _____	205
<b>Figure 96.</b> Motor function changes measured by tube test in MutSMA and SMNDelta7 treated mice _____	207
<b>Figure 97.</b> Analysis by western blot of calpain and calpain activation in MutSMA cultured MNs	213
<b>Figure 98.</b> Analysis by western blot of calpain and calpain activation in SMNDelta7 cultured MNs _____	214
<b>Figure 99.</b> Analysis of calpastatin protein levels in MutSMA and SMNDelta7 cultured MNs ____	215
<b>Figure 100.</b> Analysis by western blot of calpain, calpain activation and calpastatin in human cultured fibroblast _____	217
<b>Figure 101.</b> Analysis by western blot of calpain, calpain activation and calpastatin in human differentiated MNs _____	218
<b>Figure 102.</b> Smn, calpain and fodrin protein level measured in spinal cord protein extracts from SMNdelta7 treated mice _____	220
<b>Figure 103.</b> Calpastatin protein level measured in spinal cord protein extracts from SMNdelta7 treated mice _____	221
<b>Figure 104.</b> MNs identification in P8 lumbar spinal cord MNs from SMNdelta7 treated mice __	222
<b>Figure 105.</b> Smn level measured in P8 spinal cord MNS from SMNdelta7 treated mice using immunofluorescence _____	223
<b>Figure 106.</b> Calpain protein level measured in P8 spinal cord MNS from SMNdelta7 treated mice using immunofluorescence _____	224
<b>Figure 107.</b> Calpastatin protein level measured in P8 spinal cord MNS from SMNdelta7 treated mice using immunofluorescence _____	225
<b>Figure 108.</b> Effect of calpastatin time-course treatment on Smn protein level in CD1 MNs ____	227
<b>Figure 109.</b> Effect of calpastatin treatment in MutSMA cultured MNs _____	228
<b>Figure 110.</b> Effect of calpastatin treatment in human fibroblast cell lines _____	229
<b>Figure 111.</b> Autophagy pathway in neurons in homeostatic and pathogenic conditions _____	237
<b>Figure 112.</b> Calpain proteolytic targets in the autophagy process _____	239
<b>Figure 113.</b> Calcium regulation of autophagy _____	241
<b>Figure 114.</b> Schematic representation of calpain involvement in SMA _____	248

## INDEX OF TABLES

<b>Table 1.</b> Characteristics of upper and lower MNs _____	10
<b>Table 2.</b> Classification and clinical features of human SMA types _____	23
<b>Table 3.</b> Number of copies and amount of produced SMN in SMA types _____	26
<b>Table 4.</b> SMN dependent therapies clinical trials (to October, 2019) _____	55
<b>Table 5.</b> SMN independent therapies clinical trials (to October, 2019) _____	59
<b>Table 6.</b> Mouse models of SMA _____	67
<b>Table 7.</b> Human calpain genes and their representative products _____	84
<b>Table 8.</b> Genotype PCR mix preparation _____	102
<b>Table 9.</b> Genotype PCR cycling parameters _____	102
<b>Table 10.</b> Primary cell culture media and solution _____	104
<b>Table 11.</b> HEK 293T cells media _____	110
<b>Table 12.</b> Fibroblast cell lines media _____	113
<b>Table 13.</b> Human MNs differentiation cell culture medium _____	115
<b>Table 14.</b> List of cell cultures drugs _____	124
<b>Table 15.</b> List of the primary antibody used in immunofluorescence analysis _____	130
<b>Table 16.</b> List of the secondary antibody used in immunofluorescence analysis _____	131
<b>Table 17.</b> Components for staking and resolving SDS-PAGE gels _____	135
<b>Table 18.</b> List of the primary antibody used in western blot analysis _____	137
<b>Table 19.</b> List of the secondary antibody used in western blot analysis _____	138
<b>Table 20.</b> Reverse transcriptase PCR mix preparation _____	141
<b>Table 21.</b> Reverse transcriptase PCR cycling parameters _____	141
<b>Table 22.</b> Quantitative PCR mix preparation _____	142
<b>Table 23.</b> Quantitative PCR cycling parameters _____	143



